

AD-A243 251



NAVAL POSTGRADUATE SCHOOL
Monterey, California



DTIC
S ELEC D
C

THESIS

TRANSITION PHENOMENA IN A STRAIGHT
CHANNEL WITH A 40 TO 1
ASPECT RATIO WITH AND WITHOUT IMPOSED
PULSATIONS
PART I: NEAR-WALL AND CENTRAL REGION
PROFILES

by

Darrell S. Morrow

March 1991

Thesis Advisor

Phillip M. Ligrani

Approved for public release; distribution is unlimited.

91-17290



Unclassified

security classification of this page

REPORT DOCUMENTATION PAGE				
1a Report Security Classification Unclassified			1b Restrictive Markings	
2a Security Classification Authority			3 Distribution Availability of Report	
2b Declassification Downgrading Schedule			Approved for public release; distribution is unlimited.	
4 Performing Organization Report Number(s)			5 Monitoring Organization Report Number(s)	
6a Name of Performing Organization Naval Postgraduate School		6b Office Symbol (if applicable) 34	7a Name of Monitoring Organization Naval Postgraduate School	
6c Address (city, state, and ZIP code) Monterey, CA 93943-5000			7b Address (city, state, and ZIP code) Monterey, CA 93943-5000	
8a Name of Funding Sponsoring Organization		8b Office Symbol (if applicable)	9 Procurement Instrument Identification Number	
8c Address (city, state, and ZIP code)			10 Source of Funding Numbers	
			Program Element No	Project No
			Task No	Work Unit Accession No
11 Title (include security classification) TRANSITION PHENOMENA IN A STRAIGHT CHANNEL WITH A 40 TO 1 ASPECT RATIO WITH AND WITHOUT IMPOSED PULSATIONS PART I: NEAR-WALL AND CENTRAL REGION PROFILES				
12 Personal Author(s) Darrell S. Morrow				
13a Type of Report Master's Thesis		13b Time Covered From To	14 Date of Report (year, month, day) March 1991	15 Page Count 184
16 Supplementary Notation The views expressed in this thesis are those of the author and do not reflect the official policy or position of the Department of Defense or the U.S. Government.				
17 Cosati Codes			18 Subject Terms (continue on reverse if necessary and identify by block number)	
Field	Group	Subgroup	Imposed Pulsations, Turbulence Intensity, Center Mode	
19 Abstract (continue on reverse if necessary and identify by block number)				
<p>A channel with a rectangular cross-section, 40 to 1 aspect ratio (height is 0.0127 m), and 4.27 m test section (336 channel heights) is used to study the effects of imposed pulsations on transitional flow phenomena. Periodic velocity variations are produced in the test section using a single rotating vane located in the flow downstream of the test section. Flows with Reynolds numbers (Re) ranging from 1100 to 3600 are studied at Stokes numbers of 4.08 and 5.79 and Strouhal numbers from 0.02 to 0.122 by imposing pulsations at 1 Hz and at 2 Hz. Time-averaged velocity profiles both within and outside of the Stokes layer are unaffected by the imposed pulsations at frequencies of 1 and 2 Hz for the entire range of Reynolds numbers studied. Longitudinal turbulence intensity profiles show a local maxima only at the channel centerline for Reynolds numbers from 1250 to 1550. This is evidence of a center mode of instability. Longitudinal turbulence intensity profiles show a local maxima at both the channel centerline and y/d of 0.85 for Reynolds number from 1710 to 2300. As the Reynolds number increases from 2350 to 3400 local maxima of longitudinal turbulence intensity occur only at y/d of 0.9. Normalized profiles of longitudinal turbulence intensity are the same with and without pulsations for all Reynolds numbers studied with the exception of Reynolds numbers 2400 and 2450. Longitudinal turbulence intensity profiles at a Reynolds number of 2400 show that magnitudes near the channel centerline are reduced at Stokes number of 5.79 (2 Hz pulsations) as compared to without pulsations. At Reynolds number of 2450 the magnitude of longitudinal turbulence intensity near the channel centerline are reduced at Stokes numbers of 4.08 and 5.79 (1 Hz and 2 Hz pulsations).</p>				
20 Distribution Availability of Abstract			21 Abstract Security Classification	
<input checked="" type="checkbox"/> unclassified unlimited <input type="checkbox"/> same as report <input type="checkbox"/> DTIC users			Unclassified	
22a Name of Responsible Individual Phillip M. Ligrani			22b Telephone (include Area code) (408) 646-3382	22c Office Symbol 69Li

DD FORM 1473.84 MAR

83 APR edition may be used until exhausted
All other editions are obsolete

security classification of this page

Unclassified

Approved for public release; distribution is unlimited.

Transition Phenomena in a Straight Channel with a 40 to 1
Aspect Ratio With and Without Imposed Pulsations
Part I: Near-Wall and Central Region Profiles

by

Darrell S. Morrow
Lieutenant, United States Navy
B.S., Texas A&M University, 1985

Submitted in partial fulfillment of the
requirements for the degree of

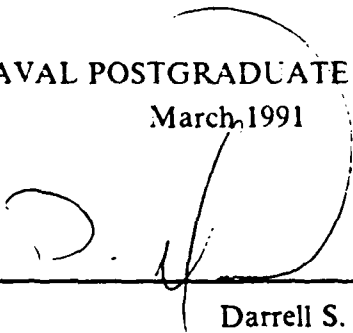
MASTER OF SCIENCE IN MECHANICAL ENGINEERING

from the

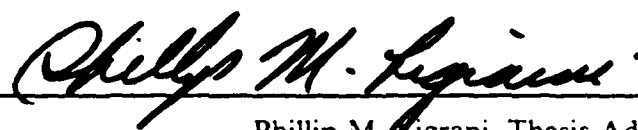
NAVAL POSTGRADUATE SCHOOL

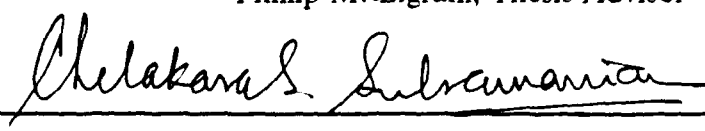
March 1991

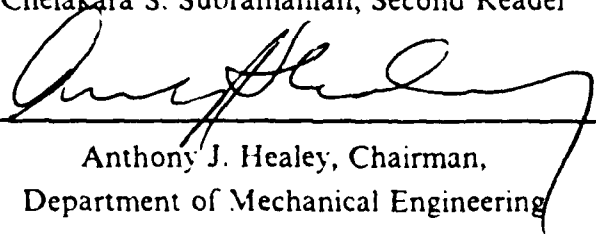
Author:


Darrell S. Morrow

Approved by:


Phillip M. Cigrani, Thesis Advisor


Chelakara S. Subramanian, Second Reader


Anthony J. Healey, Chairman,
Department of Mechanical Engineering

ABSTRACT

A channel with a rectangular cross-section, 40 to 1 aspect ratio (height is 0.0127 m), and 4.27 m test section (336 channel heights) is used to study the effects of imposed pulsations on transitional flow phenomena. Periodic velocity variations are produced in the test section using a single rotating vane located in the flow downstream of the test section. Flows with Reynolds numbers (Re) ranging from 1100 to 3600 are studied at Stokes numbers of 4.08 and 5.79 and Strouhal numbers from 0.02 to 0.122 by imposing pulsations at 1 Hz and at 2 Hz. Time-averaged velocity profiles both within and outside of the Stokes layer are unaffected by the imposed pulsations at frequencies of 1 and 2 Hz for the entire range of Reynolds numbers studied. Longitudinal turbulence intensity profiles show a local maxima only at the channel centerline for Reynolds numbers from 1250 to 1550. This is evidence of a center mode of instability. Longitudinal turbulence intensity profiles show a local maxima at both the channel centerline and y/d of 0.85 for Reynolds number from 1710 to 2300. As the Reynolds number increases from 2350 to 3400 local maxima of longitudinal turbulence intensity occur only at y/d of 0.9. Normalized profiles of longitudinal turbulence intensity are the same with and without pulsations for all Reynolds numbers studied with the exception of Reynolds numbers 2400 and 2450. Longitudinal turbulence intensity profiles at a Reynolds number of 2400 show that magnitudes near the channel centerline are reduced at Stokes number of 5.79 (2 Hz pulsations) as compared to without pulsations. At Reynolds number of 2450 the magnitude of longitudinal turbulence intensity near the channel centerline are reduced at Stokes numbers of 4.08 and 5.79 (1 Hz and 2 Hz pulsations).

Accession For	
NTIS Unshel	✓
771 741	
Available	
Classification	
By	
Classification	
Availability Codes	
Availability	
Time	
A-1	

TABLE OF CONTENTS

I. INTRODUCTION	1
A. BACKGROUND	1
B. OBJECTIVES	3
C. THESIS ORGANIZATION	4
II. EXPERIMENTAL FACILITIES	5
A. CHANNEL	5
B. UNSTEADINESS DEVICE	6
C. FLOW MEASUREMENT INSTRUMENTS	7
1. Hot-wire Probe and Probe Positioning	7
2. Hot-wire Bridge and Signal Conditioner	7
3. High Speed Data Acquisition System and Data Storage	8
III. EXPERIMENTAL PROCEDURES	9
A. HOT-WIRE CALIBRATION	9
B. DATA PROCESSING	9
1. Bulk Velocity	9
2. Instantaneous Velocity	9
3. Phase Averaging	9
IV. DISCUSSION OF RESULTS	11
A. INLET TURBULENCE INTENSITY MAGNITUDES	11
B. FLOW DEVELOPMENT VALIDATION	11
C. PROFILE DATA	11
1. Mean Velocity Profiles	12
2. Longitudinal Turbulence Intensity Profiles	12
D. NEAR-WALL DATA	12
1. Shear Velocity Determination	13
2. Local Mean Velocity Profiles	13
3. Longitudinal Turbulence Intensity Profiles	14
E. PHASE AVERAGED VELOCITY MAGNITUDE RESULTS	14

V. SUMMARY AND CONCLUSIONS	16
APPENDIX A. SOFTWARE DIRECTORY	17
APPENDIX B. FIGURES	18
LIST OF REFERENCES	164
INITIAL DISTRIBUTION LIST	167

LIST OF FIGURES

Figure 1. Experimental Channel	19
Figure 2. Unsteadiness Device	20
Figure 3. Quasi-Steady Flow Variations With Vane Positions	21
Figure 4. Schematic of Flow Measurement Equipment	22
Figure 5. Bulk Channel Velocity vs Pressure Differential Across Orifice	23
Figure 6. Instantaneous and Phase Averaged Velocity Trace	24
Figure 7. Normalized Longitudinal Turbulence Intensity at the Inlet of the Channel	25
Figure 8. Pressure Distribution of the Channel in the x-Direction	26
Figure 9. Profile Data: Mean Velocity vs y/d ; Re: 1100	27
Figure 10. Profile Data: Mean Velocity vs y/d ; Re: 1250	28
Figure 11. Profile Data: Mean Velocity vs y/d ; Re: 1350	29
Figure 12. Profile Data: Mean Velocity vs y/d ; Re: 1440	30
Figure 13. Profile Data: Mean Velocity vs y/d ; Re: 1550	31
Figure 14. Profile Data: Mean Velocity vs y/d ; Re: 1710	32
Figure 15. Profile Data: Mean Velocity vs y/d ; Re: 1850	33
Figure 16. Profile Data: Mean Velocity vs y/d ; Re: 1920	34
Figure 17. Profile Data: Mean Velocity vs y/d ; Re: 2000	35
Figure 18. Profile Data: Mean Velocity vs y/d ; Re: 2040	36
Figure 19. Profile Data: Mean Velocity vs y/d ; Re: 2090	37
Figure 20. Profile Data: Mean Velocity vs y/d ; Re: 2200	38
Figure 21. Profile Data: Mean Velocity vs y/d ; Re: 2300	39
Figure 22. Profile Data: Mean Velocity vs y/d ; Re: 2350	40
Figure 23. Profile Data: Mean Velocity vs y/d ; Re: 2400	41
Figure 24. Profile Data: Mean Velocity vs y/d ; Re: 2450	42
Figure 25. Profile Data: Mean Velocity vs y/d ; Re: 2500	43
Figure 26. Profile Data: Mean Velocity vs y/d ; Re: 2800	44
Figure 27. Profile Data: Mean Velocity vs y/d ; Re: 3100	45
Figure 28. Profile Data: Mean Velocity vs y/d ; Re: 3400	46
Figure 29. Profile Data: Mean Velocity vs y/d ; Composite Profiles	47
Figure 30. Profile Data: Mean Velocity vs y/d ; Composite Profiles	48

Figure 31. Profile Data: Mean Velocity vs y/d ; Composite Profiles	49
Figure 32. Profile Data: Mean Velocity vs y/d ; Composite Profiles	50
Figure 33. Profile Data: Mean Velocity Normalized by the Centerline Velocity vs y/d ; Re: 1100	51
Figure 34. Profile Data: Mean Velocity Normalized by the Centerline Velocity vs y/d ; Re: 1250	52
Figure 35. Profile Data: Mean Velocity Normalized by the Centerline Velocity vs y/d ; Re: 1350	53
Figure 36. Profile Data: Mean Velocity Normalized by the Centerline Velocity vs y/d ; Re: 1440	54
Figure 37. Profile Data: Mean Velocity Normalized by the Centerline Velocity vs y/d ; Re: 1550	55
Figure 38. Profile Data: Mean Velocity Normalized by the Centerline Velocity vs y/d ; Re: 1710	56
Figure 39. Profile Data: Mean Velocity Normalized by the Centerline Velocity vs y/d ; Re: 1850	57
Figure 40. Profile Data: Mean Velocity Normalized by the Centerline Velocity vs y/d ; Re: 1920	58
Figure 41. Profile Data: Mean Velocity Normalized by the Centerline Velocity vs y/d ; Re: 2000	59
Figure 42. Profile Data: Mean Velocity Normalized by the Centerline Velocity vs y/d ; Re: 2040	60
Figure 43. Profile Data: Mean Velocity Normalized by the Centerline Velocity vs y/d ; Re: 2090	61
Figure 44. Profile Data: Mean Velocity Normalized by the Centerline Velocity vs y/d ; Re: 2200	62
Figure 45. Profile Data: Mean Velocity Normalized by the Centerline Velocity vs y/d ; Re: 2300	63
Figure 46. Profile Data: Mean Velocity Normalized by the Centerline Velocity vs y/d ; Re: 2350	64
Figure 47. Profile Data: Mean Velocity Normalized by the Centerline Velocity vs y/d ; Re: 2400	65
Figure 48. Profile Data: Mean Velocity Normalized by the Centerline Velocity vs y/d ; Re: 2450	66

Figure 49. Profile Data: Mean Velocity Normalized by the Centerline Velocity vs y/d; Re: 2500	67
Figure 50. Profile Data: Mean Velocity Normalized by the Centerline Velocity vs y/d; Re: 2800	68
Figure 51. Profile Data: Mean Velocity Normalized by the Centerline Velocity vs y/d; Re: 3100	69
Figure 52. Profile Data: Mean Velocity Normalized by the Centerline Velocity vs y/d; Re: 3400	70
Figure 53. Profile Data: Longitudinal Trubulence Intensity vs y/d; Re: 1100	71
Figure 54. Profile Data: Longitudinal Turbulence Intensity vs y/d; Re: 1250	72
Figure 55. Profile Data: Longitudinal Turbulence Intensitiy vs y/d; Re: 1350	73
Figure 56. Profile Data: Longitudinal Turbulence Intensity vs y/d; Re: 1440	74
Figure 57. Profile Data: Longitudinal Turbulence Intensity vs y/d; Re: 1550	75
Figure 58. Profile Data: Longitudinal Turbulence Intensity vs y/d; Re: 1710	76
Figure 59. Profile Data: Longitudinal Turbulence Intensity vs y/d; Re: 1850	77
Figure 60. Profile Data: Longitudinal Turbulence Intensity vs y/d; Re: 1920	78
Figure 61. Profile Data: Longitudinal Turbulence Intensity vs y/d; Re: 2000	79
Figure 62. Profile Data: Longitudinal Turbulence Intensity vs y/d; Re: 2040	80
Figure 63. Profile Data: Longitudinal Trubulence Intensity vs y/d; Re: 2090	81
Figure 64. Profile Data: Longitudinal Turbulence Intensity vs y/d; Re: 2200	82
Figure 65. Profile Data: Longitudinal Turbulence Intensitiy vs y/d; Re: 2300	83
Figure 66. Profile Data: Longitudinal Turbulence Intensity vs y/d; Re: 2350	84
Figure 67. Profile Data: Longitudinal Turbulence Intensity vs y/d; Re: 2400	85
Figure 68. Profile Data: Longitudinal Turbulence Intensity vs y/d; Re: 2450	86
Figure 69. Profile Data: Longitudinal Turbulence Intensity vs y/d; Re: 2500	87
Figure 70. Profile Data: Longitudinal Turbulence Intensity vs y/d; Re: 2800	88
Figure 71. Profile Data: Longitudinal Turbulence Intensity vs y/d; Re: 3100	89
Figure 72. Profile Data: Longitudinal Turbulence Intensity vs y/d; Re: 3400	90
Figure 73. Profile Data: Longitudinal Turbulence Intensity vs y/d; Composite Profiles	91
Figure 74. Profile Data: Longitudinal Turbulence Intensity vs y/d; Composite Profiles	92
Figure 75. Profile Data: Longitudinal Turbulence Intensity vs y/d; Composite Profiles	93

Figure 76. Profile Data: Longitudinal Turbulence Intensity vs y/d ; Composite Profiles	94
Figure 77. Profile Data: Longitudinal Turbulence Intensity Normalized by the Centerline Velocity vs y/d ; Re: 1100	95
Figure 78. Profile Data: Longitudinal Turbulence Intensity Normalized by the Centerline Velocity vs y/d ; Re: 1250	96
Figure 79. Profile Data: Longitudinal Turbulence Intensity Normalized by the Centerline Velocity vs y/d ; Re: 1350	97
Figure 80. Profile Data: Longitudinal Turbulence Intensity Normalized by the Centerline Velocity vs y/d ; Re: 1440	98
Figure 81. Profile Data: Longitudinal Turbulence Intensity Normalized by the Centerline Velocity vs y/d ; Re: 1550	99
Figure 82. Profile Data: Longitudinal Turbulence Intensity Normalized by the Centerline Velocity vs y/d ; Re: 1710	100
Figure 83. Profile Data: Longitudinal Turbulence Intensity Normalized by the Centerline Velocity vs y/d ; Re: 1850	101
Figure 84. Profile Data: Longitudinal Turbulence Intensity Normalized by the Centerline Velocity vs y/d ; Re: 1920	102
Figure 85. Profile Data: Longitudinal Turbulence Intensity Normalized by the Centerline Velocity vs y/d ; Re: 2000	103
Figure 86. Profile Data: Longitudinal Turbulence Intensity Normalized by the Centerline Velocity vs y/d ; Re: 2040	104
Figure 87. Profile Data: Longitudinal Turbulence Intensity Normalized by the Centerline Velocity vs y/d ; Re: 2090	105
Figure 88. Profile Data: Longitudinal Turbulence Intensity Normalized by the Centerline Velocity vs y/d ; Re: 2200	106
Figure 89. Profile Data: Longitudinal Turbulence Intensity Normalized by the Centerline Velocity vs y/d ; Re: 2300	107
Figure 90. Profile Data: Longitudinal Turbulence Intensity Normalized by the Centerline Velocity vs y/d ; Re: 2350	108
Figure 91. Profile Data: Longitudinal Turbulence Intensity Normalized by the Centerline Velocity vs y/d ; Re: 2400	109
Figure 92. Profile Data: Longitudinal Turbulence Intensity Normalized by the Centerline Velocity vs y/d ; Re: 2450	110

Figure 93. Profile Data: Longitudinal Turbulence Intensity Normalized by the Centerline Velocity vs y/d ; Re: 2500	111
Figure 94. Profile Data: Longitudinal Turbulence Intensity Normalized by the Centerline Velocity vs y/d ; Re: 2800	112
Figure 95. Profile Data: Longitudinal Turbulence Intensity Normalized by the Centerline Velocity vs y/d ; Re: 3100	113
Figure 96. Profile Data: Longitudinal Turbulence Intensity Normalized by the Centerline Velocity vs y/d ; Re: 3400	114
Figure 97. Profile Data: Longitudinal Turbulence Intensity Normalized by the Mean Velocity vs y/d ; Re: 1100	115
Figure 98. Profile Data: Longitudinal Turbulence Intensity Normalized by the Mean Velocity vs y/d ; Re: 1250	116
Figure 99. Profile Data: Longitudinal Turbulence Intensity Normalized by the Mean Velocity vs y/d ; Re: 1350	117
Figure 100. Profile Data: Longitudinal Turbulence Intensity Normalized by the Mean Velocity vs y/d ; Re: 1440	118
Figure 101. Profile Data: Longitudinal Turbulence Intensity Normalized by the Mean Velocity vs y/d ; Re: 1550	119
Figure 102. Profile Data: Longitudinal Turbulence Intensity Normalized by the Mean Velocity vs y/d ; Re: 1710	120
Figure 103. Profile Data: Longitudinal Turbulence Intensity Normalized by the Mean Velocity vs y/d ; Re: 1850	121
Figure 104. Profile Data: Longitudinal Turbulence Intensity Normalized by the Mean Velocity vs y/d ; Re: 1920	122
Figure 105. Profile Data: Longitudinal Turbulence Intensity Normalized by the Mean Velocity vs y/d ; Re: 2000	123
Figure 106. Profile Data: Longitudinal Turbulence Intensity Normalized by the Mean Velocity vs y/d ; Re: 2040	124
Figure 107. Profile Data: Longitudinal Turbulence Intensity Normalized by the Mean Velocity vs y/d ; Re: 2090	125
Figure 108. Profile Data: Longitudinal Turbulence Intensity Normalized by the Mean Velocity vs y/d ; Re: 2200	126
Figure 109. Profile Data: Longitudinal Turbulence Intensity Normalized by the Mean Velocity vs y/d ; Re: 2300	127

Figure 110. Profile Data: Longitudinal Turbulence Intensity Normalized by the Mean Velocity vs y/d ; Re: 2350	128
Figure 111. Profile Data: Longitudinal Turbulence Intensity Normalized by the Mean Velocity vs y/d ; Re: 2400	129
Figure 112. Profile Data: Longitudinal Turbulence Intensity Normalized by the Mean Velocity vs y/d ; Re: 2450	130
Figure 113. Profile Data: Longitudinal Turbulence Intensity Normalized by the Mean Velocity vs y/d ; Re: 2500	131
Figure 114. Profile Data: Longitudinal Turbulence Intensity Normalized by the Mean Velocity vs y/d ; Re: 2800	132
Figure 115. Profile Data: Longitudinal Turbulence Intensity Normalized by the Mean Velocity vs y/d ; Re: 3100	133
Figure 116. Profile Data: Longitudinal Turbulence Intensity Normalized by the Mean Velocity vs y/d ; Re: 3400	134
Figure 117. Near-Wall Data: Mean Velocity vs y/d ; Re: 1150	135
Figure 118. Near-Wall Data: Mean Velocity vs y/d ; Re: 2010	136
Figure 119. Near-Wall Data: Mean Velocity vs y/d ; Re: 3585	137
Figure 120. Near-Wall Data: Mean Velocity Normalized by the Centerline Velocity vs y/d ; Re: 1150	138
Figure 121. Near-Wall Data: Mean Velocity Normalized by the Centerline Velocity vs y/d ; Re: 2010	139
Figure 122. Near-Wall Data: Mean Velocity Normalized by the Centerline Velocity vs y/d ; Re: 3585	140
Figure 123. Near-Wall Data: Mean Velocity Normalized by the Centerline Velocity vs y/d ; Composite Near-Wall Profiles	141
Figure 124. Near-Wall Data: Mean Velocity Normalized by the Bulk Velocity vs y/d ; Re: 1150	142
Figure 125. Near-Wall Data: Mean Velocity Normalized by the Bulk Velocity vs y/d ; Re: 2010	143
Figure 126. Near-Wall Data: Mean Velocity Normalized by the Bulk Velocity vs y/d ; Re: 3585	144
Figure 127. Near-Wall Data: Mean Velocity Normalized by the Shear Velocity vs $\log(yU^*/Nu)$; Re: 1150	145
Figure 128. Near-Wall Data: Mean Velocity Normalized by the Shear Velocity vs $\log(yU^*/Nu)$; Re: 2010	146

Figure 129. Near-Wall Data: Mean Velocity Normalized by the Shear Velocity vs $\log(yU^*/\nu)$; Re: 3585	147
Figure 130. Near-Wall Data: Longitudinal Turbulence Intensity vs y/d ; Re: 1150	148
Figure 131. Near-Wall Data: Longitudinal Turbulence Intensity vs y/d ; Re: 2010	149
Figure 132. Near-Wall Data: Longitudinal Turbulence Intensity vs y/d ; Re: 3585	150
Figure 133. Near-Wall Data: Longitudinal Turbulence Intensity Normalized by the Centerline Velocity vs y/d ; Re: 1150	151
Figure 134. Near-Wall Data: Longitudinal Turbulence Intensity Normalized by the Centerline Velocity vs y/d ; Re: 2010	152
Figure 135. Near-Wall Data: Longitudinal Turbulence Intensity Normalized by the Centerline Velocity vs y/d ; Re: 3585	153
Figure 136. Near-Wall Data: Longitudinal Turbulence Intensity Normalized by the Bulk Velocity vs y/d ; Re: 1150	154
Figure 137. Near-Wall Data: Longitudinal Turbulence Intensity Normalized by the Bulk Velocity vs y/d ; Re: 2010	155
Figure 138. Near-Wall Data: Longitudinal Turbulence Intensity Normalized by the Bulk Velocity vs y/d ; Re: 3585	156
Figure 139. Near-Wall Data: Longitudinal Turbulence Intensity Normalized by the Shear Velocity vs y/d ; Re: 1150	157
Figure 140. Near-Wall Data: Longitudinal Turbulence Intensity Normalized by the Shear Velocity vs y/d ; Re: 2010	158
Figure 141. Near-Wall Data: Longitudinal Turbulence Intensity Normalized by the Shear Velocity vs y/d ; Re: 3585	159
Figure 142. Phase Averaged Amplitude Normalized by the Bulk Velocity vs y/d ; Composite Near-Wall Profiles	160
Figure 143. Phase Averaged Amplitude Normalized by the Bulk Velocity vs y/d ; Composite of Pre-Transition Profiles	161
Figure 144. Phase Averaged Amplitude Normalized by the Bulk Velocity vs y/d ; Composite of Transitional Profiles	162
Figure 145. Near-Wall Data: Phase Shift vs y/d ; Re: 1150	163

LIST OF SYMBOLS

d	channel height
f_{osc}	frequency of imposed pulsation
n_{cycl}	number of imposed pulsation cycles
Re	Reynolds number, $V_{blk}d/\nu$
Str	Strouhal number, $2\pi f_{osc}d/V_{blk}$
δ_s	Stokes layer thickness, $\sqrt{\frac{\nu}{2\pi f_{osc}}}$
U	instantaneous longitudinal velocity
V_{blk}	bulk mean velocity
V_{max}	centerline velocity ($Y/d = 0.50$)
V_{avg}, \bar{u}	mean streamwise velocity
V_{rms}	longitudinal turbulence intensity, $\sqrt{\overline{u'^2}}$
\hat{u}	phase-averaged streamwise velocity
\bar{u}	periodic streamwise velocity component from imposed pulsations
u'	instantaneous streamwise fluctuating velocity
x	longitudinal coordinate, measured from nozzle exit
y, Y	normal coordinate, measured from the bottom wall

z	spanwise coordinate, measured from the channel centerline
Ω	Stokes number, $d/2t_s$
ν	kinematic viscosity (m^2/s)
ϕ	constant of proportionality in Han's equation
U'	shear velocity
ρ_{air}	density of air
τ_w	shear stress at the channel wall
$\frac{dP}{dx}$	pressure gradient along channel length
k	constant of proportionality in the law of the wall equation
θ	phase shift

ACKNOWLEDGEMENTS

The author wishes to acknowledge, with gratitude and appreciation, Professors Ligrani and Subramanian for their guidance and direction pertaining to the research and drafting of this document.

I. INTRODUCTION

A. BACKGROUND

Flow pulsations and unsteadiness are present in many practical flow situations occurring in aerodynamics, naval engineering, bioengineering, and wind engineering. Most of these flows, especially those of technological interest, also undergo transition from a laminar state to a turbulent state. Transition is extremely complex by itself, but when it interacts with flow pulsations, modeling and computations to accurately predict the location and extent of transition and the accompanying changes of important flow properties are near impossible. Thus, information on the changes of important flow properties under these conditions are generally obtained experimentally. According to Shemer [Ref. 1], such experiments should be "restricted to the simplest and most well-defined conditions," in order to "obtain a clear physical description of a fluid dynamical process."

The present study employs a straight channel not only to investigate a situation consistent with Shemer's suggestion, but also because this flow has not yet been studied experimentally. Even though some experimental results are available for pipe flows, and some analytic and numeric results are available for channel flows, the author knows of no other experiments, other than the current work, performed to study the stability or transition of plane channel flow with imposed pulsations.

The imposed flow pulsations are induced using a single rotating vane located downstream of the test section. The device is similar to the rotating profiled sleeves employed by Tu and Ramaprian [Ref. 2], Ramaprian and Tu [Ref. 3] and Stettler and Hussain [Ref. 4] to study the influences of sinusoidal pulsations on pipe flows. Their sleeves are used in water and operate simply by altering the exit flow area. Other studies of the influences of imposed pulsations on pipe flows use reciprocating pistons in cylinders to produce the unsteadiness [Ref. 5; Ref. 6; Ref. 7; Ref. 8; Ref. 9; Ref. 10; Ref. 11]. Simpson et al [Ref. 12] uses a rotating blade damper system at the inlet of their wind tunnel, upstream of screens and honeycomb, in order to study the effects of unsteadiness on turbulent boundary layer. By changing the motion of the five individual damper blades, sinusoidal perturbations to the flow are produced with amplitudes amounting to 11-93 % of the maximum velocity over frequencies from 0.6-2 Hz.

Of the experimental studies of transitional flows in pipes, Merkli and Thomann [Ref. 5], Sergeev [Ref. 6], Hino and Swamoto [Ref. 7], Hino et al [Ref. 8], Gerrard [Ref. 9], Gilbrech and Combs [Ref. 10], Sarpkaya et al [Ref. 11], Ramaprian and Tu [Ref. 3], Shemer [Ref. 1] and Stettler and Hussain [Ref. 4] also examine the effects of imposed pulsations. Of these studies, [Ref. 5] to [Ref. 8] investigate the instability of sinusoidally modulated pipe flow with zero mean flow. Gerrard [Ref. 9] relates variations of turbulent flow over individual flow pulsations to magnitudes of vorticity diffusion. Diffusion rates are then determined by a Stokes number equal to the ratio of the pipe radius to distance the vorticity diffuses during the period of one pulsation cycle. Gerrard also suggests that, with high pulsation frequency, viscous effects are confined to a very thin Stokes layer near the wall where the fluid is retarded. Gilbrech and Combs [Ref. 10] and Sarpkaya [Ref. 11] examine the effects of amplitude and frequency of imposed oscillations on the growth rate of artificially introduced plugs. Both investigators indicate that oscillations increase the critical Reynolds number as long as they are not so large as to cause local flow reversals. Ramaprian and Tu [Ref. 3] study transitional pipe flow at a mean Reynolds number of 2100. Due to pulsations, their Reynolds number based on instantaneous velocity varied between 1278 (fully laminar) and 2872 (fully turbulent). They indicate that flow pulsations at frequencies ranging from 0.05 to 1.75 Hz increase the critical Reynolds number only when the turbulent intermittency is small. With higher intermittency levels, the authors suggest that imposed pulsations affect the flow only when the pulsation frequency is near the characteristic frequency of the turbulence. Shemer's [Ref. 1] work focuses on large pulsation amplitudes at a single low frequency. For a mean Reynolds number of about 4000 and a pulsation frequency of 0.37 Hz, he concludes that transition is governed primarily by the instantaneous Reynolds number. Stettler and Hussain [Ref. 4] present results for Stokes numbers as high as 70. The authors provide a three-dimensional map of the stability-transition boundary, and also indicate that transition in pipes is associated with plugs of turbulence which can grow or shrink in size.

Numerical and analytical investigations of the influences of imposed periodic unsteadiness on flow in a plane channel are described by Grosch and Salwen [Ref. 13], Herbert [Ref. 14], Hall [Ref. 15], von Kerczek [Ref. 16] and Singer et al [Ref. 17; Ref. 18]. In addition to these studies, Tozzi [Ref. 19] provides results of a numerical investigation of the influences of imposed periodic unsteadiness on flow in a pipe, and Davies [Ref. 20] provides a review of work done on the stability of time periodic flows. Of the above mentioned analytic studies of plane channel flow, Grosch and Salwen [Ref. 13]

solve a set of linearized equations by integrating through one period of pulsation. They conclude that flows with small amplitudes of imposed periodic unsteadiness are more stable than steady flows, where the degree of stabilization depends upon interactions between shear waves generated by the imposed pulsation and flow disturbances. A modified version of Grosch and Salwen's energy analysis is described by Herbert [Ref. 14]. Hall [Ref. 15] reports results obtained with high frequency pulsations and concludes that such pulsations are slightly destabilizing irrespective of amplitude. von Kerczek [Ref. 16] modulates the pressure gradient in a perturbation analysis, and shows that the pulsating flow is more stable than the steady flow for frequencies of imposed pulsations greater than about one tenth of the frequency of the steady flow neutral disturbance. However, at both very low and very high frequencies of imposed pulsations, the flow is slightly unstable. Singer et al [Ref. 17; Ref. 18] describe results from a direct Navier-Stokes simulation of flow in a plane channel with imposed periodic unsteadiness and indicate that imposed sinusoidal pulsations provide a stabilizing effect at all but very low frequencies. Significant variations in the amplitudes of Tollmein-Schlichting waves are also noted which depend upon the Strouhal number and the amplitude of the pulsations, as well as on initial amplitudes of the Tollmein-Schlichting waves. Tozzi's [Ref. 19] study of pipe flow shows that imposed pulsations are stabilizing up to very high amplitudes of imposed pulsation, a result in contradiction to a number of experimental studies which show that flow is destabilized even at low amplitudes.

B. OBJECTIVES

The present study is conducted to provide experimental data which show the influences of imposed pulsations on laminar, transitional, and turbulent flows in a rectangular cross-section channel with a 40 to 1 aspect ratio and a L/d of 336 ($d = 0.0127$ m). Results are given on longitudinal turbulent intensity profiles and mean velocity profiles both with and without imposed pulsations. The imposed pulsation device is based on other existing designs, but is applied to a new flow condition: channel flow with air. Imposed pulsation frequencies are presented as Stokes numbers,

$$\Omega = \frac{d}{2t_{st}} \quad 1.1$$

where t_{st} is the Stokes layer thickness, given by

$$t_{st} = \sqrt{\frac{\nu}{2\pi f_{osc}}} \quad 1.2$$

t_{v} is described by Gerrard [Ref. 9] as the distance vorticity diffuses away from the wall in a single pulsation cycle. The Stokes number then represents the ratio of the channel half-width to Stokes layer thickness. These definitions of Stokes number and Stokes layer thickness are strictly applicable only to laminar flows [Ref. 1]. In turbulent flows, the kinematic viscosity should be replaced by an equivalent eddy viscosity giving a Stokes layer thickness that is significantly greater.

Strouhal numbers are also provided in situations where the ratio of bulk flow time scale to imposed pulsation time scale is of interest. Stokes numbers of 4.08 and 5.79 and Strouhal numbers from 0.033 to 0.121 are produced at Reynolds numbers ranging from 1100 to 3600 ($V_{b,u}$ from 1.3 m/s to 4.4 m/s), where each of the latter two quantities is based on bulk mean velocity and channel height. Experimental results in the transition regime are included, which is important since the authors know of no other experimental studies in this area.

C. THESIS ORGANIZATION

In the sections which follow, details of the experimental facilities, the unsteadiness generating device, and the data acquisition system are given in section II. The experimental procedure, including calibration of the Hot-Wire Probe, channel validation, and flow measurement are described in section III. Discussion of Results are given in section IV. Section V contains the summary and conclusions.

II. EXPERIMENTAL FACILITIES

A. CHANNEL

The experimental facility is designed to study the effects of imposed pulsations on channel flow. The facility is located in the laboratories of the Department of Mechanical Engineering of the Naval Postgraduate School, and is shown schematically in Figure 1. With the present coordinate system, x is the longitudinal coordinate measured from the downstream edge of the nozzle, y is normal to the top and bottom surfaces of the channel and measured from the bottom wall, and z is the transverse coordinate measured from the spanwise center of the channel.

The straight test section of the channel is 4.27 meters in length with inside dimensions of 1.27 cm in height and 50.8 cm in width, giving an aspect ratio of 40 to 1. The top and bottom walls of the channel are made of 6.35 mm thick plexiglass and supported by ribs and cross beams along the length of the straight section. The side walls are removable to allow for access to the inside of the channel. The inlet flow is through a honeycomb, screens and a 20:1 contraction ratio nozzle. Two layers of cheese cloth are placed at the inlet to remove contaminants from the air entering the channel.

At the exit of the 4.27 m long test section are three 10.16 cm long frames. Between the flanges of these frames are four screens and a honeycomb placed just upstream of the last screen. The middle frame houses the device used to impose unsteadiness onto the flow. A two dimensional 3 degree diffuser, 45.72 cm long is located downstream of the honeycomb section. This diffuser connects to an exit plenum chamber which provides a volume of uniform low pressure air to prevent transients from the blower from affecting the flow of air in the test section of the channel. The inside dimensions of the plenum are 60.96 cm by 60.96 cm by 60.96 cm. The plenum chamber is connected to the suction side of a 5 hp blower via a 5.08 cm inside diameter pipe. Flow through the channel is metered using a 3.81 cm orifice plate located between the plenum chamber and the blower.

Bulk flow velocities V_{bulk} up to 15 m/s may be achieved in the channel. The channel is designed such that transition occurs after the flow in the channel becomes fully developed, as indicated by the pressure gradient in the x direction of the channel which is discussed in the results and discussion section.

B. UNSTEADINESS DEVICE

Periodic variations of the flow rate are induced in the test section of wind tunnels, channel flows and pipe flows by introducing a periodic blockage at the inlet or exit of flow passages. The most important requirement of such an unsteadiness device is that it be controllable and periodic without adding other disturbances. To achieve this in an open circuit induction channel, the unsteadiness device is located just downstream of the test section. By placing the unsteadiness device downstream of the test section, wakes and other flow disturbances resulting from the operation of the unsteadiness device are not convected into the test section.

The design used in this study is shown in Figure 2. Since the height of the channel interior is only 1.27 cm, a single rotating vane is used to impose the required pulsations in the flow. The vane is made of a 3.2 mm thick 8.7 mm wide brass strip with rounded edges that span a portion of the channel height when oriented normal to the flow. The vane is supported at the ends by a 3.2 mm diameter shaft and bushings that are fitted to the side walls of the frame. Three intermediate spanwise struts are provided to increase the rigidity of the vane as it rotates. One end of the shaft is fixed to a 48 tooth spur gear exterior to the channel. This gear is driven by a spur pinion with 12 teeth mounted on the shaft of a Superior Electric, M092-FD310 Stepper Motor. The motor is driven by a Modulynx MITAS PMS085-D050 Drive, which is controlled by a Modulynx MITAS PMS085-C2AR Drive Controller. The motor shaft may be positioned at 1/200th increments of one motor shaft revolution, and operated at speeds up to 100 revolutions per second. For each revolution of the vane there are two cycles of imposed flow pulsations as shown in Figure 3. Figure 3 shows that in position 2 resistance to flow is maximized and velocity in the straight section of the channel is minimized. The flow resistance is minimized and the velocity is maximized when the vane is in position 4. A gearing ratio of 1 to 4 and two cycles of imposed flow pulsations per vane rotation equates to one half of one cycle of an imposed flow pulsation for every motor revolution. The imposed pulsation frequency is set by programming the Drive Controller for a particular motor speed which then sets the vane rotation rate. The amplitude of the imposed unsteadiness can be altered by changing the width of the vane. The variation of the mean velocity due to vane rotation when the flow is fully laminar or turbulent, is approximately sinusoidal. This waveform results because the velocity is proportional to the flow restriction of the vane [Ref. 21].

Under actual conditions, the flow around the rotating vane is quite complex. Velocity and pressure variations are affected not only by the varying flow resistance from

the vane, but also by other fluid dynamic effects such as dynamic flow separation and flow inertia. Imposed oscillatory flow behavior is thus different and difficult to predict compared to quasi-steady flow. The assessment of the performance of the rotating vane as it produces imposed velocity oscillations in the test section is given by Lagrani et al [Ref. 21].

C. FLOW MEASUREMENT INSTRUMENTS

A schematic of the flow measurement equipment is presented in Figure 4.

1. Hot-wire Probe and Probe Positioning

A DANTEC 55P51 hot-wire probe with sensor diameter of $5\mu\text{m}$ and sensor length of 1.25 mm, is used for instantaneous velocity measurements. The probe is mounted with the wire horizontal and normal to the flow direction. The probe position is controlled by a rotatable lever arm for the profile data and a mechanical traverse for near-wall data. The rotatable lever arm has a y/d range of 0.25 to 0.95, and the mechanical traverse has a y/d range of 0.75 to 0.99. The probe position was calibrated using a plexiglass insert to the channel. The insert, which is the height of the channel, was etched starting at y/d of 0.5 and incremented at 0.05 y/d units to y/d of 0.95. Since the mechanical traverse is motor controlled it could be stepped up in microns, therefore it is used for near-wall measurements. The mechanical traverse is an ORIEL Motor Mike Motorized Micrometer and is operated by an ORIEL Dual Control Unit, Model 18009. The rotatable lever arm is operated manually, and therefore a scale is calibrated against the y/d probe position as marked on the plexiglass insert. The probe is fixed with respect to the longitudinal and horizontal axes for both the near-wall and the profile data. The profile data probe position is at x/d of 294.3 and 27.7 z/d units left of the spanwise center, while the near-wall probe position is at x/d of 309.4 and 29.8 z/d units left of the spanwise center.

2. Hot-wire Bridge and Signal Conditioner

A DISA 55M10 constant temperature bridge is used to operate the hot-wire probe at an overheat ratio of 1.8. The hot-wire is calibrated in the potential flow of a wind tunnel. The DC voltage from the hot-wire bridge is measured using a Hewlett-Packard 3466A digital multimeter. The velocity is measured using Kiel probe and wall static taps in conjunction with a digital manometer. A DANTEC Model 56N20 signal conditioner is used to amplify and filter the voltage from the bridge. During measurements, an amplifier gain of 10 is used. To reduce the high frequency noise and DC bias, the low pass filter is set to 10kHz and the high pass filter is set at 0.1 Hz.

3. High Speed Data Acquisition System and Data Storage

The output of the signal conditioner is fed into a Hewlett-Packard 6944 Multiprogrammer with a buffered high speed A/D conversion system. The Multiprogrammer cards are driven using Hewlett-Packard CAT 14752A software on a Hewlett-Packard 9000 series Model 310 computer.

For phase sampling, data are acquisitioned so that data are obtained at different phases of each cycle of flow pulsation. The pulses used for triggering originate in the motor used to drive the vane, which generates voltage pulses sequentially in each of the four field windings used to step the motor. Fifty pulses are available to each field winding for each revolution of the motor shaft, giving a total of 200 pulses per revolution. The pulses from one of the four field windings are used to trigger the data acquisition system, thus providing a situation in which data acquisition is precisely synchronized with the vane rotation. For a given vane imposed pulsation frequency, f_{osc} , the data sampling rate (TR) is given by:

$$\begin{aligned} TR(\text{samples/sec}) &= f_{osc} \cdot (\text{pulses/motor shaft rev.}) \\ &\quad \cdot (\text{motor shaft rev./imposed flow pulsations}) \\ &= f_{osc} \cdot 50 \cdot 2 \end{aligned}$$

$$TR(\text{samples/sec}) = 100 \cdot f_{osc} \quad 2.1$$

With this approach, 100 samples of data are obtained, spaced uniformly, over each period of flow pulsation, providing a phase resolution of 1/100 of the imposed pulsation cycle. Data is acquired for 640 flow pulsations to fill the memory buffer of the Multiprogrammer (64 kbytes), after which, data is stored in the computer memory. In the memory, the data is packed into 640 arrays of 100 samples each and stored on a disk for processing. Because non-uniform width voltage pulses are generated by the motor drive as the motor is started and stopped, the first 6000 points are ignored as data is processed, and all acquisitions are completed well before the vane motor is stopped. When no unsteadiness is imposed on the flow, data acquisition is triggered by a square wave function from a Hewlett-Packard 3311A function generator which is set to the same frequency as the imposed pulsation. The instantaneous voltage is stored on 3.5 inch disks for processing. The heading to each data set includes the time and date, the bulk velocity, the pulsation frequency, and the average voltage from the digital multimeter.

III. EXPERIMENTAL PROCEDURES

A. HOT-WIRE CALIBRATION

The hot-wire sensors are calibrated in the freestream of the wind tunnel located in the laboratories of the Mechanical Engineering Department of the Naval Postgraduate School. During calibration, the hot-wire probe is mounted normal to the flow in the potential freestream of the wind tunnel, and connected to the same hot-wire bridge previously discussed. Output from the hot-wire bridge is read on a Keithly 169 Digital Multimeter. Freestream velocity in the wind tunnel is measured utilizing a Kiel pressure probe, a wall static pressure tap, and a Validyne PS 309 Digital Manometer. Voltage and differential pressure readings are taken for a range of velocities between 1.0 and 4.0 m/s. Following the calibration, the hot-wire is installed in the straight channel.

B. DATA PROCESSING

1. Bulk Velocity

The bulk flow velocity of the channel is determined from the pressure drop across the orifice plate located in the outlet piping which connects the outlet plenum and the blower. The pressure differential across the orifice plate is measured in inches of water using a Validyne Model PS 309 Digital Manometer. Figure 5 shows the relationship of bulk velocity to pressure differential across the orifice plate. This same bulk velocity is then used to determine the channel Reynolds number and Strouhal number.

2. Instantaneous Velocity

Instantaneous voltages from the hot-wire are converted into instantaneous velocities using a look-up table that accounts for hot-wire calibration coefficients, amplifier gains and mean voltage levels. Such instantaneous velocity data are shown in Figure 6 along with the corresponding phased-averaged velocity trace for a Reynolds number of 3660 ($V_{bulk} = 4.38$ m/s) and a Strouhal number of 0.036 (f_{osc} is 2 Hz).

3. Phase Averaging

With imposed periodic flow, instantaneous velocities can be considered to be the sum of three components such that $U = \bar{u} + \tilde{u} + u'$, where \bar{u} is the time-averaged velocity, \tilde{u} is the periodic velocity, and u' is the fluctuating component. In the present study, \tilde{u} and \bar{u} are combined as the phase-averaged velocity (\hat{u}) such that $U = \hat{u} + u'$, following Ramaprian and Tu [Ref. 3]. Thus, for a steady flow with no periodic velocity, \hat{u} is then

equal to \bar{u} . \hat{u} is then determined from phase-averaging instantaneous velocity results using the equation given by

$$\hat{u}(n) \big|_{n=1}^{100} = \frac{1}{ncycl} \sum_{m=1}^{ncycl} U(m,n) \big|_{n=1}^{100} \quad 3.1$$

Here, m and n correspond to the number of cycles and to the number of locations across each phase, respectively, where data are sampled. Typically 580 cycles are ensemble averaged to obtain a phase-averaged velocity trace. When time averaged velocity \bar{u} is determined, averages are again obtained from 58 thousand points.

Occasionally the digitized hot-wire signal is contaminated by noise. The source of the noise is the electromagnetic field present in the laboratory. This noise is a disturbance of the data signal that appears as a singular high voltage spike which saturates the ± 10 volt analog-to-digital converter. These data samples could not be due to flow behavior because of their magnitudes, abrupt random nature, and because they are not apparent in analog voltages from the DANTEC hot-wire bridge or in analog spectra of these voltage signals. When the noise causes individual data samples to drop out, they are replaced using the sample acquisitioned 100 points, before which, with phase averaging, is the point at the same phase from the previous flow pulsation. These occurrences happen less than 1% of the data sampling time, and consequently, no evidence of these corrections is evident in ensemble and time averaged results.

IV. DISCUSSION OF RESULTS

A. INLET TURBULENCE INTENSITY MAGNITUDES

The normalized longitudinal turbulence intensity ($\sqrt{\overline{u'^2}}/\bar{u}$) at the exit of the nozzle (and the inlet of the straight section) of the channel was measured using a single hot-wire sensor placed at y/d of 0.5 and x/d of 4.17. Figure 7 shows the magnitudes for three Reynolds numbers: 1103, 2005, and 3585. Data for Reynolds number of 1103 and 2005 vary between 0.001 and 0.0014 over the pulsation frequency range of 0 to 4 Hz. The normalized longitudinal turbulence intensities are somewhat higher for a Reynolds number of 3585. At this higher Reynolds number, the normalized longitudinal turbulence intensity varies between 0.0017 and 0.0024 over the pulsation range of 0 to 4 Hz, with a minimum value of 0.0017 occurring at 3 Hz.

B. FLOW DEVELOPMENT VALIDATION

The present experiment was planned so that measurements are taken downstream of the portion of the channel where the flow is developing. To determine where the flow becomes fully developed, the pressure gradient along the length of the channel was measured. The flow is considered to be fully developed when the pressure gradient is linear. Figure 8 shows that this occurs at a x/d position of approximately 54 when Re is 1100, at a x/d position of approximately 108 when Re is 2010, and at a x/d position of approximately 168 when Re is 3585. Probe positions are in the fully developed region at x/d of 294.3 for profile data and at x/d of 309.4 for near-wall data.

Han [Ref. 22] gives the following equation to predict fully developed channel flow:

$$\frac{x}{d} = 4\phi Re \quad 4.1$$

where $\phi = 0.0115$ for the present channel. From this equation, fully developed flow is present at $x/d = 165.6$ for a Reynolds number of 3600, and at $x/d = 50.6$ for a Reynolds number of 1100.

C. PROFILE DATA

Profile data are taken using a single hot-wire sensor placed at an x/d of 294.3 and a z/d of 27.7. A manual traverse is used to position the hot-wire sensor over y/d from 0.5 to 0.95.

1. Mean Velocity Profiles

Dimensional mean velocity (V_{avg}) profiles are shown in Figures 9 through 32. As the Reynolds number increases, magnitudes of mean velocity increase, and profiles become less parabolic. Profiles with imposed pulsations are quantitatively similar to profiles without imposed pulsations. Mean velocity profiles normalized by the centerline mean velocity (V_{avg}/V_{max}) are presented in Figures 33 through 52.

2. Longitudinal Turbulence Intensity Profiles

Longitudinal turbulence intensity (V_{rms}) profiles are presented in Figures 53 through 76. Longitudinal turbulence intensity values are normalized by the centerline velocity (V_{rms}/V_{max}) in Figures 77 through 96, and by the local mean velocity (V_{rms}/V_{avg}) in Figures 97 through 116.

Figures 53 to 57 show that maximum turbulence intensity occurs at the channel centerline for Reynolds numbers from 1100 to 1550. Such behavior evidences a center mode of instability described by Zang and Krist [Ref. 23]. As Reynolds number increases to 1710 and higher, profiles show a local maxima which increases in magnitude near the wall at $y/d=0.85$ as channel center magnitudes decrease (Figures 58 through 72). At Reynolds numbers of 2400 and 2450, Figures 67 and 68 show that centerline magnitudes are further reduced by pulsations. Figure 67 for the lower Reynolds number shows the centerline magnitude is reduced by 2 Hz pulsations. Figure 68 for the higher Reynolds number shows the centerline magnitude is reduced by both 1 Hz and 2 Hz pulsations. Figures 77 through 96 present profiles of the longitudinal turbulence intensity normalized by the centerline velocity (V_{rms}/V_{max}) which show the same trends as the dimensional longitudinal turbulence intensity profiles. Longitudinal turbulence intensity profiles normalized by the local mean velocity (V_{rms}/V_{avg}) in Figures 97 through 116 show magnitude increases with Reynolds number which are most rapid near the wall. Of course these profiles are unaffected by pulsations with the exception of profiles at Reynolds numbers of 2400 and 2450.

D. NEAR-WALL DATA

Near-wall data are taken using a single hot-wire sensor placed at an x/d of 309.4 and a z/d of 29.8. The mechanical traverse is used to position the hot-wire sensor over y/d from 0.75 to 0.99 for Reynolds numbers of 1150 and 2010, and over y/d from 0.7 to 0.99 for a Reynolds number of 3585. Near-wall data are presented in graphs along with results from the previous section and from Koth's [Ref. 24] experiments.

1. Shear Velocity Determination

In several of the near-wall profiles, the shear velocity is used to normalize the local mean velocity and the longitudinal turbulence intensity. The shear velocity (U^+) is given by the following equation:

$$U^+ = \sqrt{\frac{\tau_w}{\rho_{air}}} \quad 4.2$$

where

ρ_{air} = density of air

τ_w = shear stress at the wall given by

$$\tau_w = -\frac{d}{2} \frac{dP}{dx}$$

where

d = channel height

$\frac{dP}{dx}$ = pressure gradient

Substituting values for the channel height and the density of air, the shear velocity is related to the pressure gradient using an equation of the form:

$$U^+ = 7.149 \sqrt{\frac{dP}{dx}} \quad 4.3$$

From this equation, for the three Reynolds numbers examined, shear velocities are 0.102 m/s for $Re = 1150$, 0.126 m/s for $Re = 2010$ and 0.278 m/s for $Re = 3585$.

2. Local Mean Velocity Profiles

Figures 117 through 129 present local mean velocity (V_{avg}) profiles and various normalized local mean velocity profiles measured in near-wall regions. Figures 117 to 119 show dimensional mean velocities (V_{avg}). These near-wall data are somewhat higher than both the profile data and Koth's [Ref. 24] data, but the trends are identical. Local mean velocity profiles normalized by the centerline velocity (V_{avg}/V_{max}) are presented in Figures 120 to 123. These figures show good agreement with profile data and Koth [Ref. 24] data, however, near the wall, magnitudes of differences increase. Figures 124 through 126 present the local mean velocity profiles normalized by the bulk velocity (V_{avg}/V_{bulk}). Again, the near-wall data is somewhat higher than the profile data in these figures.

Local mean velocity profiles normalized by the shear velocity (V_{τ}/U^+) plotted against $\log(y U^+/\nu)$ are presented in Figures 127 through 129. Figures 128 and 129 include the equation for the turbulent law of the wall, given by:

$$\frac{V_{avg}}{U^+} = \frac{1}{k} \ln \frac{y U^+}{\nu} + 5.0 \quad 4.4$$

where

$$k = 0.4$$

Included on Figures 127, 128, and 129 is the equation for laminar flow given by:

$$\frac{V_{avg}}{U^+} = \frac{y U^+}{\nu} \quad 4.5$$

Very near the wall, mean data for $Re = 1150$ show agreement with this equation. Log law region turbulent data for $Re = 3585$ lie above the law of the wall equation.

3. Longitudinal Turbulence Intensity Profiles

Near-wall longitudinal turbulence intensity profiles are shown in Figures 130 through 141. As for the local mean velocity results, the dimensional plots are presented first, followed by the various normalized plots. Figures 130 through 132 give dimensional longitudinal turbulence intensity (V_{rms}) profiles. Near-wall data, profile data, and Koth's [Ref. 24] results agree well. Figure 133 through 135 show longitudinal turbulence intensity profiles normalized by the centerline velocity (V_{rms}/V_{max}). Figures 136 through 138 show near-wall longitudinal turbulence intensity profiles normalized by bulk velocities (V_{rms}/V_{bulk}). Both sets of normalized near-wall profiles show slight disagreement with profile data and Koth's [Ref. 24] results. Longitudinal turbulence intensity profiles normalized by the shear velocity (V_{rms}/U^+) are presented in Figures 139 through 141. For all three Reynolds numbers investigated, intensity profiles with and without imposed pulsations are the same.

E. PHASE AVERAGED VELOCITY MAGNITUDE RESULTS

Figures 142 through 144 show peak to peak amplitudes of phase-averaged velocities normalized by the bulk velocity ($\Delta \hat{u}/V_{bulk}$) with imposed pulsations at a Stokes number of 5.79. Near-wall results are given in Figure 142 for Reynolds numbers of 1150, 2010, and 3585. Data at Reynolds numbers of 1100 and 3400 are shown in Figures 143 and 144. Figure 143 also shows profiles for Reynolds numbers from 1920 to 2200, whereas Figure 144 shows profiles for Reynolds numbers from 2300 to 2500. The laminar profile

for $Re = 1100$ in Figures 143 and 144 shows a local maxima of 0.07 for y/d of 0.65 and approaches zero near the wall. The turbulent profile for $Re = 3400$ also shows a local maxima of 0.15 for y/d of 0.9, and also approaches zero near the wall.

Phase shift data for a Reynolds number of 1150 are shown in Figure 145. These data, designated as θ , were measured in the near-wall region, and actually represent the phase angle minus 270 degrees. θ varies from a high of 29 degrees at y/d of 0.75 to a minimum of 7 degrees at y/d of 0.97.

V. SUMMARY AND CONCLUSIONS

The effects of imposed pulsations on profile and near-wall flow characteristics at Stokes numbers of 4.08 and 5.79 are studied in a straight channel with laminar, transitional and turbulent flows. Imposed pulsations at 1 Hz and 2 Hz are produced using a single rotating vane located downstream of the test section. Profile data are taken for Reynolds numbers from 1100 to 3400. Near-wall data for three Reynolds numbers, 1150, 2010, and 3585 are also examined.

Longitudinal turbulence intensity profiles show a local maxima only at the channel centerline for Reynolds numbers from 1250 to 1550. This is evidence of a center mode of instability. Longitudinal turbulence intensity profiles show a local maxima at both the channel centerline and y/d of 0.85 for Reynolds number from 1710 to 2300. As the Reynolds number increases from 2350 to 3400 local maxima of longitudinal turbulence intensity occur only at y/d of 0.9.

Effects due to imposed pulsations are apparent only at Reynolds numbers of 2400 and 2450. Longitudinal turbulence intensity profiles at a Reynolds number of 2400 show that magnitudes near the channel centerline are reduced at Stokes number of 5.79 (2 Hz pulsations). At a Reynolds number of 2450, the magnitude of longitudinal turbulence intensity near the channel centerline are reduced at Stokes numbers of 4.08 and 5.79 (1 Hz and 2 Hz pulsations). These changes are believed to result from destabilizing influences of pulsations which cause the flow to become fully turbulent at Reynolds numbers lower than if no pulsations are imposed. The fluctuations in a fully turbulent flow are less intense than in a transitional flow at slightly lower Reynolds numbers resulting in lower longitudinal turbulence intensities.

APPENDIX A. SOFTWARE DIRECTORY

DEANIS : Determines channel mass flow rate, bulk velocity and Reynolds number from orifice plate pressure drop. The program requires ambient temperature and pressure inputs which can be entered manually or via a data acquisition system connected to thermocouples and or pressure transducers. Once ambient conditions are established, air density is calculated and orifice pressure drop is entered manually. Originally designed for curved channel applications, this version has been specifically modified for straight channel use.

HWCAL : Determines the constants for the King's Law calibration of the hot-wire. The program also provides a polynomial fit of the calibration data.

HOTWIREPAV : Reads the data stored in the A/D buffer of the high speed data acquisition system and stores the information on micro diskettes. Manual inputs are : triggering frequency, hot-wire DC voltage (ungained), oscillation frequency (flow blockage), bulk velocity, Reynolds number, and date and time of run.

DATAP : Calculates instantaneous and phase-averaged velocities. Initially a look up table is created. Effective velocities are calculated from the effective voltage values and stored for follow-on calculations. The hot-wire calibration constants obtained from HWCAL, and the amplifier gain are incorporated into these calculations. The velocity calibration is given by :

$$U_{eff} = k(E_{eff}^2 - E_0^2)^{1/N}$$

where k is the proportionality constant, E_{eff} is the effective voltage, and E_0 is the reference voltage at no flow. N is a constant (0.45) for moderate Reynolds numbers. Once the look up table is created, the program reads the instantaneous voltage values from the data file and converts them to instantaneous velocities. A plot of the instantaneous velocity versus time can be generated for any of 580 cycles (the first 60 cycles are discarded to allow for flow stabilization as the unsteady device is started).

Next the program phase averages the 580 cycles, and velocity versus phase angle (of the flow blockage) plots are available. Two plots are available from the averaged values : \hat{u} versus phase angle and $\sqrt{\hat{u}'^2} / \bar{u}$ versus phase angle. \hat{u} is the phase averaged velocity, $\sqrt{\hat{u}'^2}$ is the phase averaged root mean squared (rms) velocity, and \bar{u} is the average velocity. In the case where there is no imposed unsteadiness, the phase averaged velocity, \hat{u} , is equal to the time averaged velocity, \bar{u} .

APPENDIX B. FIGURES

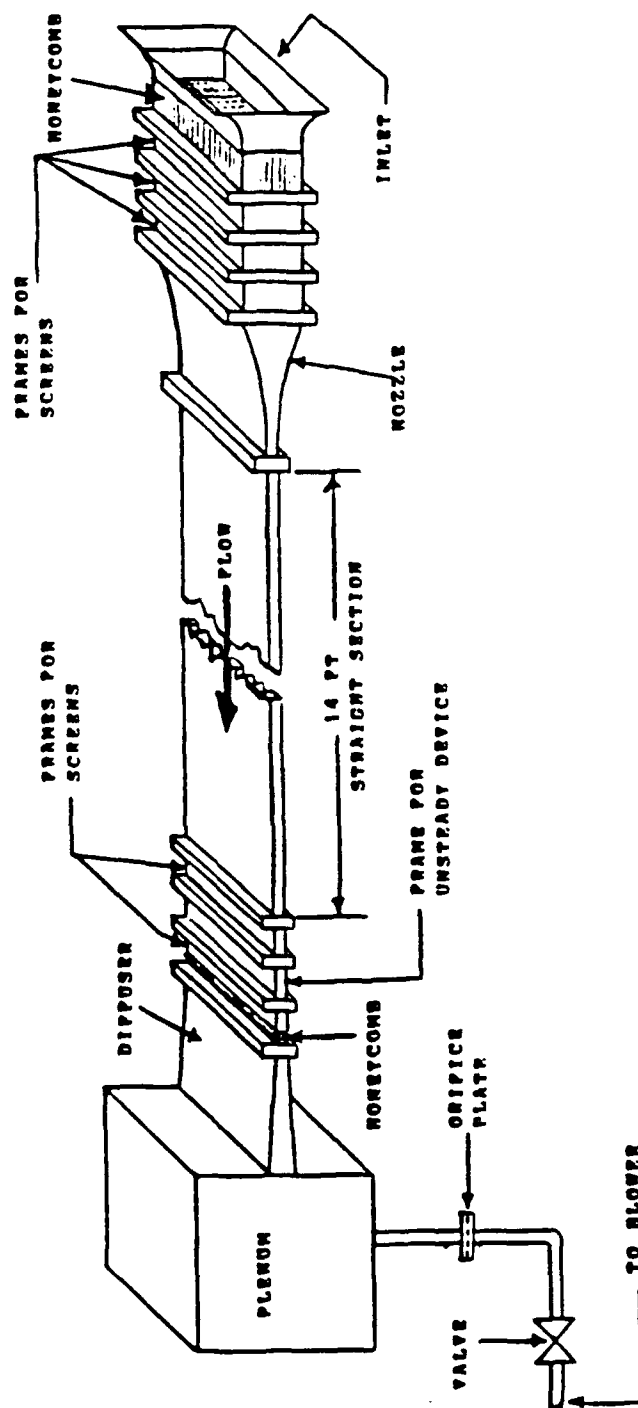


Figure 1. Experimental Channel

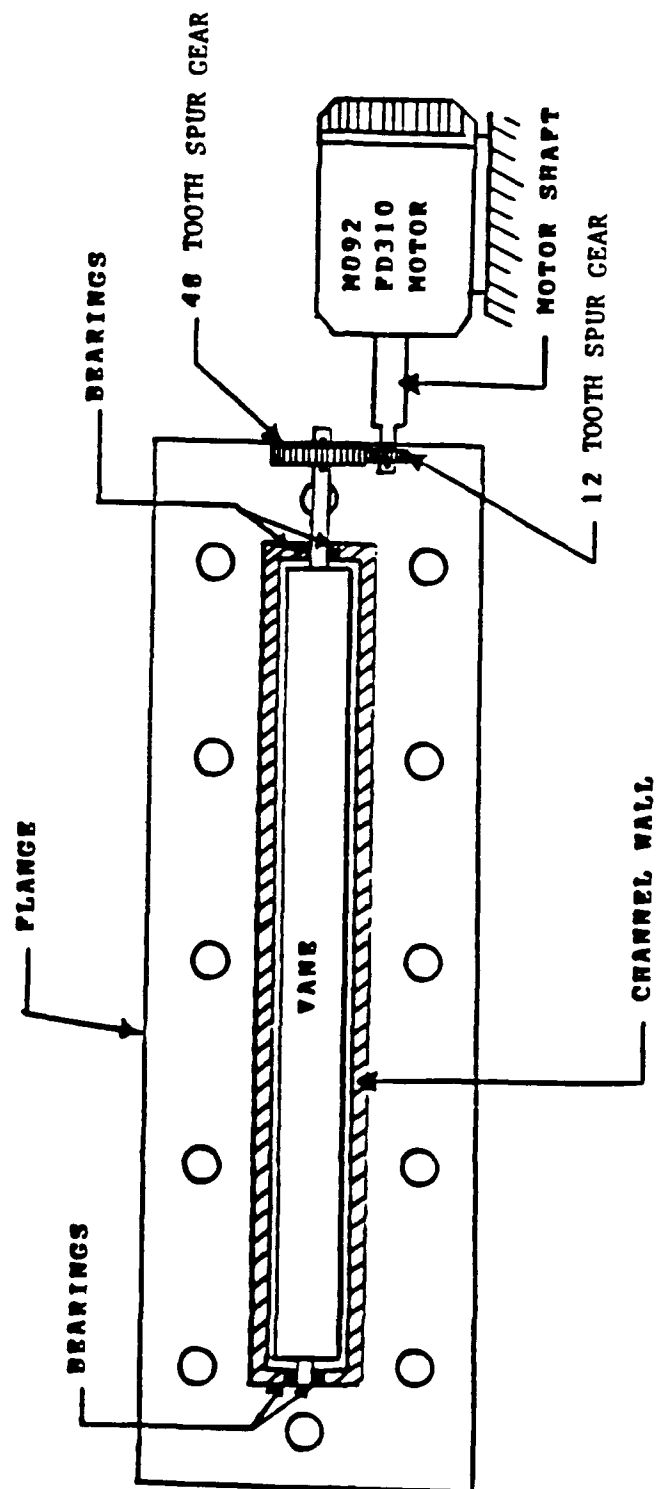


Figure 2. Unsteadiness Device

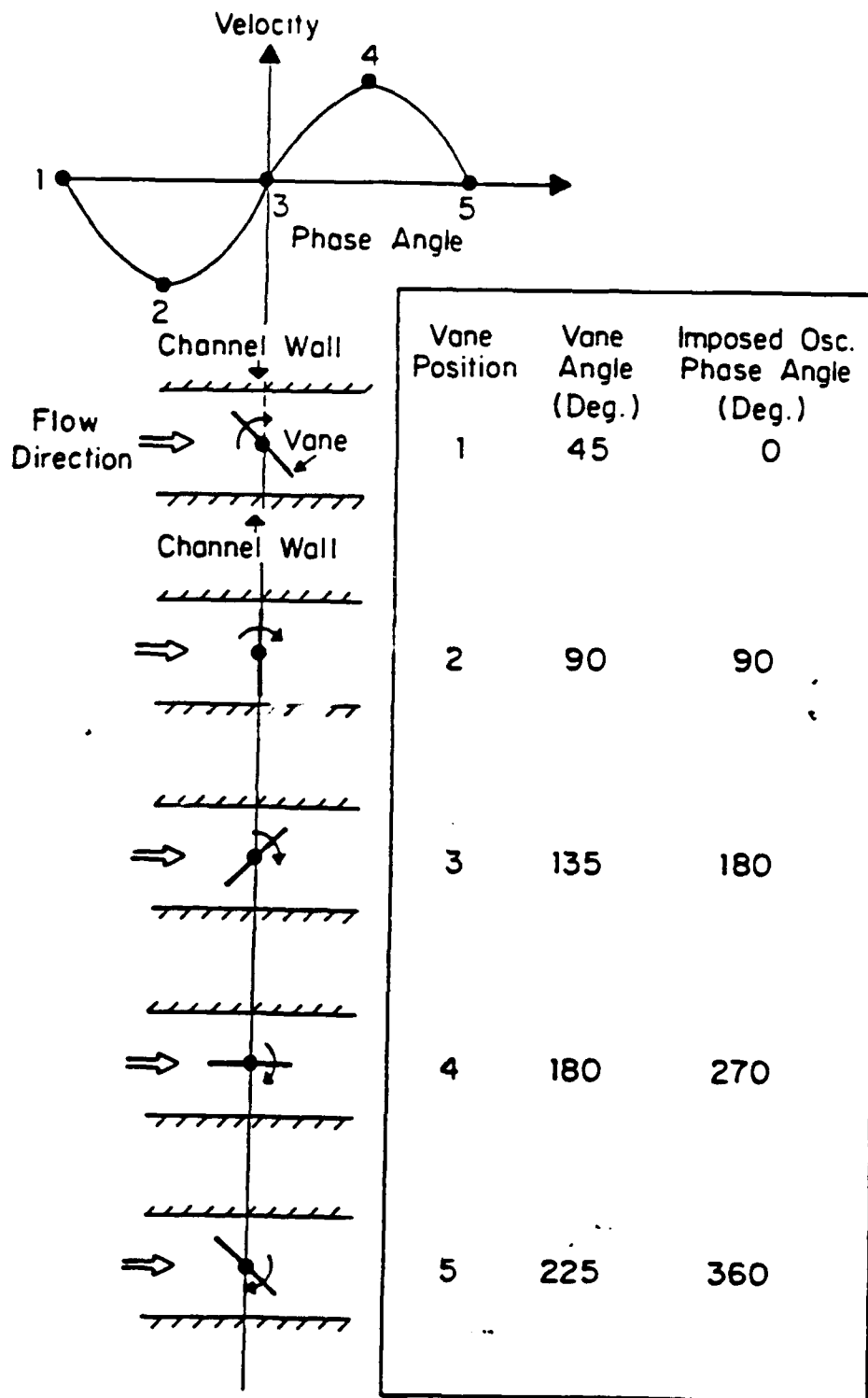


Figure 3. Quasi-Steady Flow Variations With Vane Positions

SCHEMATIC OF FLOW MEASUREMENT EQUIPMENT

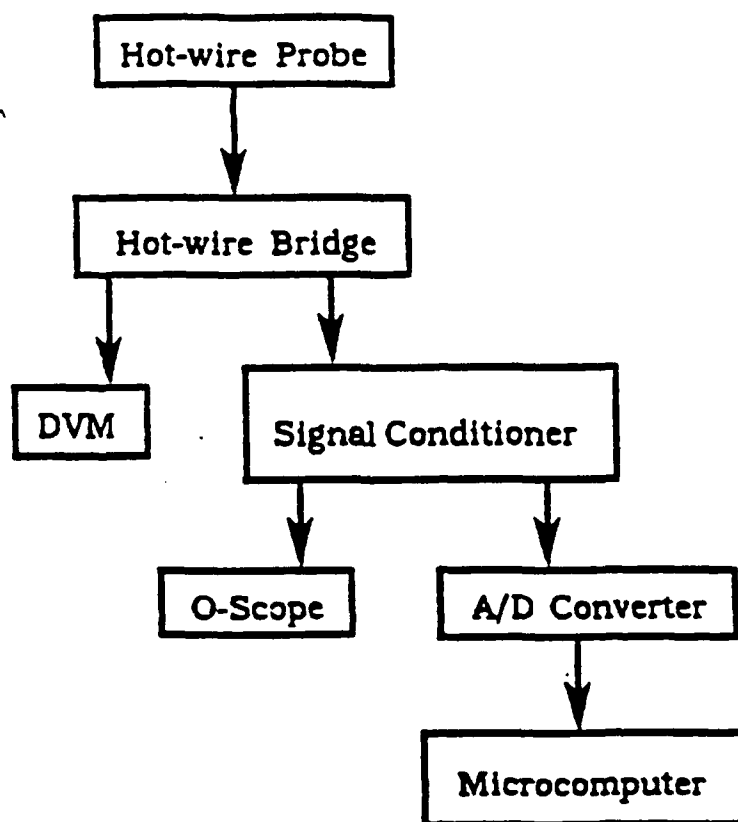


Figure 4. Schematic of Flow Measurement Equipment

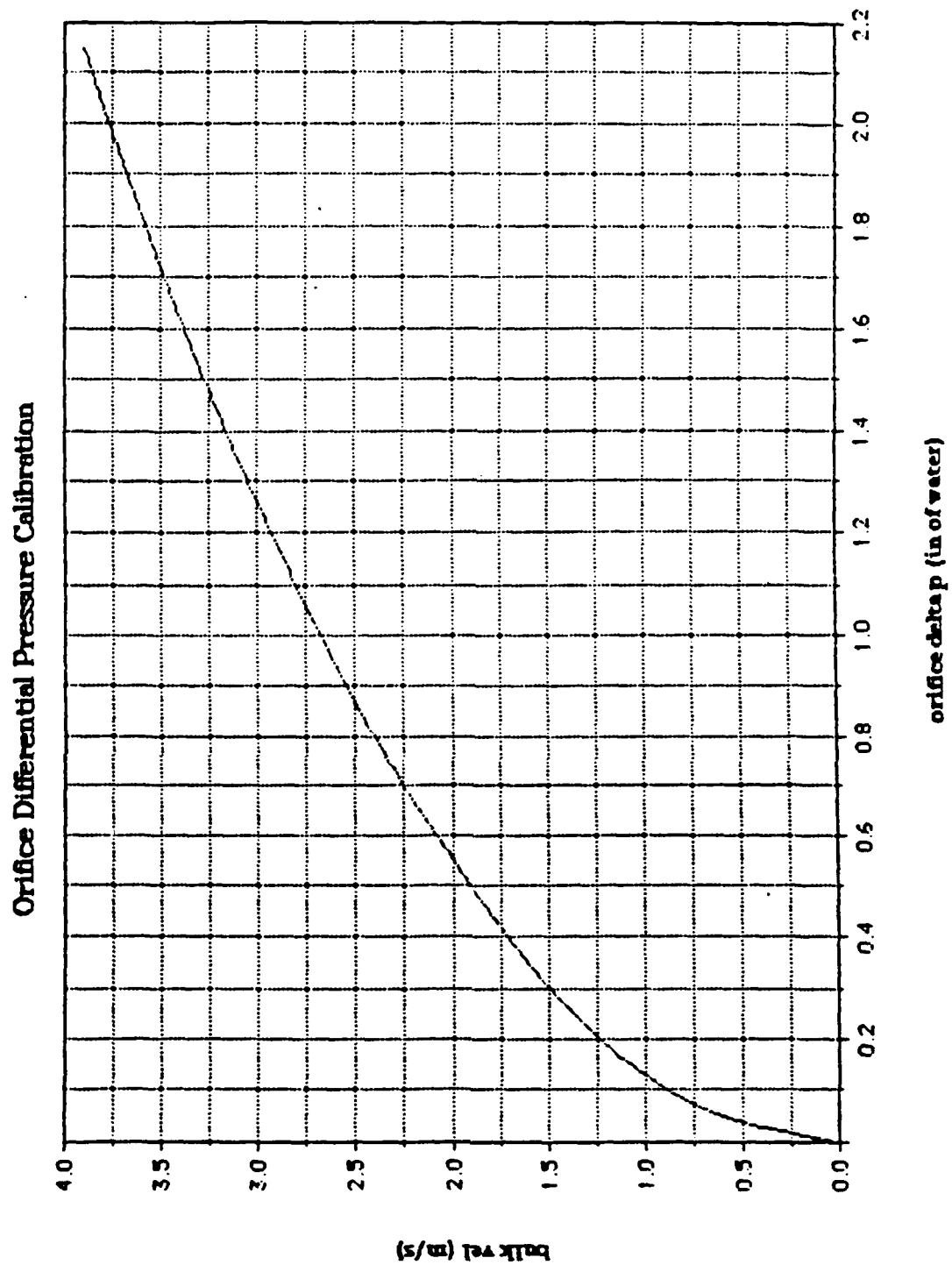


Figure 5. Bulk Channel Velocity vs Pressure Differential Across Orifice Plate

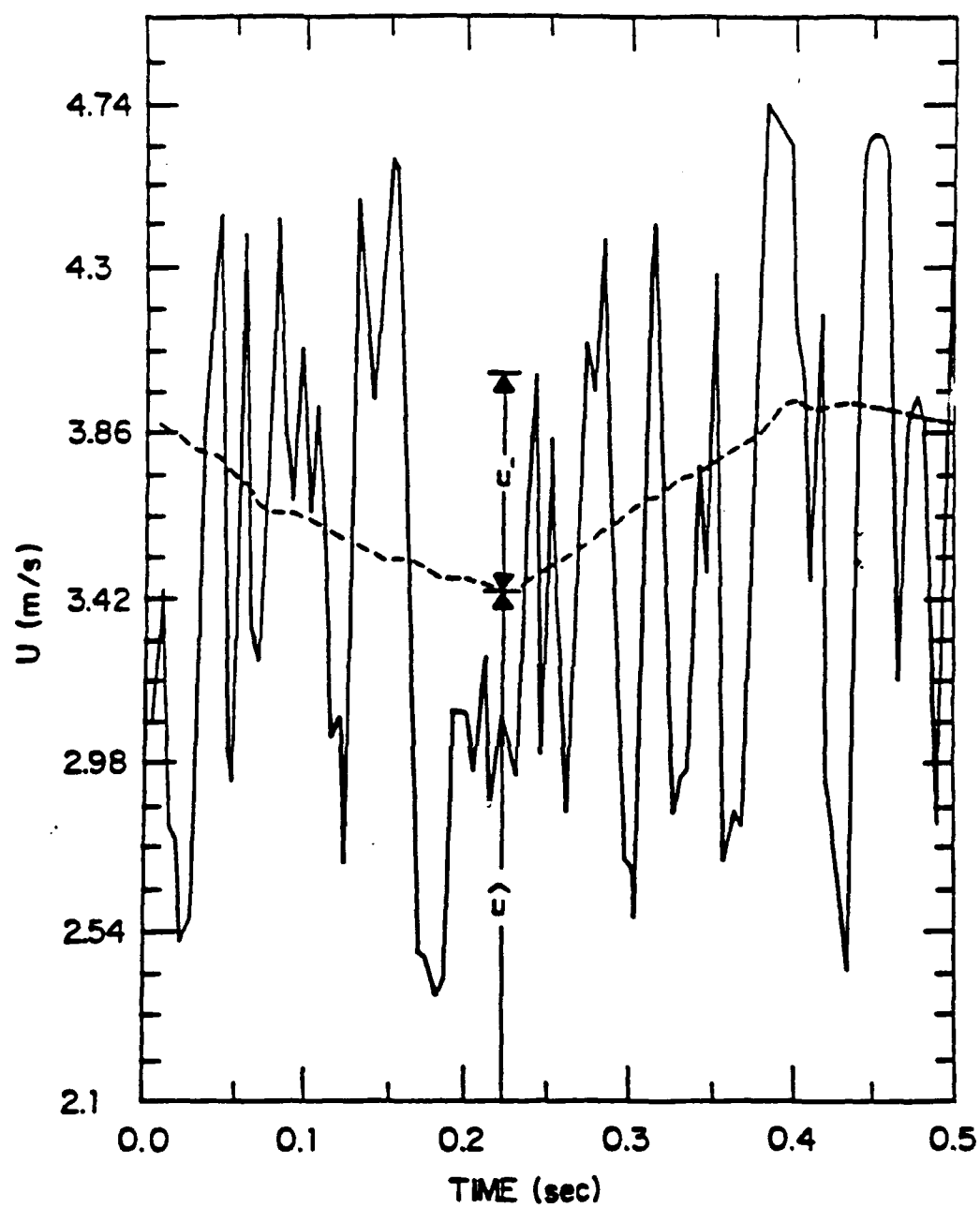


Figure 6. Instantaneous and Phase Averaged Velocity Trace

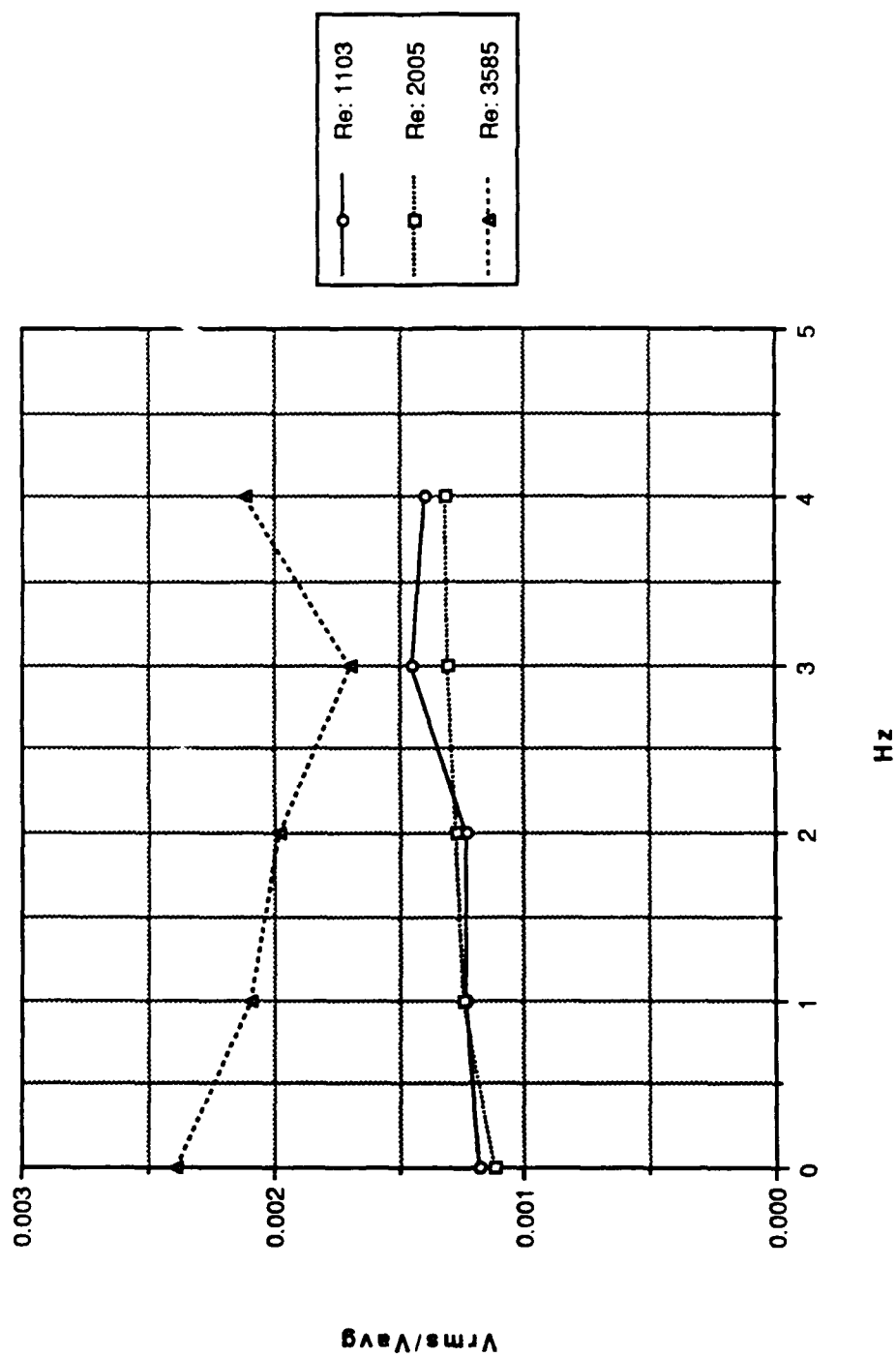


Figure 7. Normalized Longitudinal Turbulence Intensity at the Inlet of the Channel

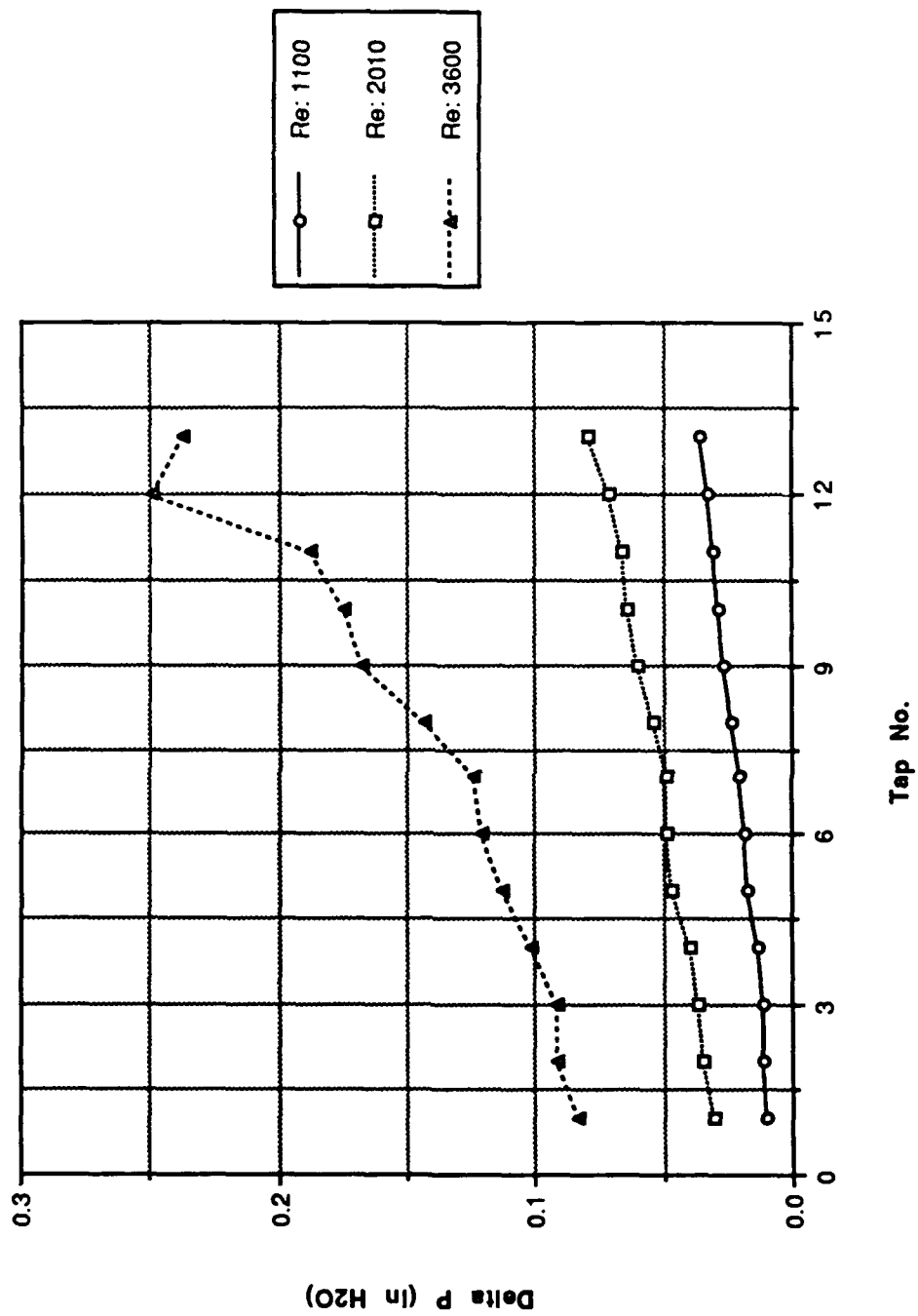


Figure 8. Pressure Distribution of the Channel in the x-Direction

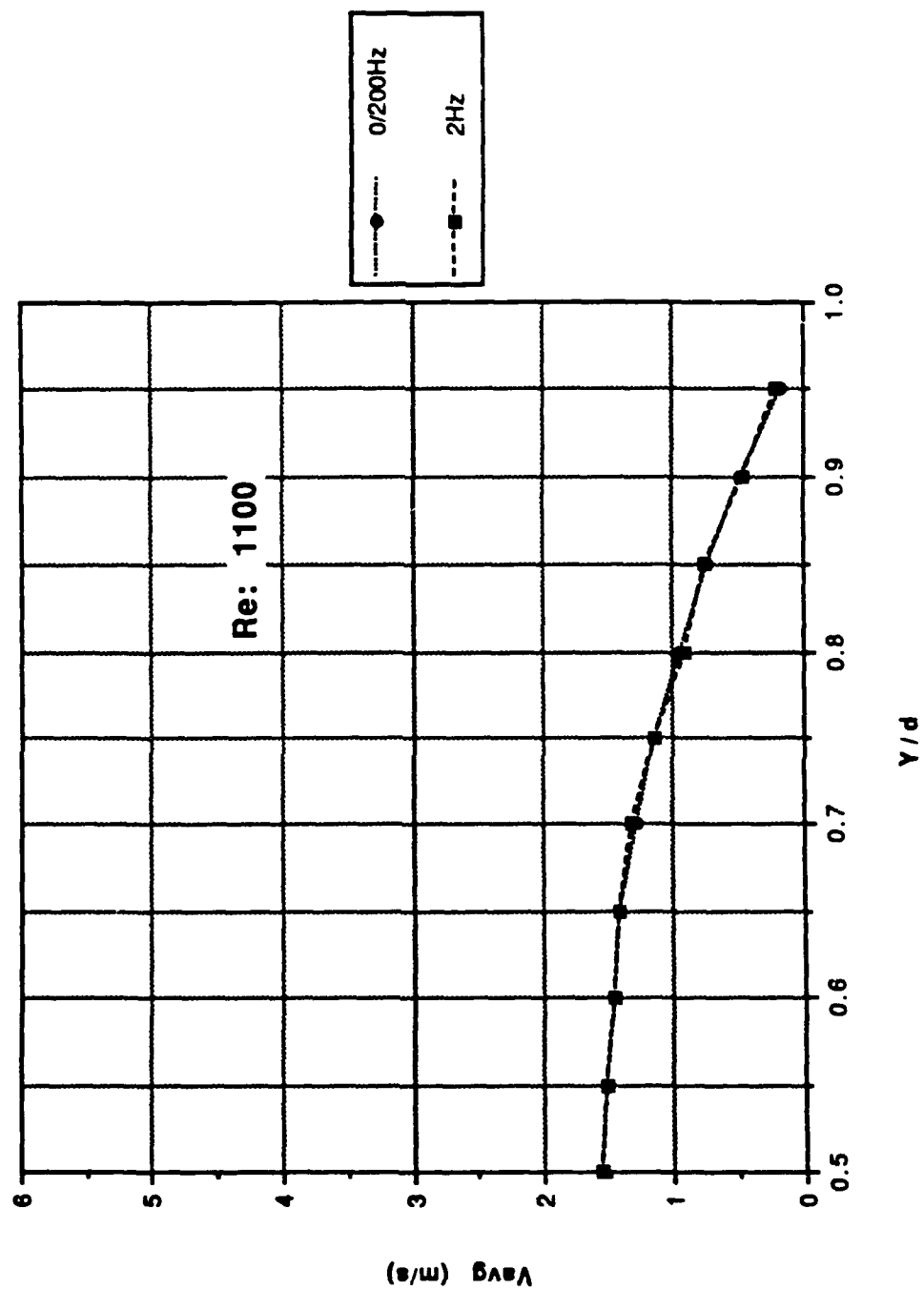


Figure 9. Profile Data: Mean Velocity vs y/d ; Re: 1100

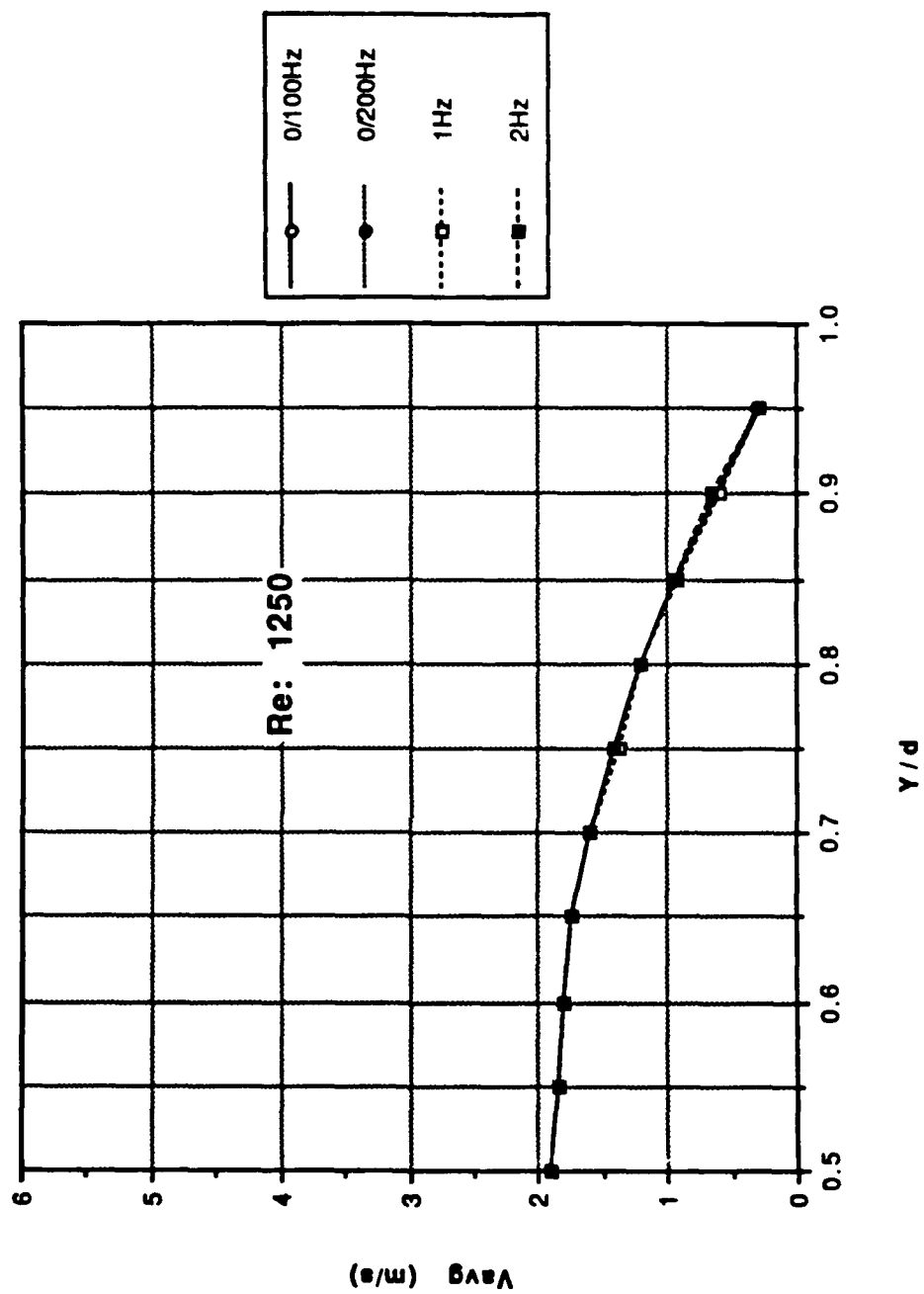


Figure 10. Profile Data: Mean Velocity vs y/d; Re: 1250

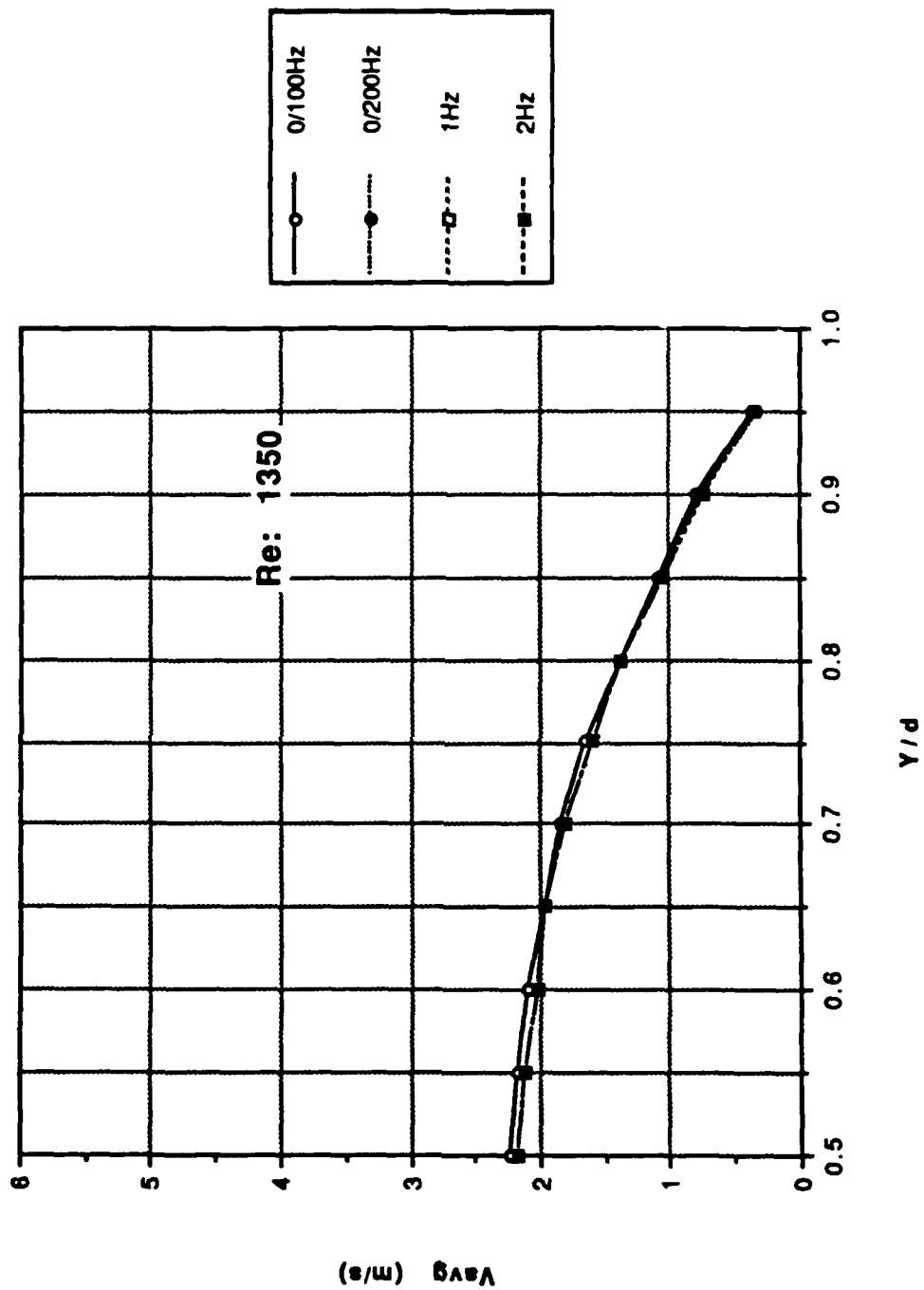


Figure 11. Profile Data: Mean Velocity vs y/d ; $Re: 1350$

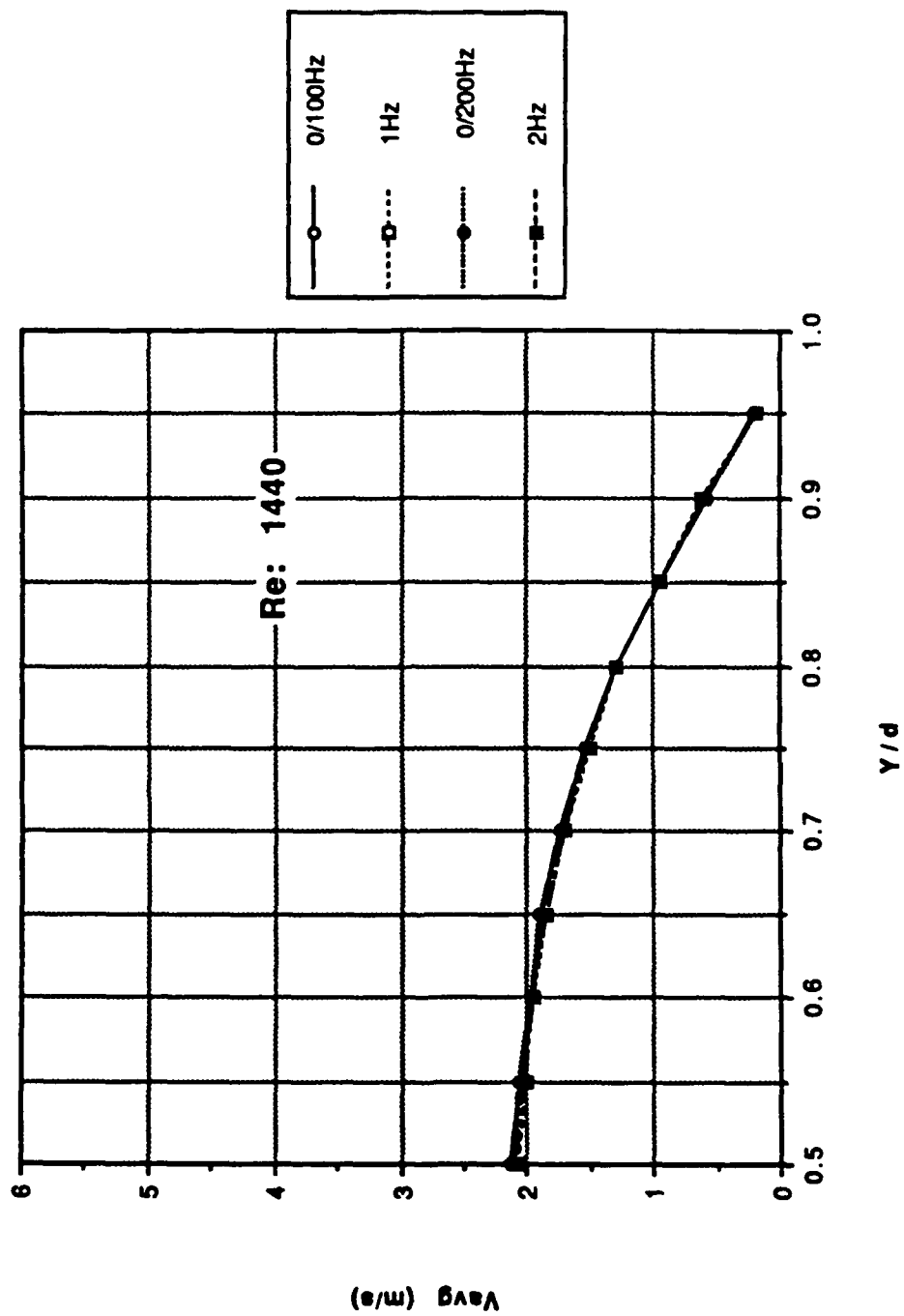


Figure 12. Profile Data: Mean Velocity vs y/d ; Re: 1440

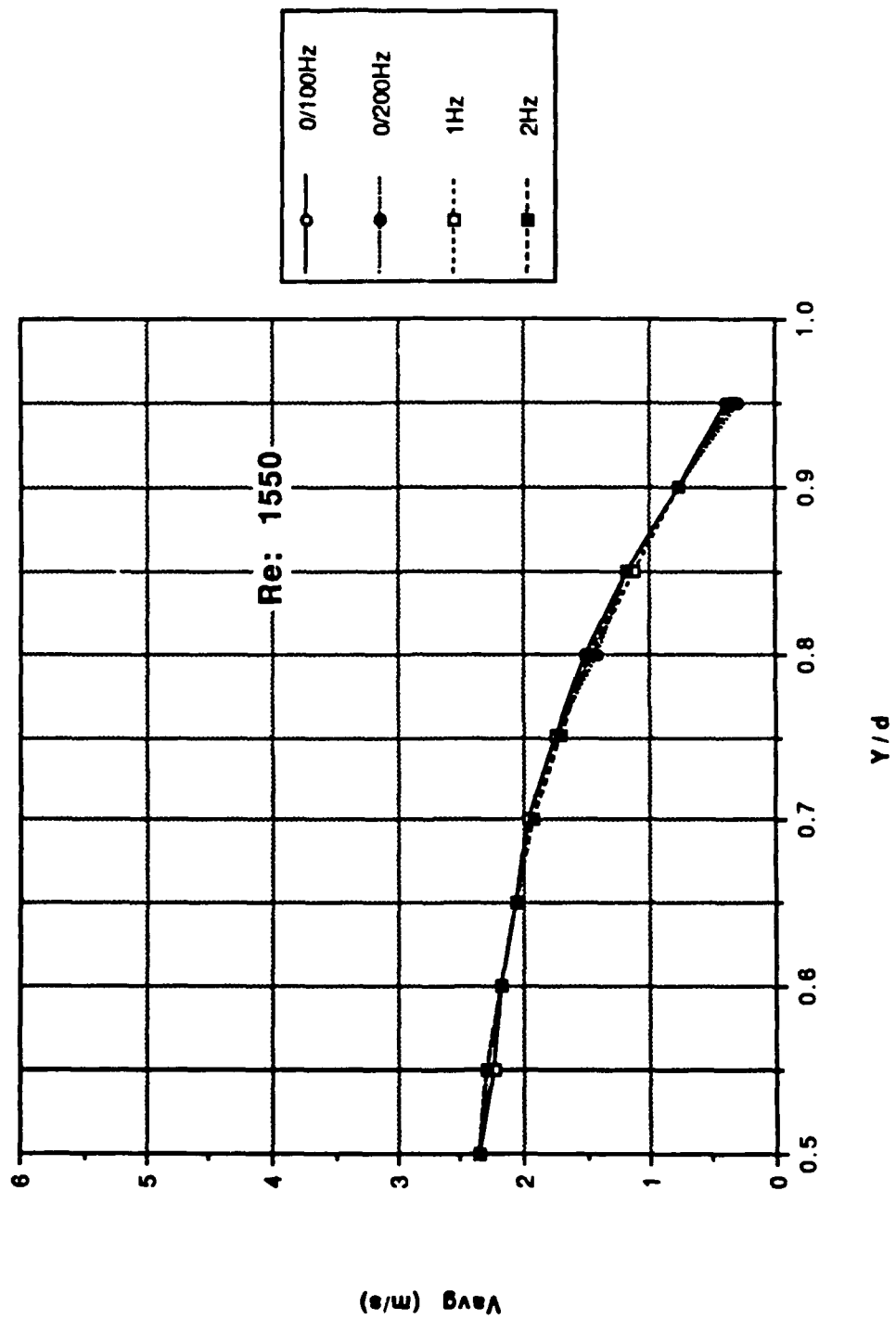


Figure 13. Profile Data: Mean Velocity vs y/d; Re: 1550

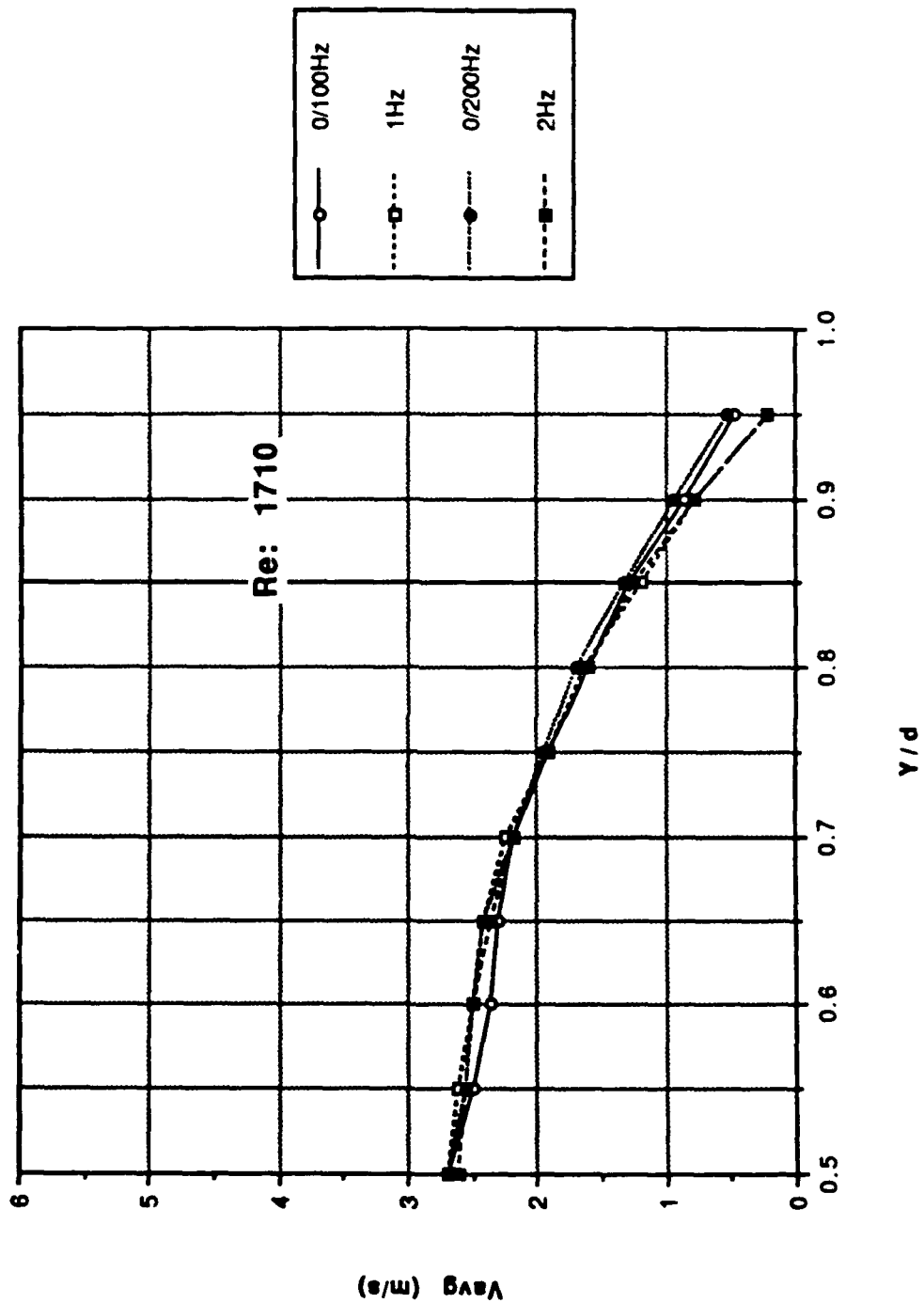


Figure 14. Profile Data: Mean Velocity vs y/d; Re: 1710

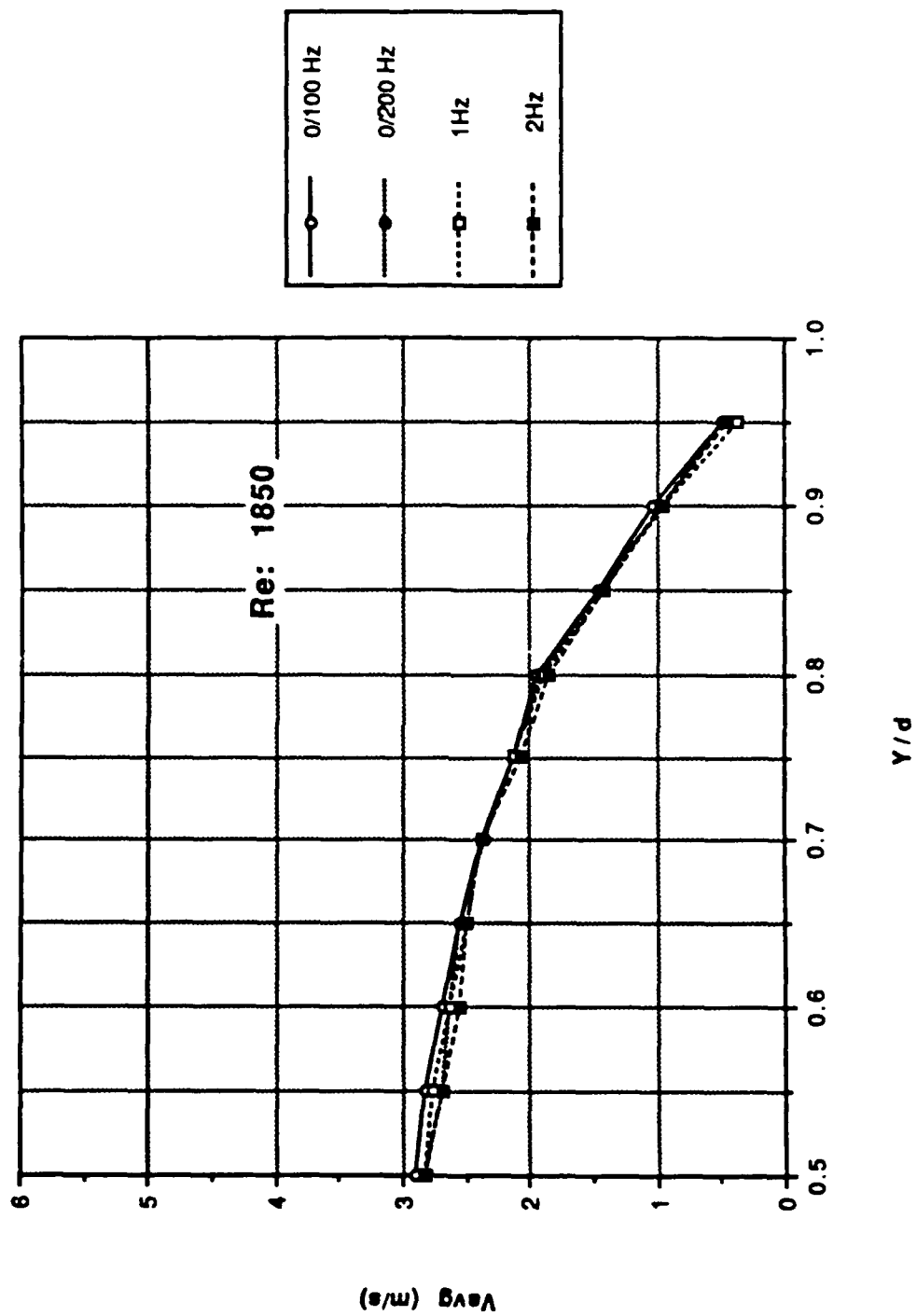


Figure 15. Profile Data: Mean Velocity vs y/d; Re: 1850

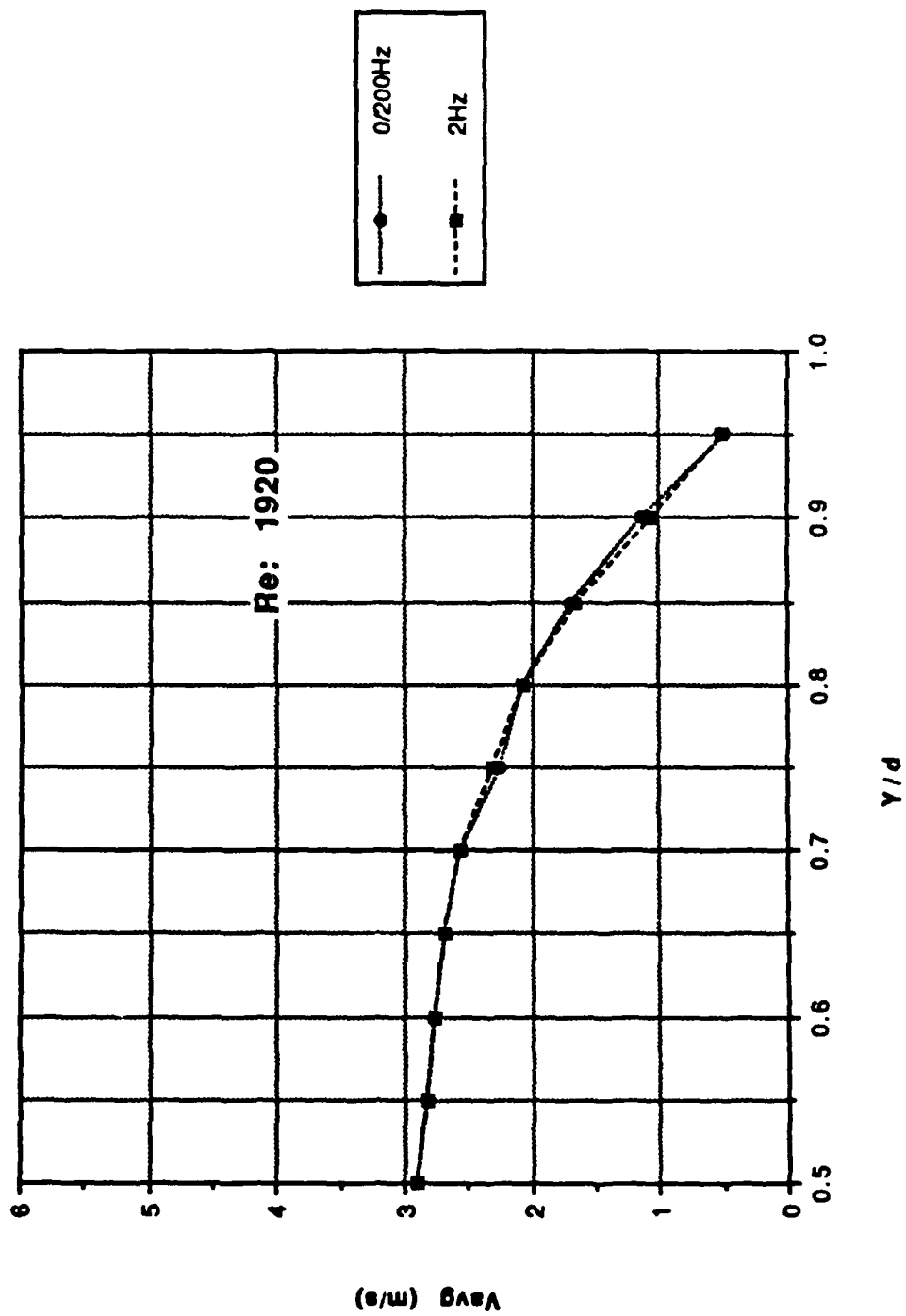


Figure 16. Profile Data: Mean Velocity vs y/d ; Re: 1920

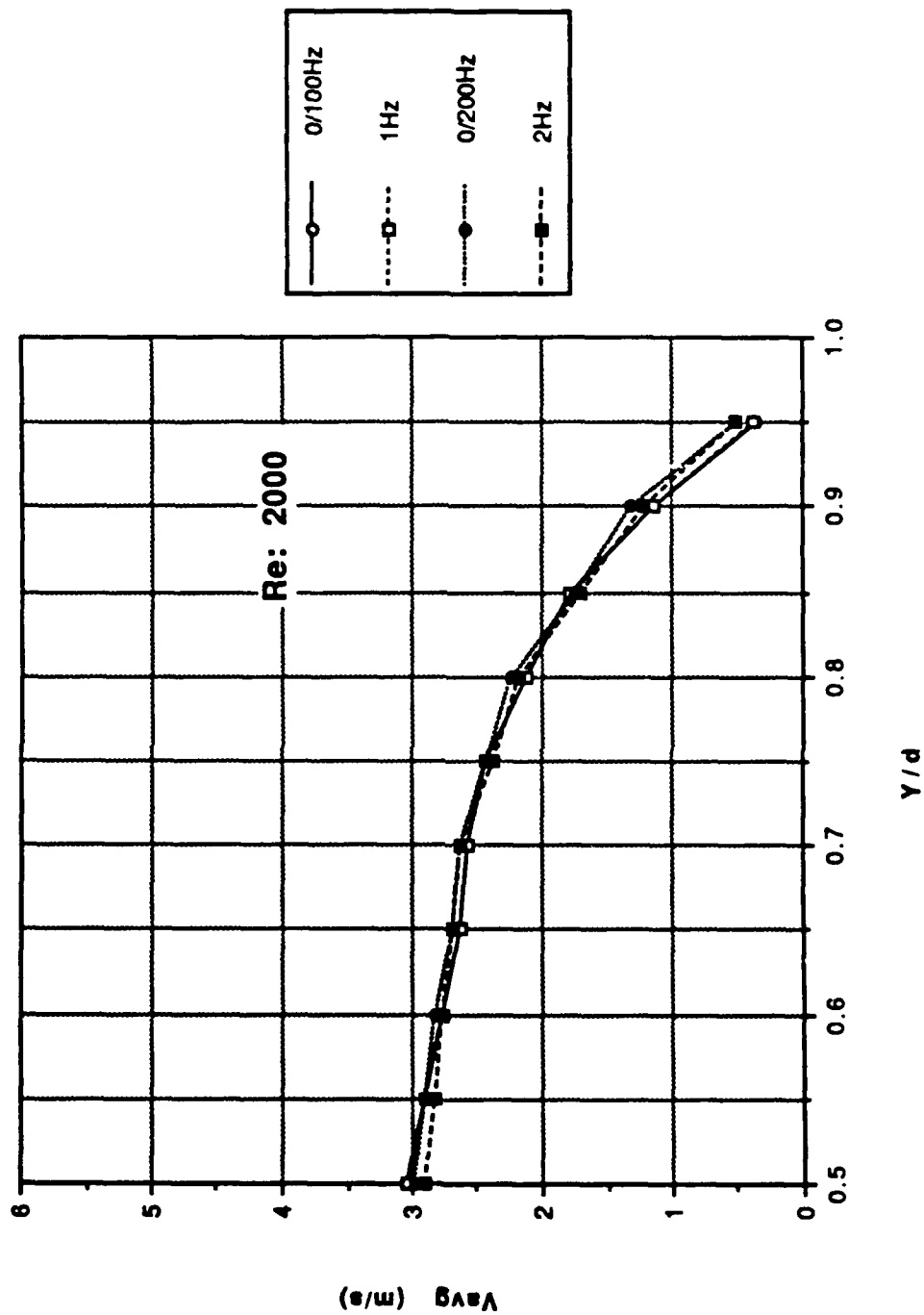


Figure 17. Profile Data: Mean Velocity vs y/d; Re: 2000

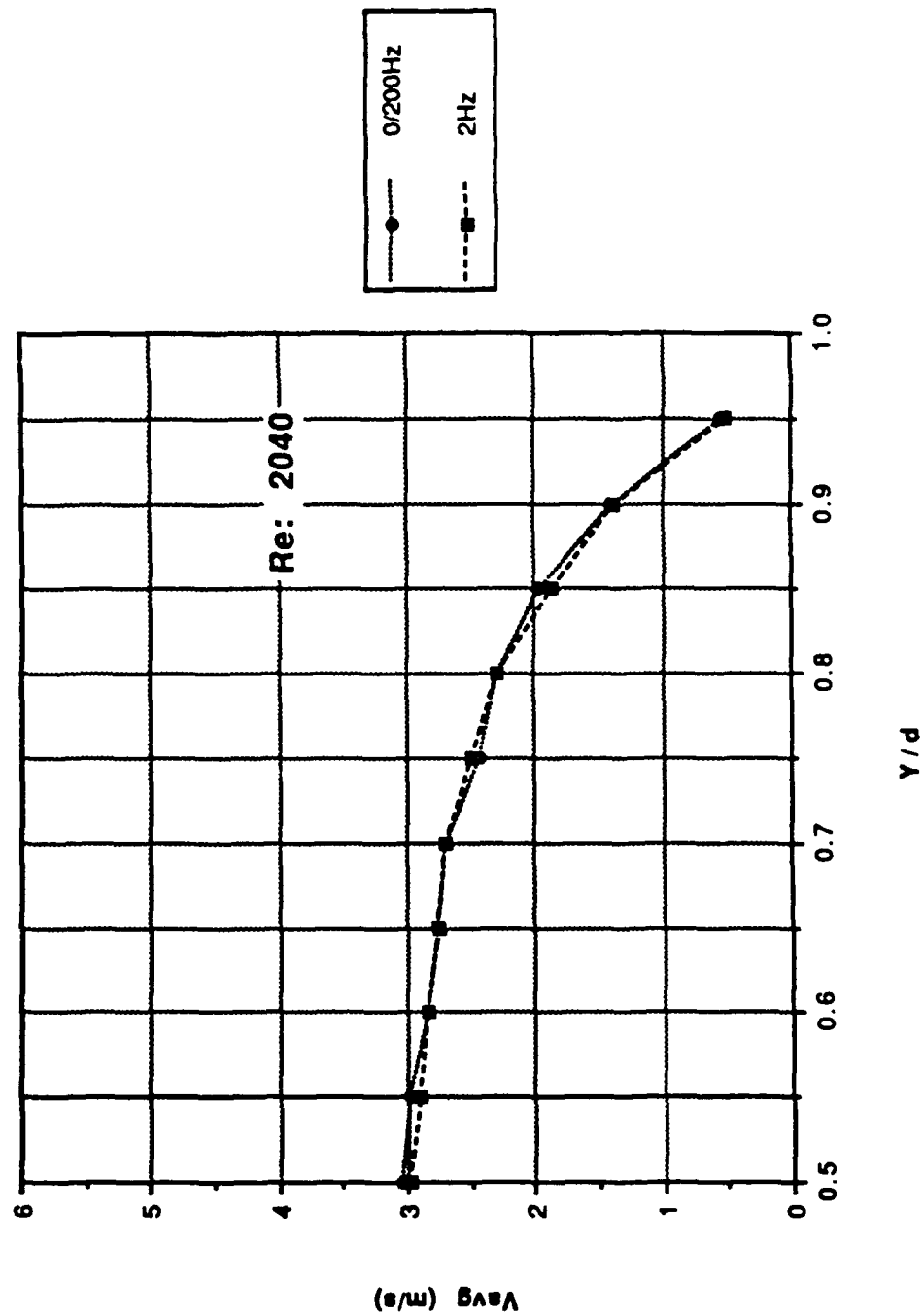


Figure 18. Profile Data: Mean Velocity vs y/d ; Re: 2040

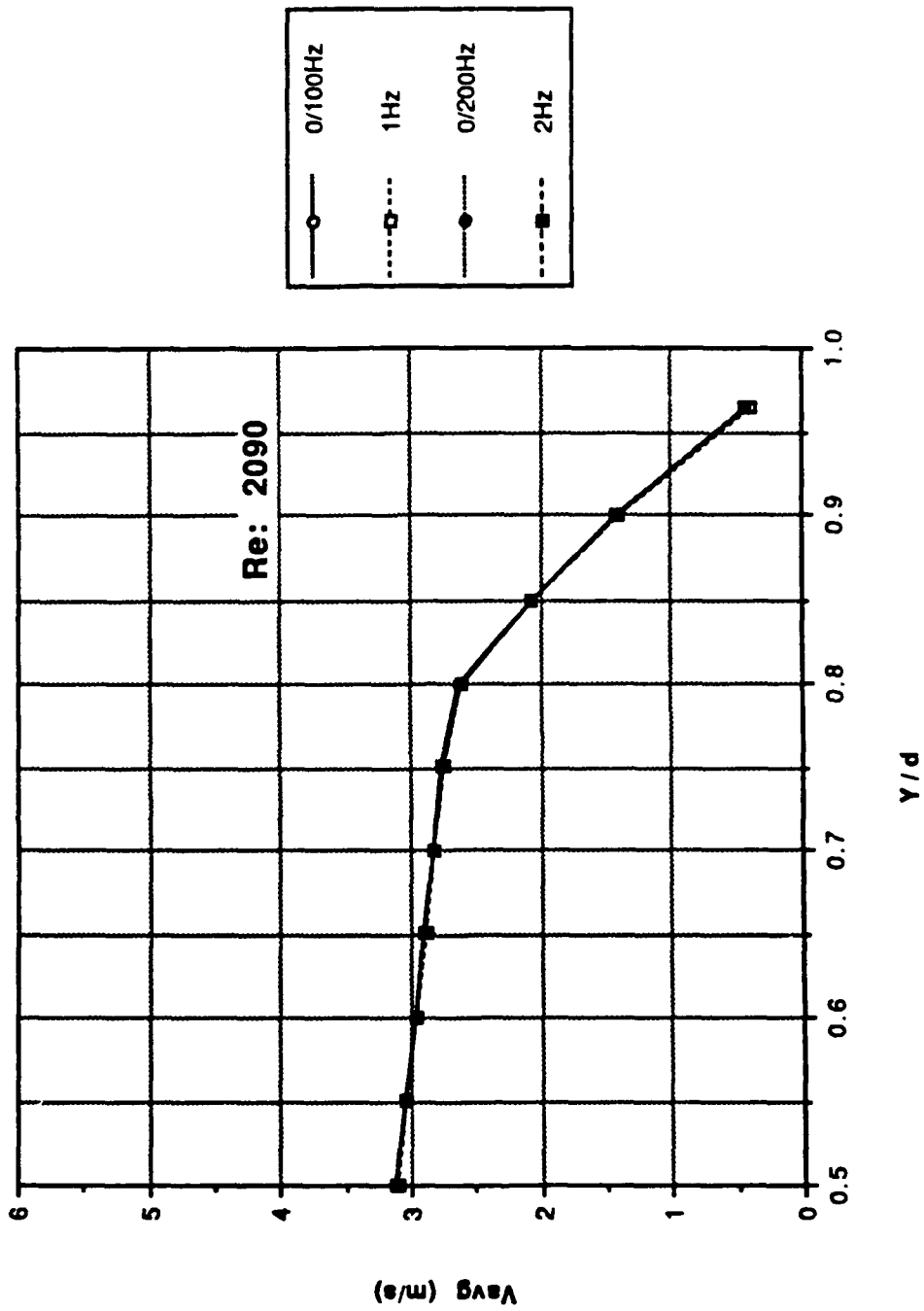


Figure 19. Profile Data: Mean Velocity vs y/d; Re: 2090

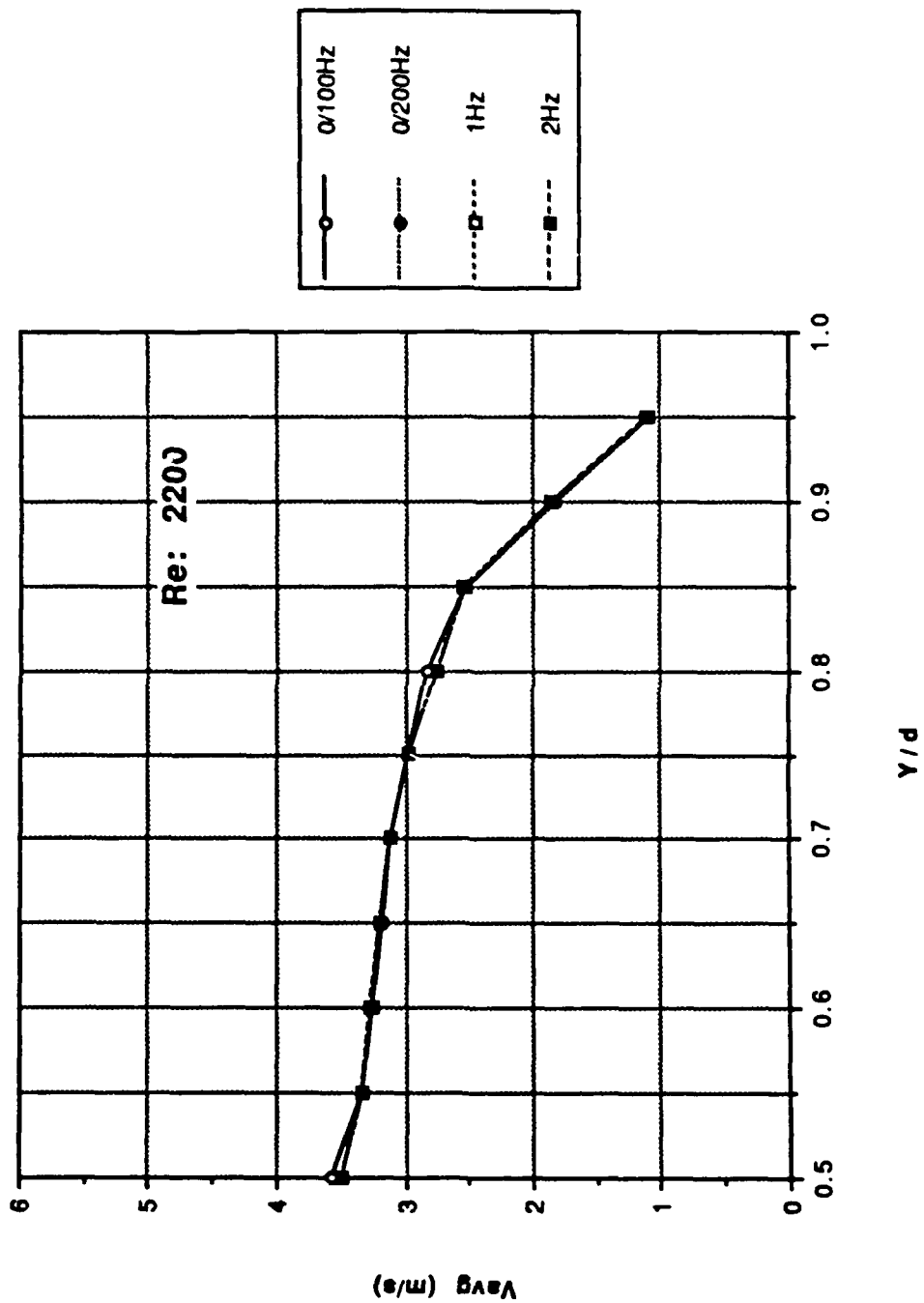


Figure 20. Profile Data: Mean Velocity vs y/d; Re: 2200

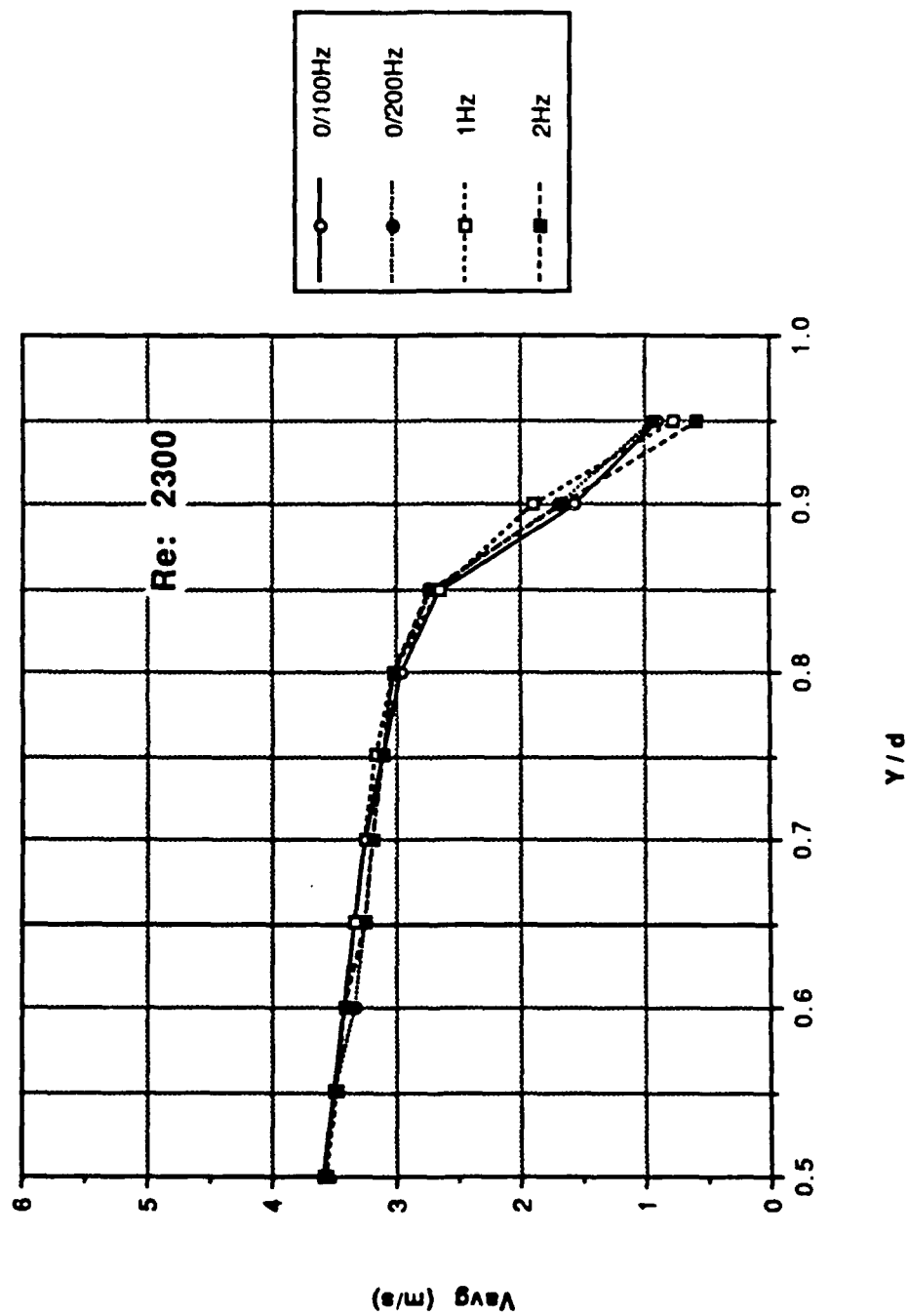


Figure 21. Profile Data: Mean Velocity vs y/d; Re: 2300

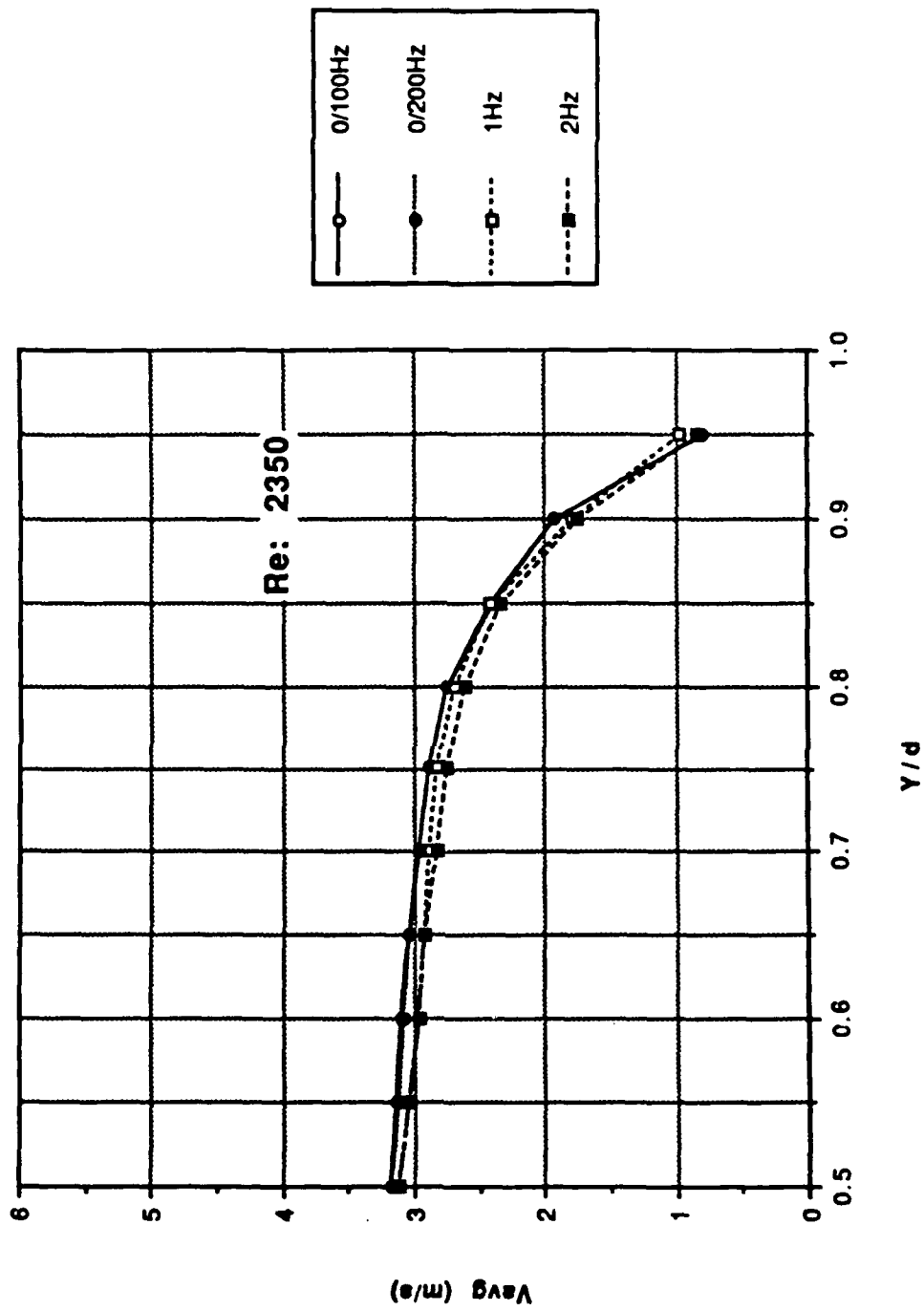


Figure 22. Profile Data: Mean Velocity vs y/d ; $Re: 2350$

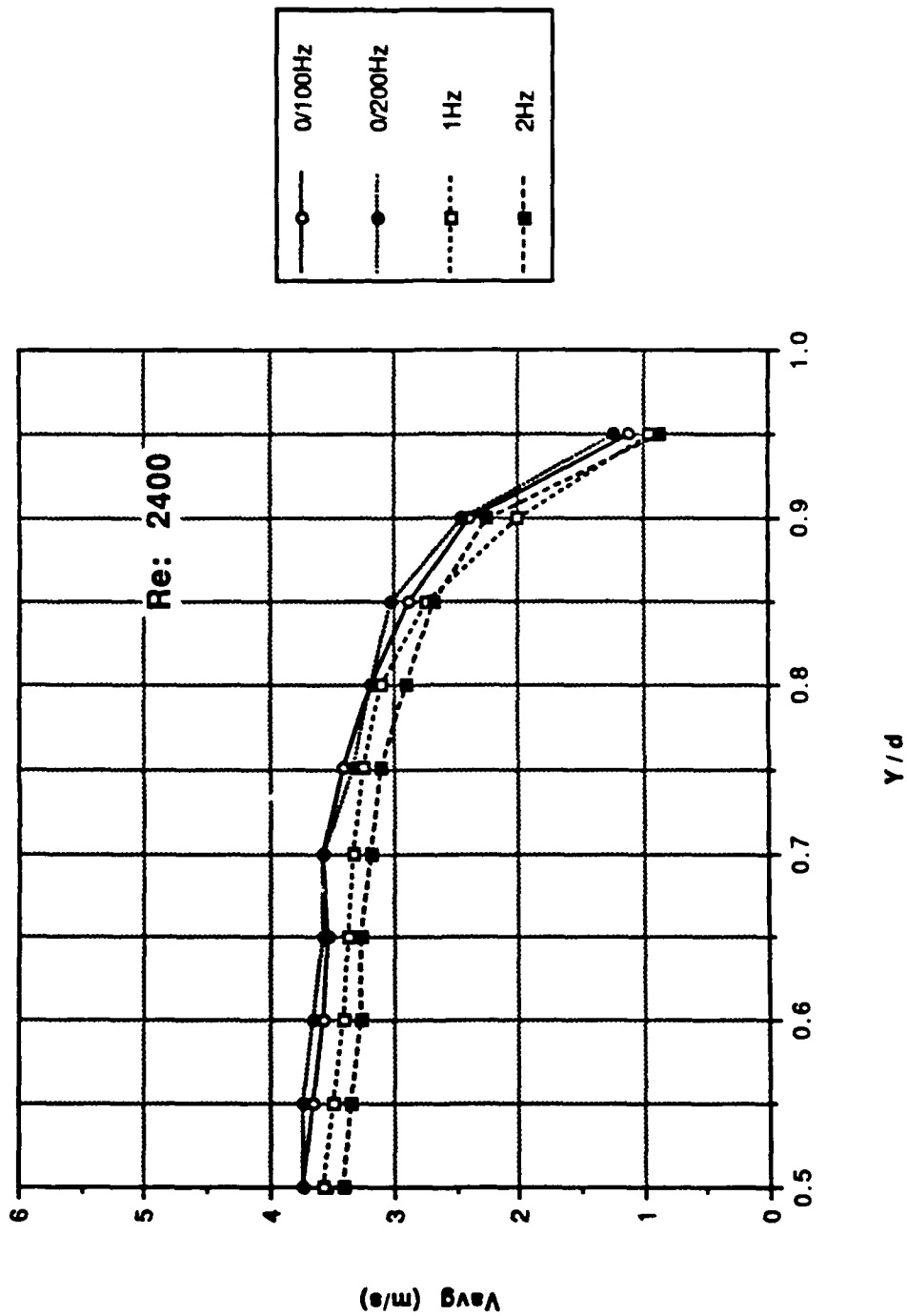


Figure 23. Profile Data: Mean Velocity vs y/d ; Re: 2400

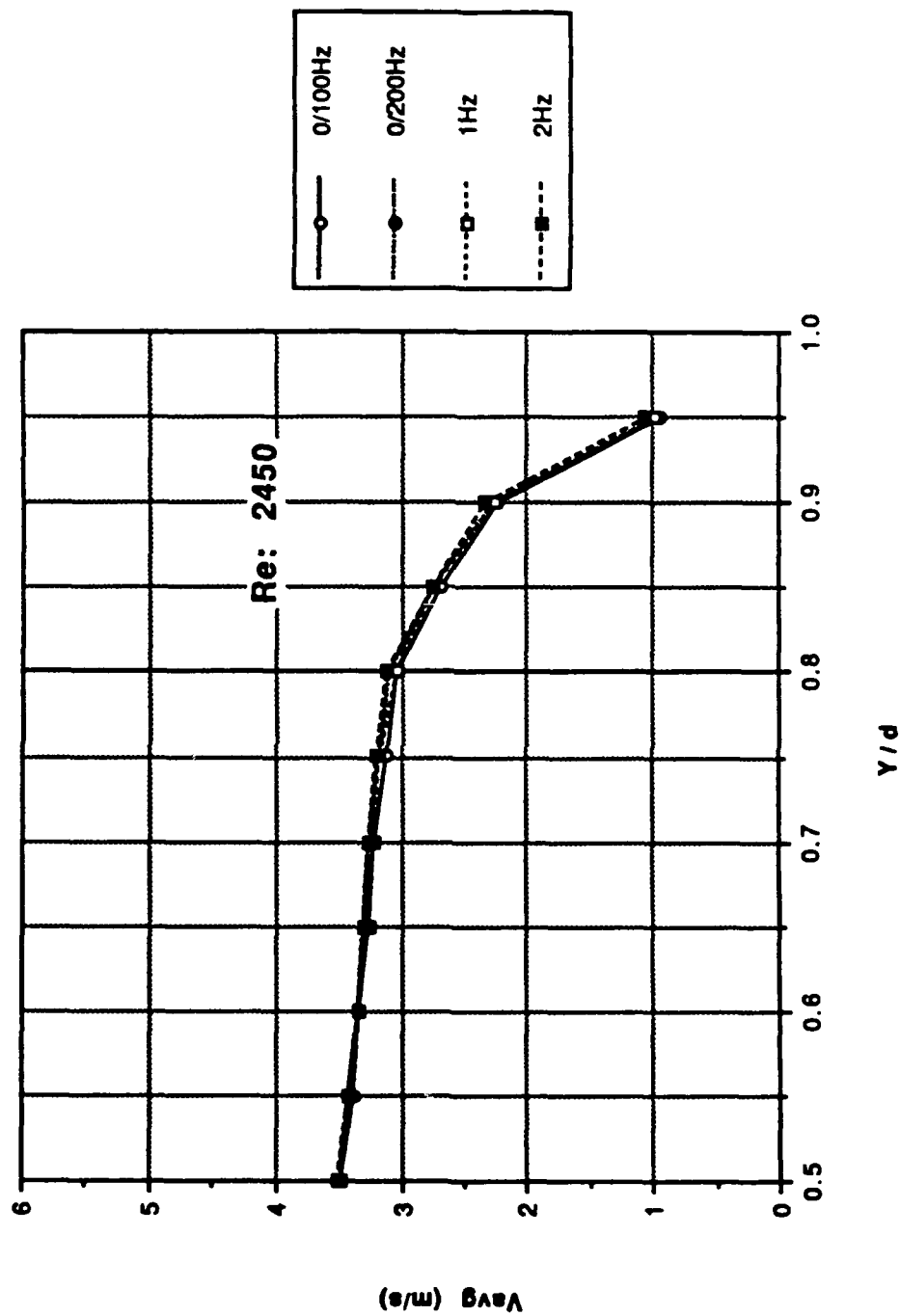


Figure 24. Profile Data: Mean Velocity vs y/d; Re: 2450

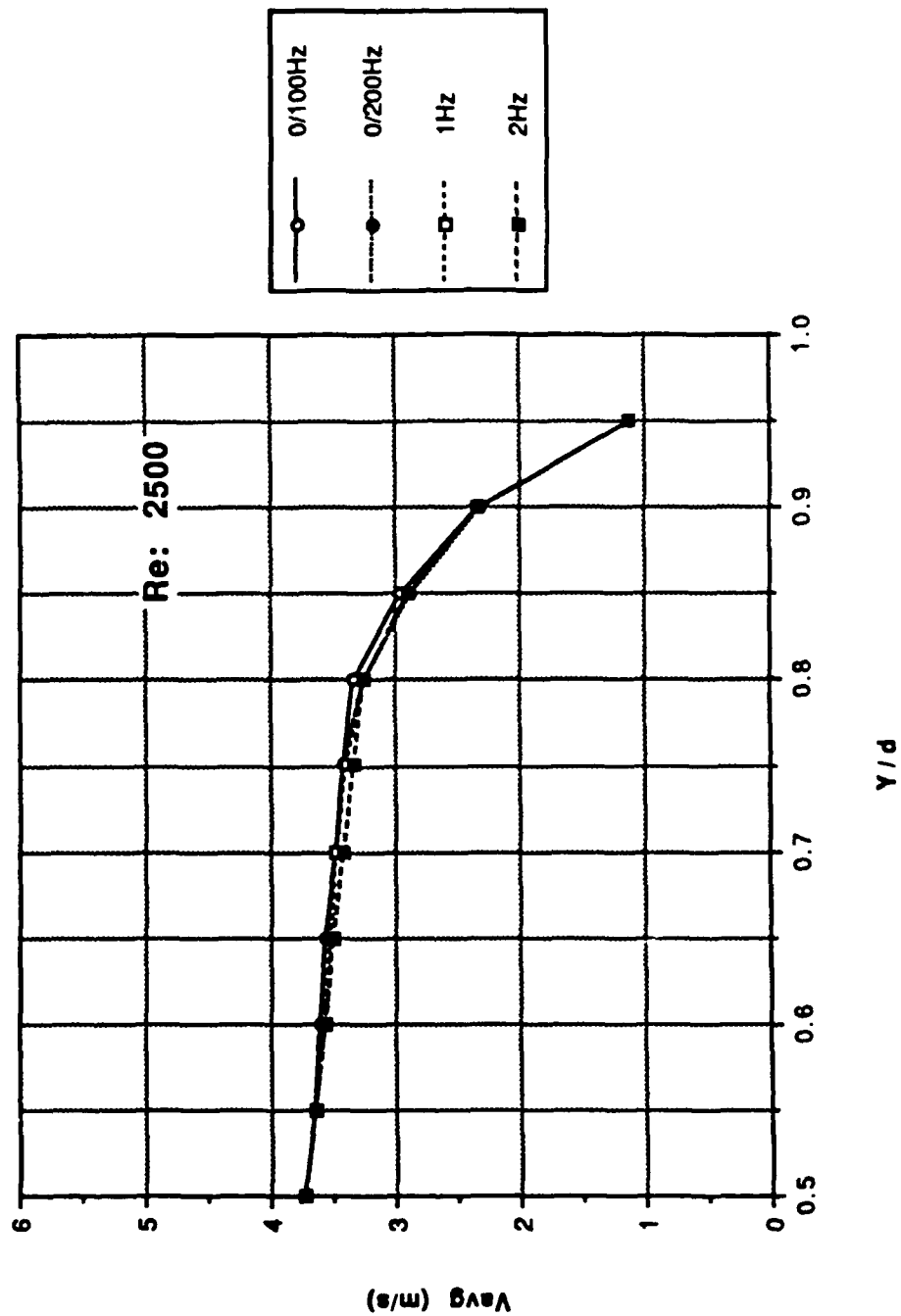


Figure 25. Profile Data: Mean Velocity vs y/d; Re: 2500

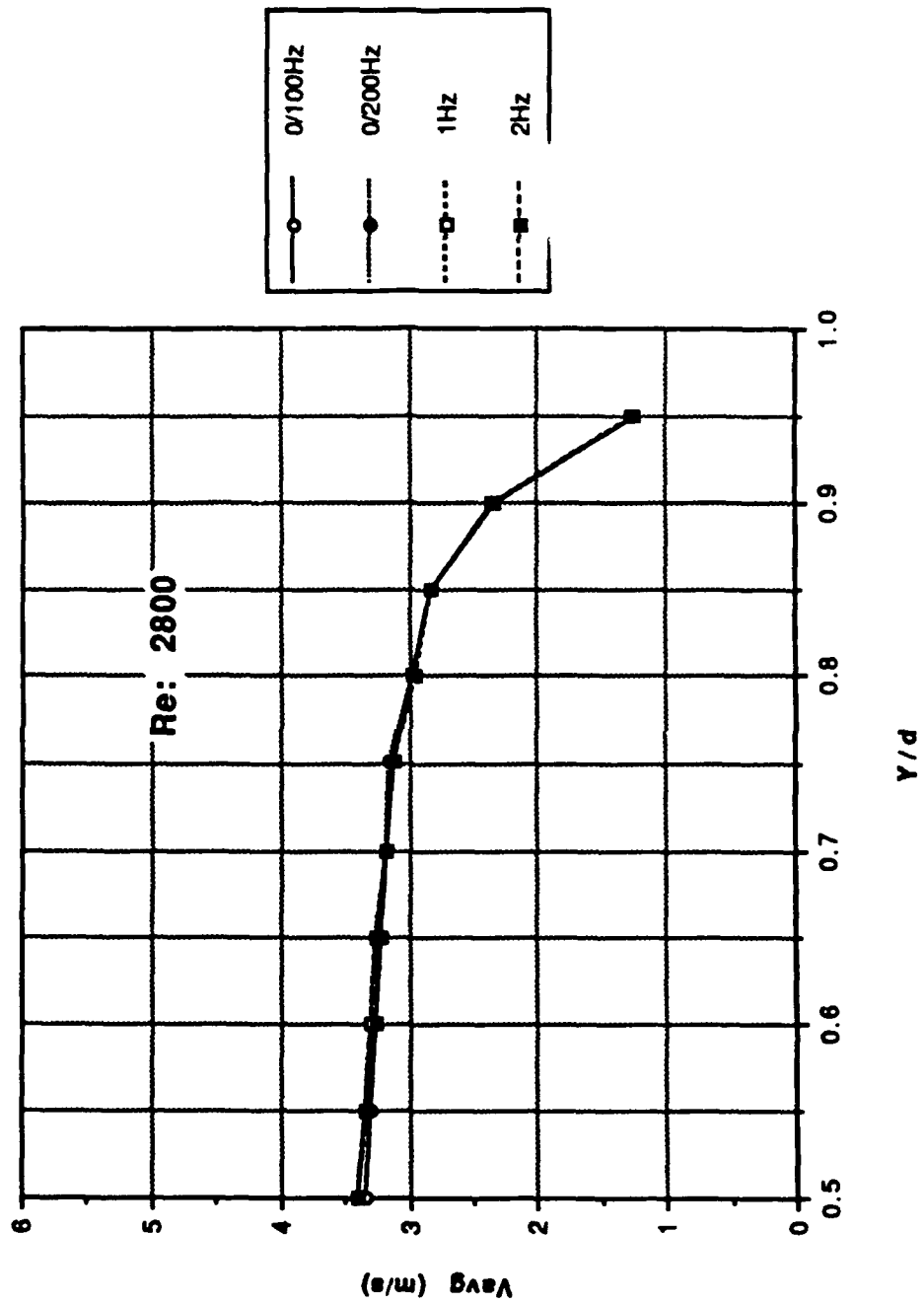


Figure 26. Profile Data: Mean Velocity vs y/d ; Re: 2800

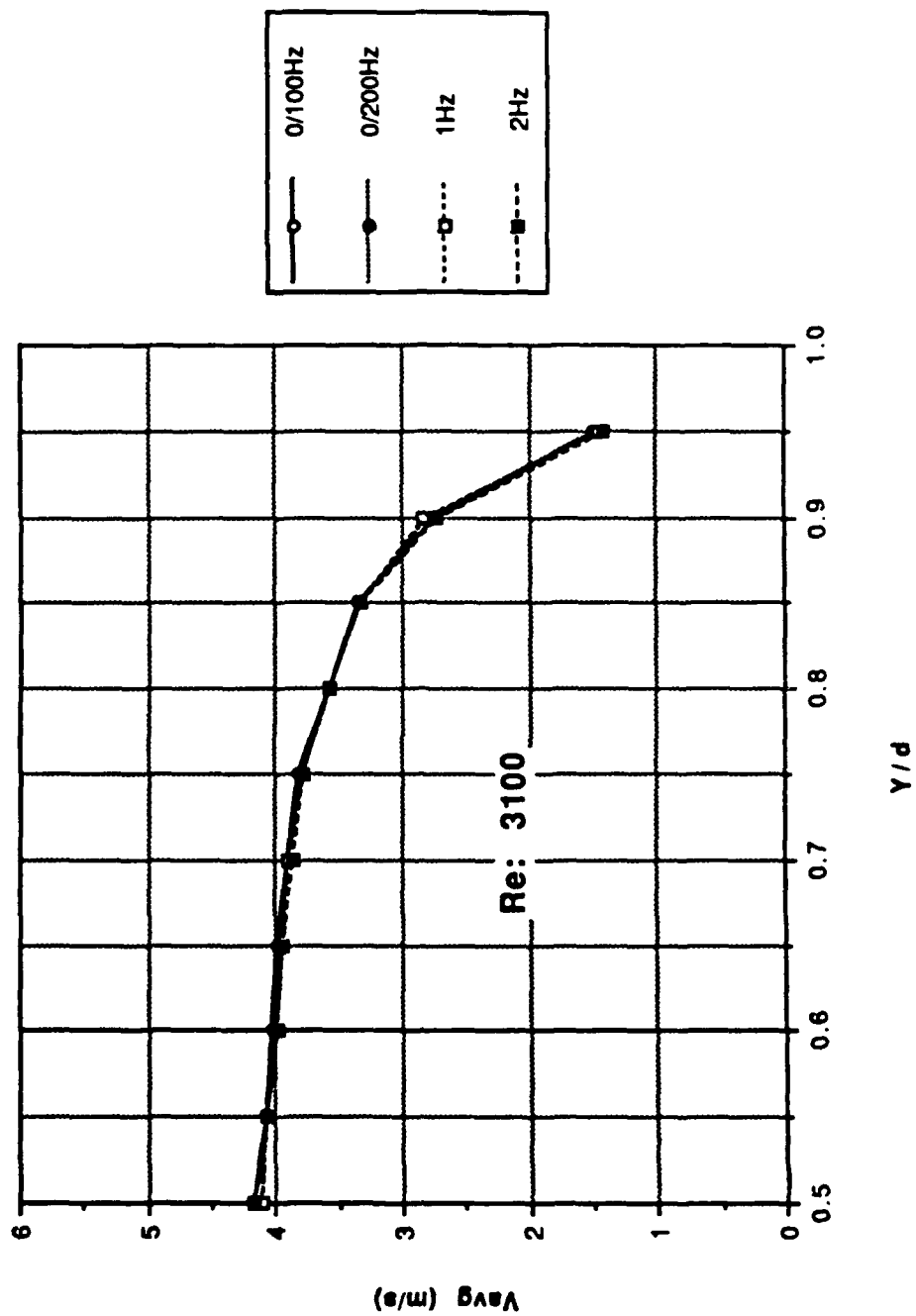


Figure 27. Profile Data: Mean Velocity vs y/d; Re: 3100

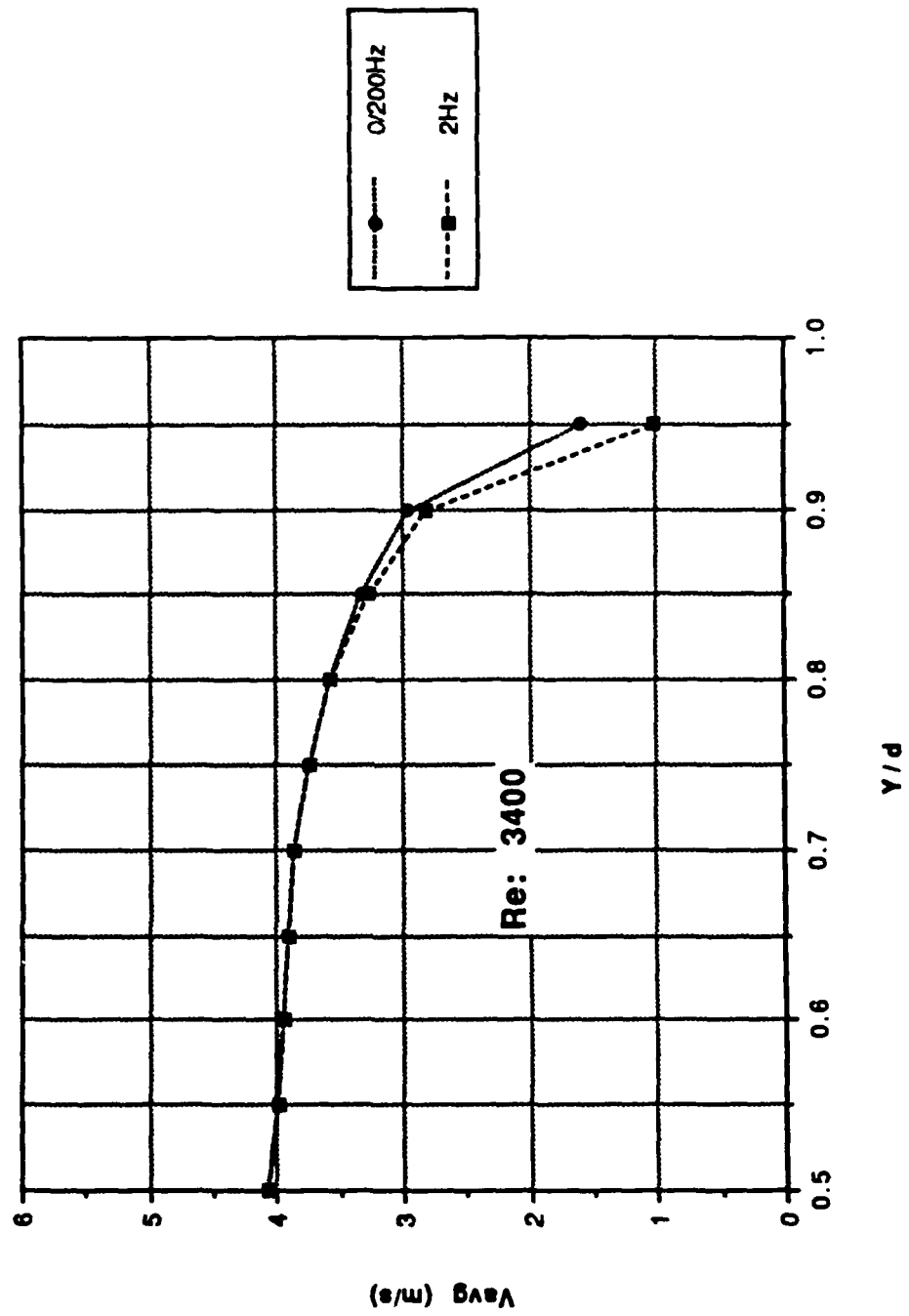


Figure 28. Profile Data: Mean Velocity vs y/d ; Re: 3400

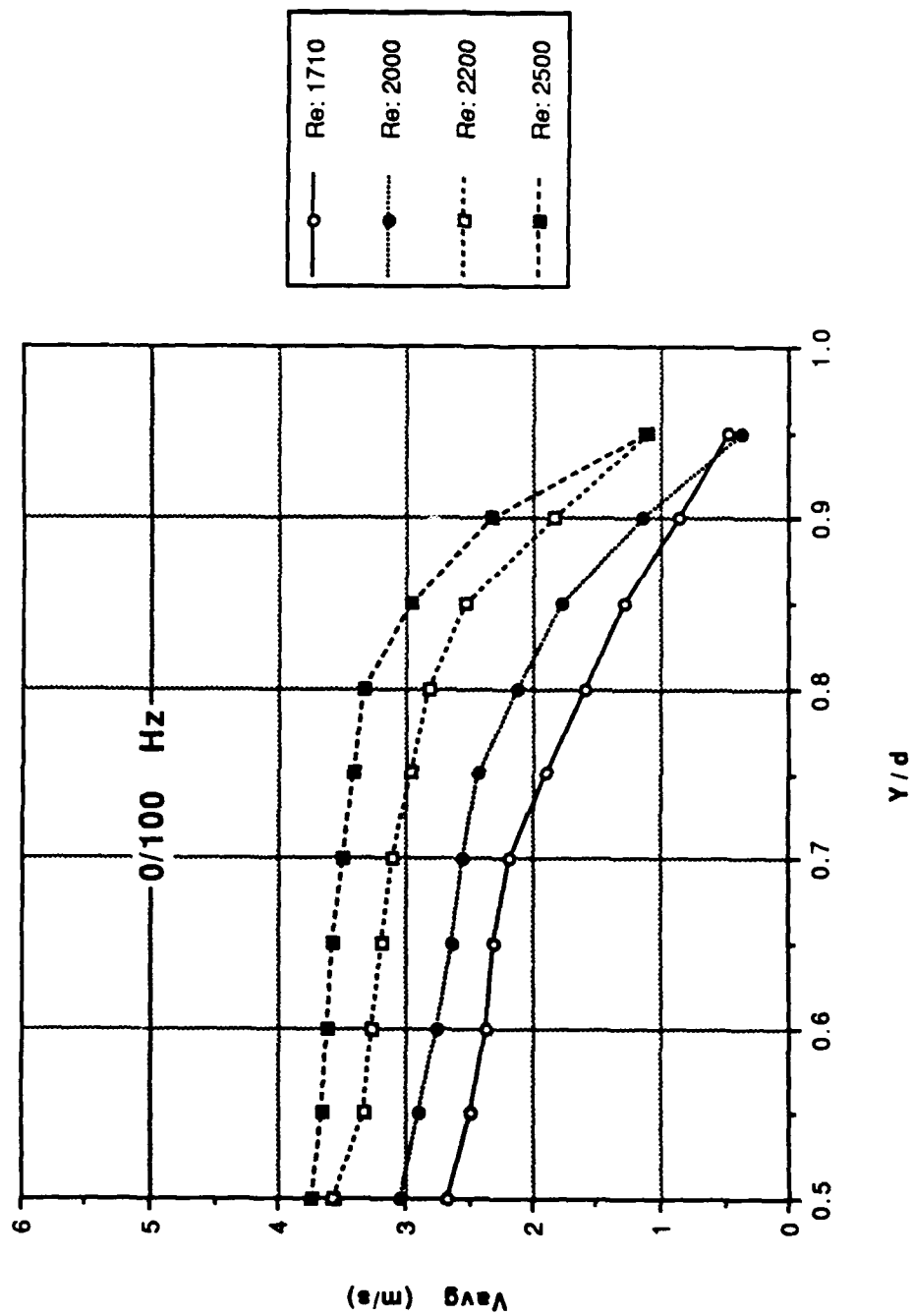


Figure 29. Profile Data: Mean Velocity vs y/d; Composite Profiles

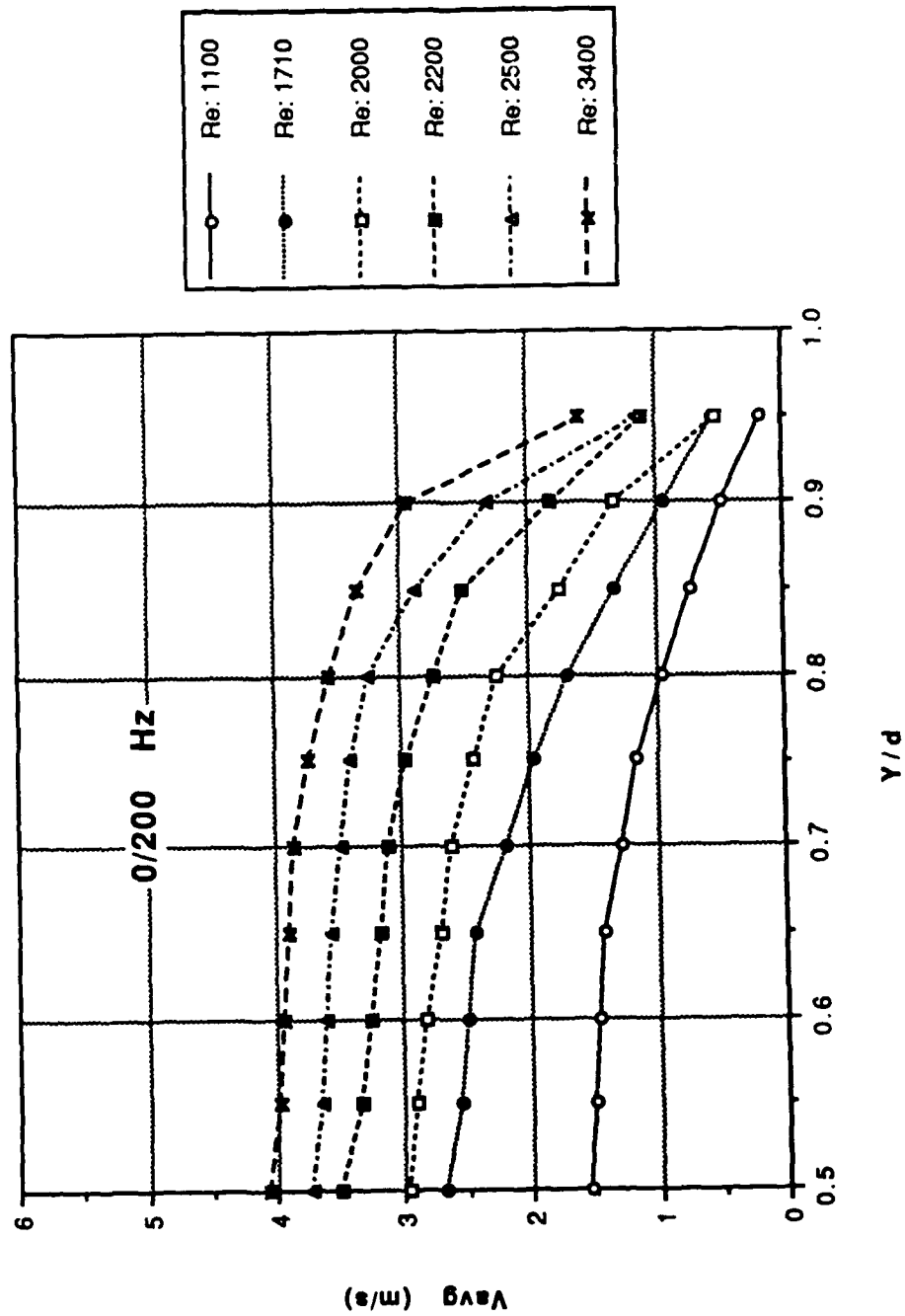


Figure 30. Profile Data: Mean Velocity vs y/d; Composite Profiles

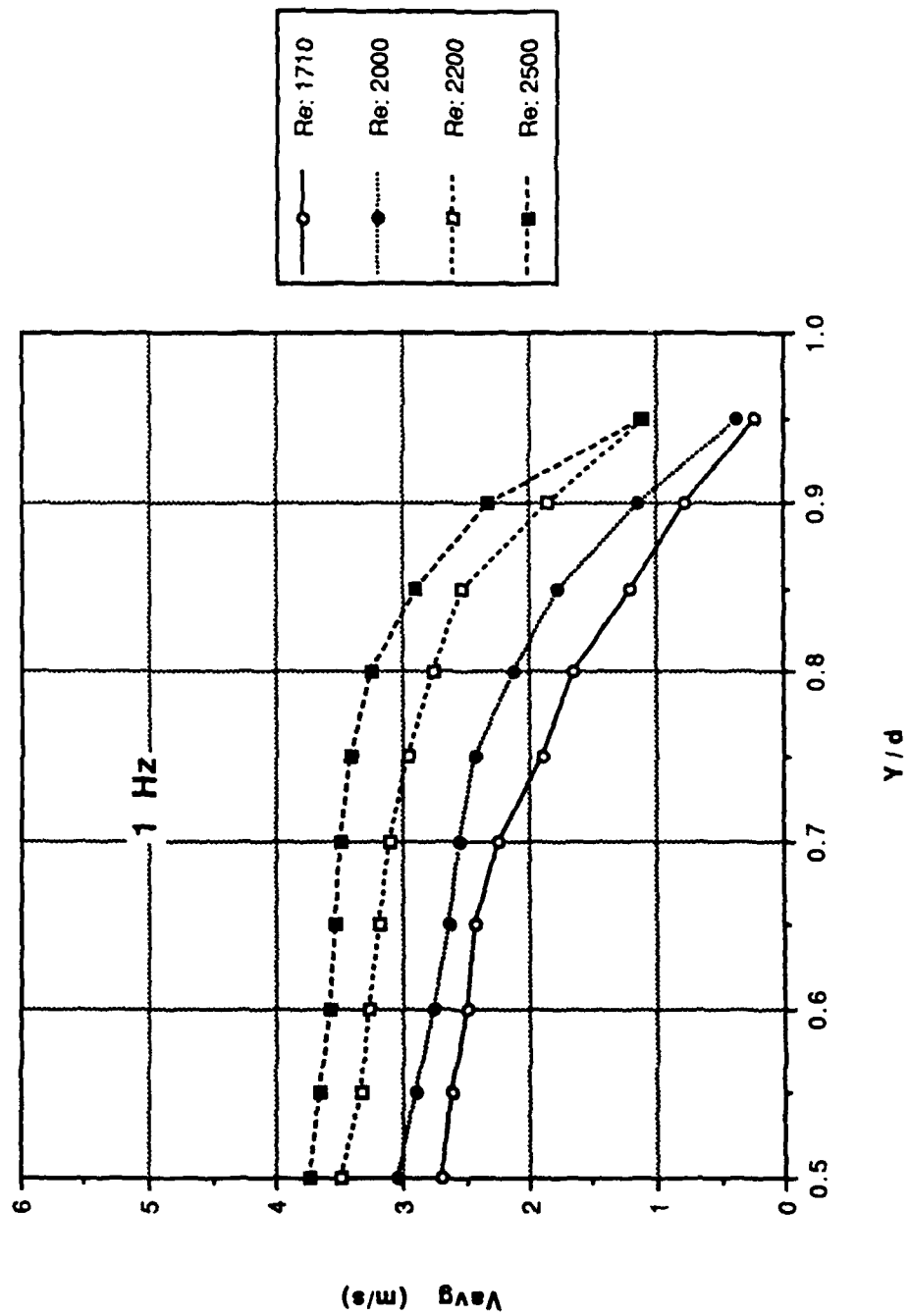


Figure 31. Profile Data: Mean Velocity vs y/d ; Composite Profiles

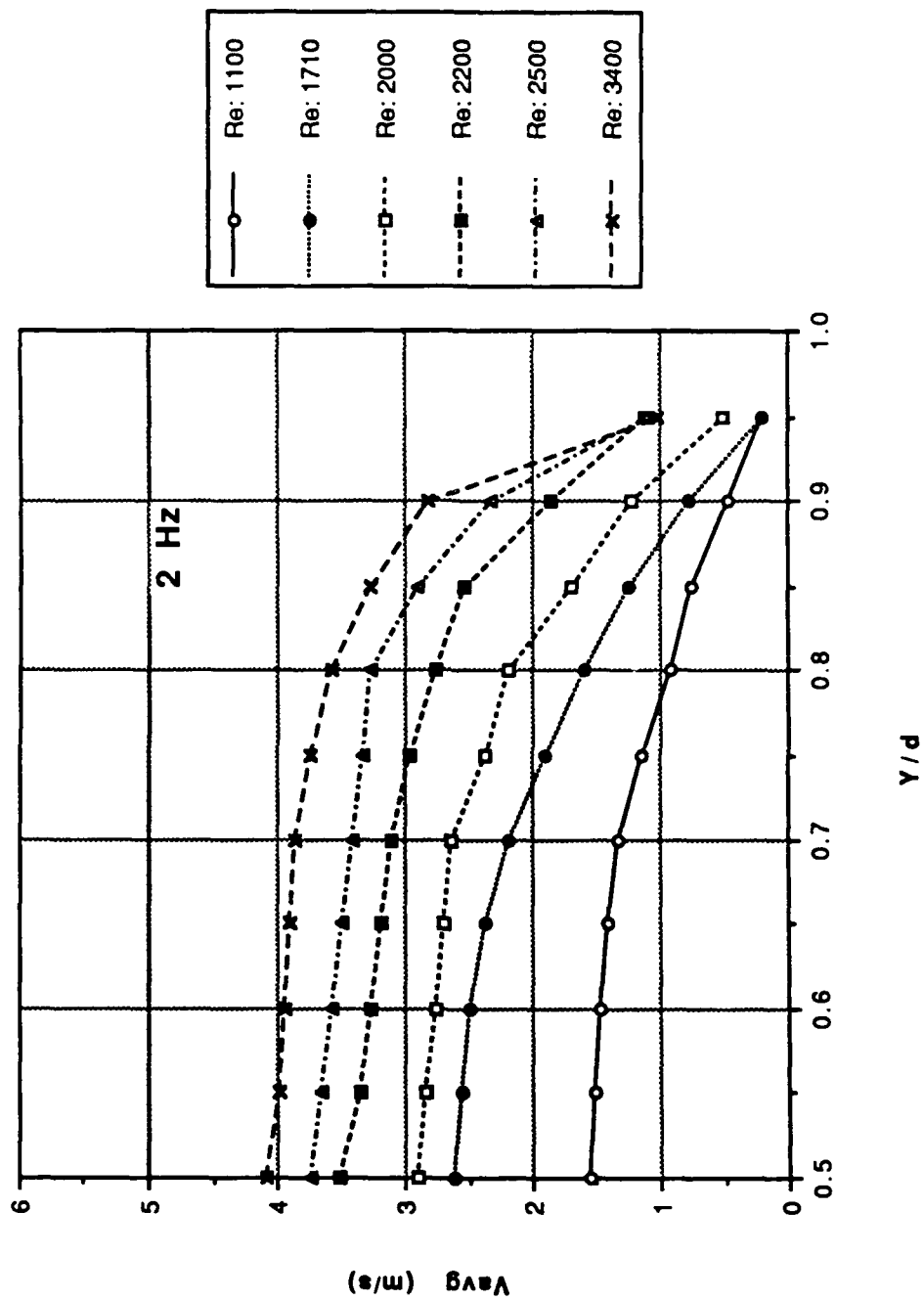


Figure 32. Profile Data: Mean Velocity vs y/d ; Composite Profiles

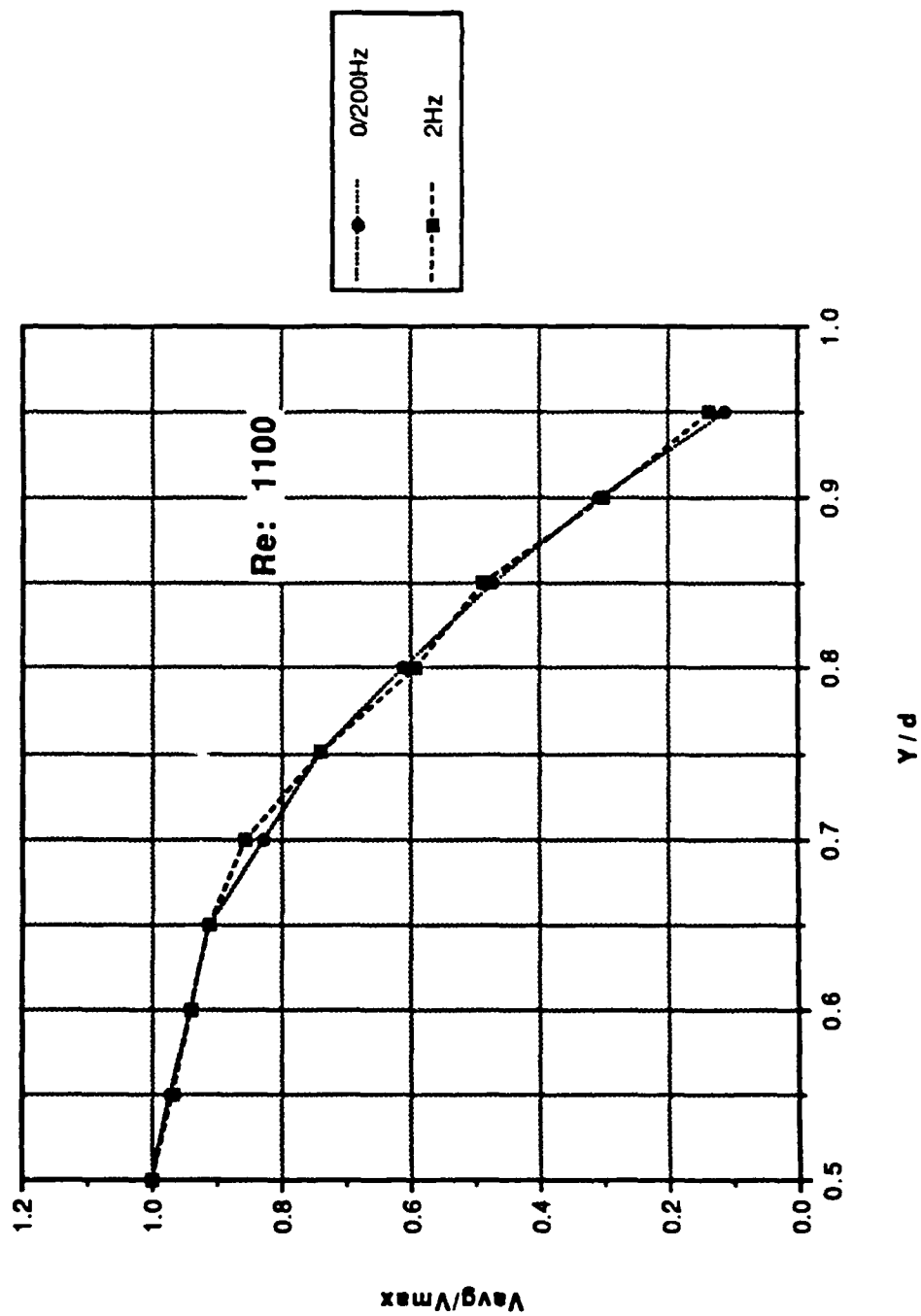


Figure 33. Profile Data: Mean Velocity Normalized by the Centerline Velocity vs y/d ; Re: 1100

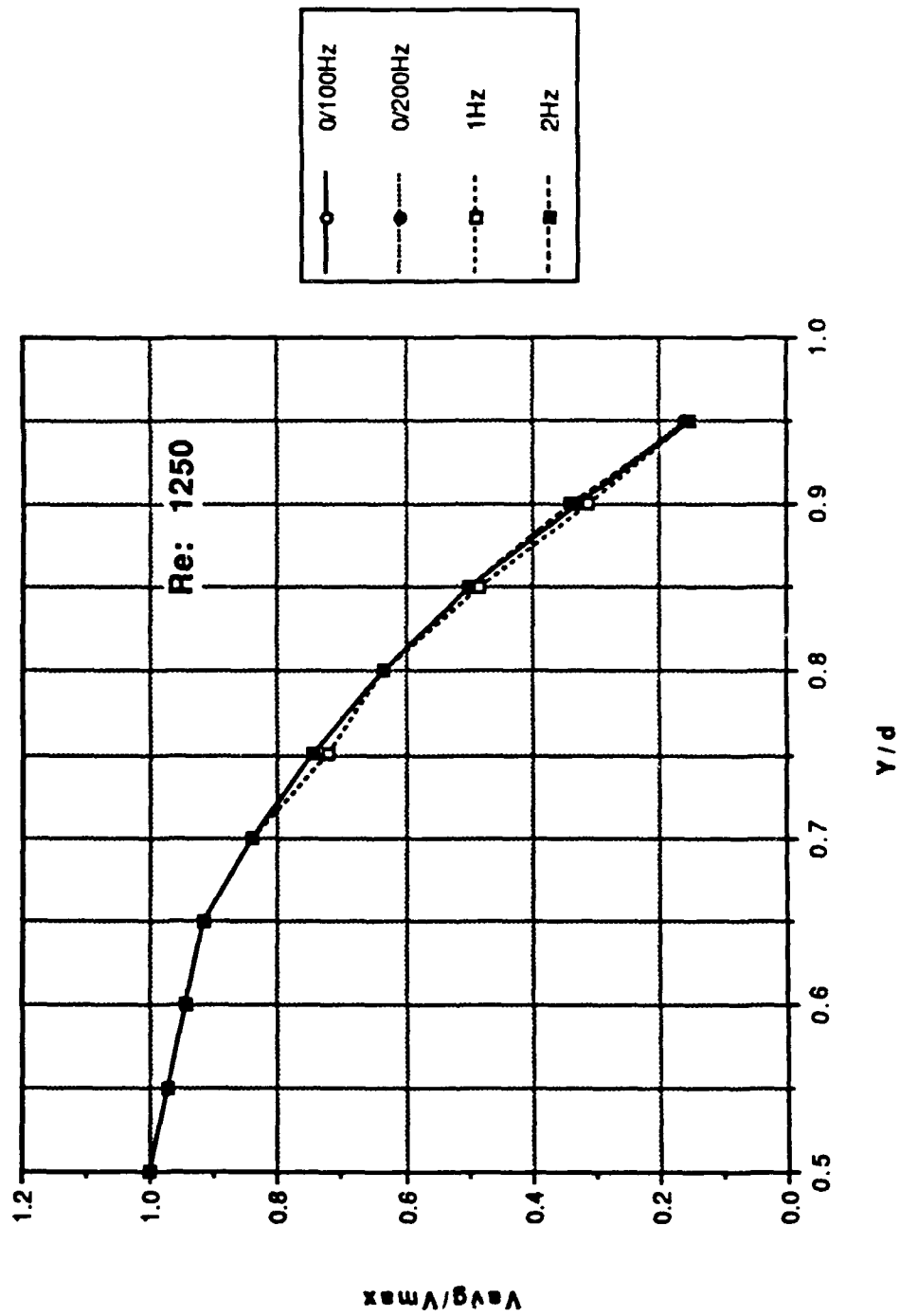


Figure 34. Profile Data: Mean Velocity Normalized by the Centerline Velocity vs y/d ; Re: 1250

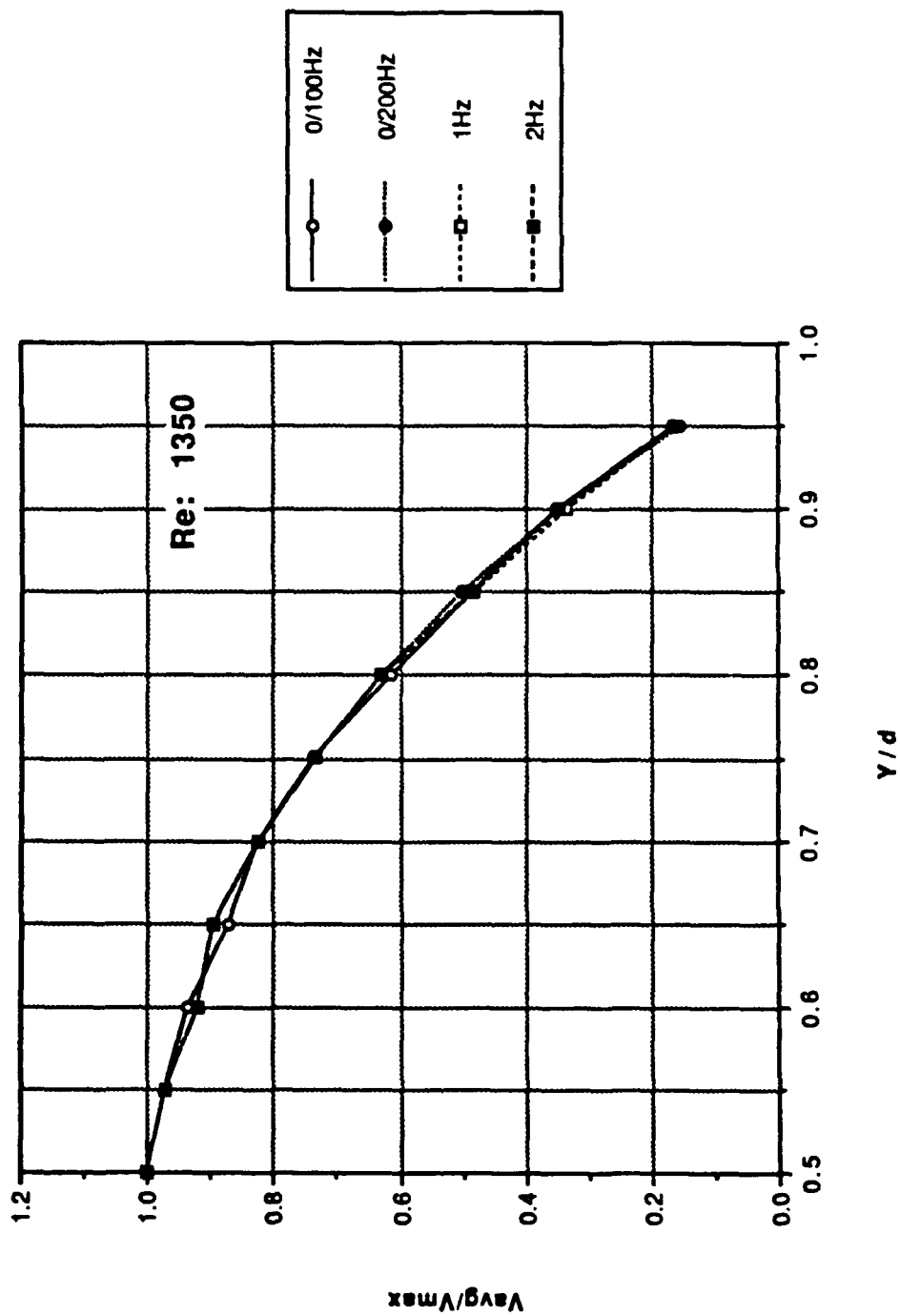


Figure 35. Profile Data: Mean Velocity Normalized by the Centerline Velocity vs y/d ; Re: 1350

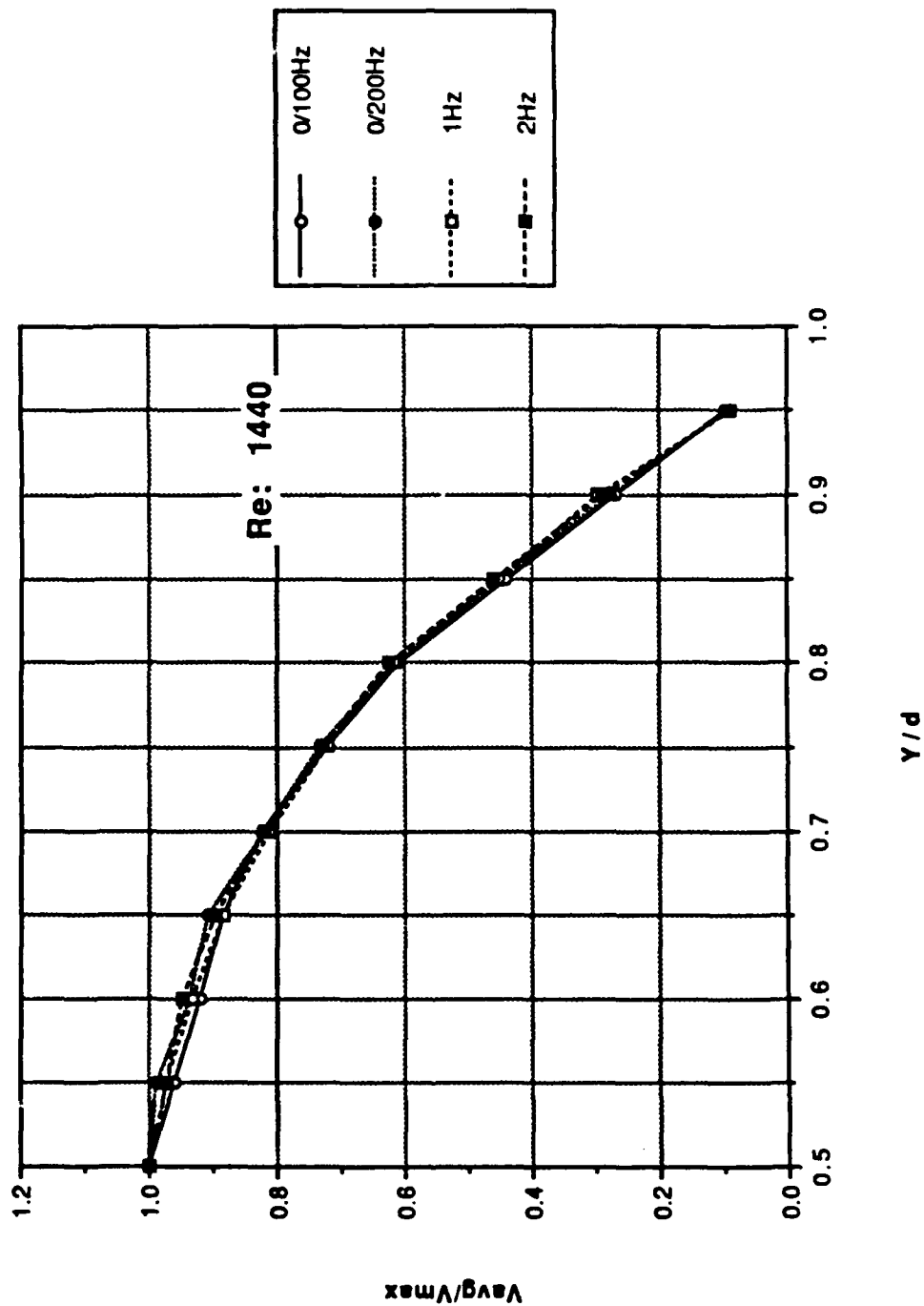


Figure 36. Profile Data: Mean Velocity Normalized by the Centerline Velocity vs y/d ; $Re: 1440$

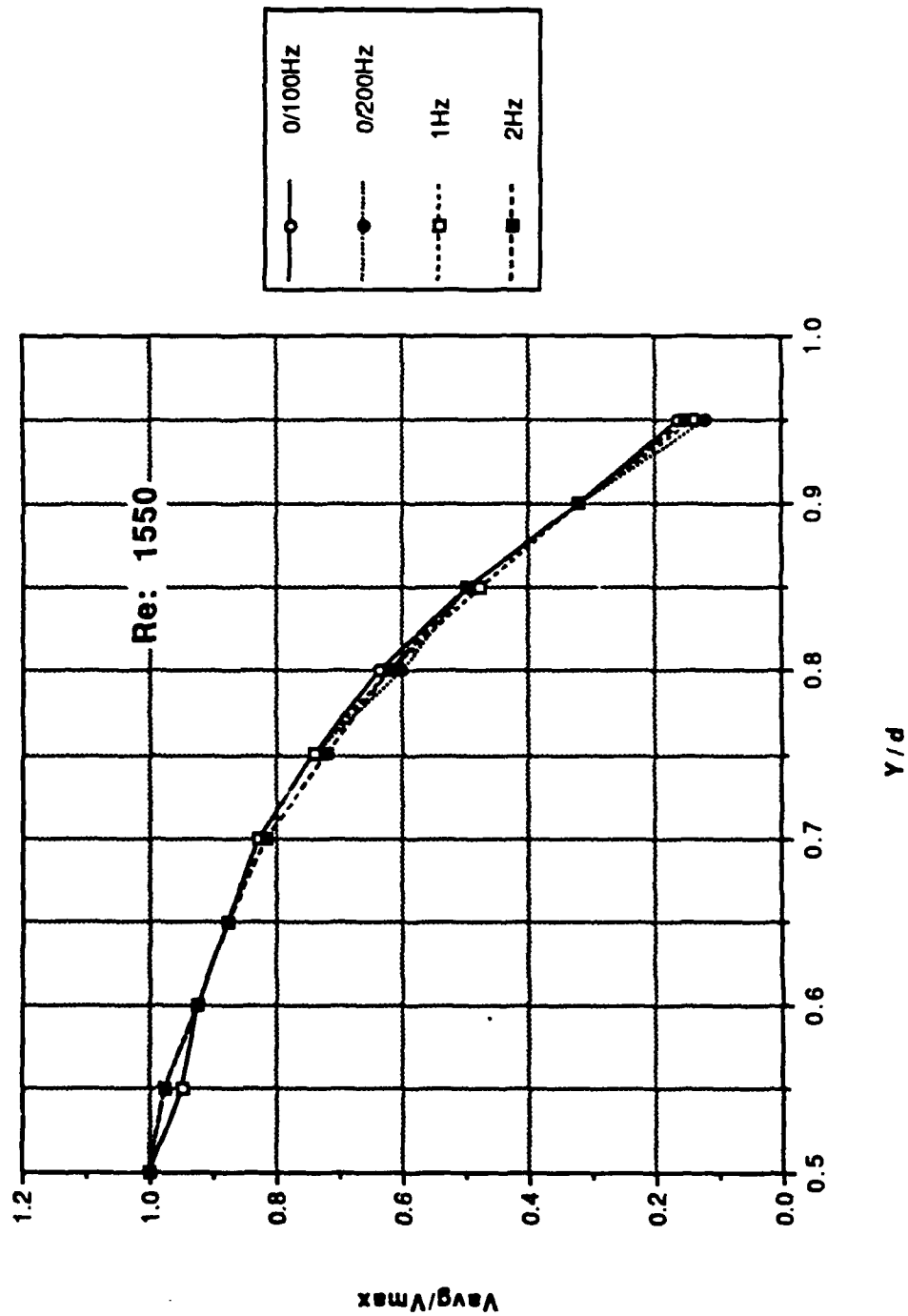


Figure 37. Profile Data: Mean Velocity Normalized by the Centerline Velocity vs y/d ; $Re: 1550$

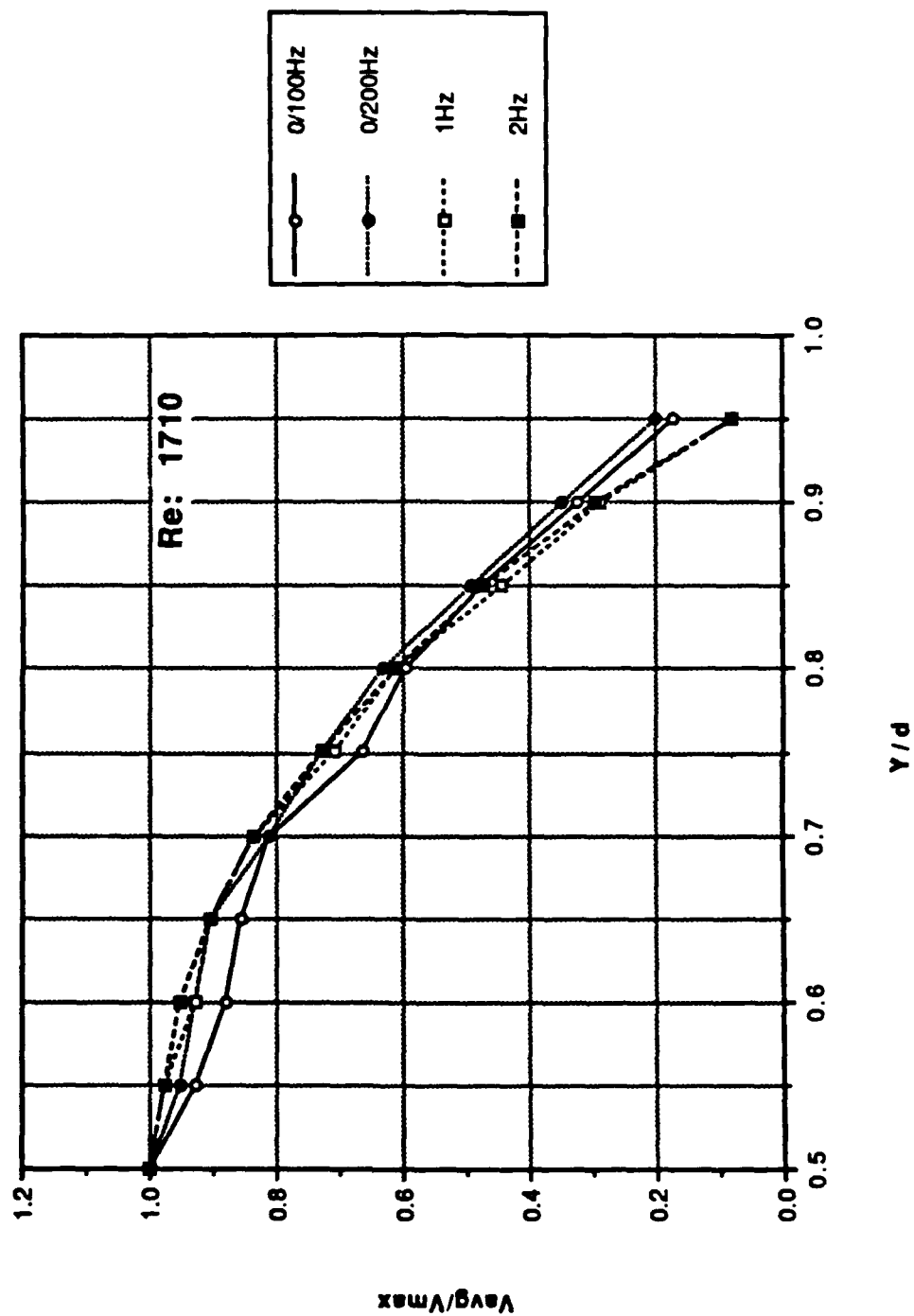


Figure 38. Profile Data: Mean Velocity Normalized by the Centerline Velocity vs y/d ; Re:1710

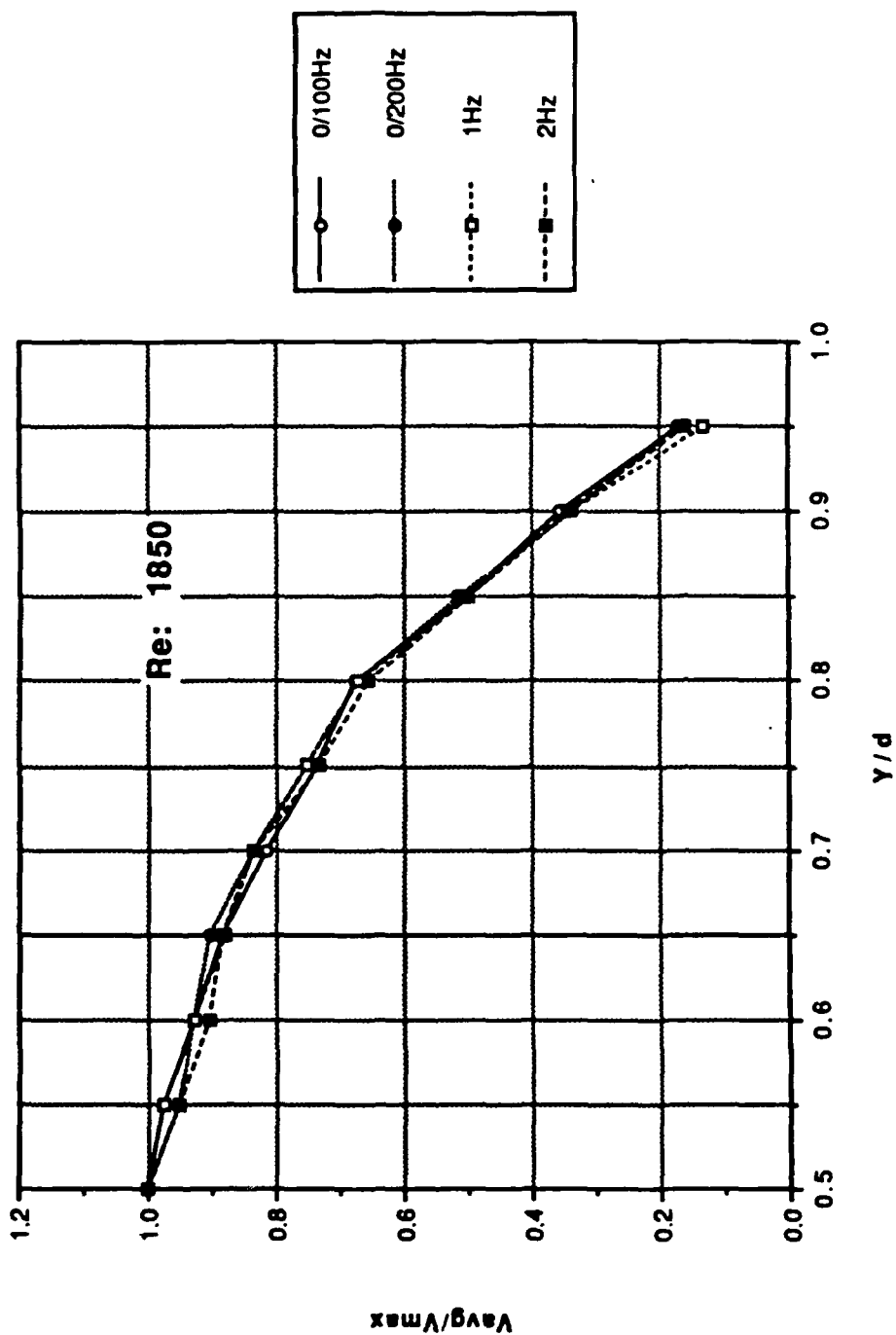


Figure 39. Profile Data: Mean Velocity Normalized by the Centerline Velocity vs y/d ; $Re: 1850$

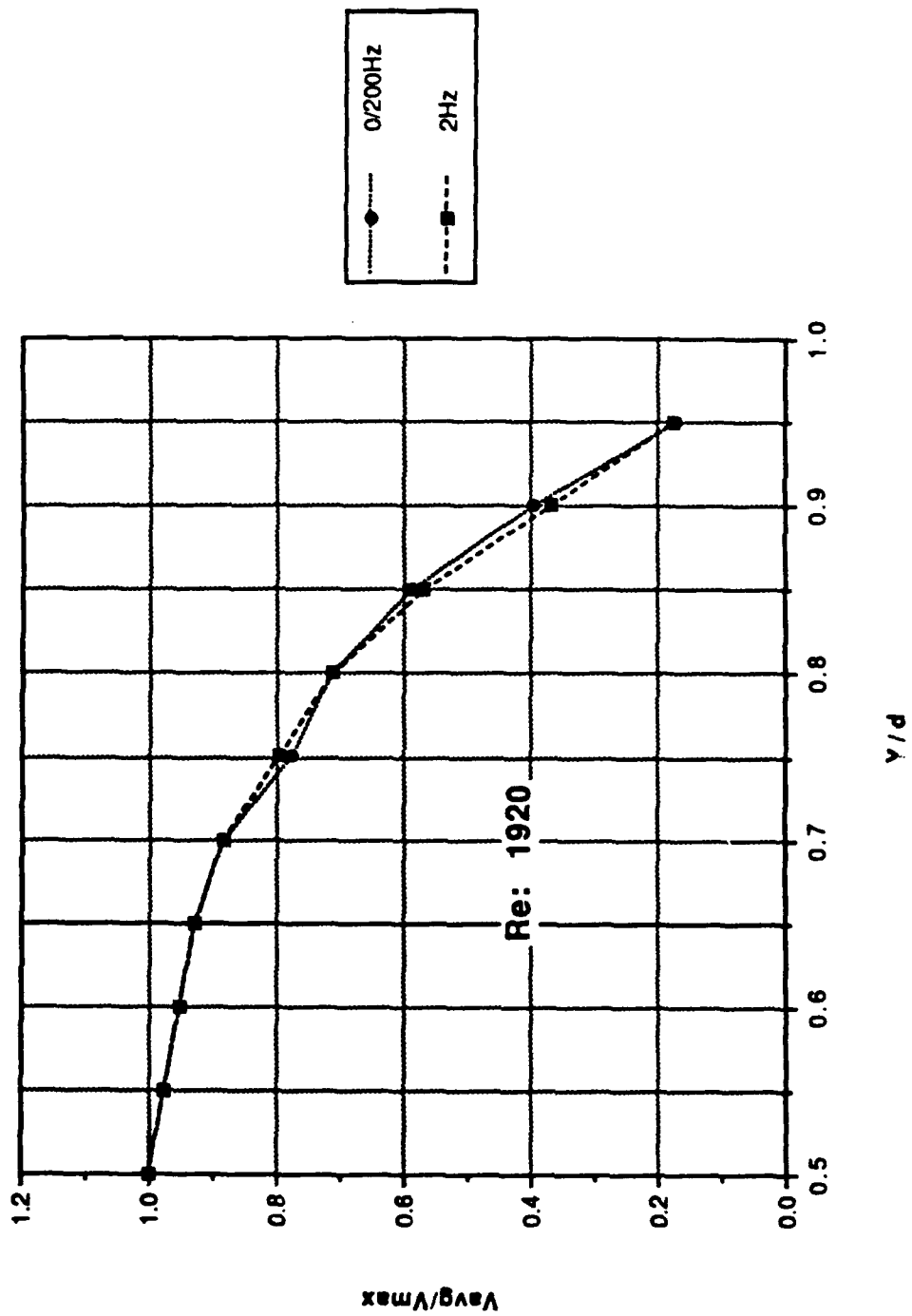


Figure 40. Profile Data: Mean Velocity Normalized by the Centerline Velocity vs y/d ; Re: 1920

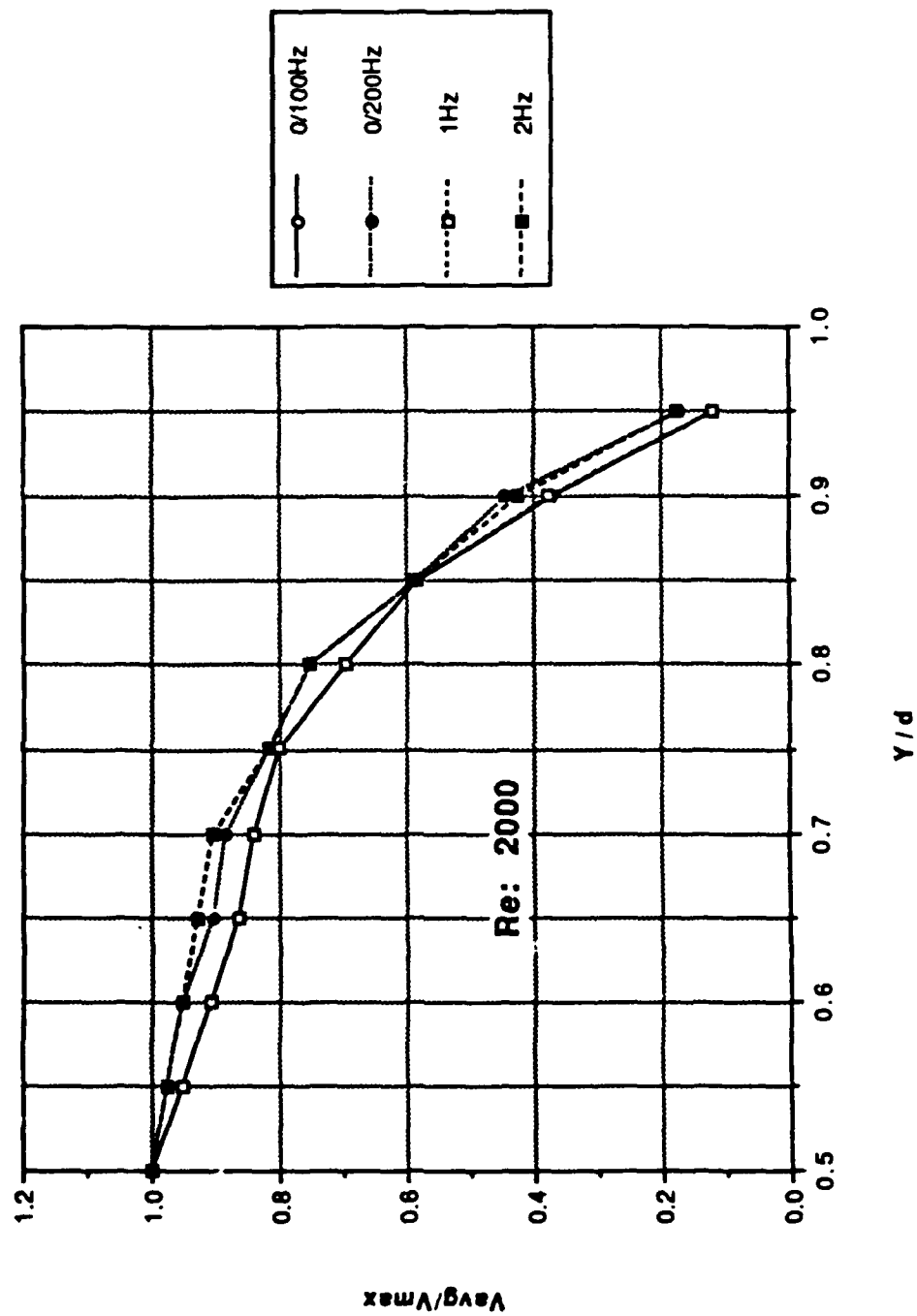


Figure 41. Profile Data: Mean Velocity Normalized by the Centerline Velocity vs y/d ; Re: 2000

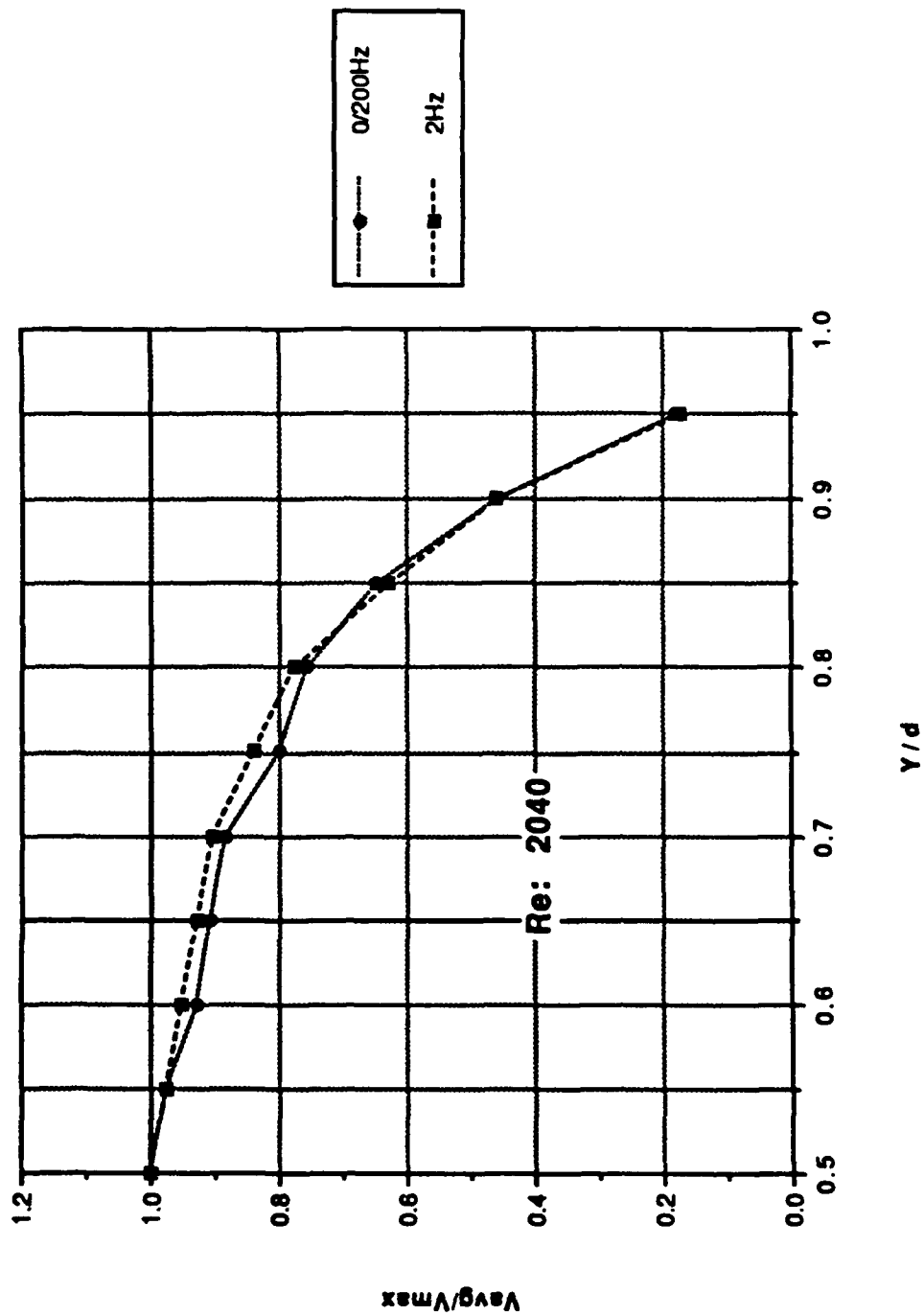


Figure 42. Profile Data: Mean Velocity Normalized by the Centerline Velocity vs y/d ; Re: 2040

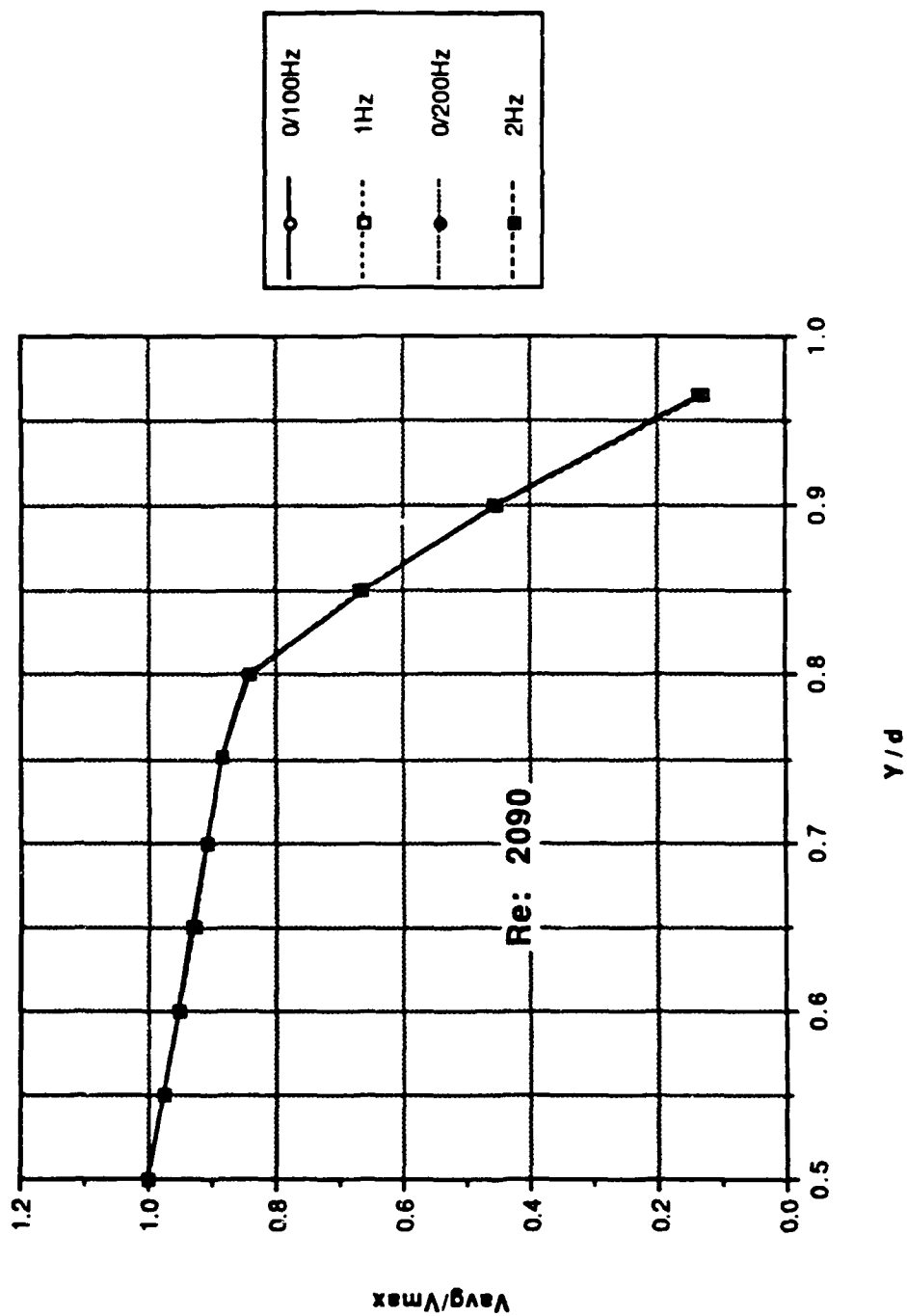


Figure 43. Profile Data: Mean Velocity Normalized by the Centerline Velocity vs y/d ; Re: 2090

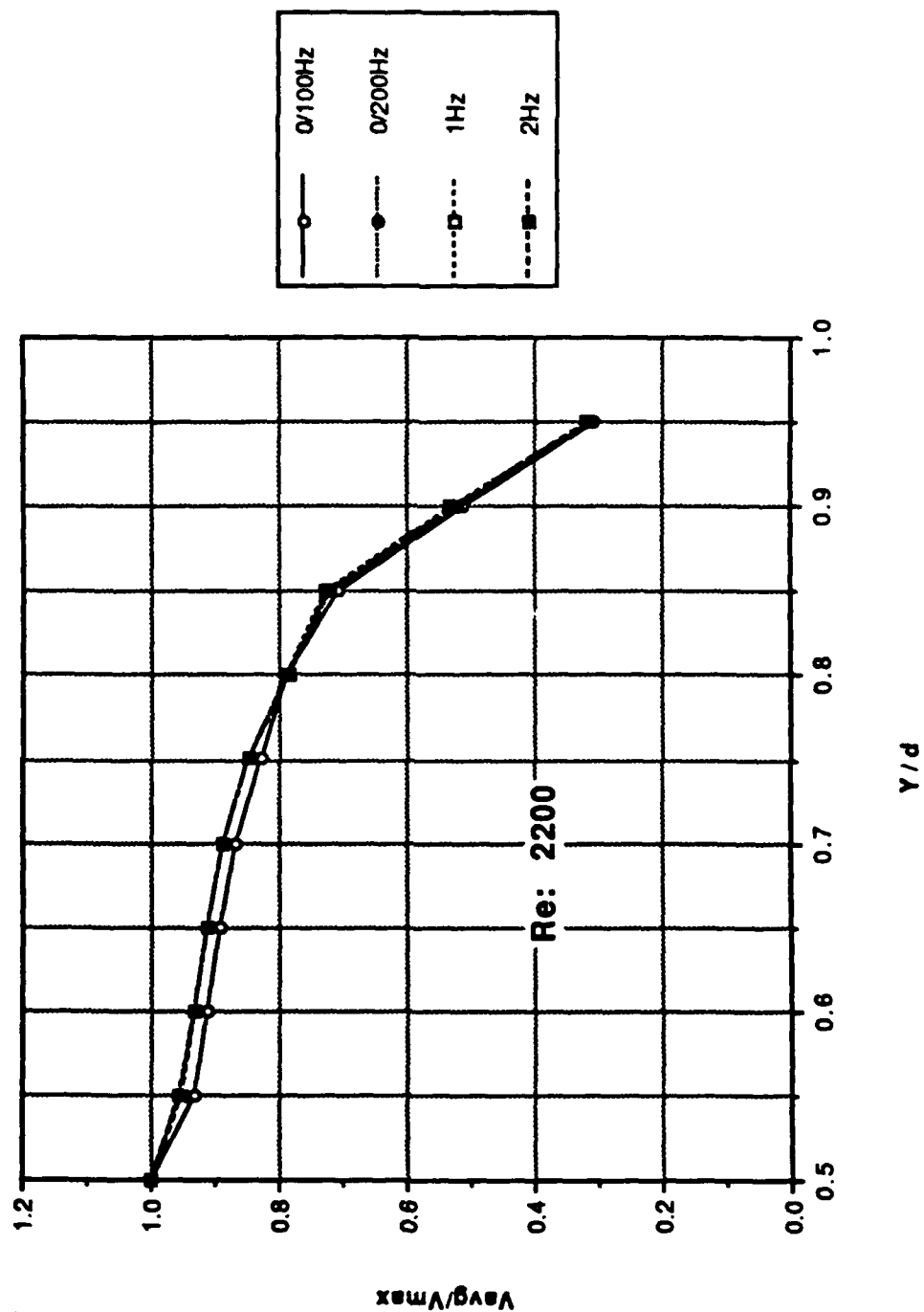


Figure 44. Profile Data: Mean Velocity Normalized by the Centerline Velocity vs y/d ; Re: 2200

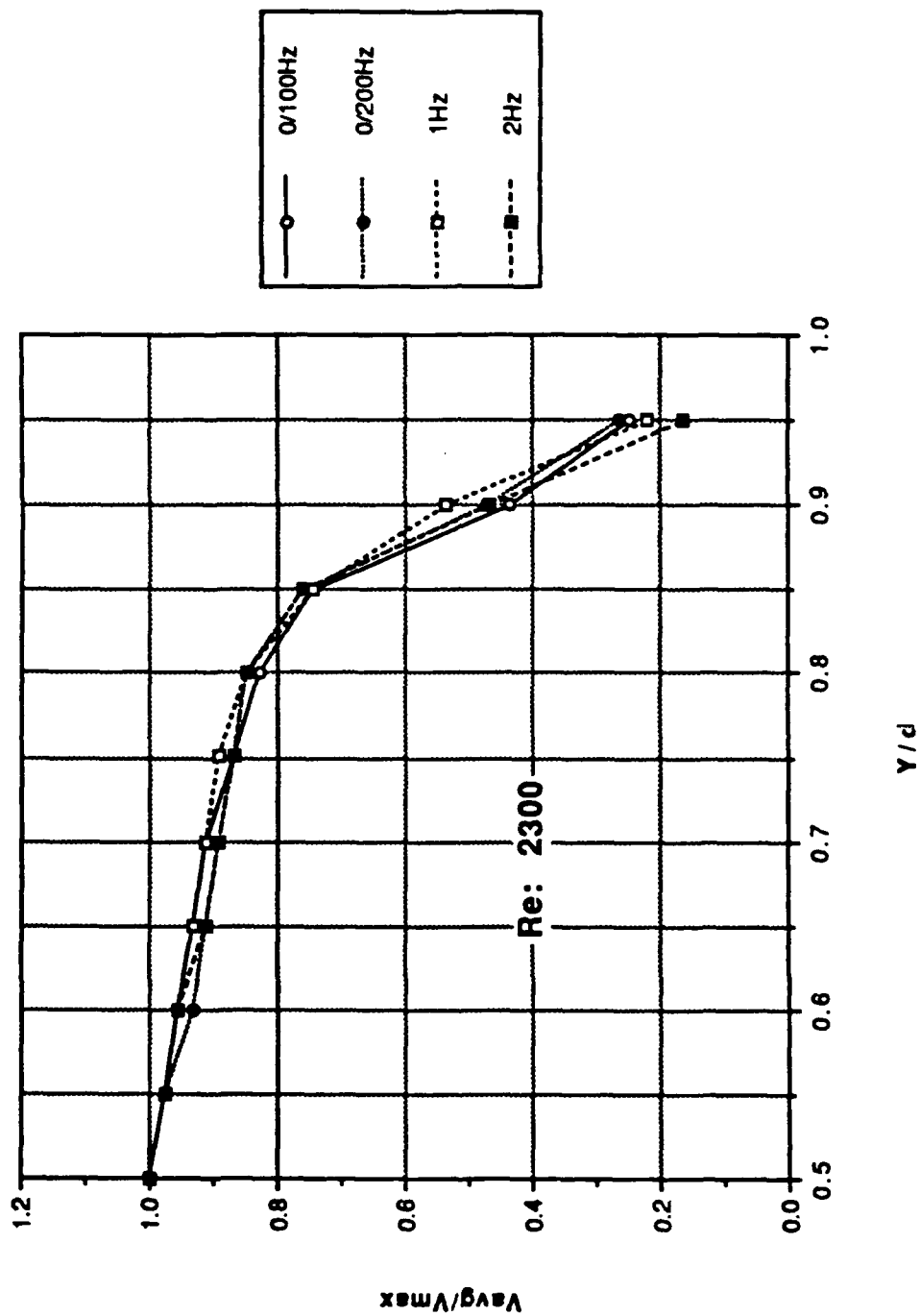


Figure 45. Profile Data: Mean Velocity Normalized by the Centerline Velocity vs y/d ; Re: 2300

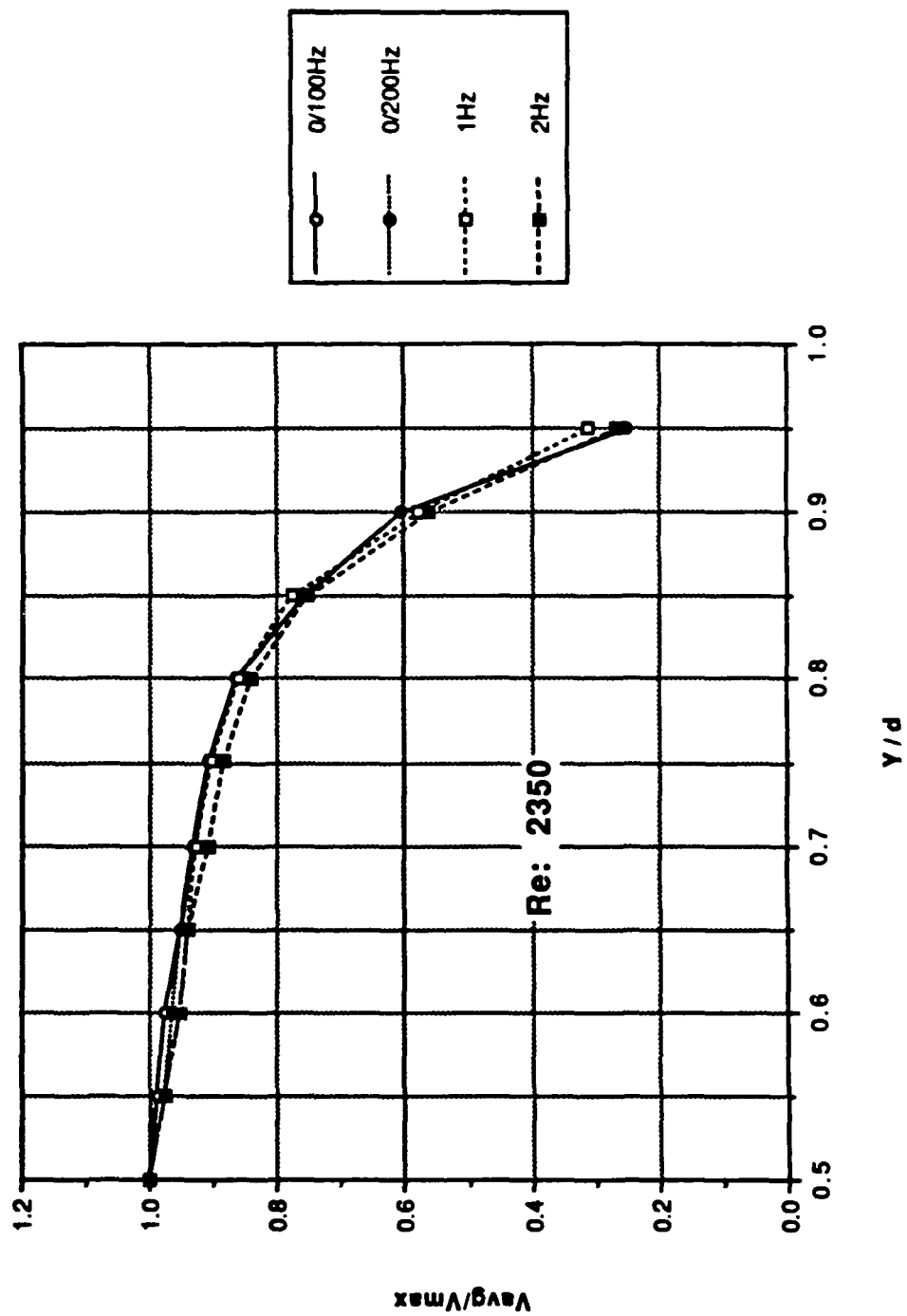


Figure 46. Profile Data: Mean Velocity Normalized by the Centerline Velocity vs y/d ; Re: 2350

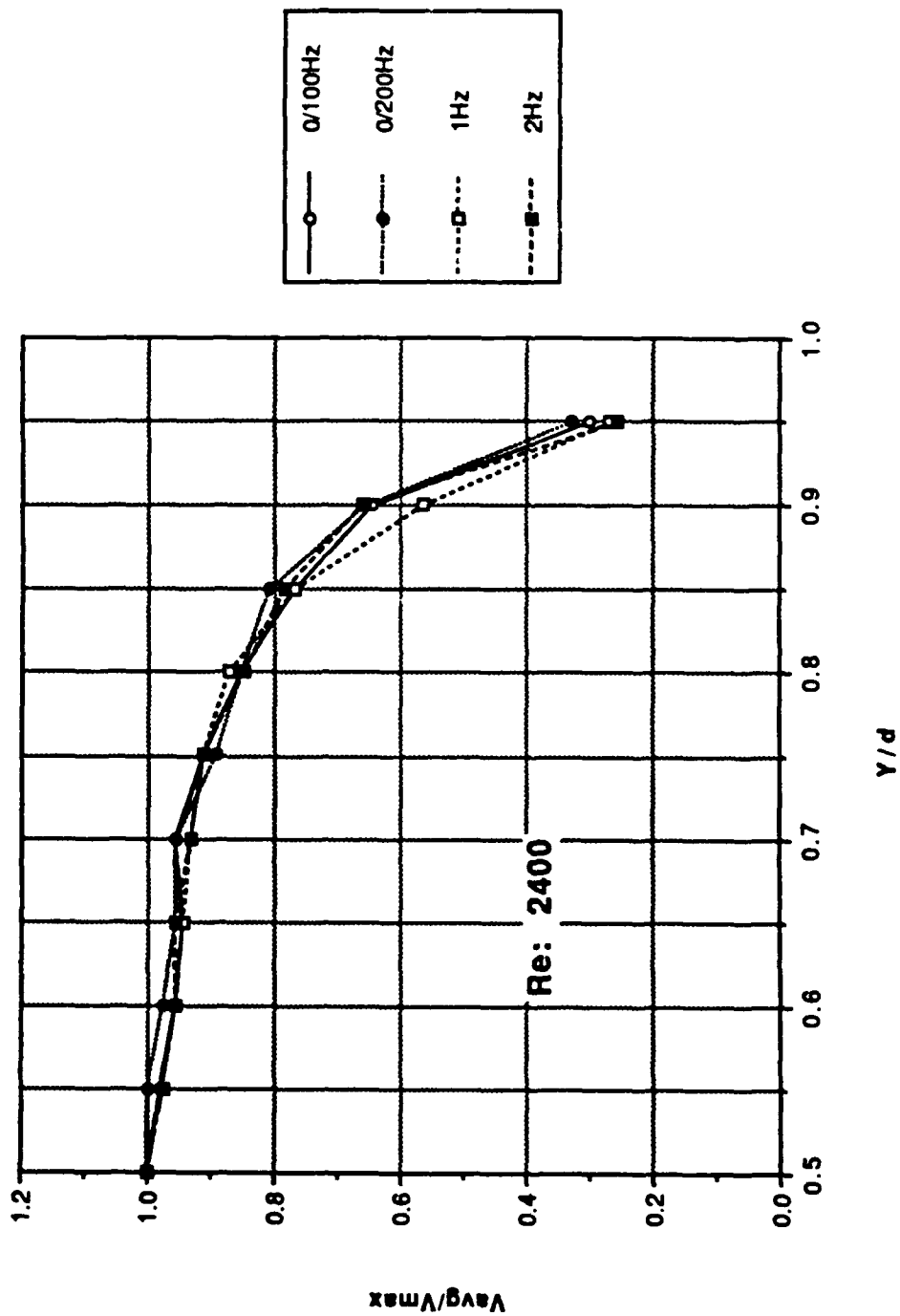


Figure 47. Profile Data: Mean Velocity Normalized by the Centerline Velocity vs y/d ; $Re: 2400$

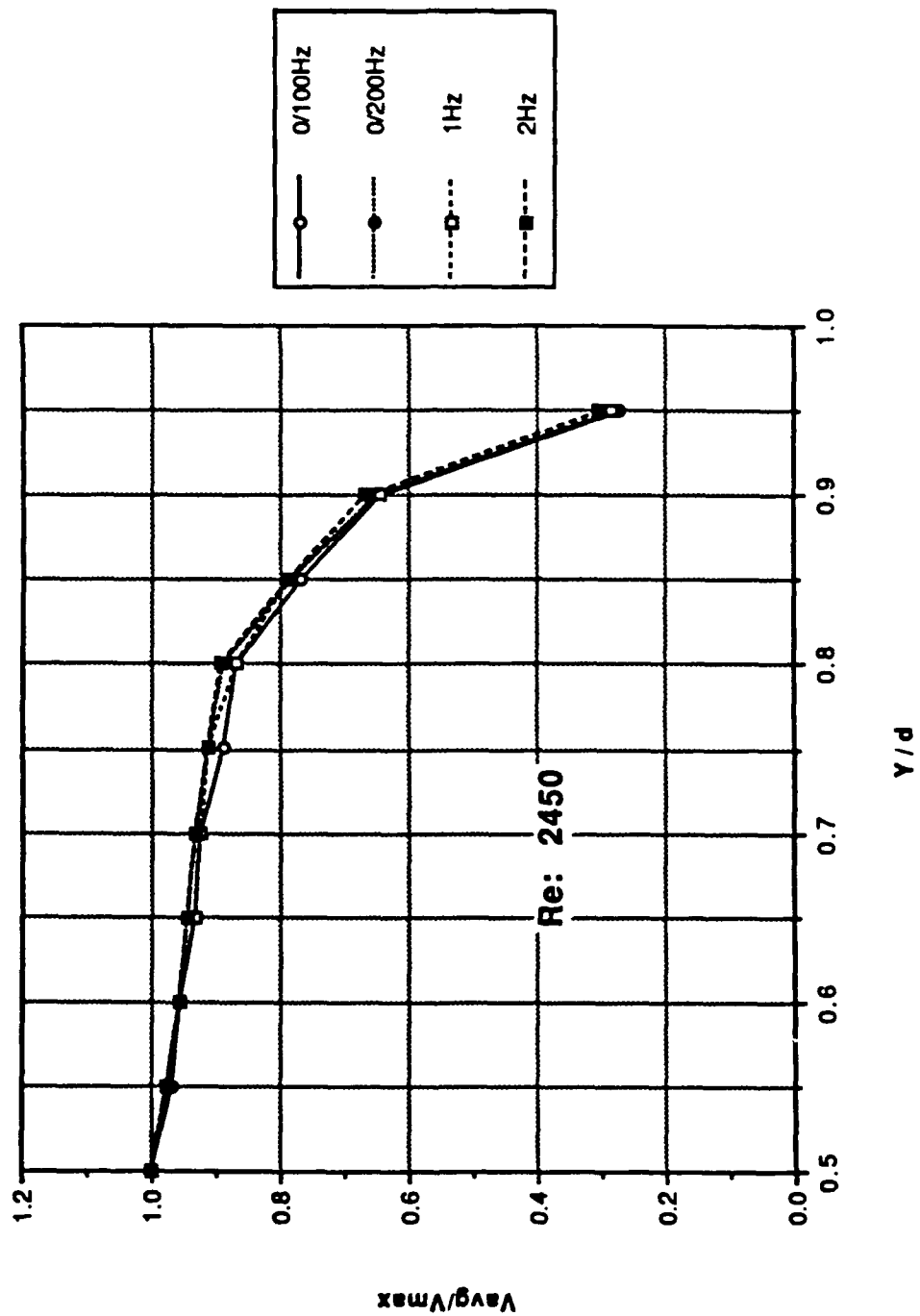


Figure 48. Profile Data: Mean Velocity Normalized by the Centerline Velocity vs y/d ; Re: 2450

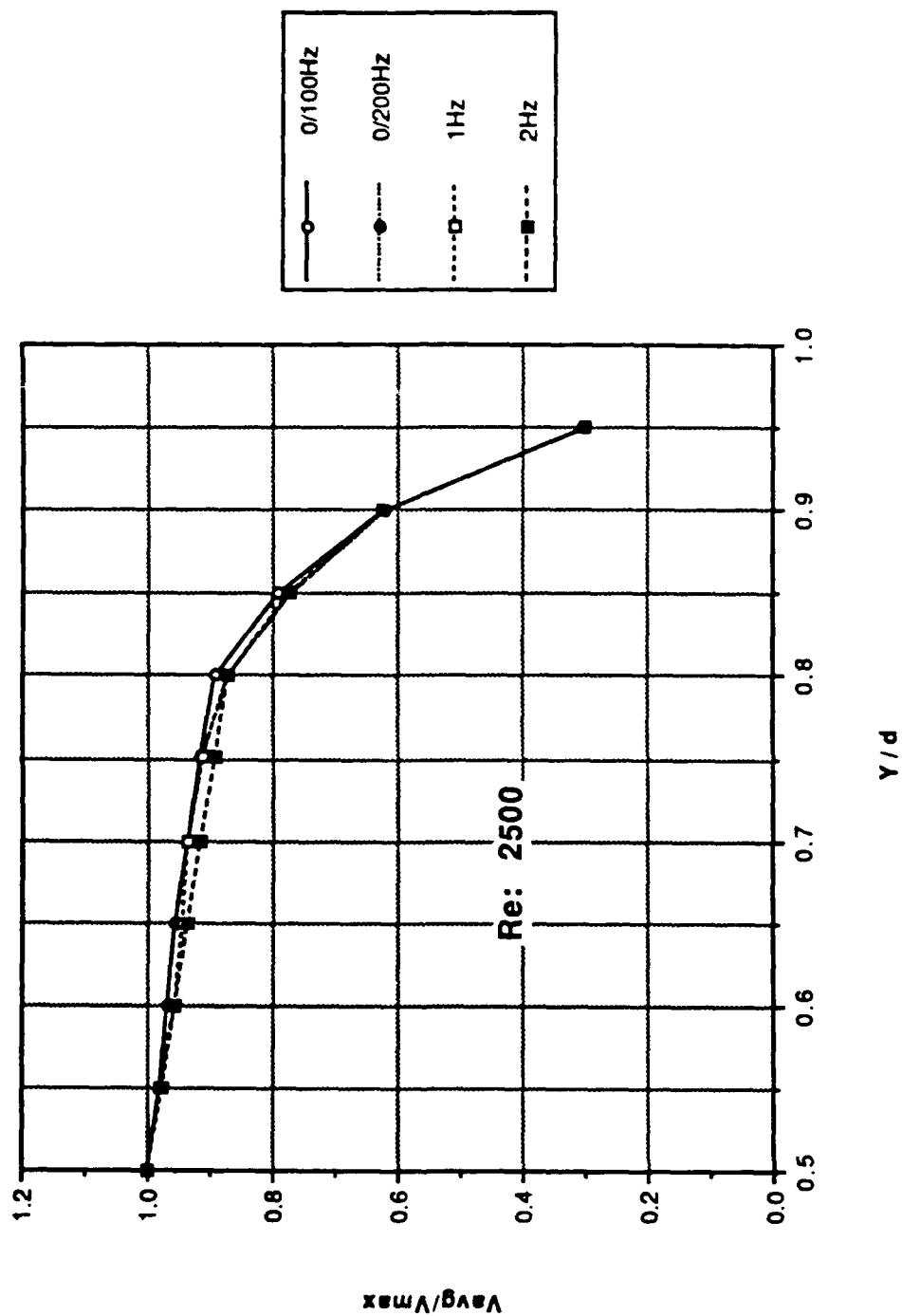


Figure 49. Profile Data: Mean Velocity Normalized by the Centerline Velocity vs y/d ; Re: 2500

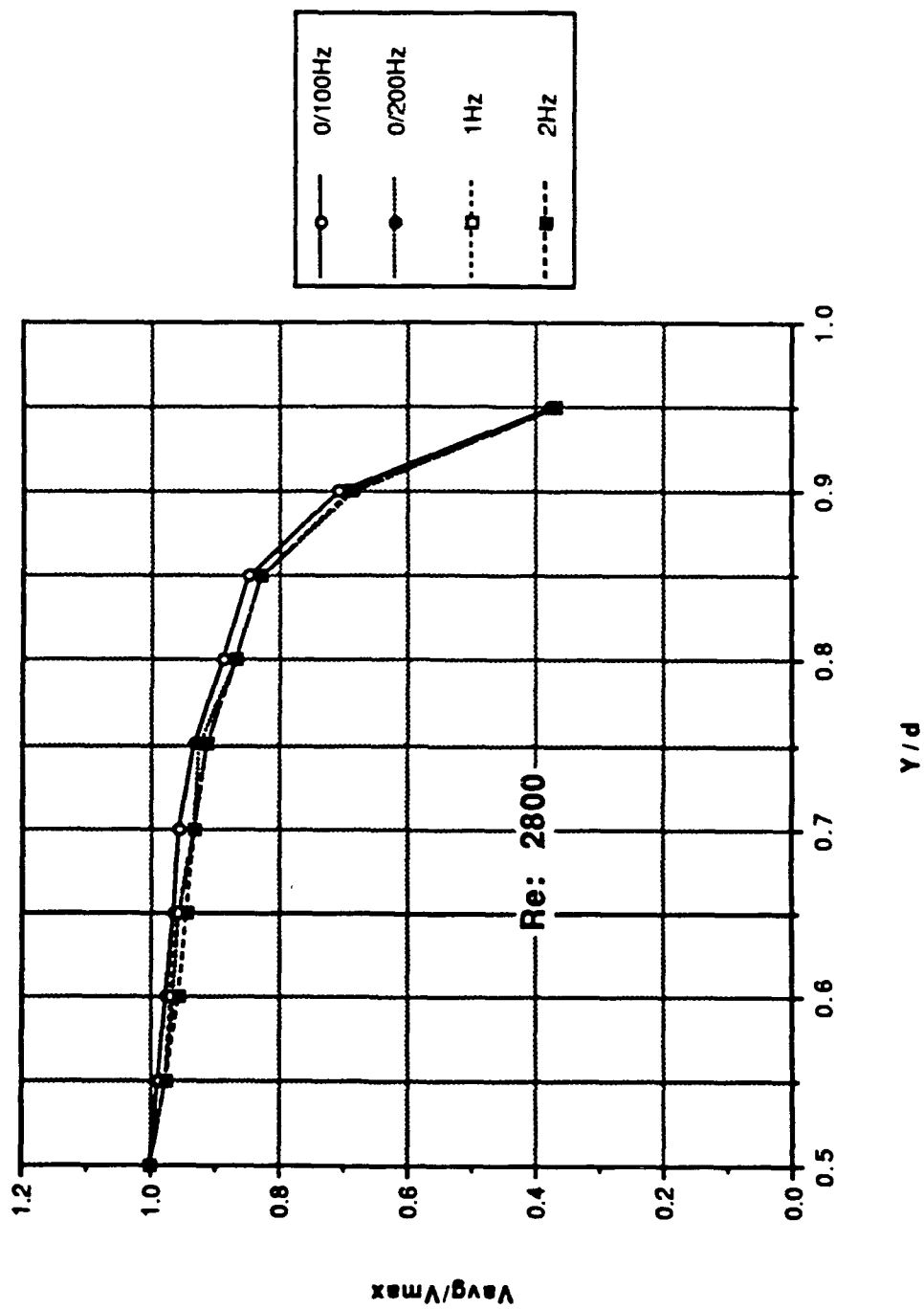


Figure 50. Profile Data: Mean Velocity Normalized by the Centerline Velocity vs y/d ; Re: 2800

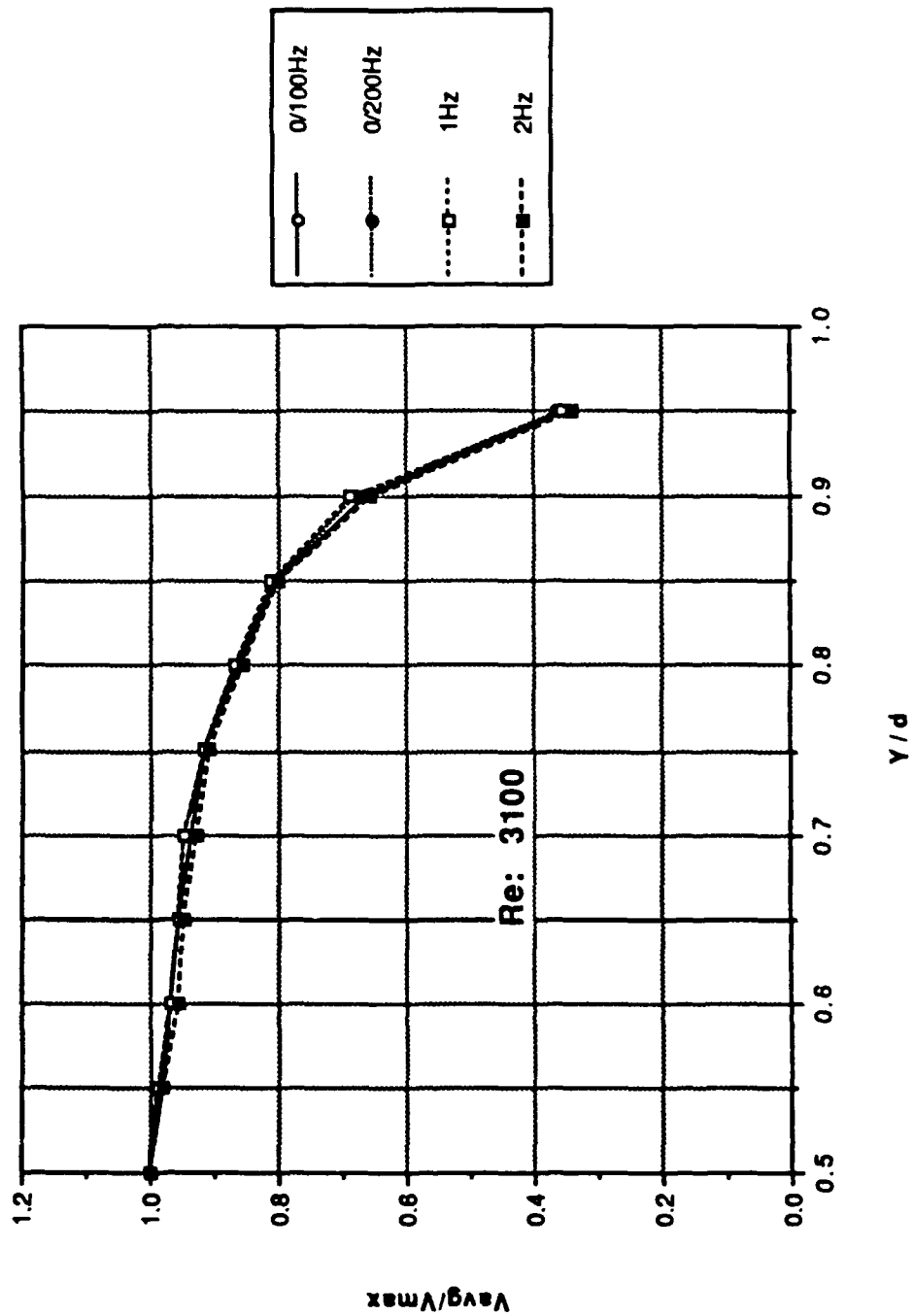


Figure 51. Profile Data: Mean Velocity Normalized by the Centerline Velocity vs y/d ; Re: 3100

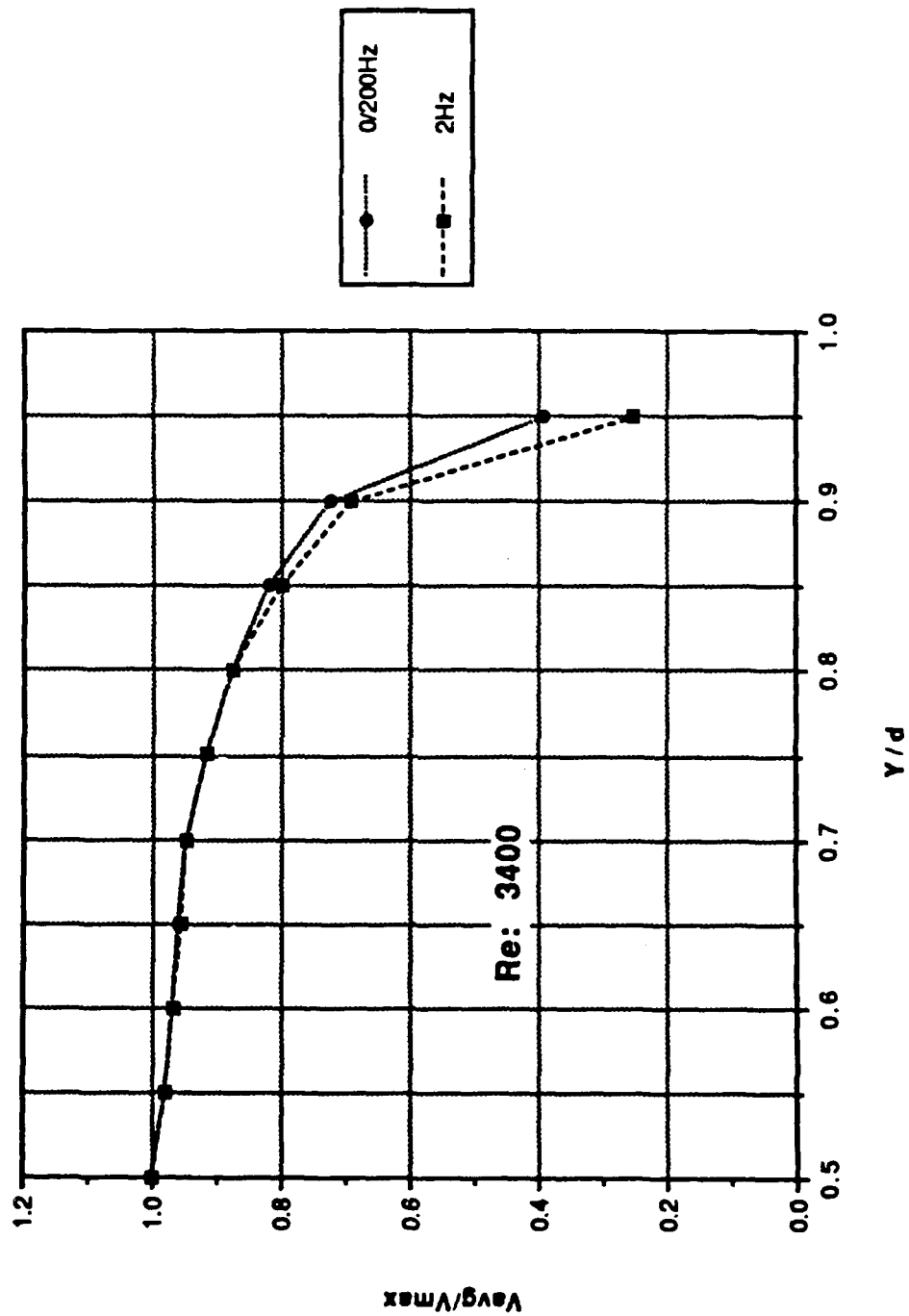


Figure 52. Profile Data: Mean Velocity Normalized by the Centerline Velocity vs y/d ; Re: 3400

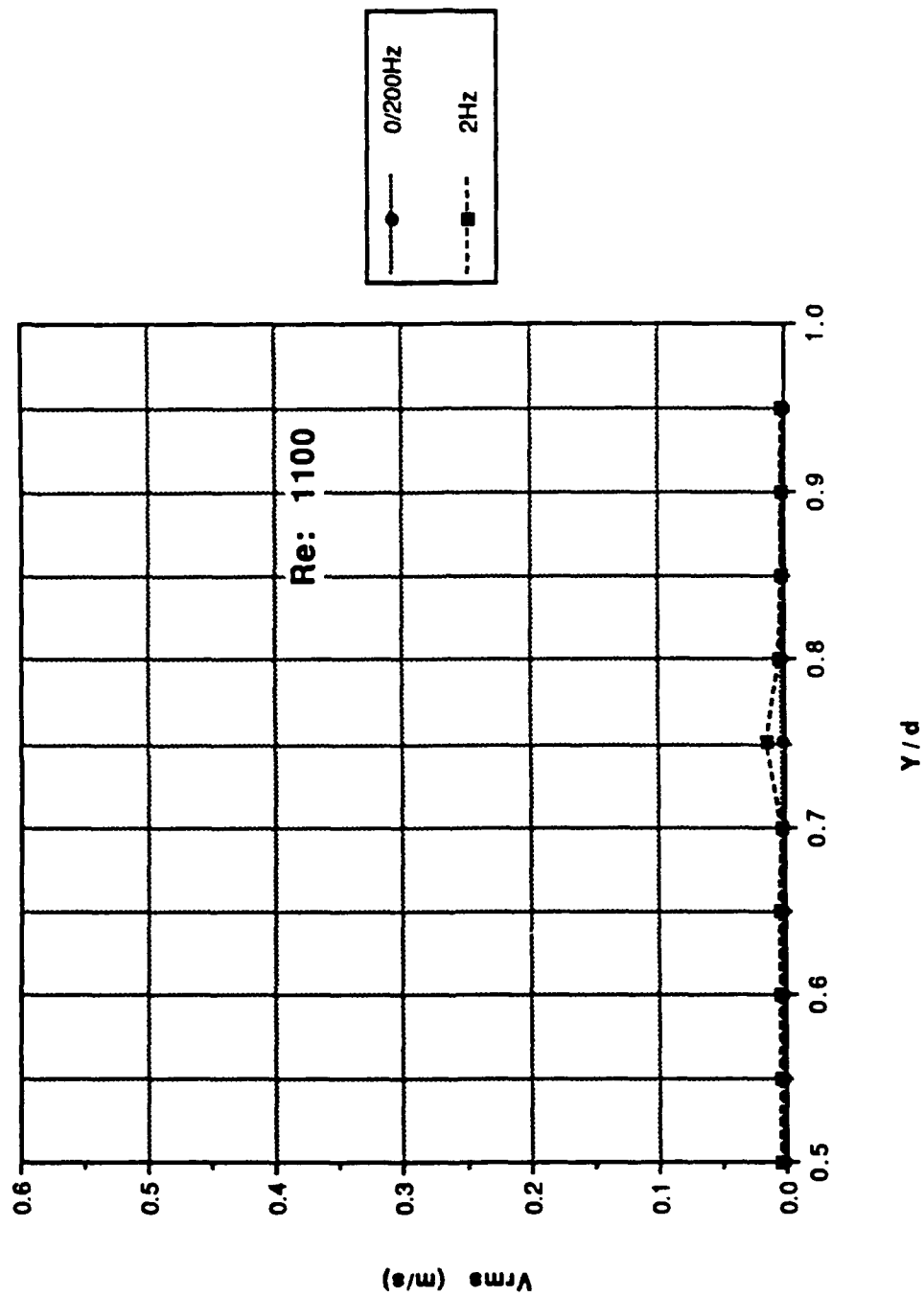


Figure 53. Profile Data: Longitudinal Trubulence Intensity vs y/d; Re: 1100

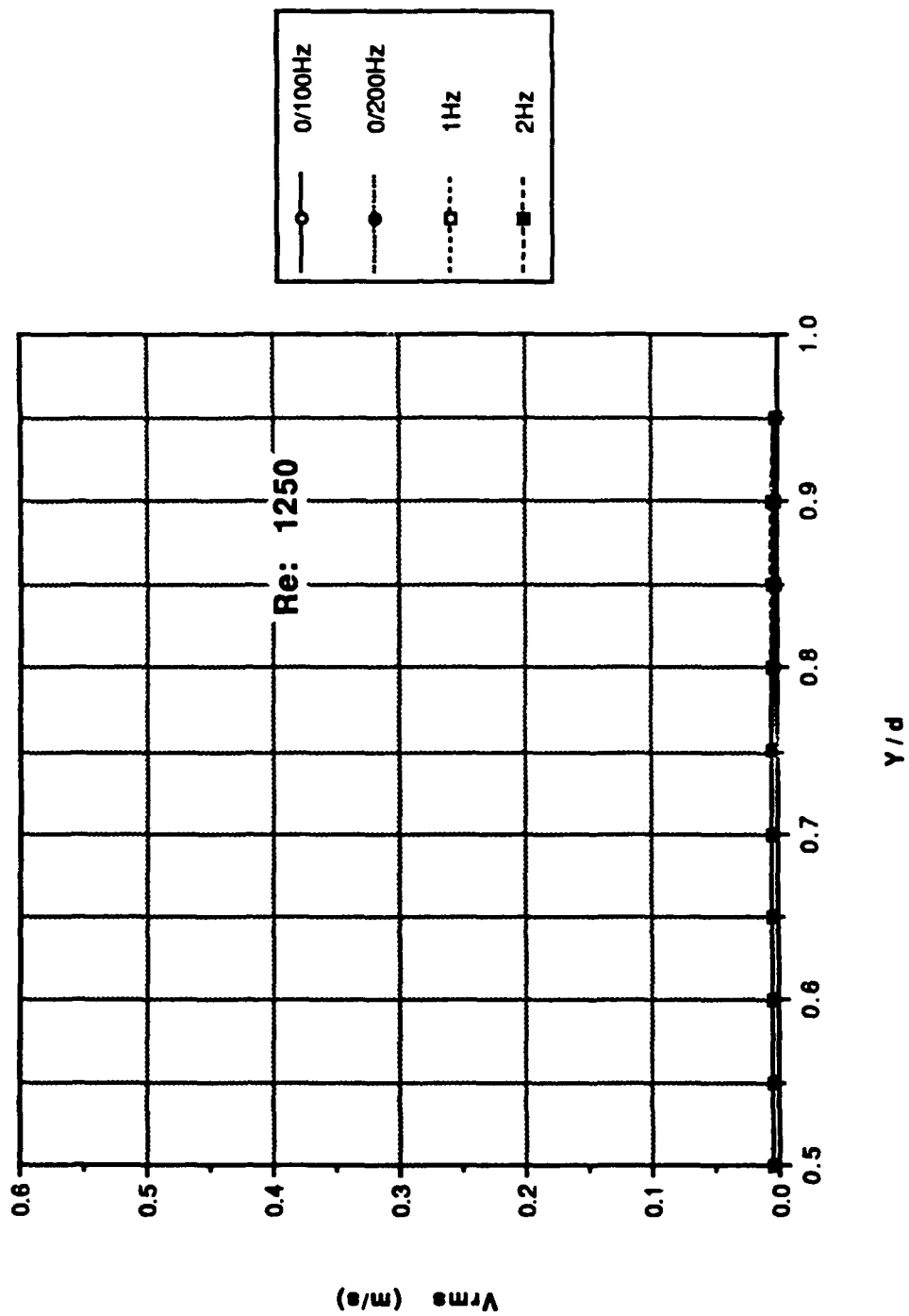


Figure 54. Profile Data: Longitudinal Turbulence Intensity vs y/d; Re: 1250

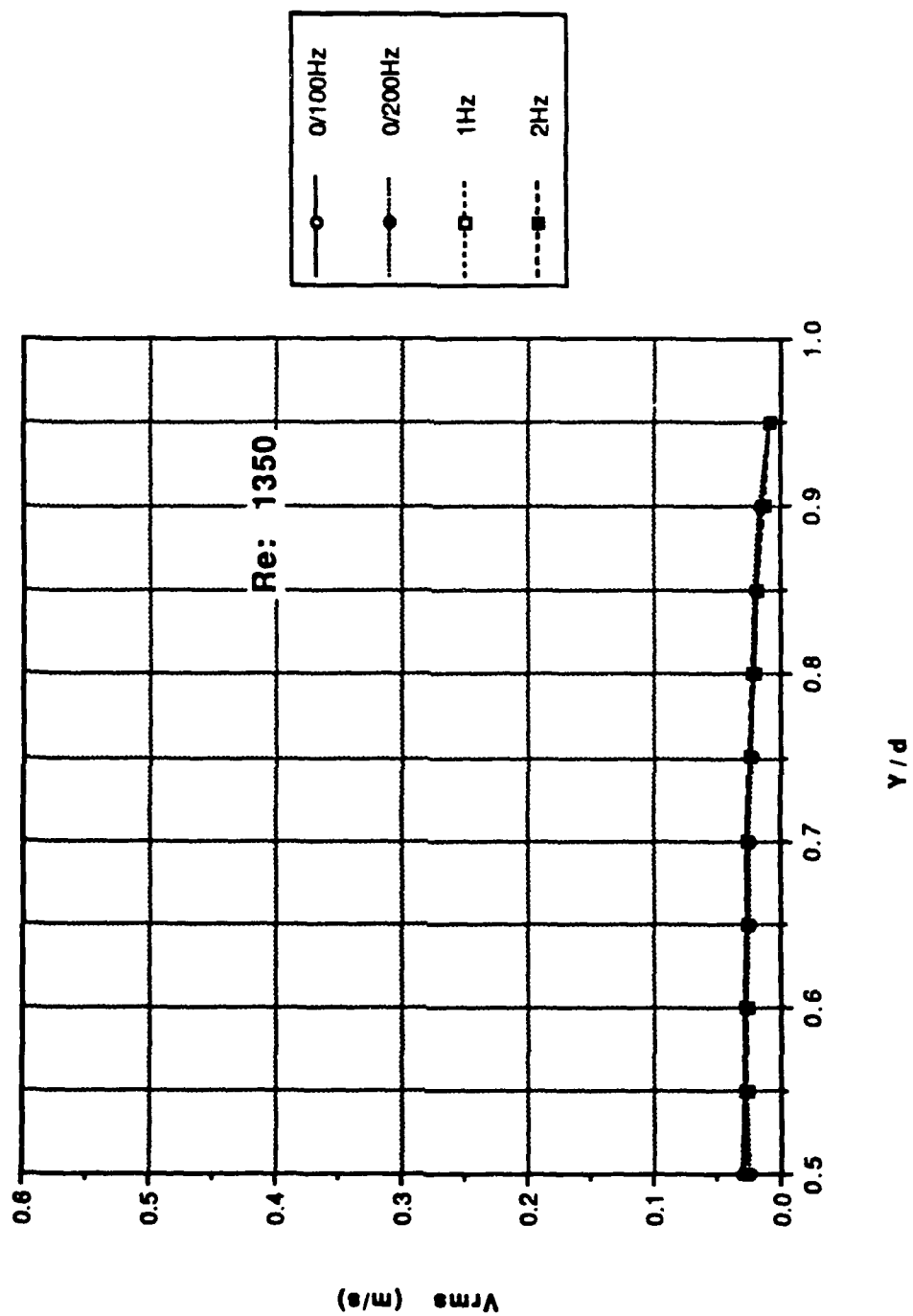


Figure 55. Profile Data: Longitudinal Turbulence Intensity vs y/d; Re: 1350

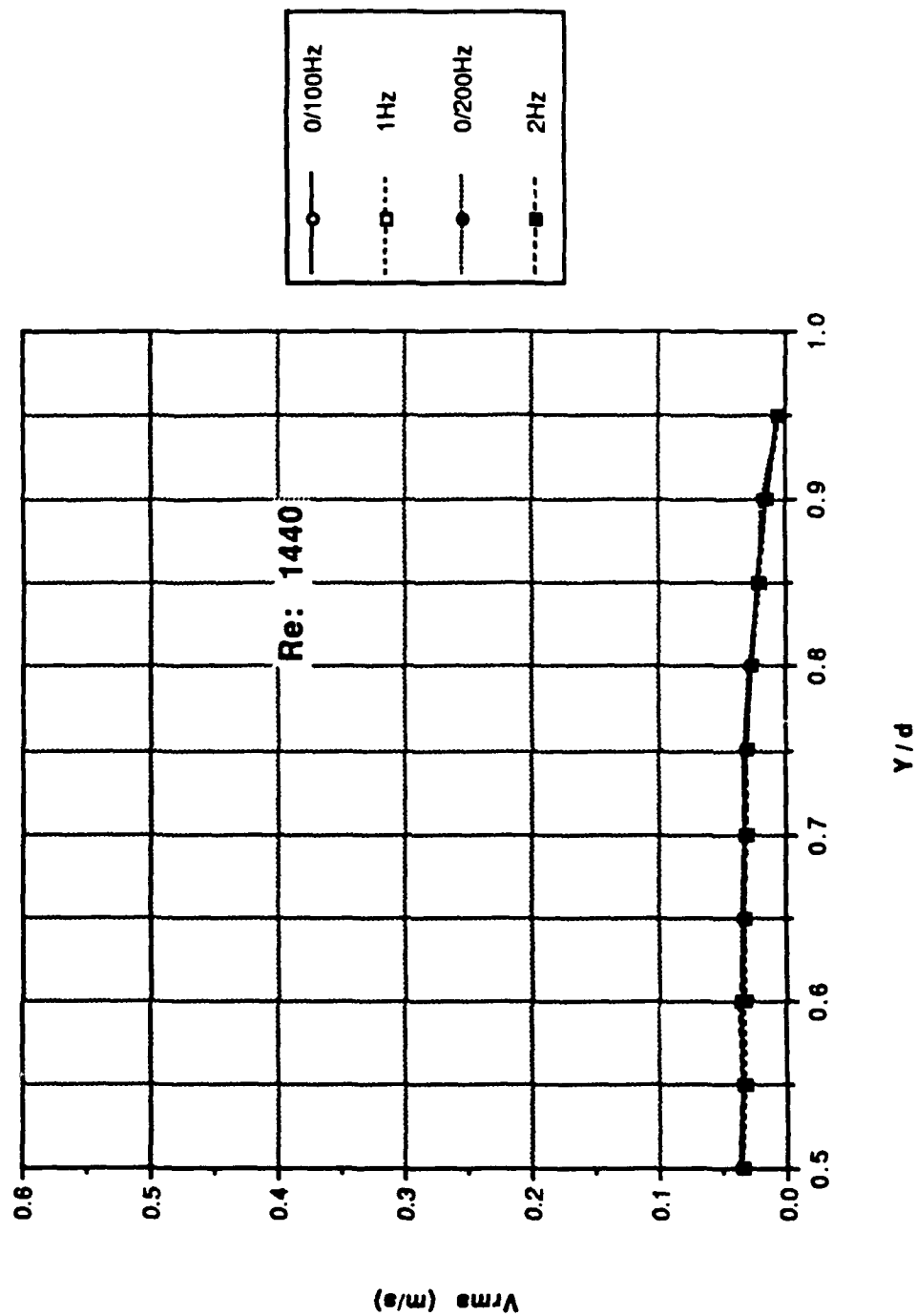


Figure 56. Profile Data: Longitudinal Turbulence Intensity vs y/d ; Re: 1440

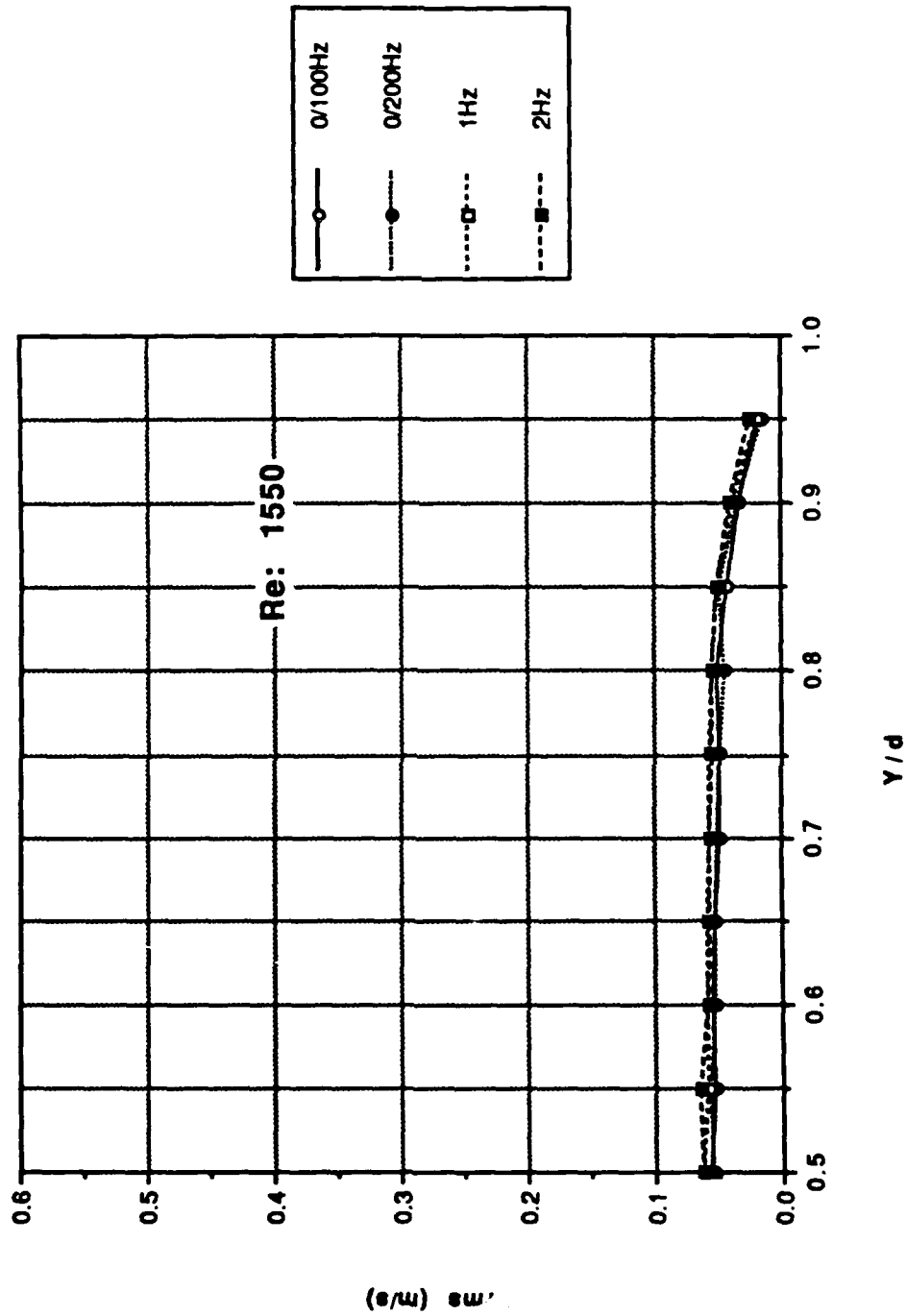


Figure 57. Profile Data: Longitudinal Turbulence Intensity vs y/d; Re: 1550

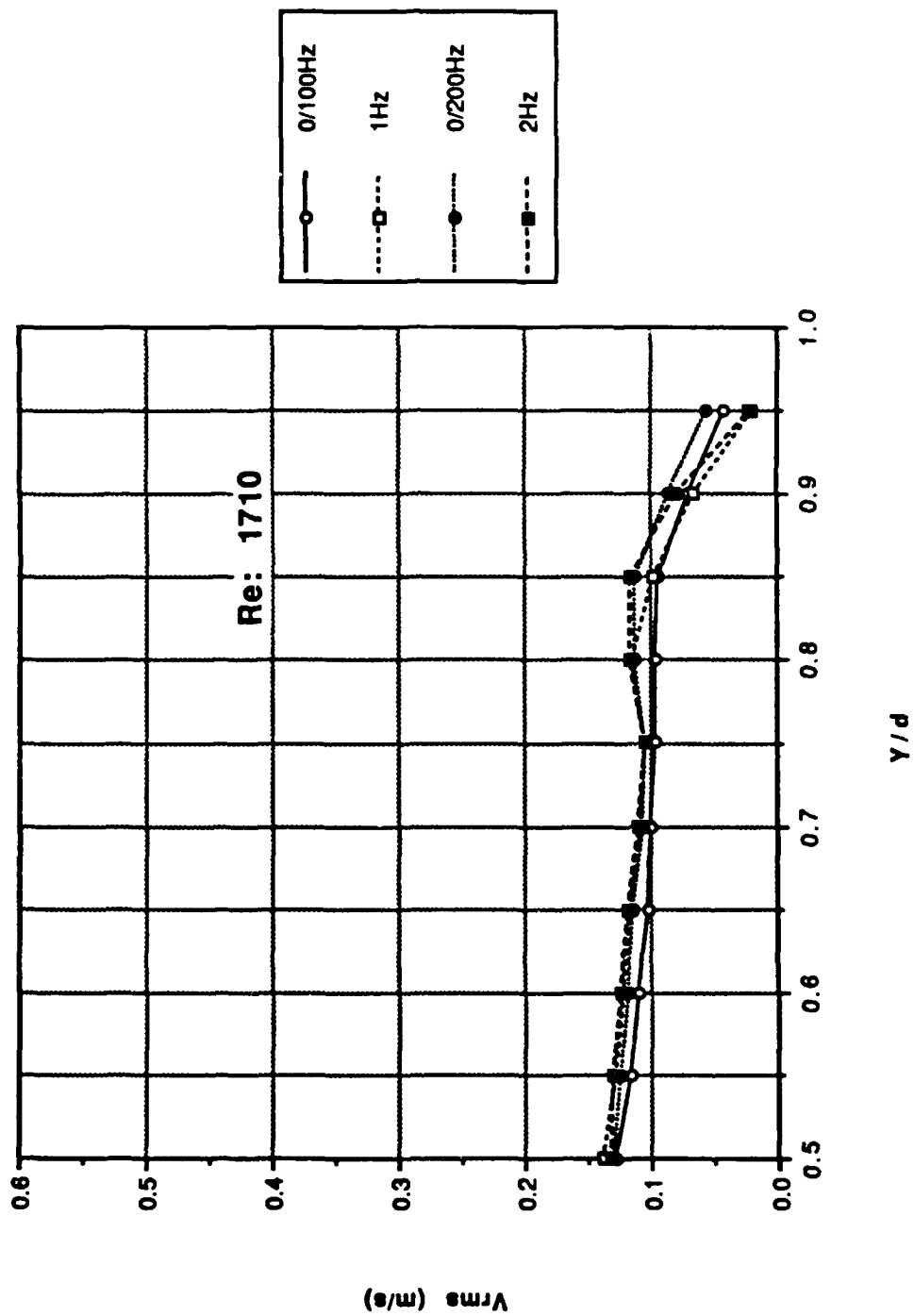


Figure 58. Profile Data: Longitudinal Turbulence Intensity vs y/d ; Re: 1710

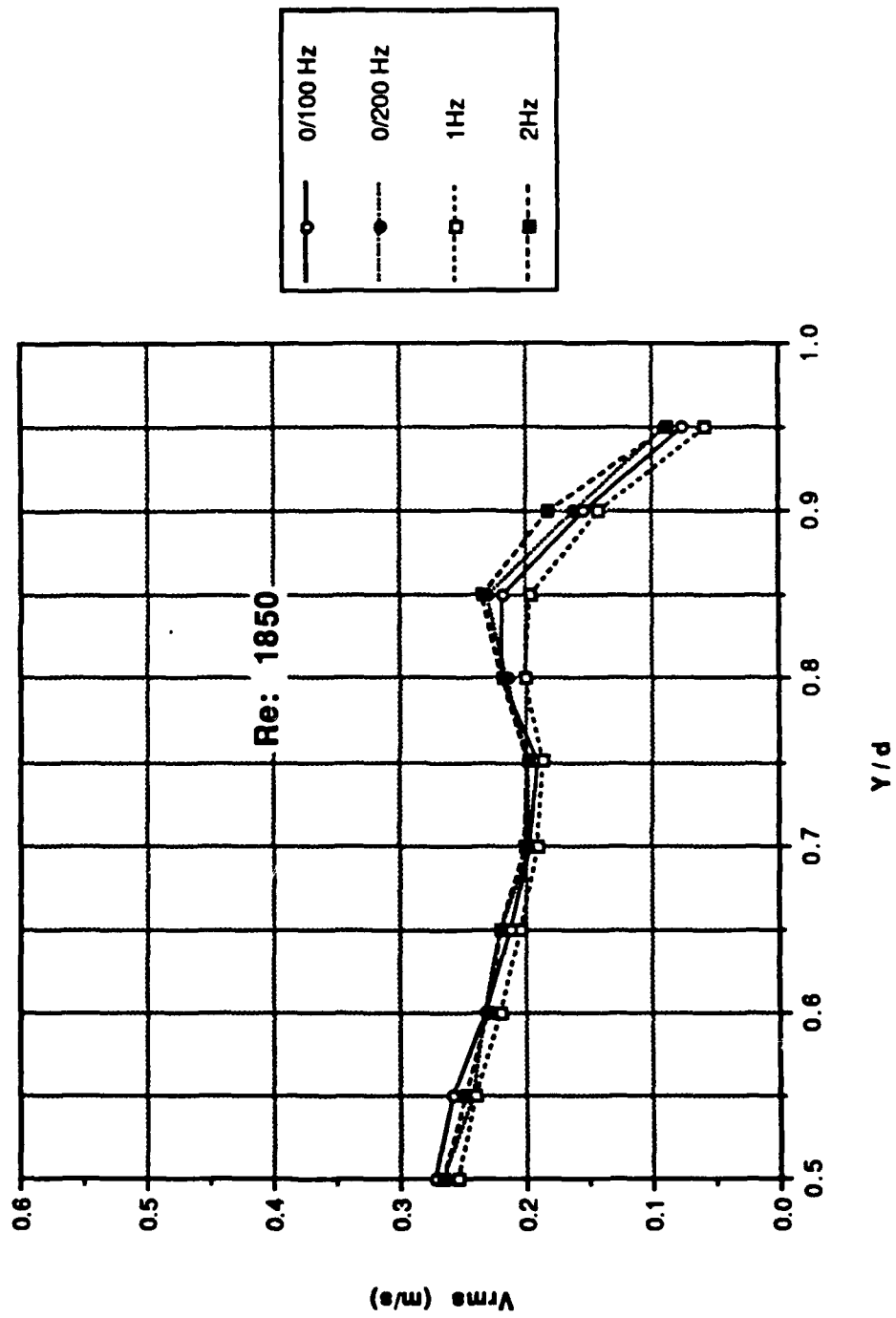


Figure 59. Profile Data: Longitudinal Turbulence Intensity vs y/d ; Re: 1850

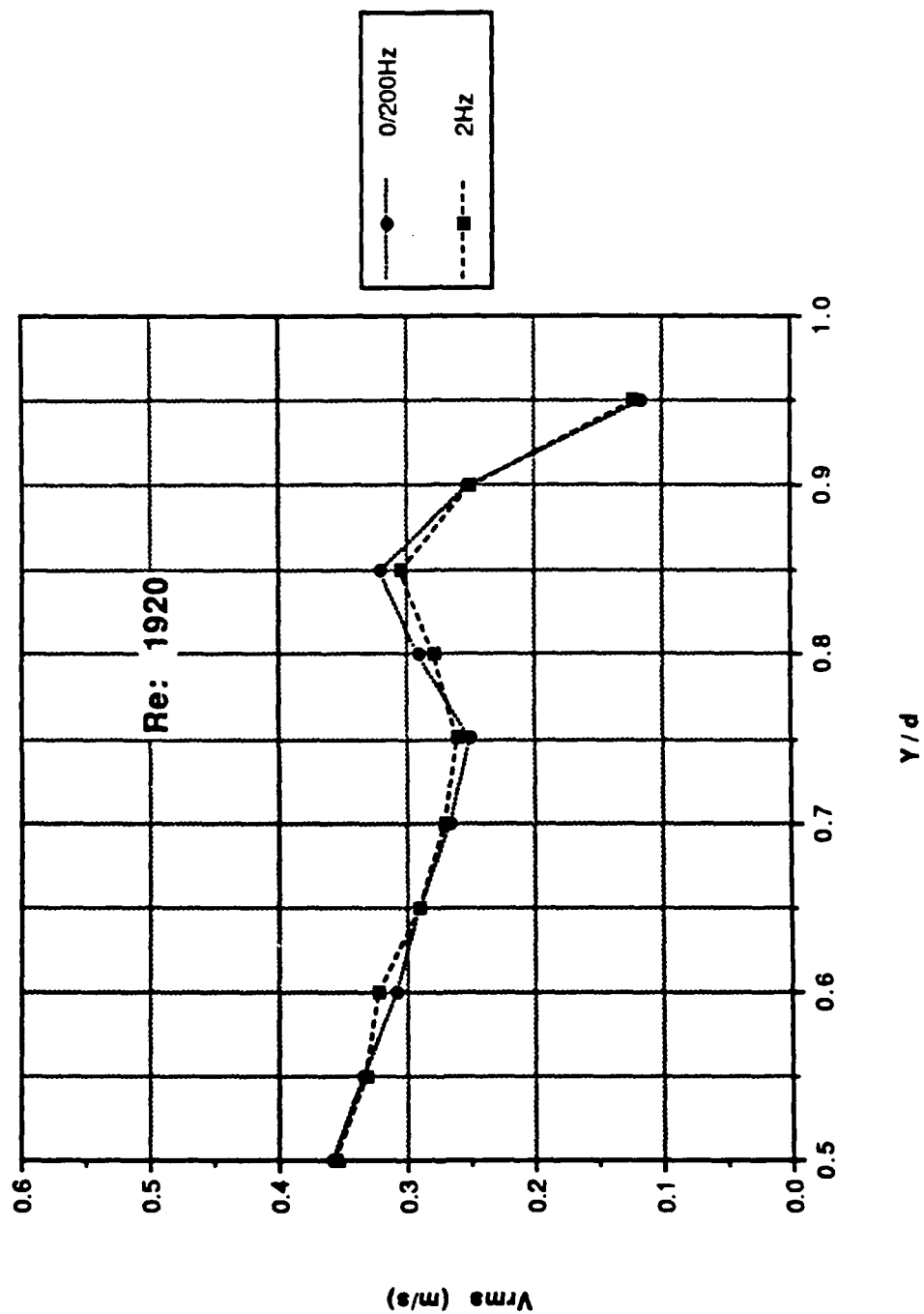


Figure 60. Profile Data: Longitudinal Turbulence Intensity vs y/d ; Re: 1920

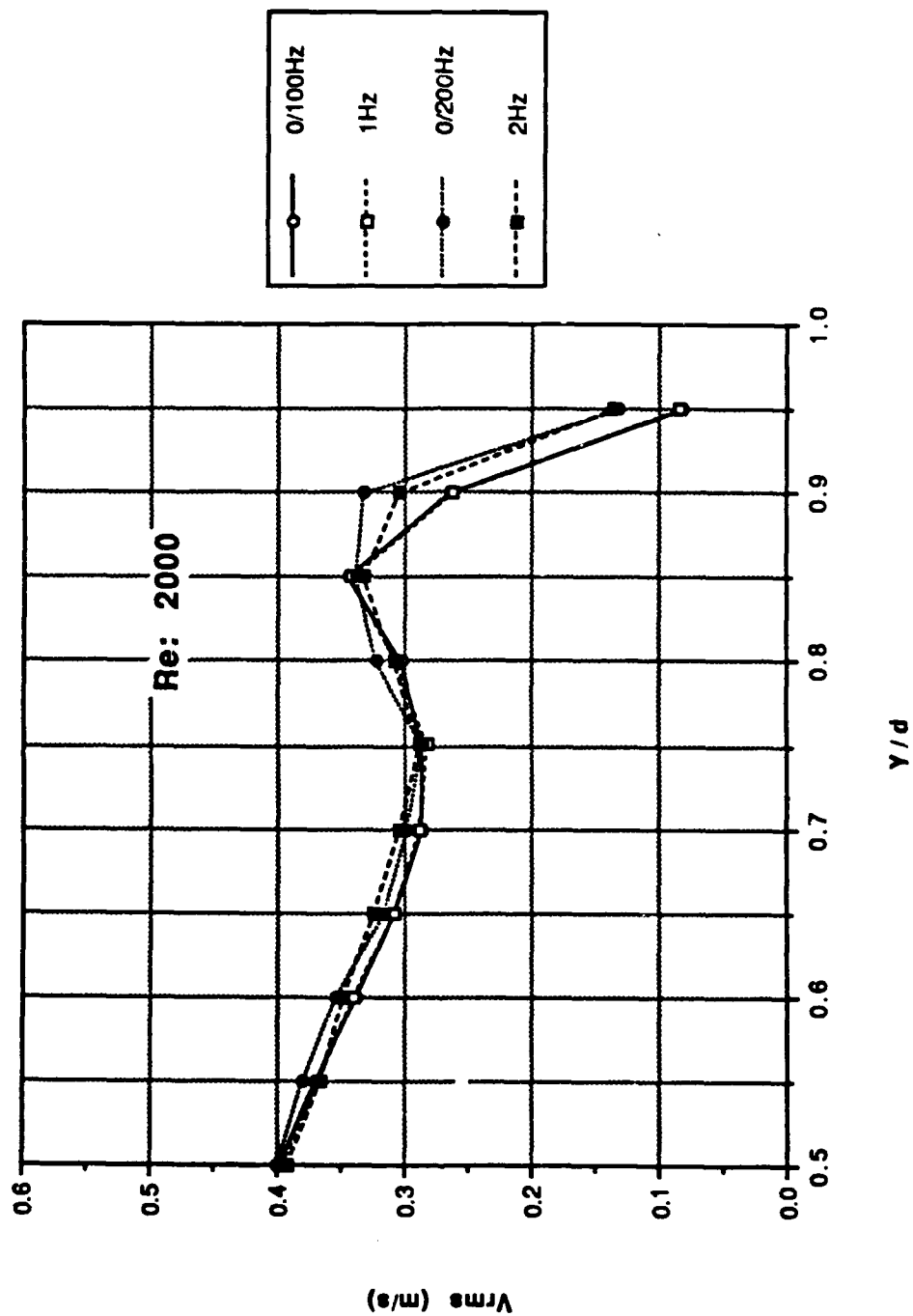


Figure 61. Profile Data: Longitudinal Turbulence Intensity vs y/d ; Re: 2000

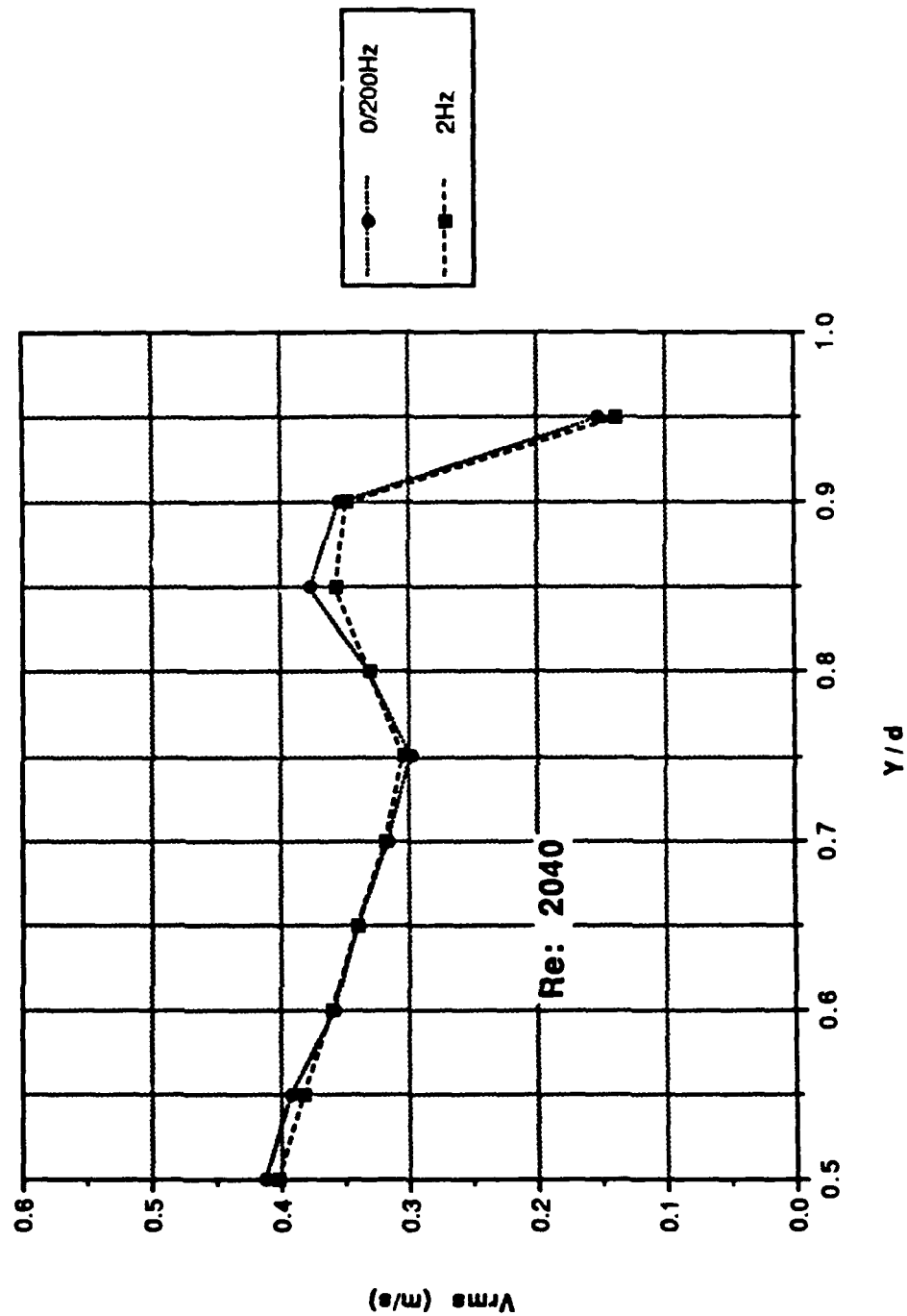


Figure 62. Profile Data: Longitudinal Turbulence Intensity vs y/d ; Re: 2040

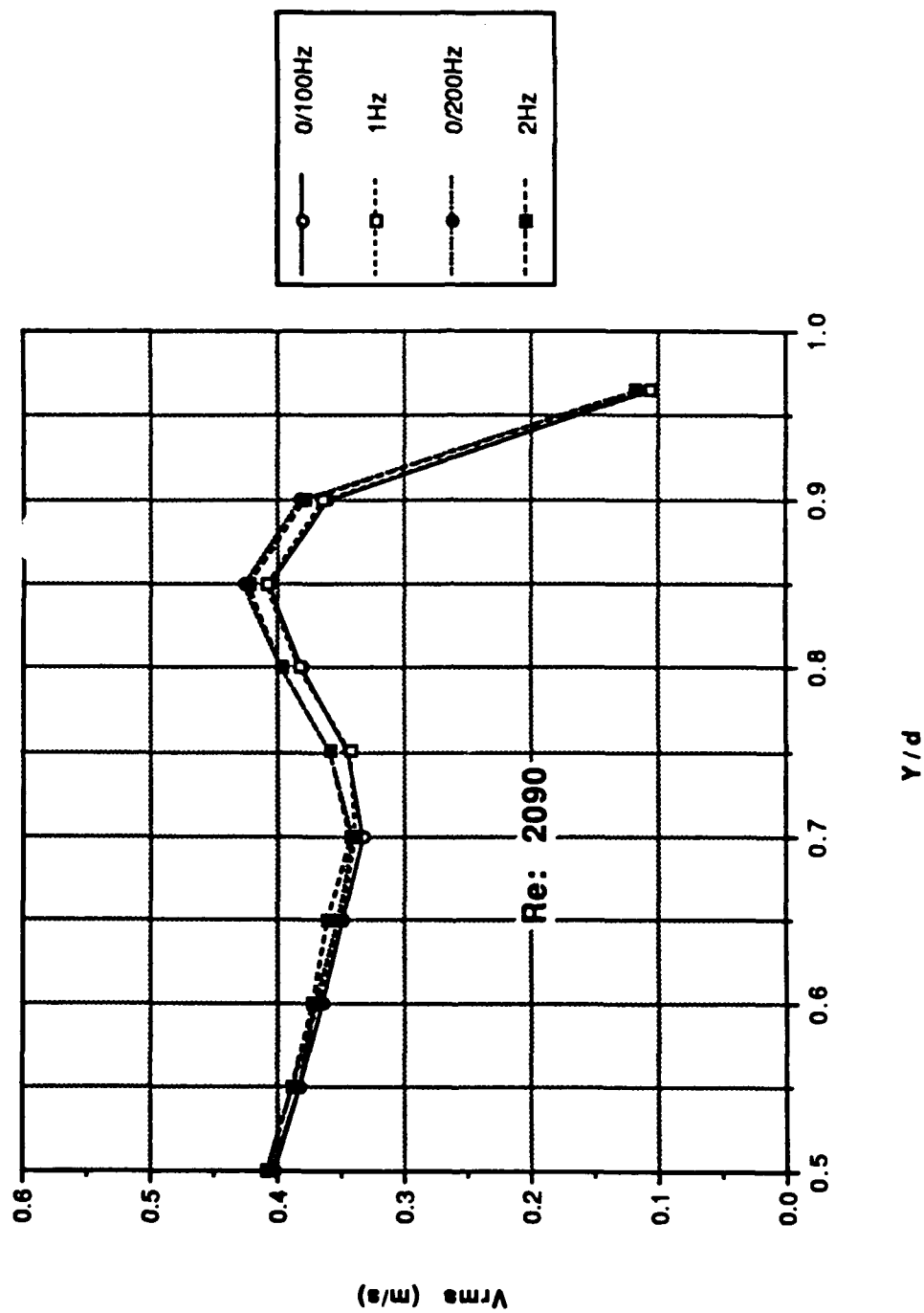


Figure 63. Profile Data: Longitudinal Trubulence Intensity vs y/d ; Re: 2090

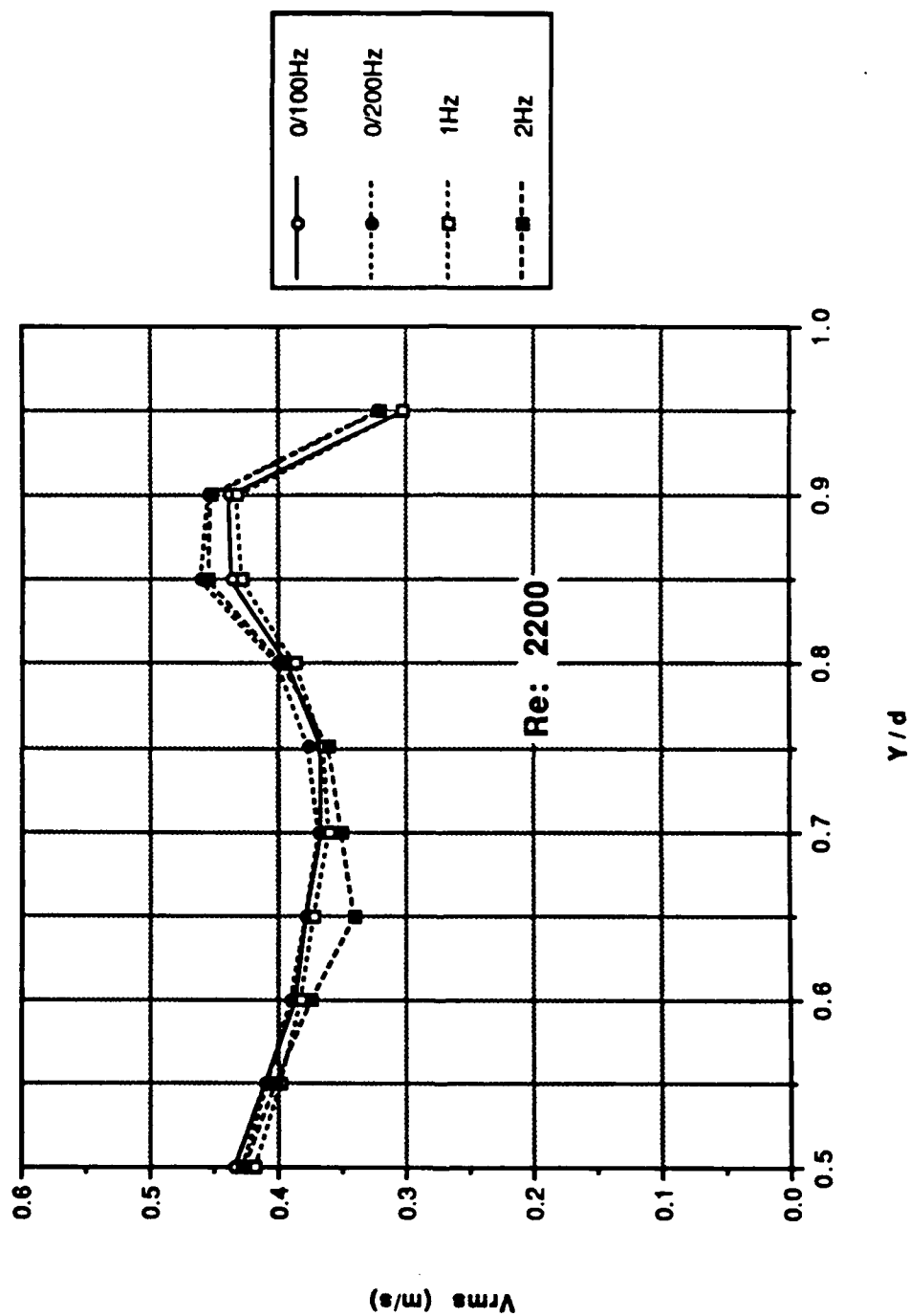


Figure 64. Profile Data: Longitudinal Turbulence Intensity vs y/d; Re: 2200

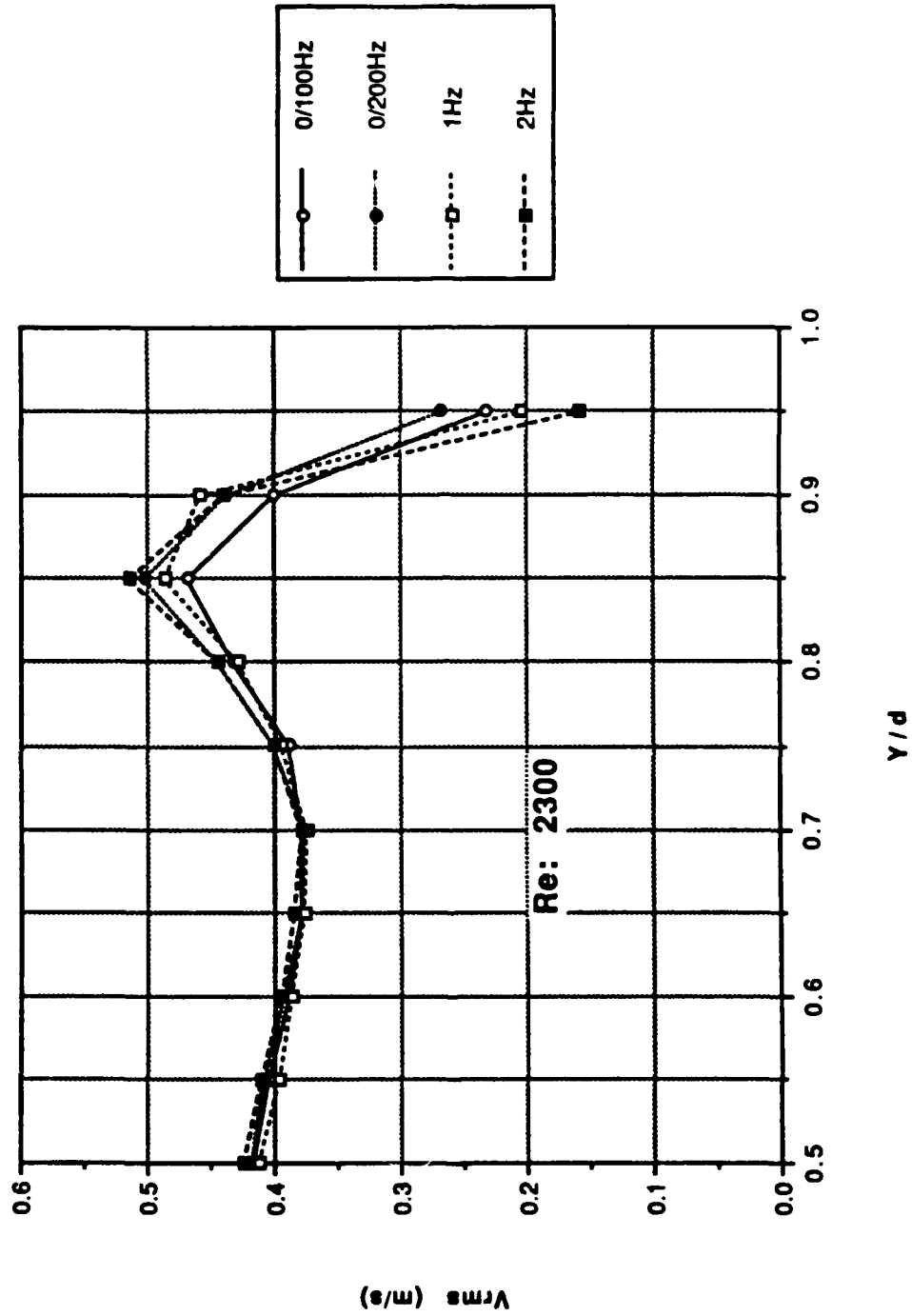


Figure 65. Profile Data: Longitudinal Turbulence Intensity vs y/d; Re: 2300

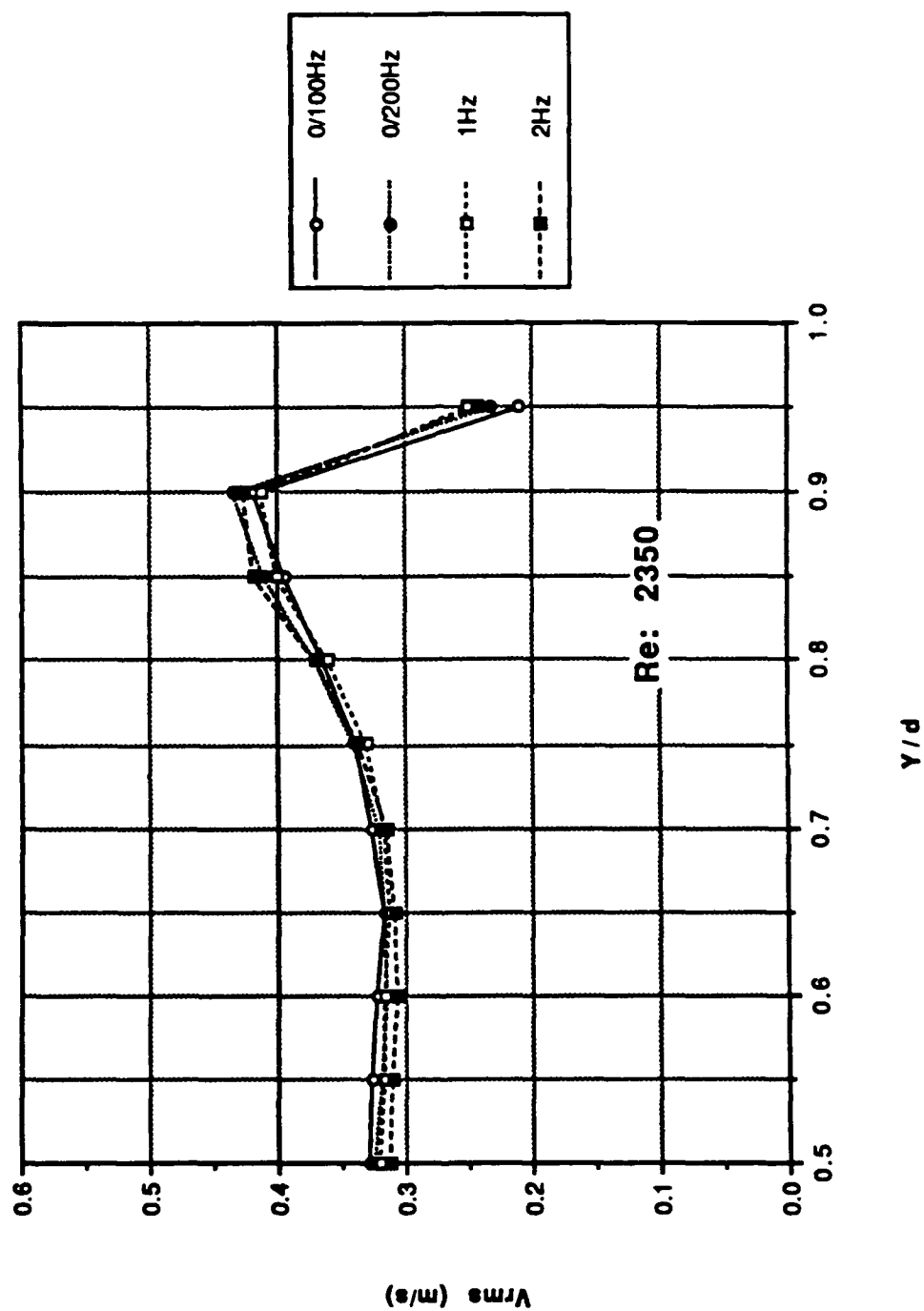


Figure 66. Profile Data: Longitudinal Turbulence Intensity vs y/d; Re: 2350

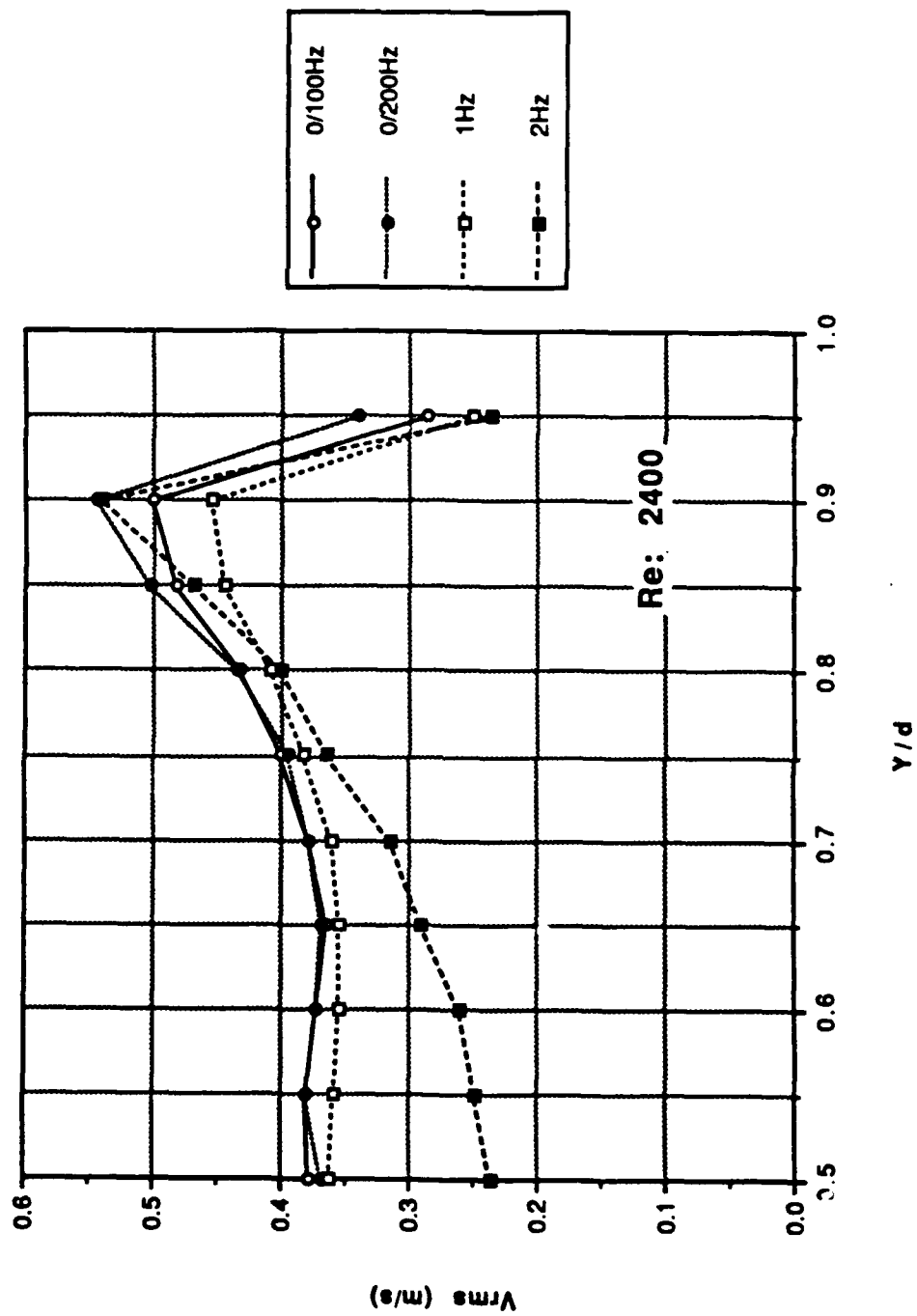


Figure 67. Profile Data: Longitudinal Turbulence Intensity vs y/d; Re: 2400

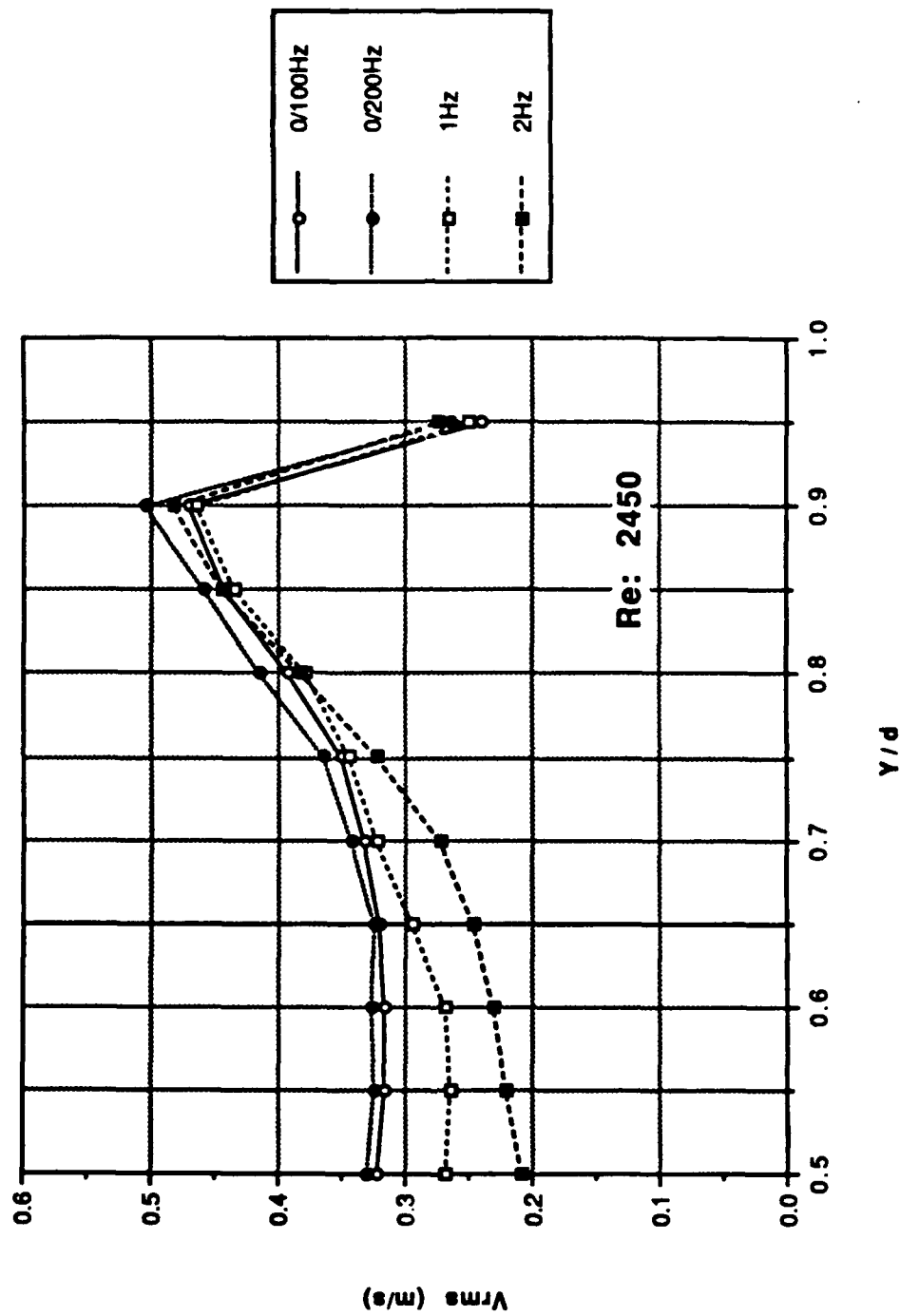


Figure 68. Profile Data: Longitudinal Turbulence Intensity vs y/d; Re: 2450

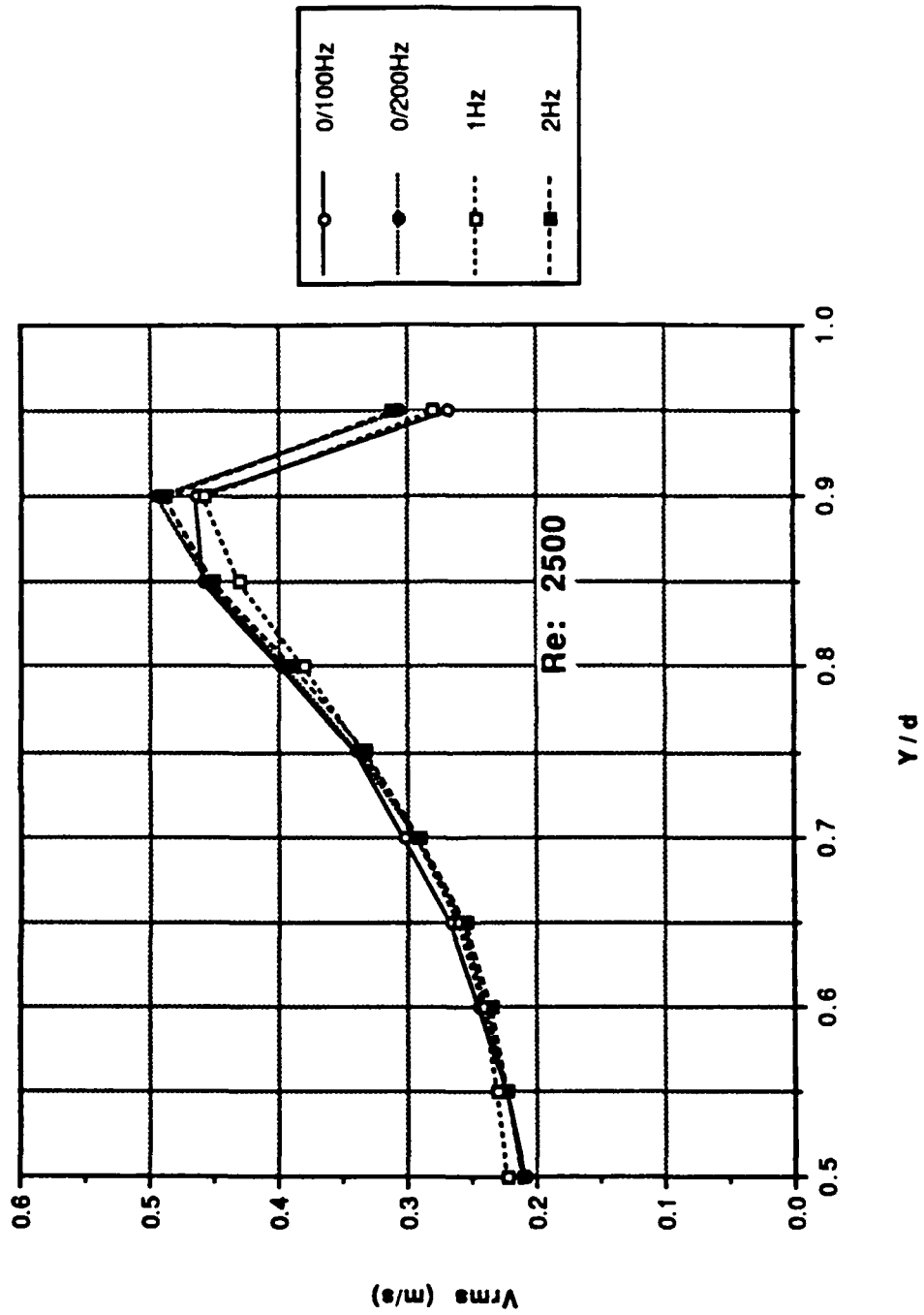


Figure 69. Profile Data: Longitudinal Turbulence Intensity vs y/d ; Re: 2500

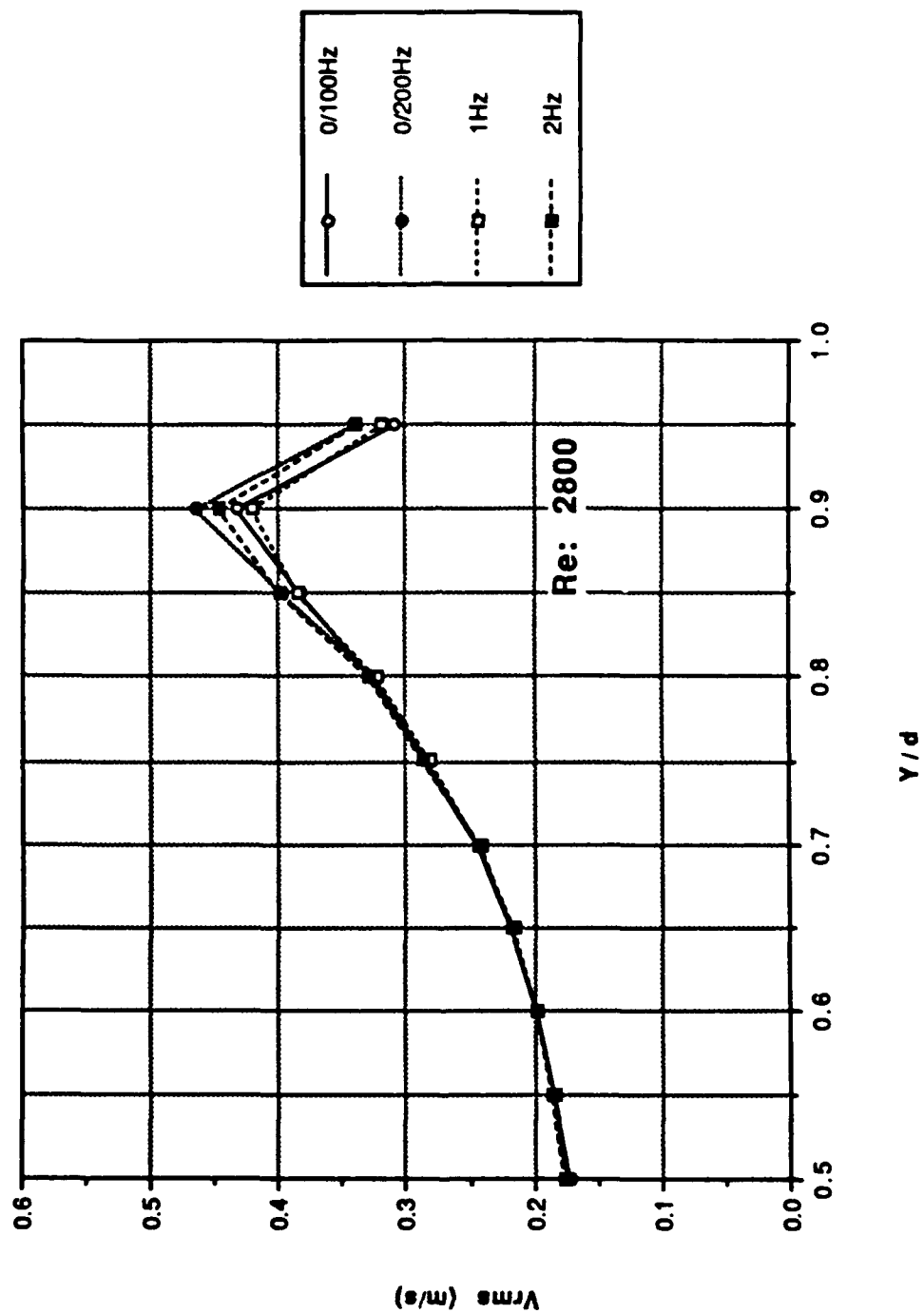


Figure 70. Profile Data: Longitudinal Turbulence Intensity vs y/d ; Re: 2800

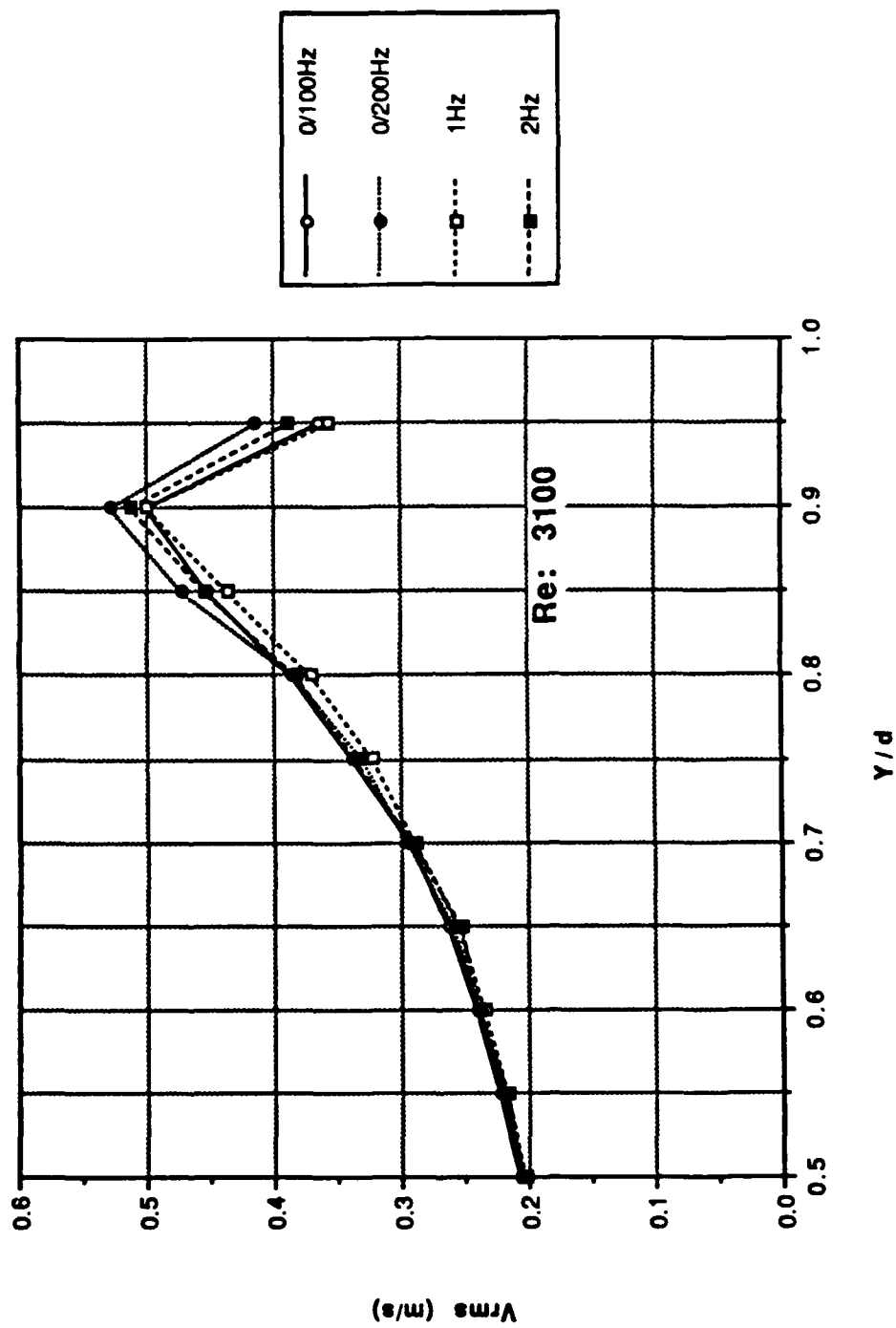


Figure 71. Profile Data: Longitudinal Turbulence Intensity vs y/d; Re: 3100

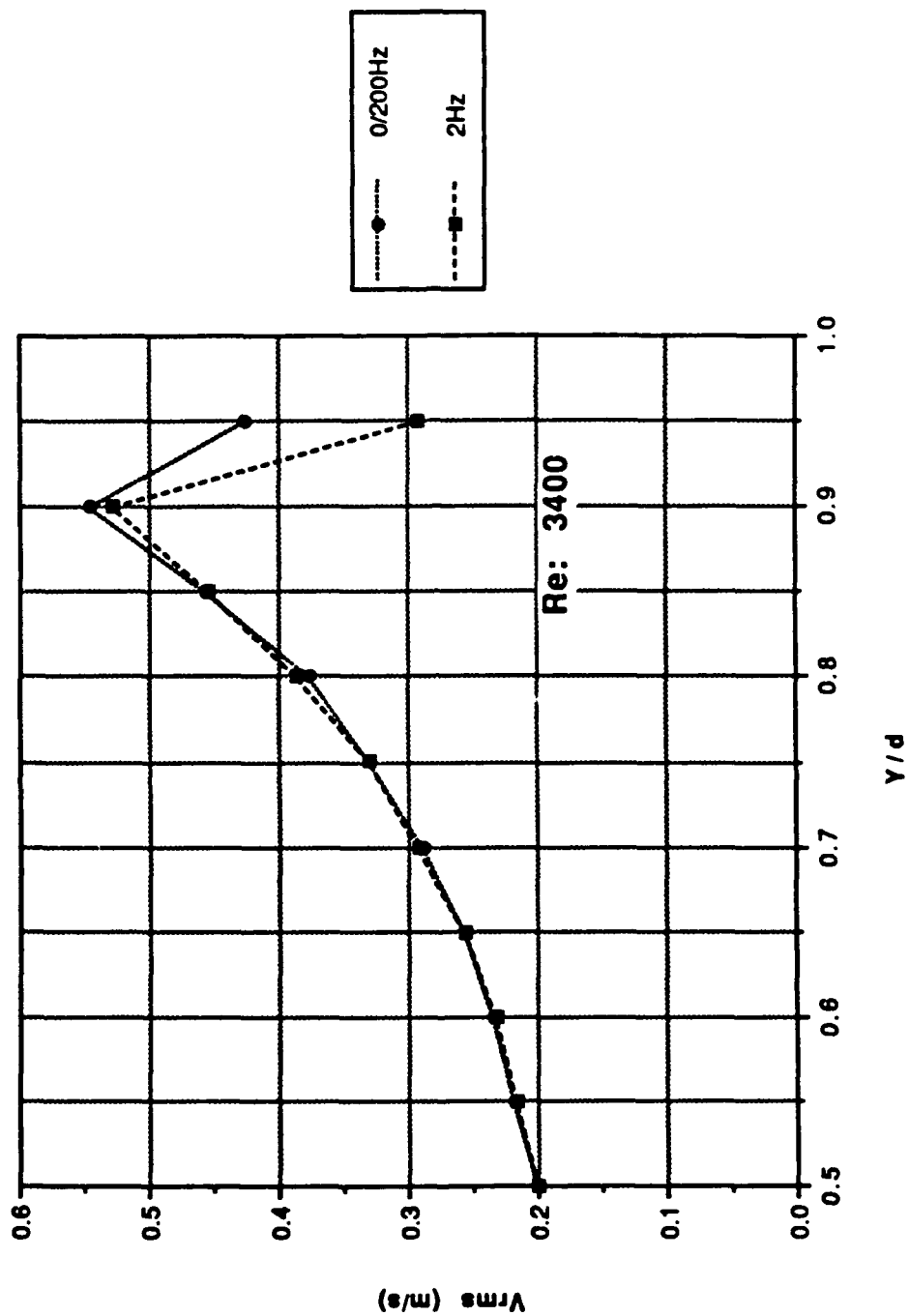


Figure 72. Profile Data: Longitudinal Turbulence Intensity vs y/d ; Re: 3400

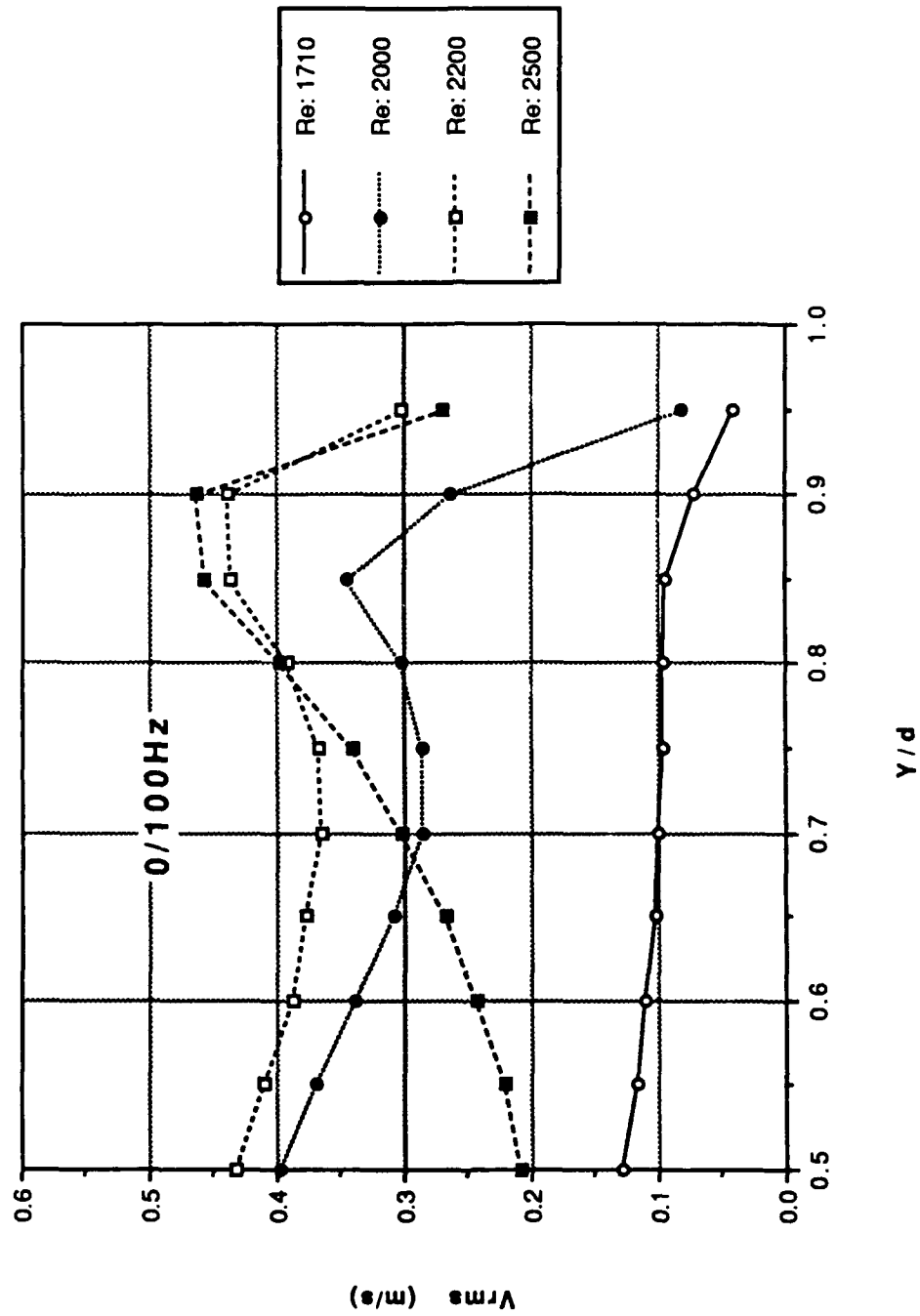


Figure 73. Profile Data: Longitudinal Turbulence Intensity vs y/d ; Composite Profiles

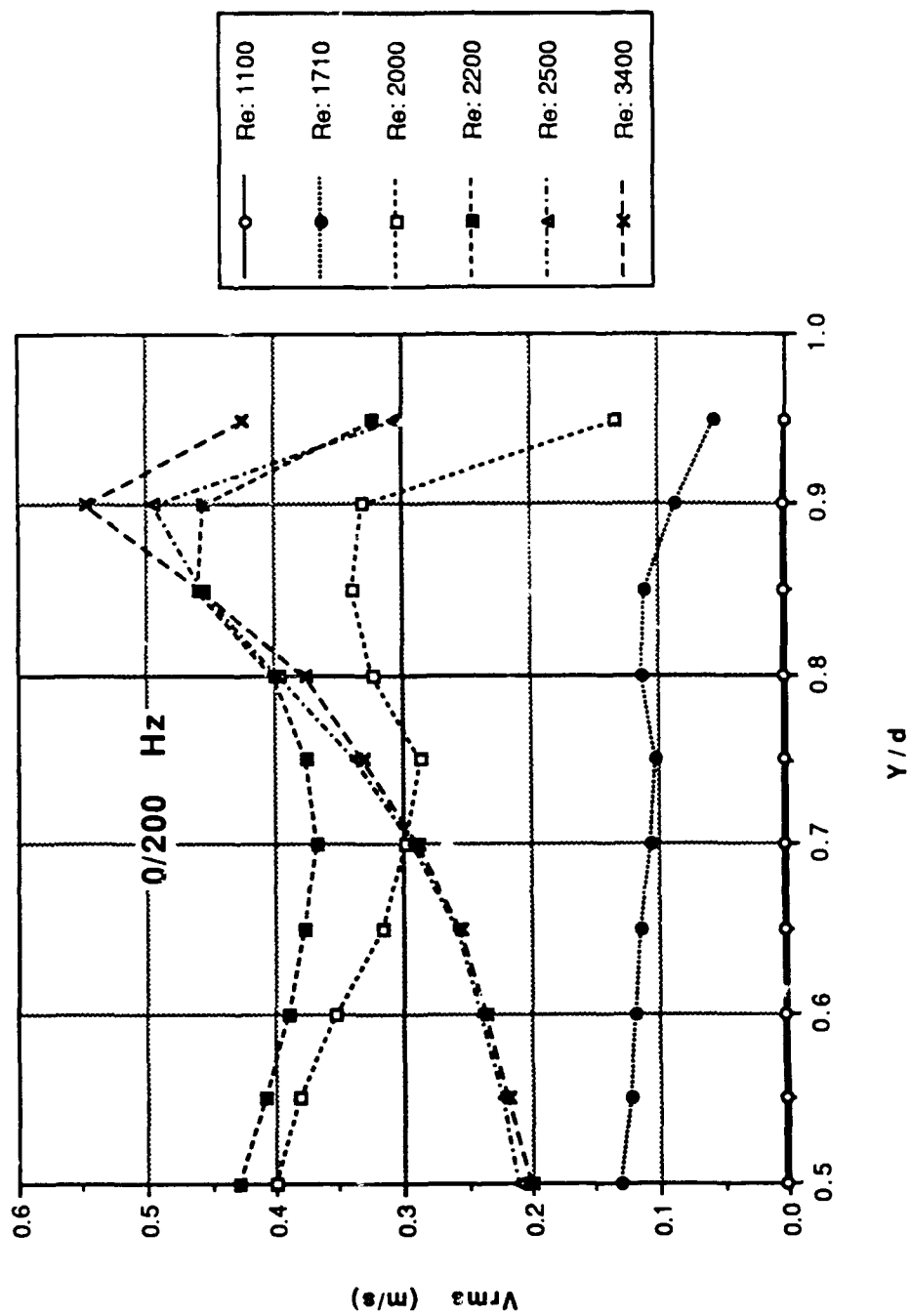


Figure 74. Profile Data: Longitudinal Turbulence Intensity vs y/d ; Composite Profiles

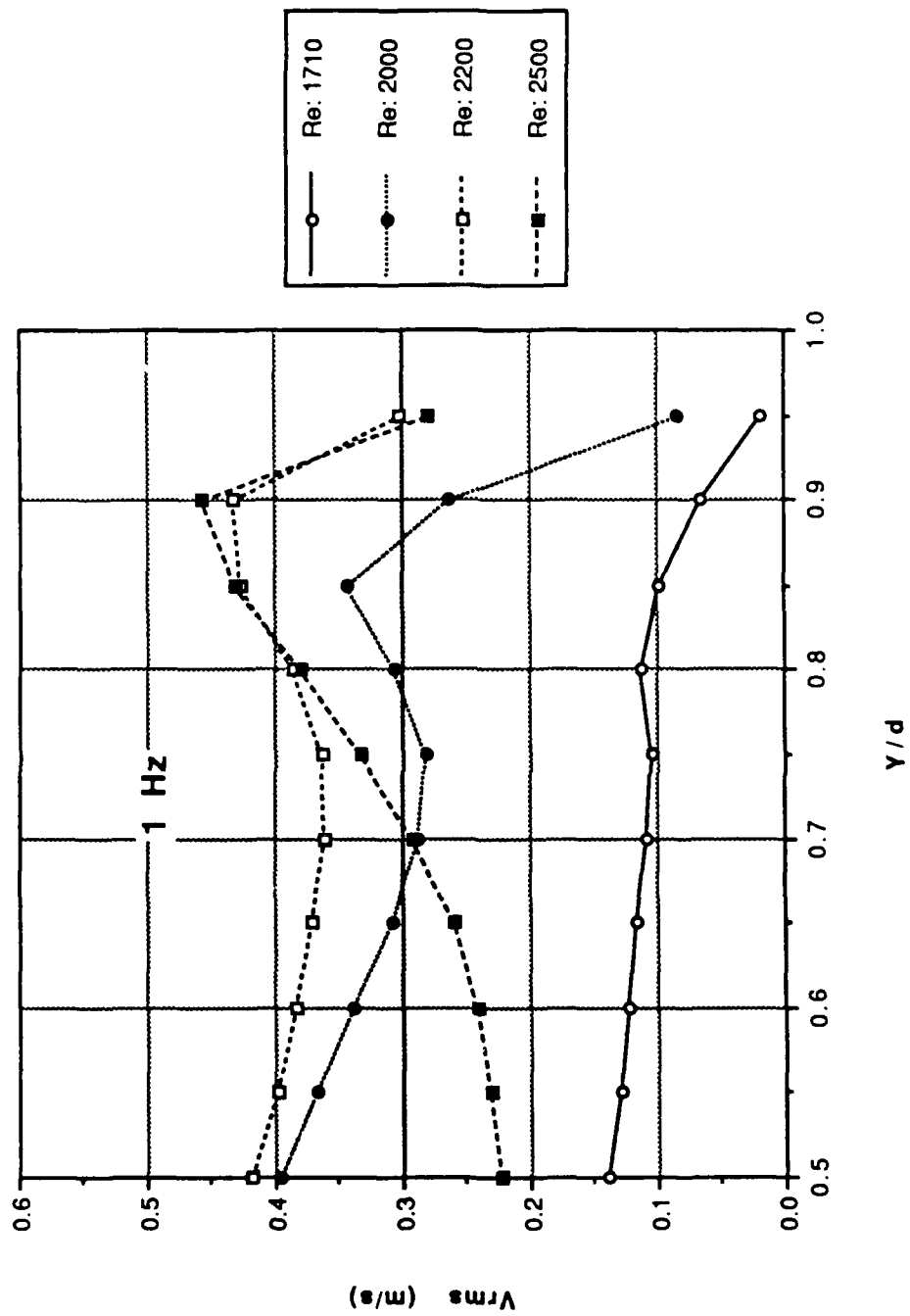


Figure 75. Profile Data: Longitudinal Turbulence Intensity vs y/d ; Composite Profiles

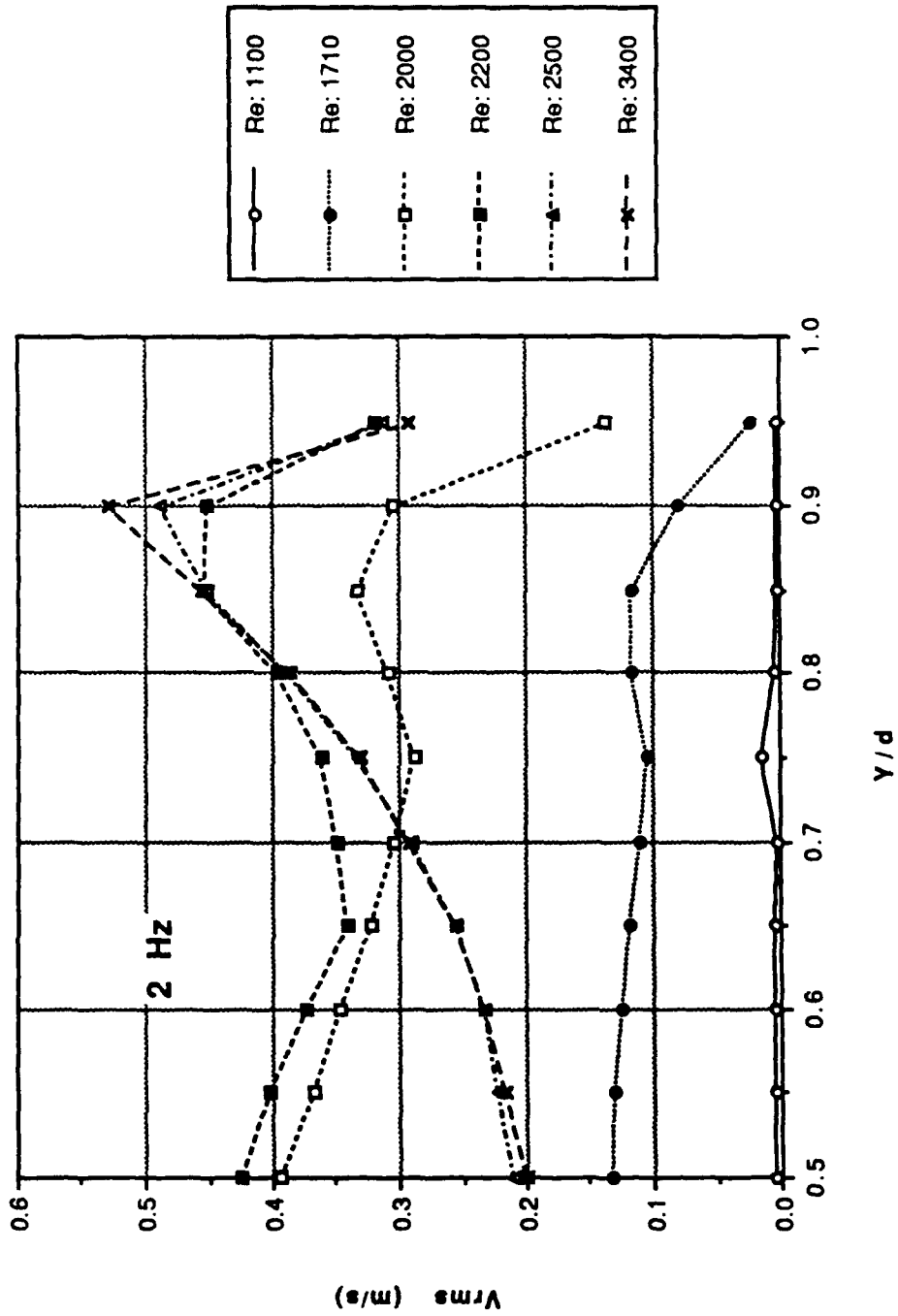


Figure 76. Profile Data: Longitudinal Turbulence Intensity vs y/d ; Composite Profiles

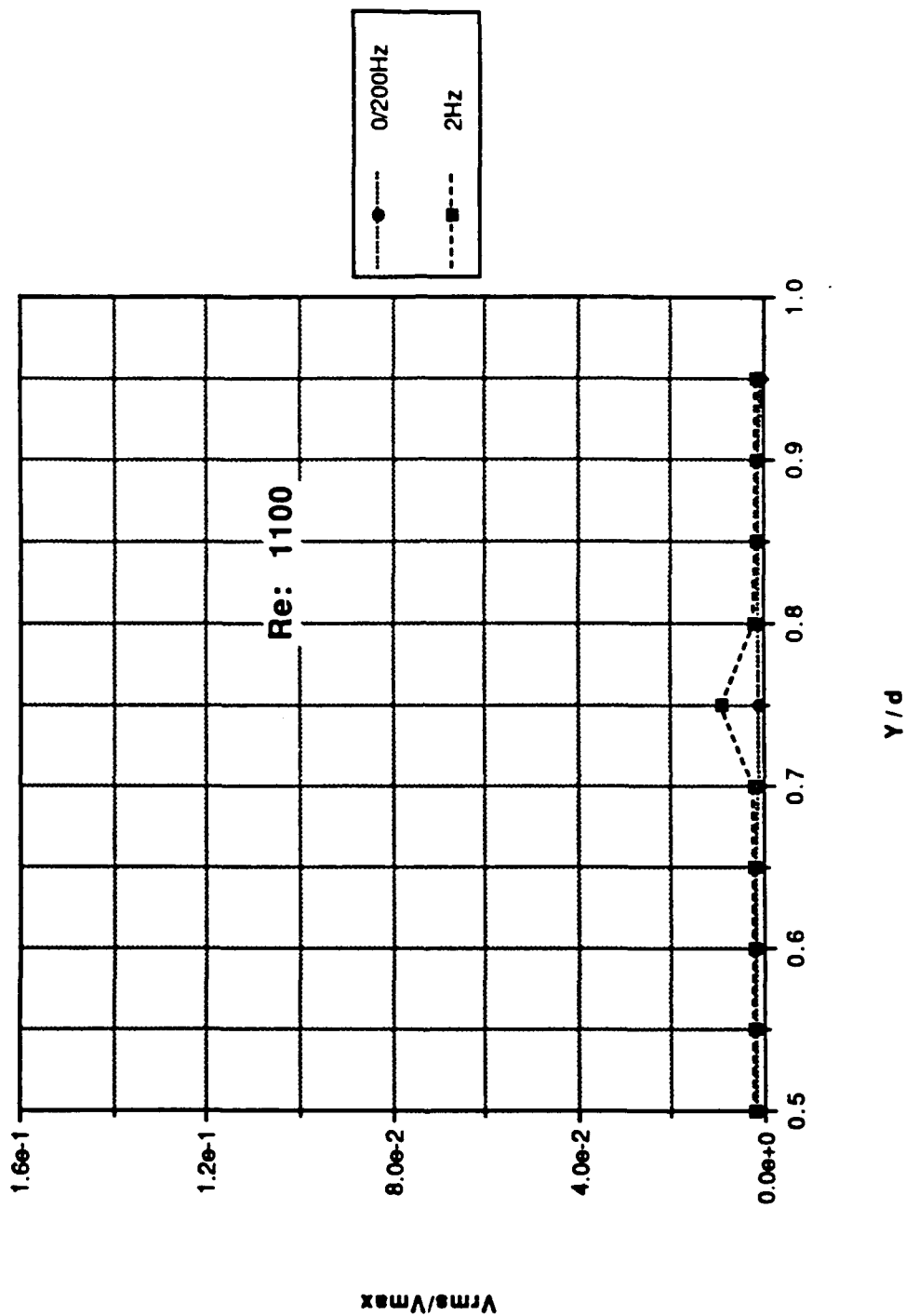


Figure 77. Profile Data: Longitudinal Turbulence Intensity Normalized by the Centerline Velocity vs y/d; Re: 1100

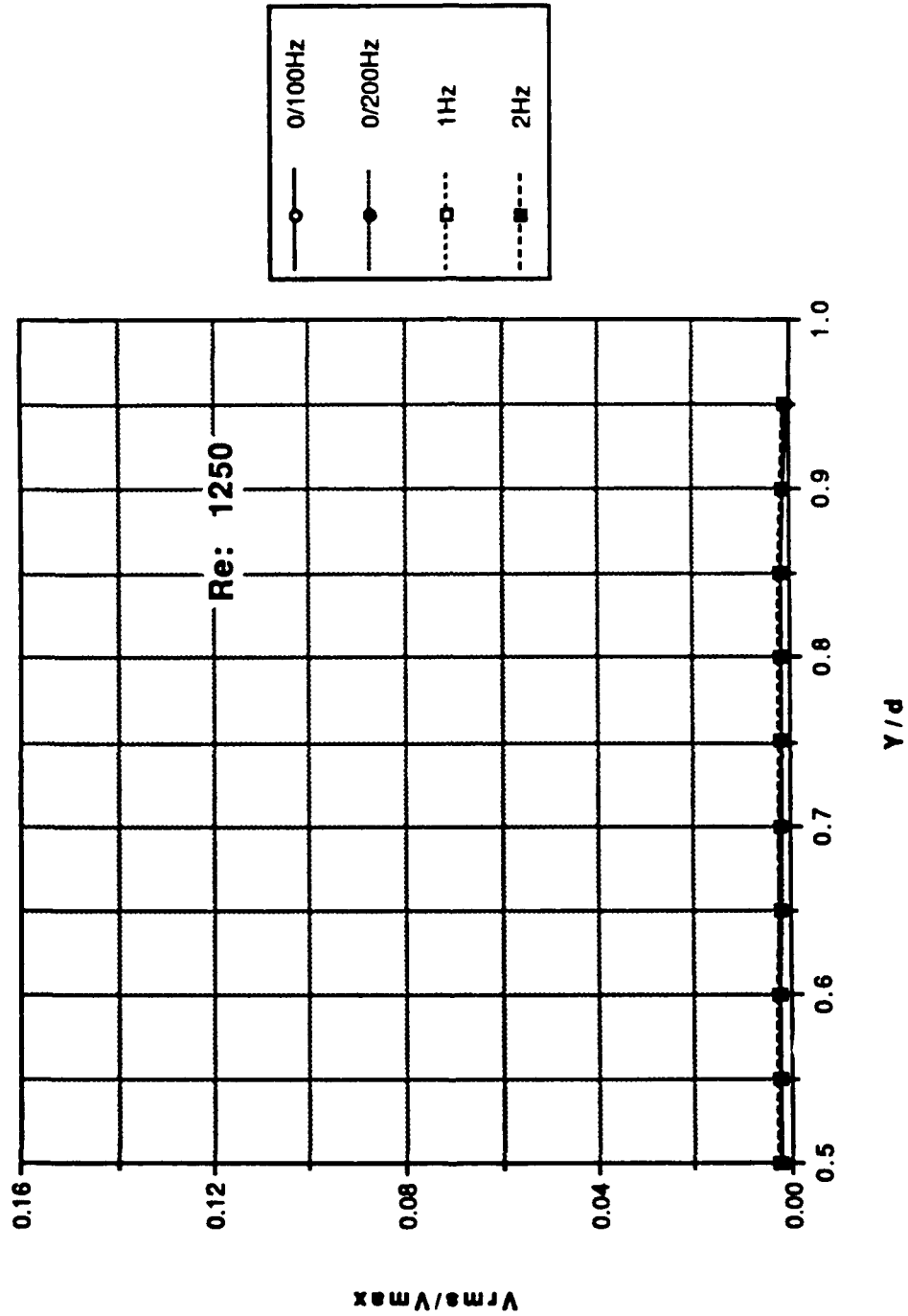


Figure 78. Profile Data: Longitudinal Turbulence Intensity Normalized by the Centerline Velocity vs y/d ; Re: 1250

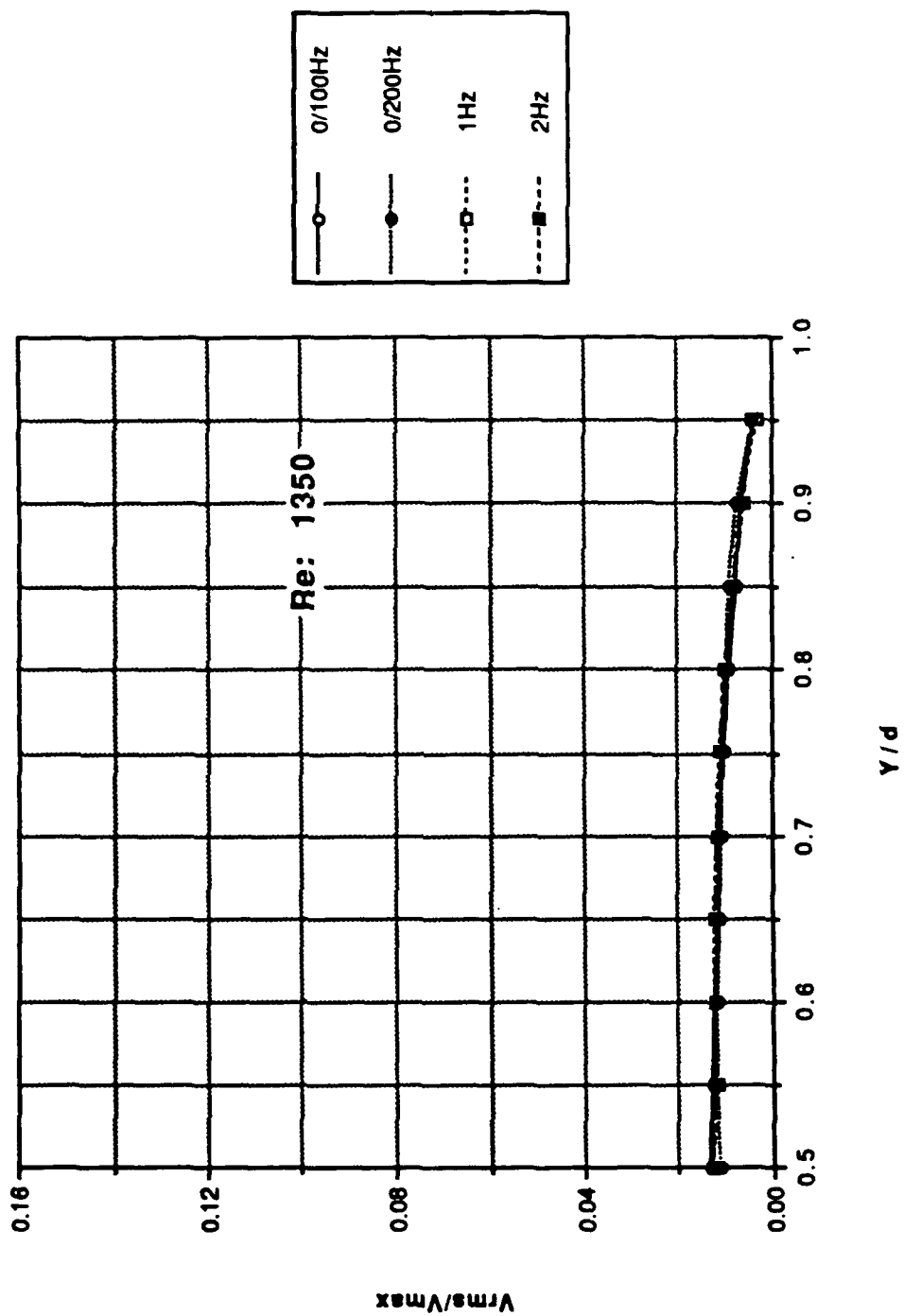


Figure 79. Profile Data: Longitudinal Turbulence Intensity Normalized by the Centerline Velocity vs y/d ; Re: 1350

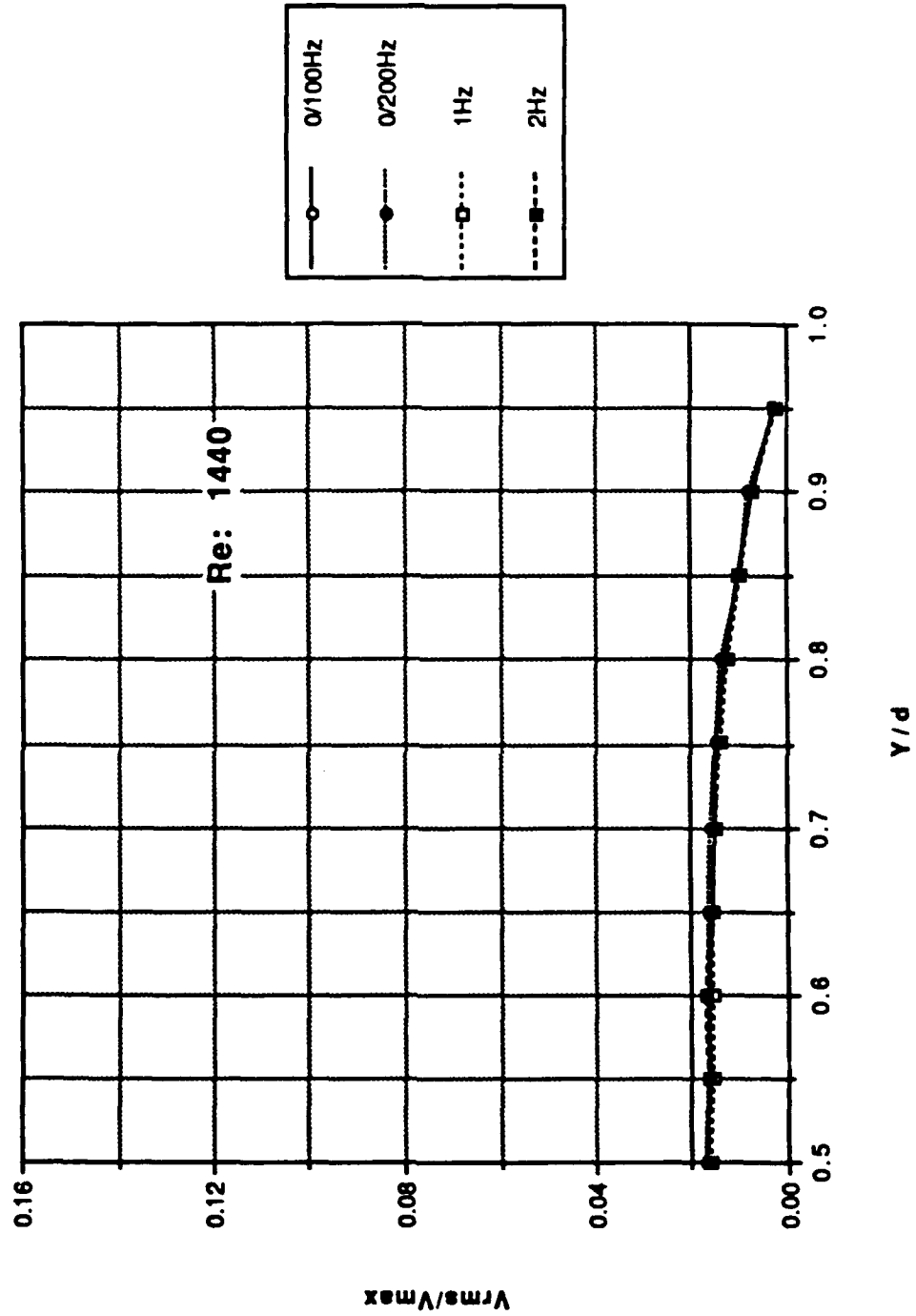


Figure 80. Profile Data: Longitudinal Turbulence Intensity Normalized by the Centerline Velocity vs y/d ; Re: 1440

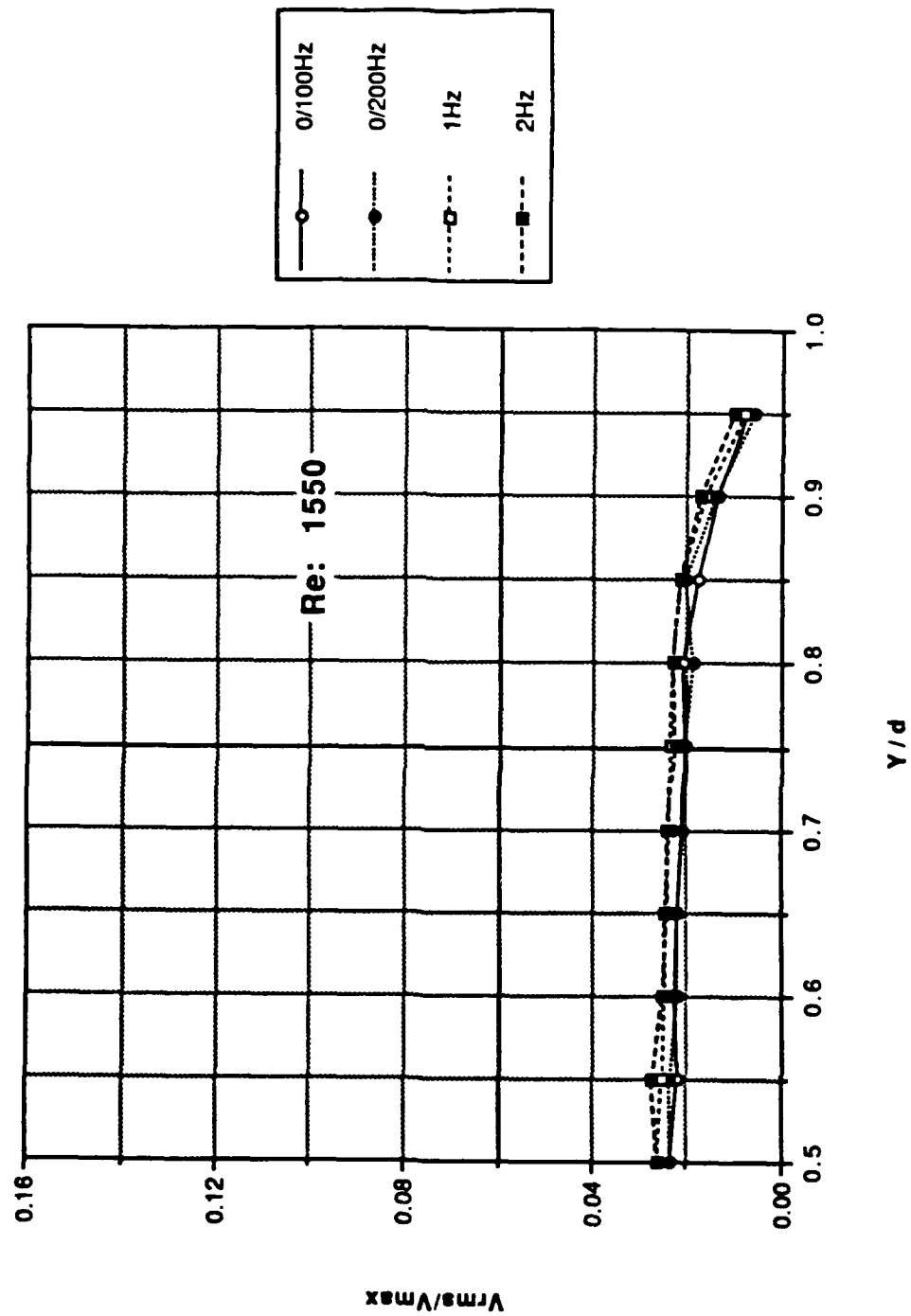


Figure 81. Profile Data: Longitudinal Turbulence Intensity Normalized by the Centerline Velocity vs y/d ; Re: 1550

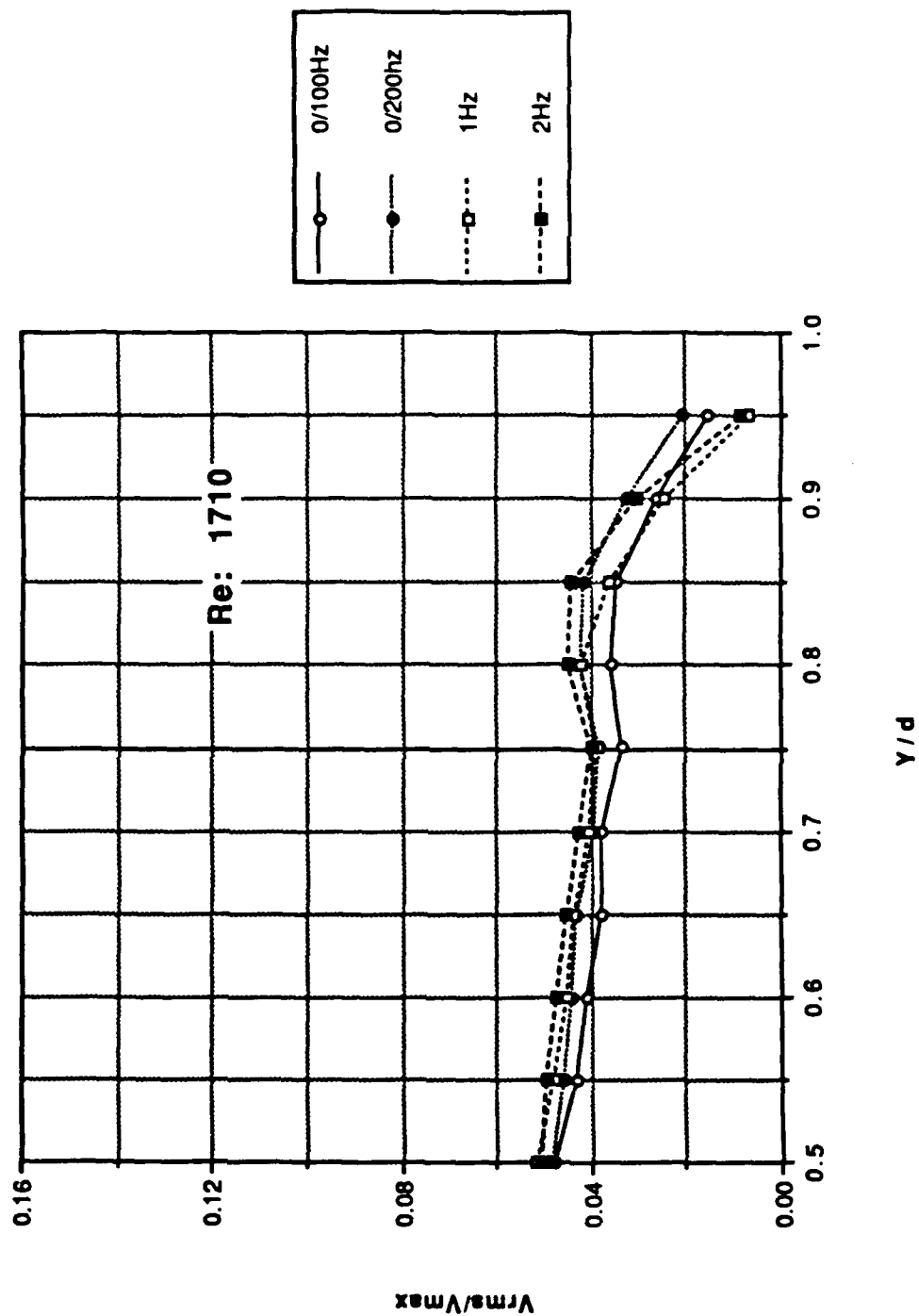


Figure 82. Profile Data: Longitudinal Turbulence Intensity Normalized by the Centerline Velocity vs y/d ; Re: 1710

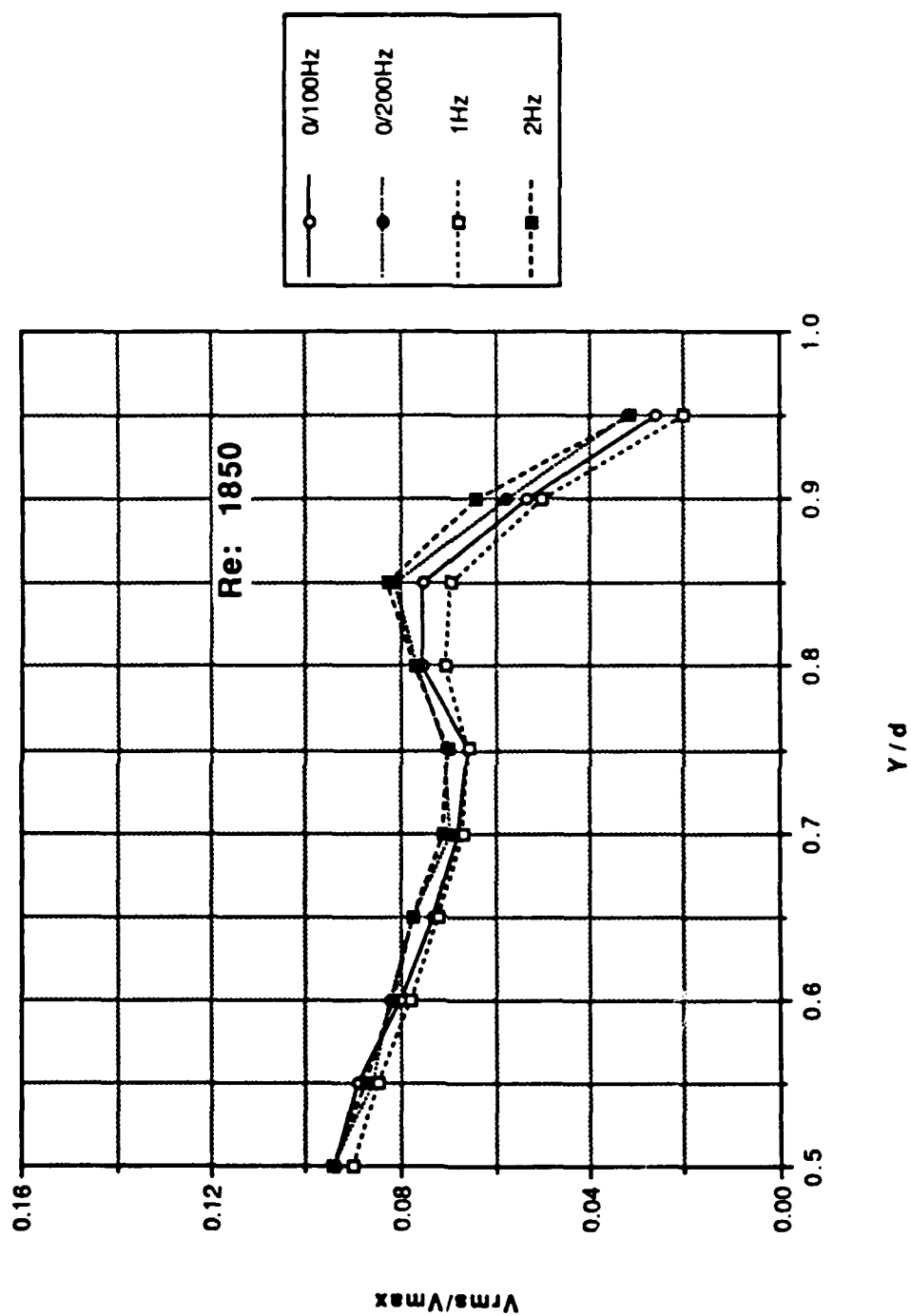


Figure 83. Profile Data: Longitudinal Turbulence Intensity Normalized by the Centerline Velocity vs y/d ; Re: 1850

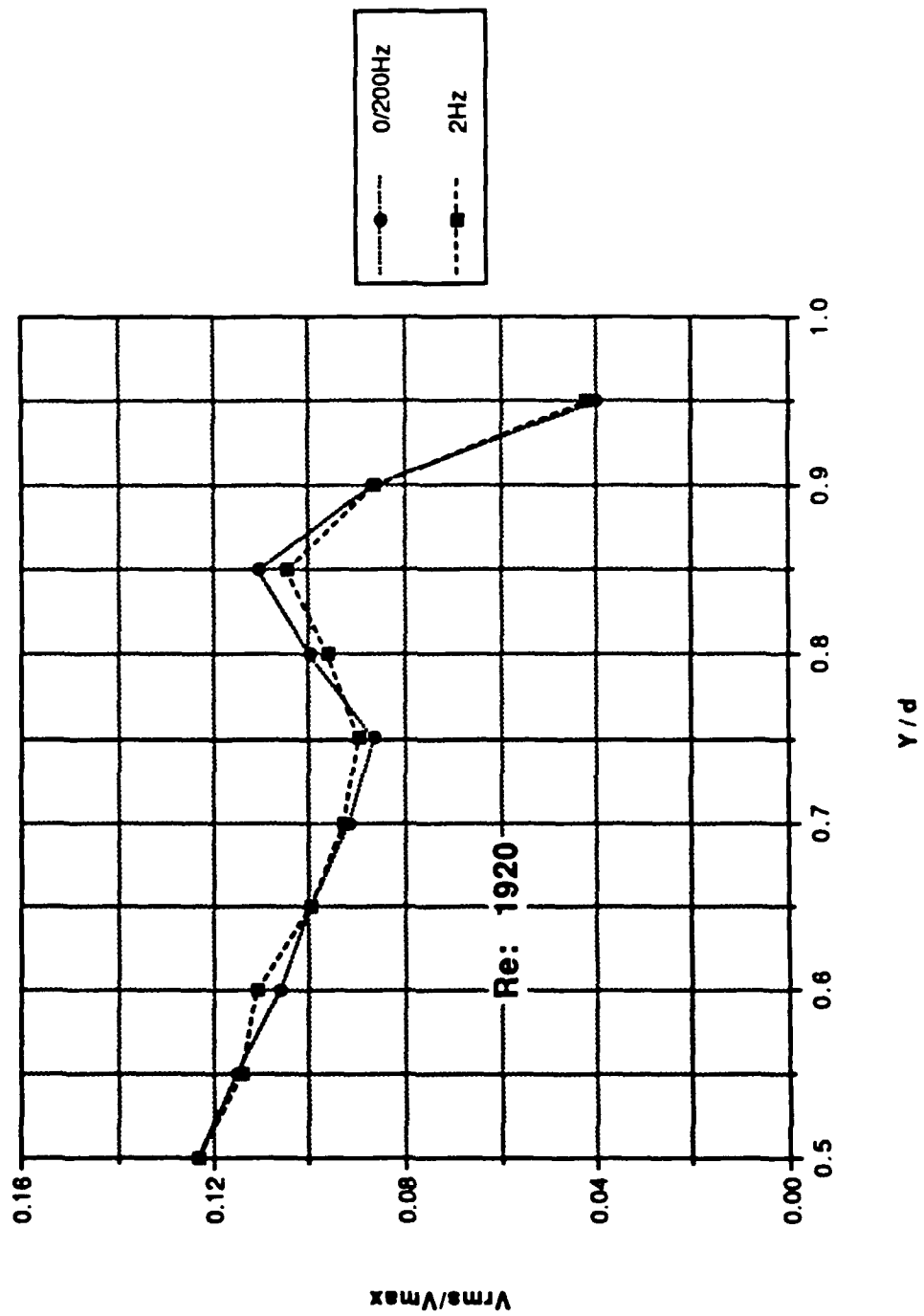


Figure 84. Profile Data: Longitudinal Turbulence Intensity Normalized by the Centerline Velocity vs y/d ; Re: 1920

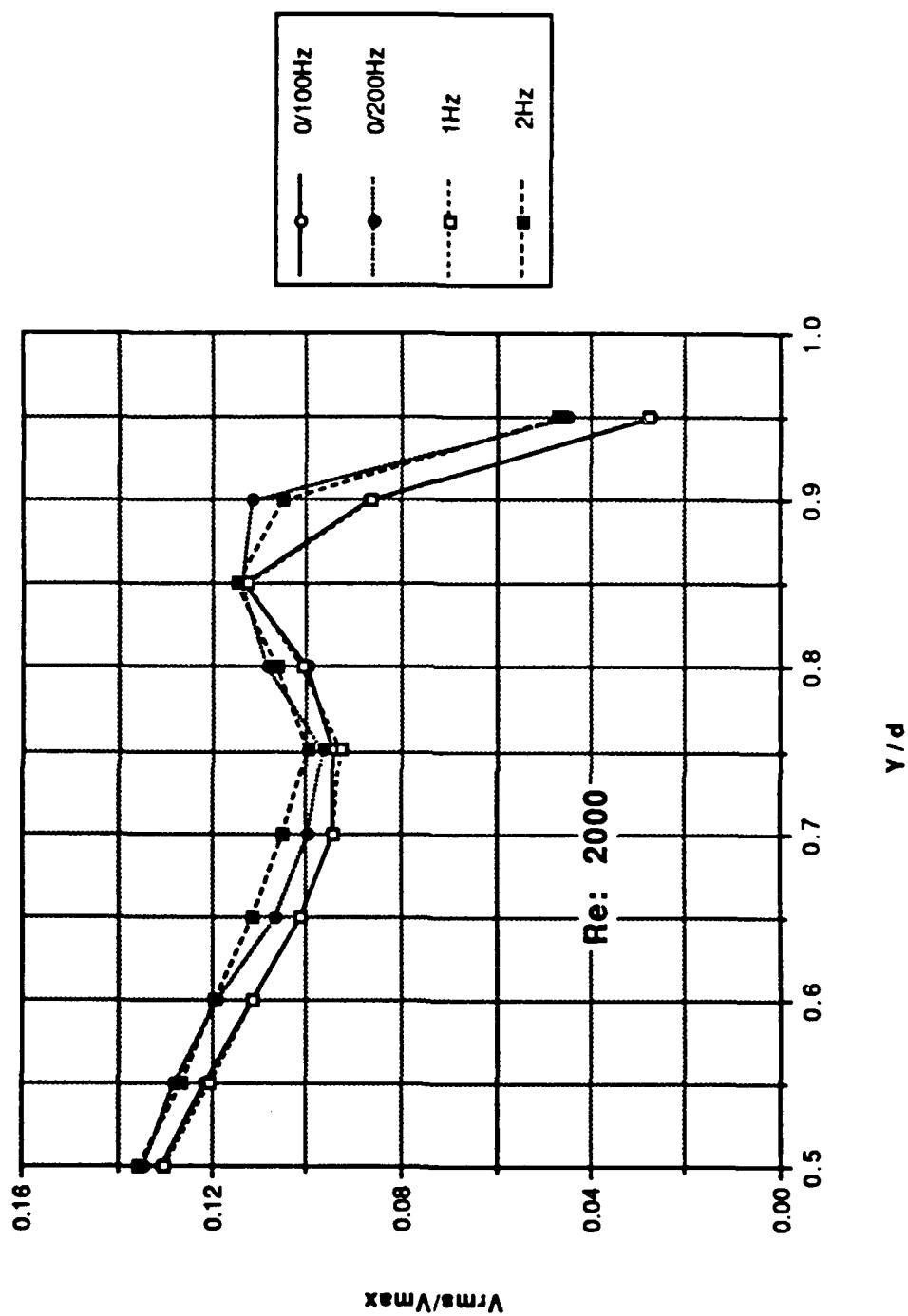


Figure 85. Profile Data: Longitudinal Turbulence Intensity Normalized by the Centerline Velocity vs y/d ; Re: 2000

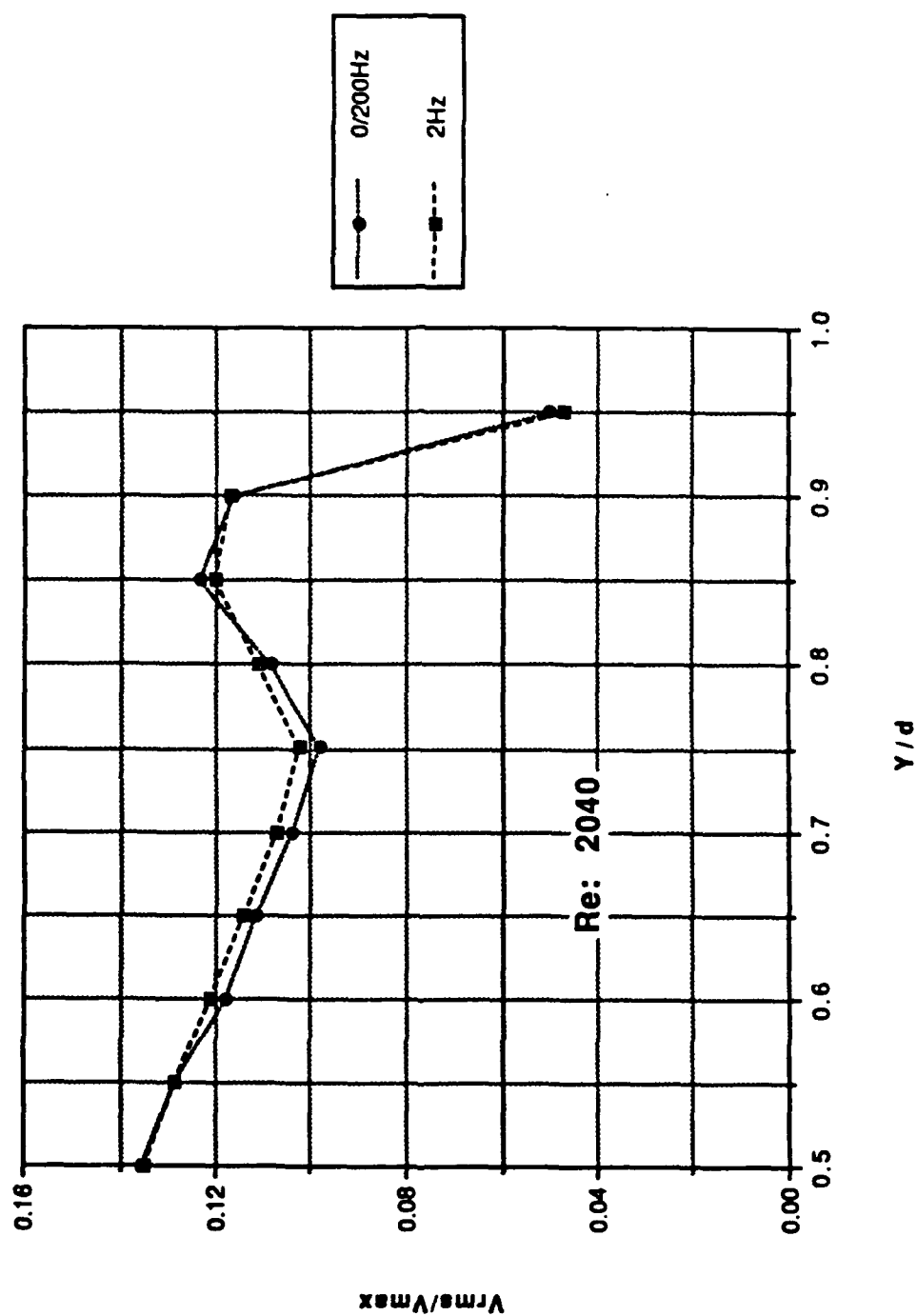


Figure 86. Profile Data: Longitudinal Turbulence Intensity Normalized by the Centerline Velocity vs y/d ; Re: 2040

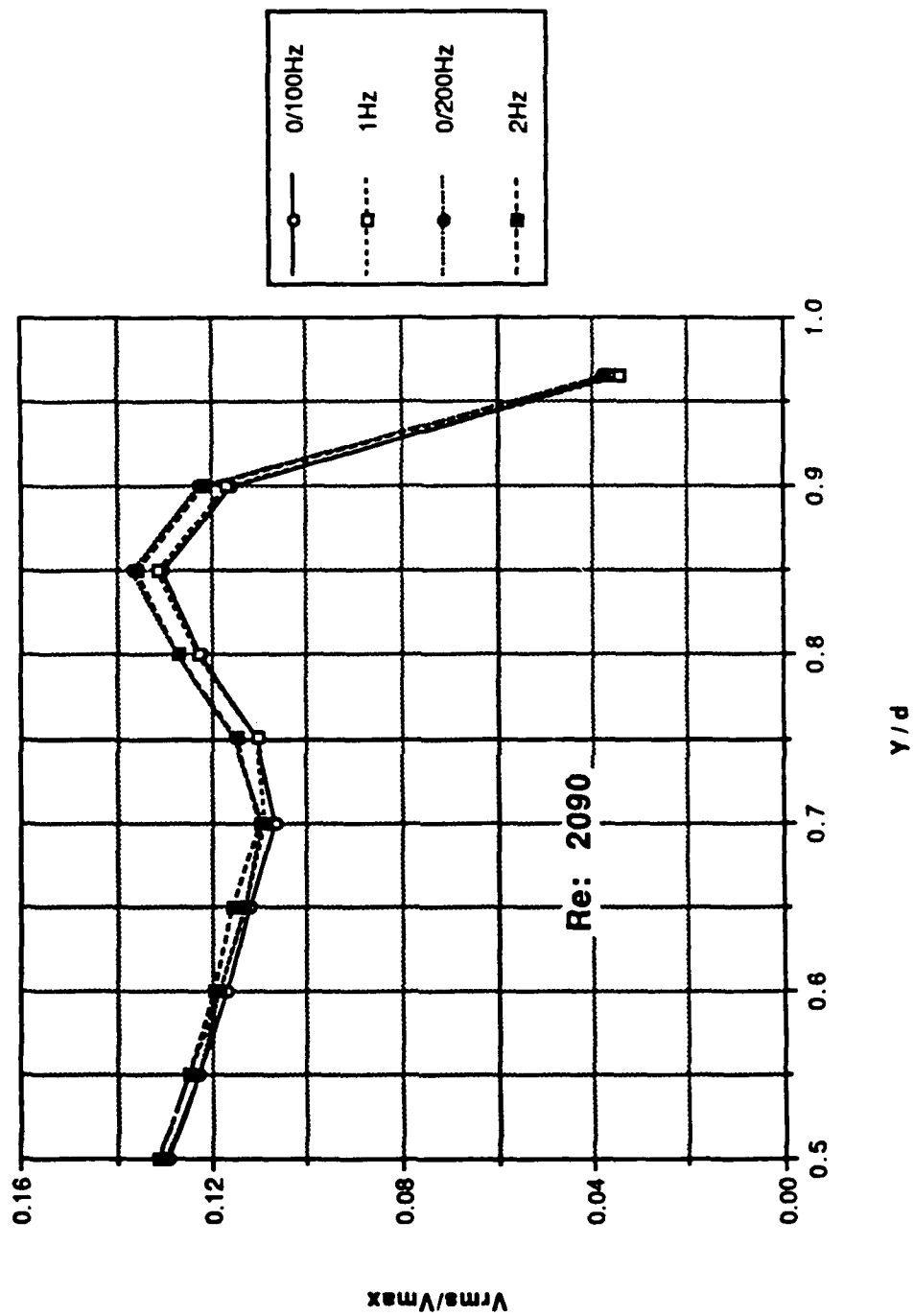


Figure 87. Profile Data: Longitudinal Turbulence Intensity Normalized by the Centerline Velocity vs y/d ; Re: 2090

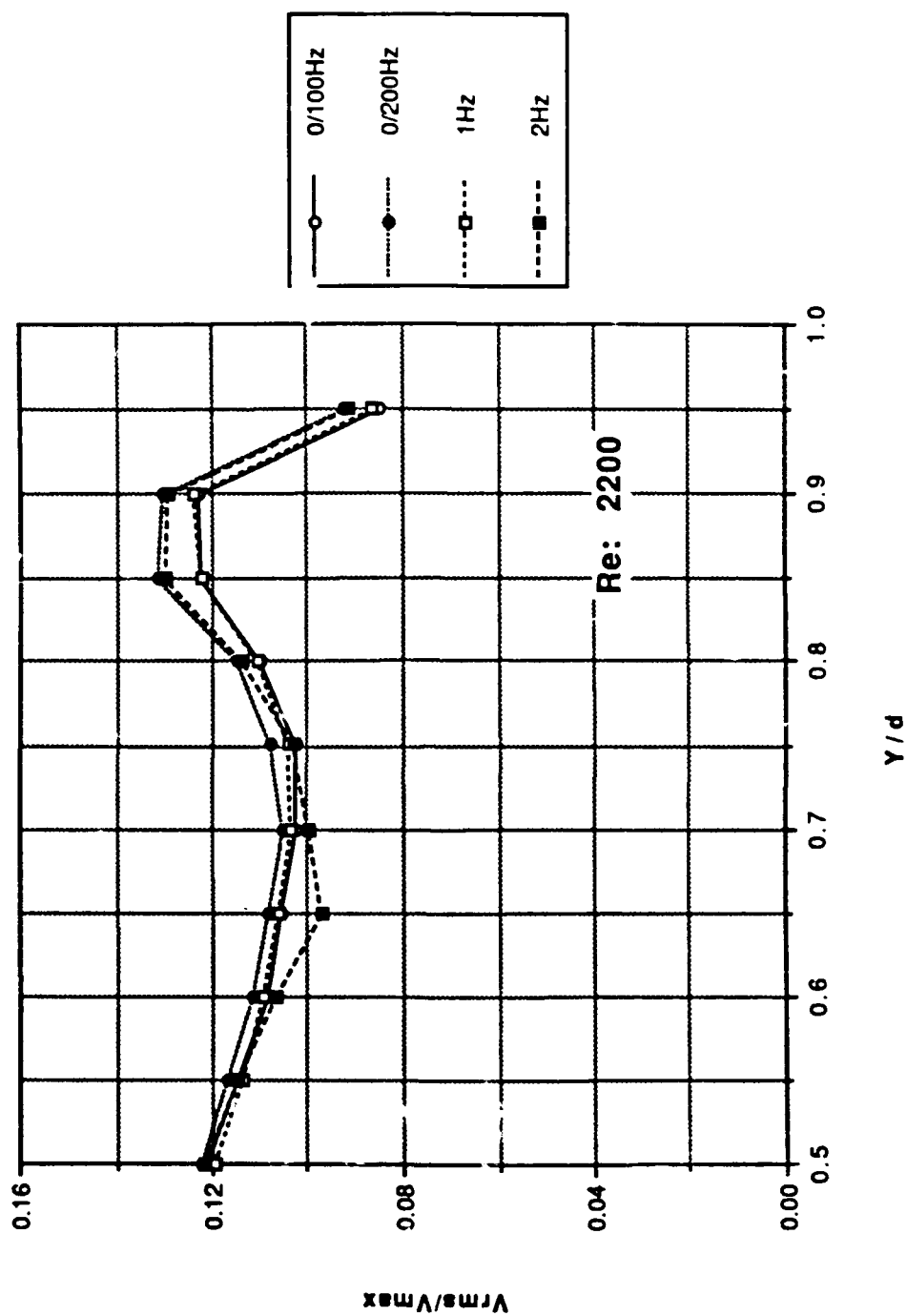


Figure 88. Profile Data: Longitudinal Turbulence Intensity Normalized by the Centerline Velocity vs y/d ; Re: 2200

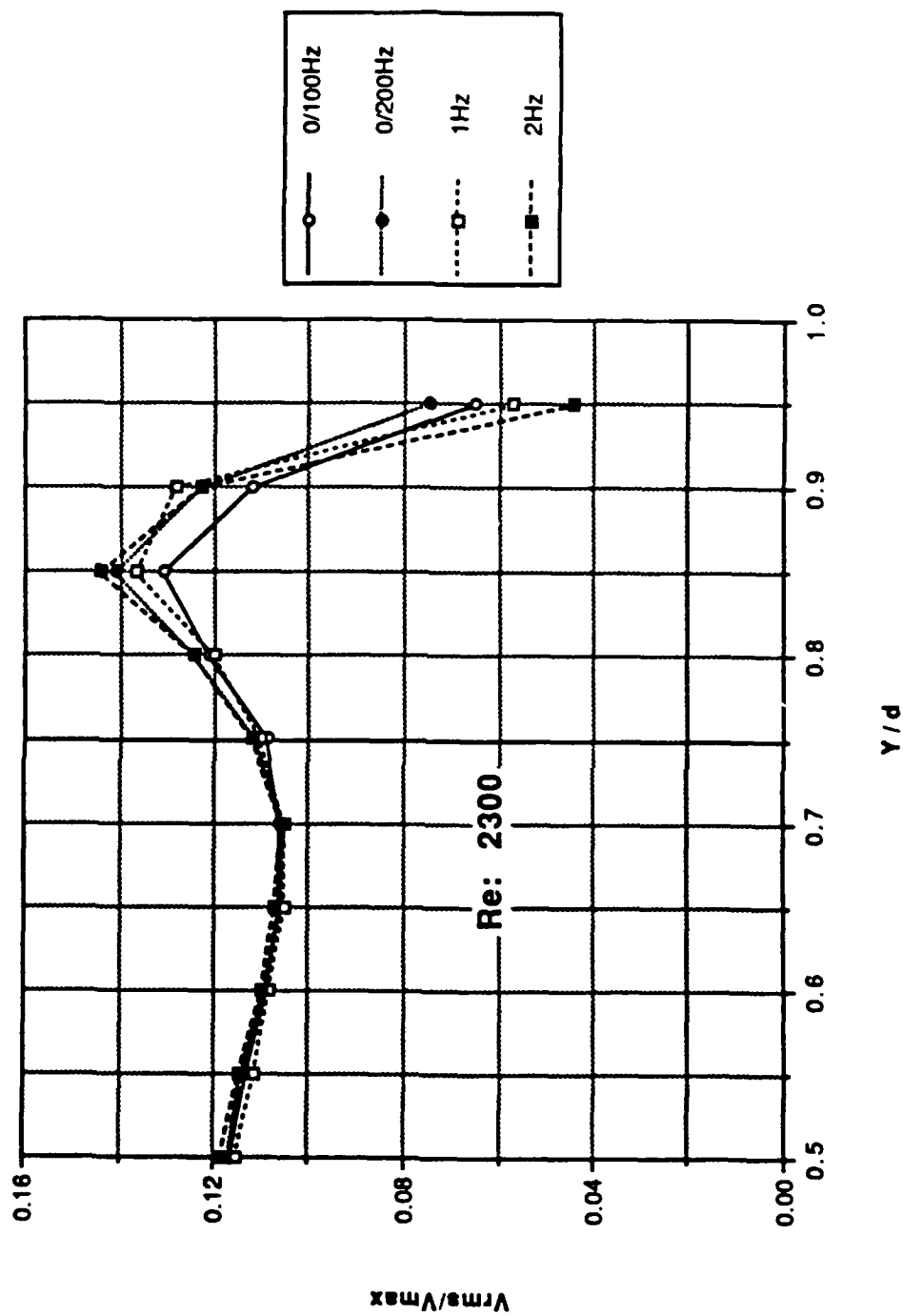


Figure 89. Profile Data: Longitudinal Turbulence Intensity Normalized by the Centerline Velocity vs y/d ; Re: 2300

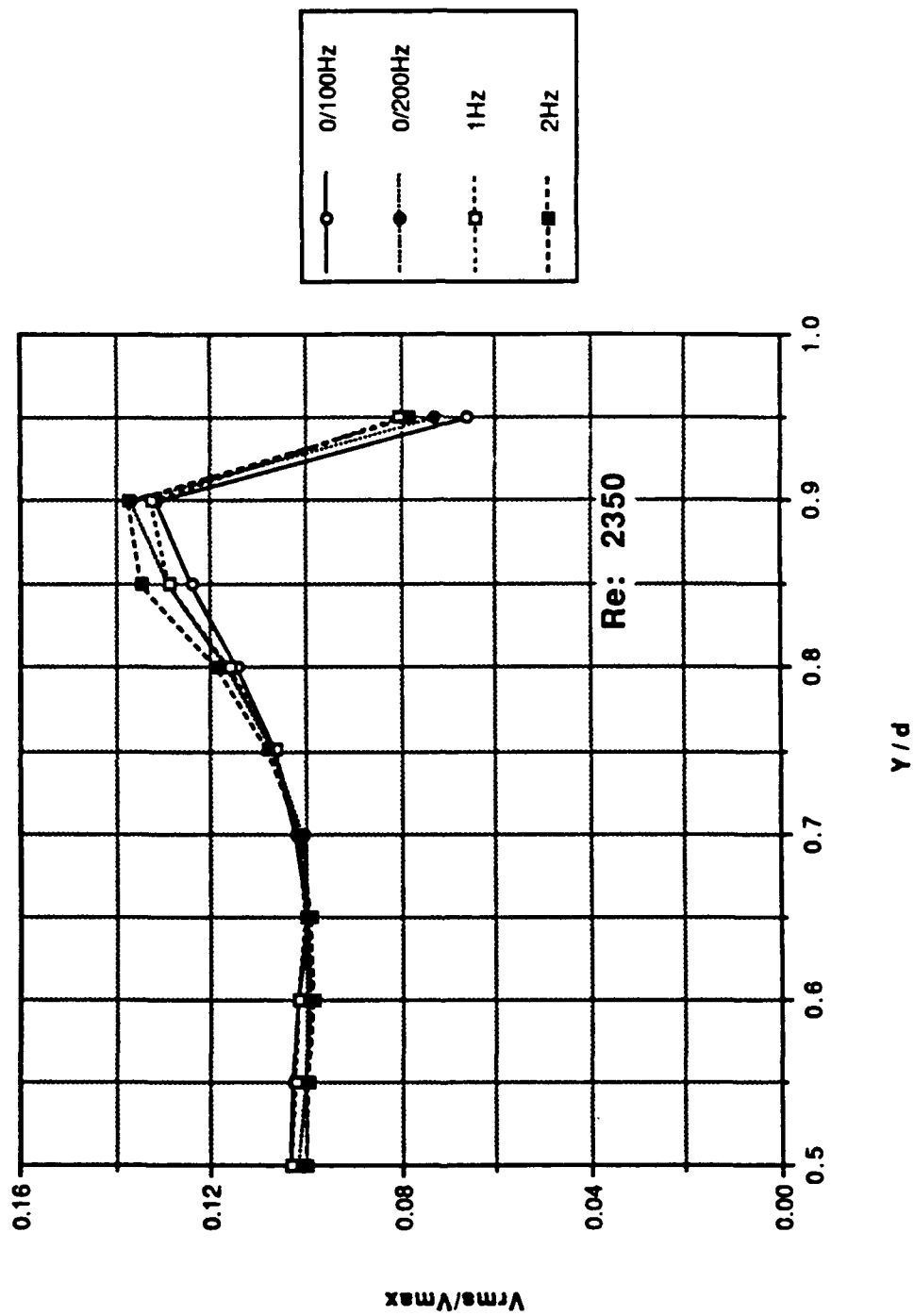


Figure 90. Profile Data: Longitudinal Turbulence Intensity Normalized by the Centerline Velocity vs y/d ; Re: 2350

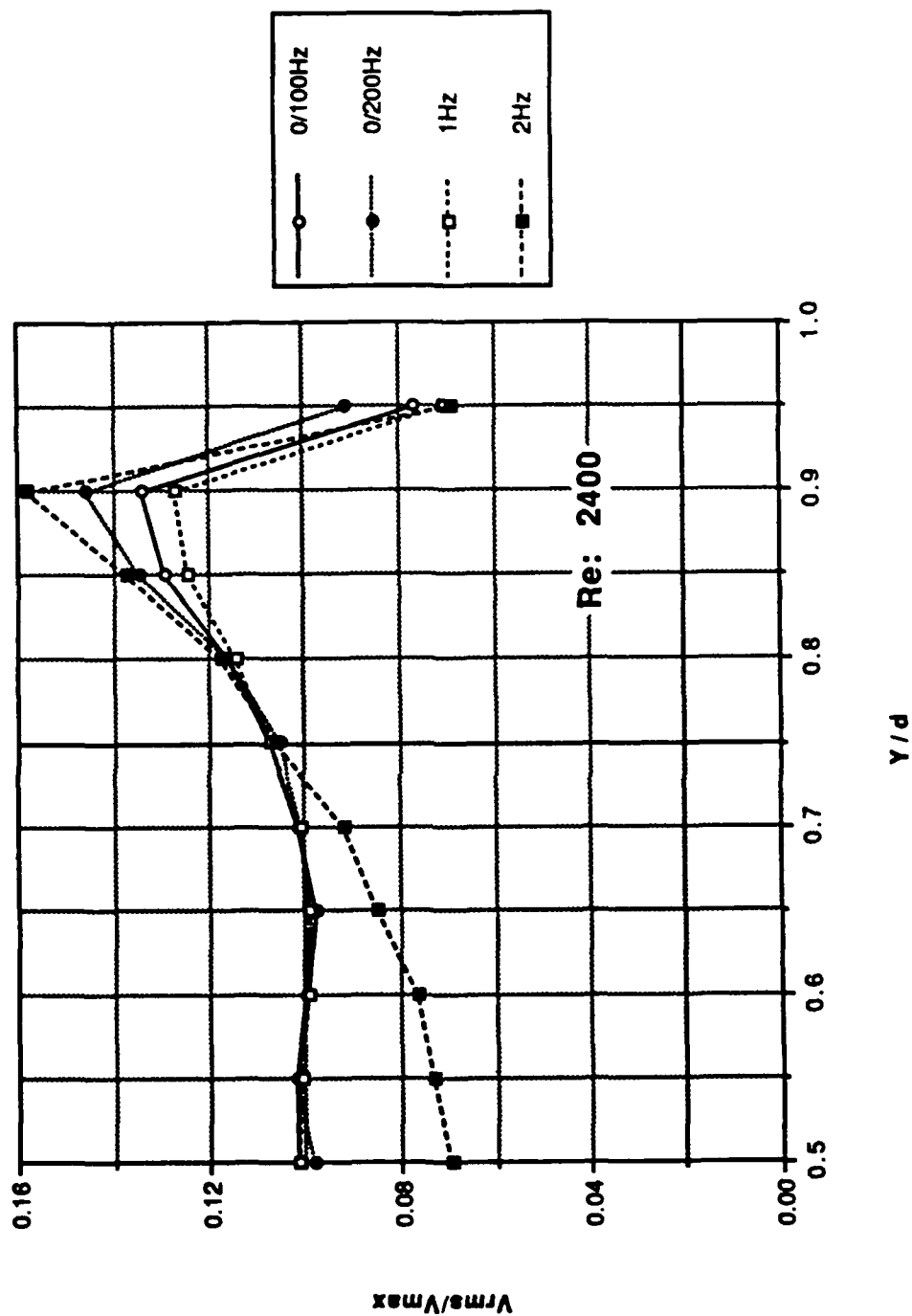


Figure 91. Profile Data: Longitudinal Turbulence Intensity Normalized by the Centerline Velocity vs y/d ; Re: 2400

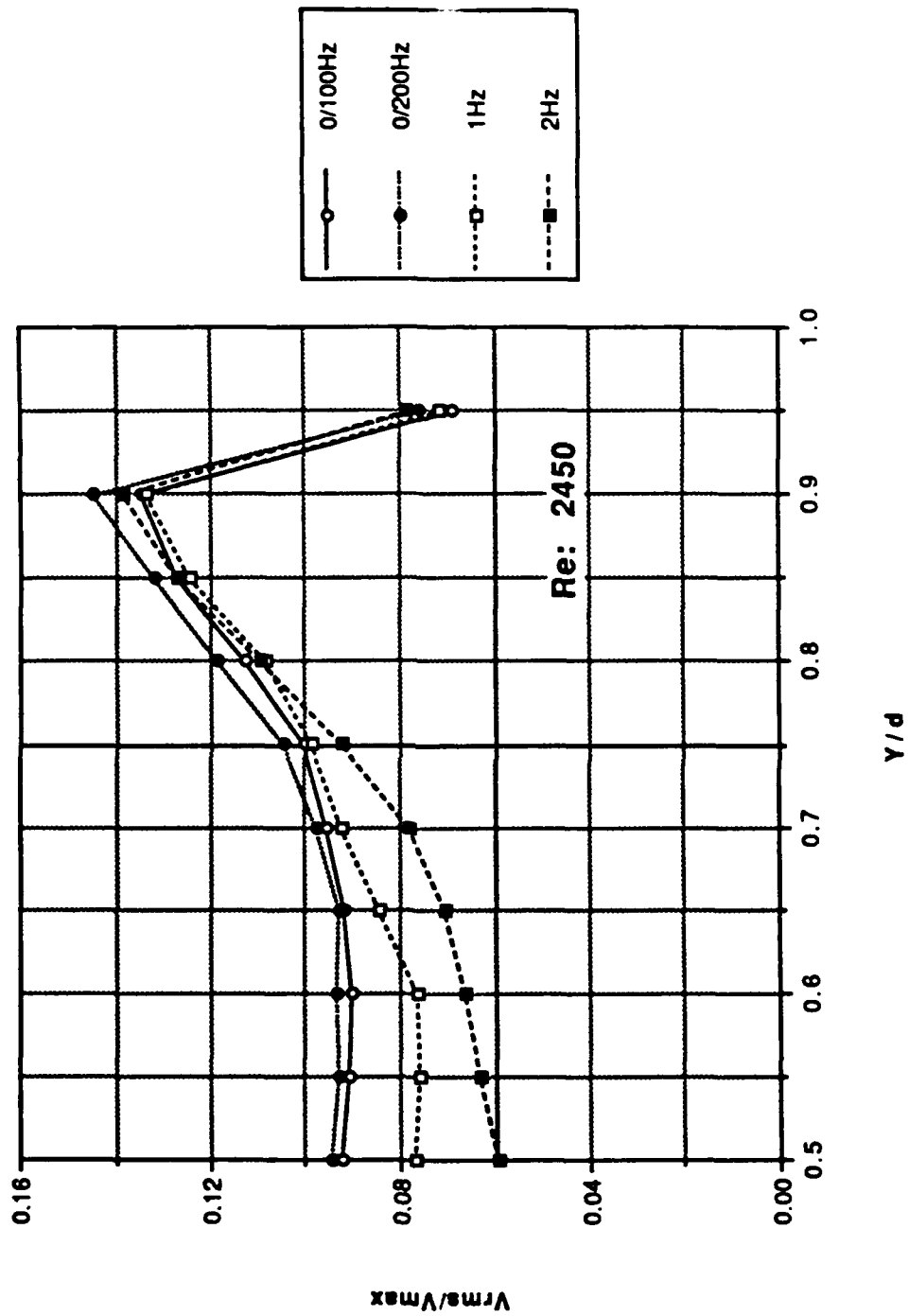


Figure 92. Profile Data: Longitudinal Turbulence Intensity Normalized by the Centerline Velocity vs y/d ; Re: 2450

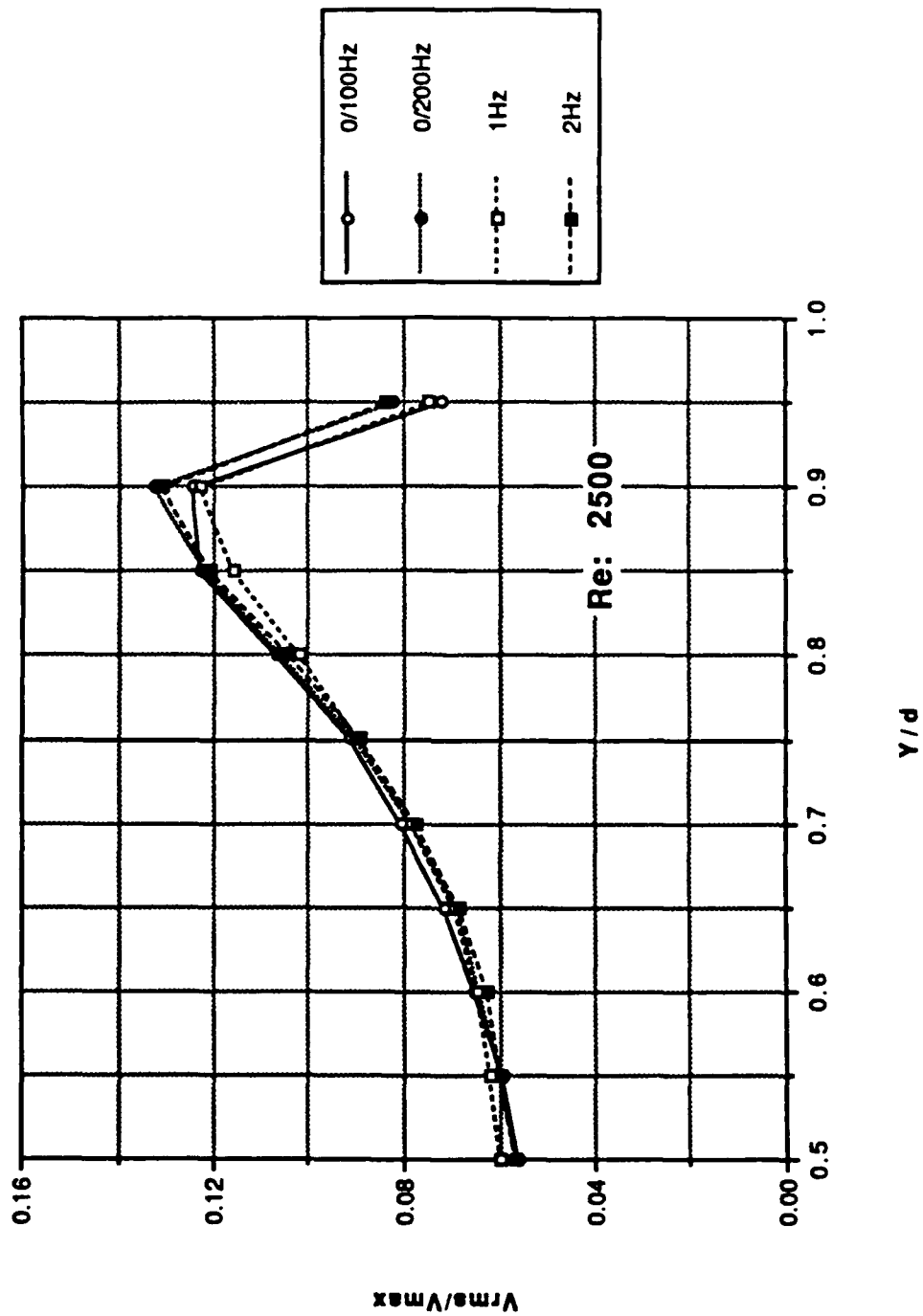


Figure 93. Profile Data: Longitudinal Turbulence Intensity Normalized by the Centerline Velocity vs y/d ; Re: 2500

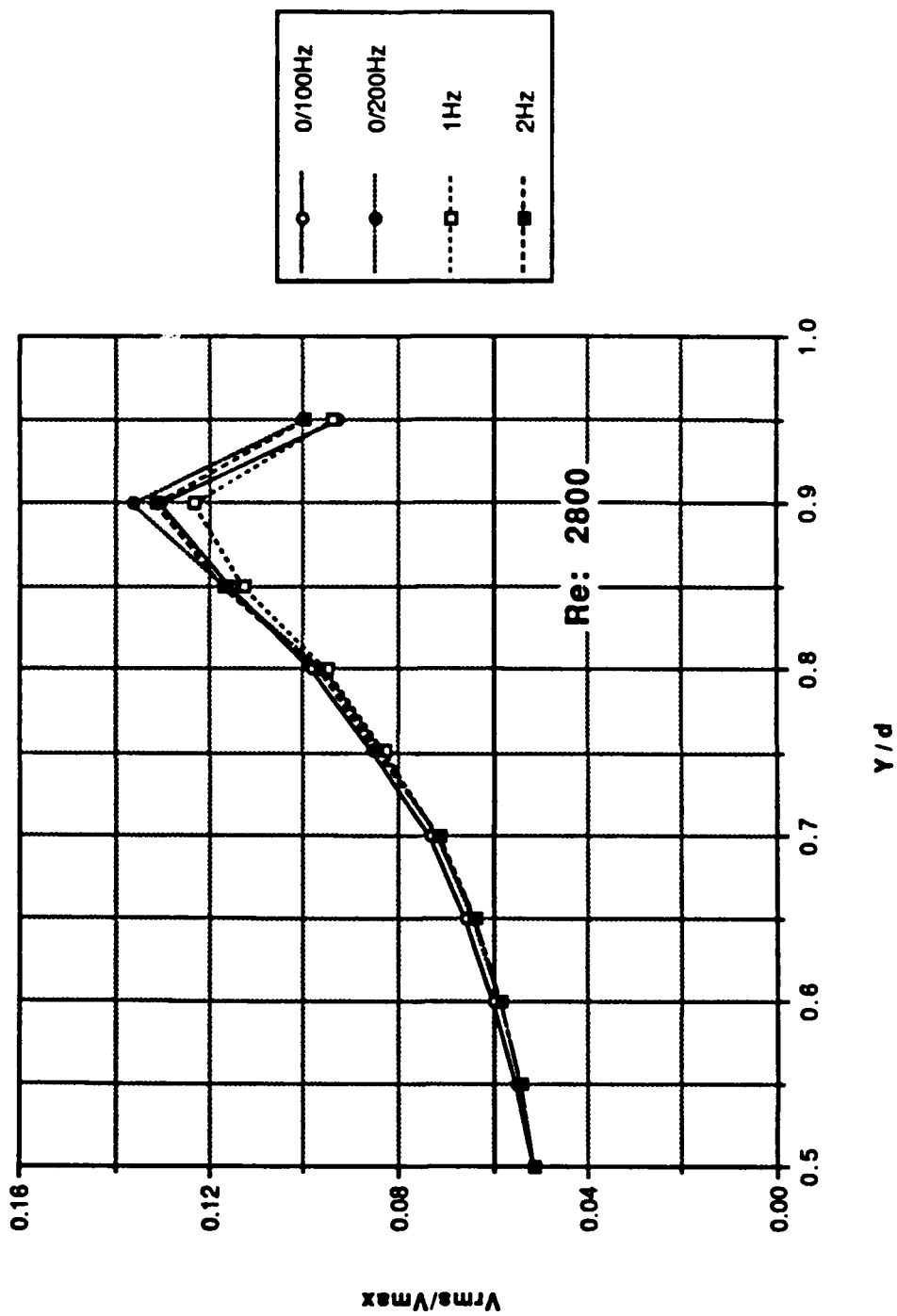


Figure 94. Profile Data: Longitudinal Turbulence Intensity Normalized by the Centerline Velocity vs y/d ; Re: 2800

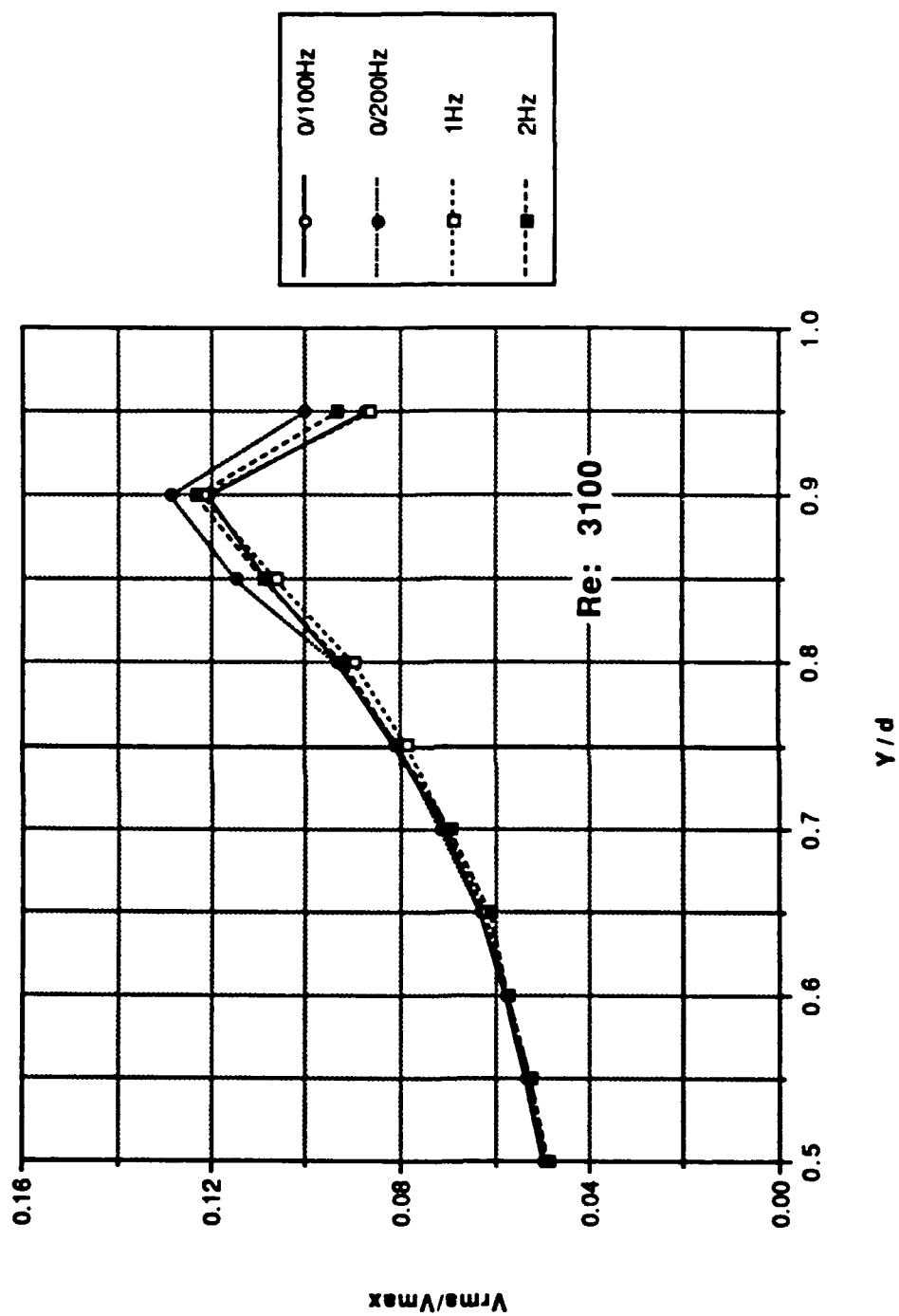


Figure 95. Profile Data: Longitudinal Turbulence Intensity Normalized by the Centerline Velocity vs y/d ; Re: 3100

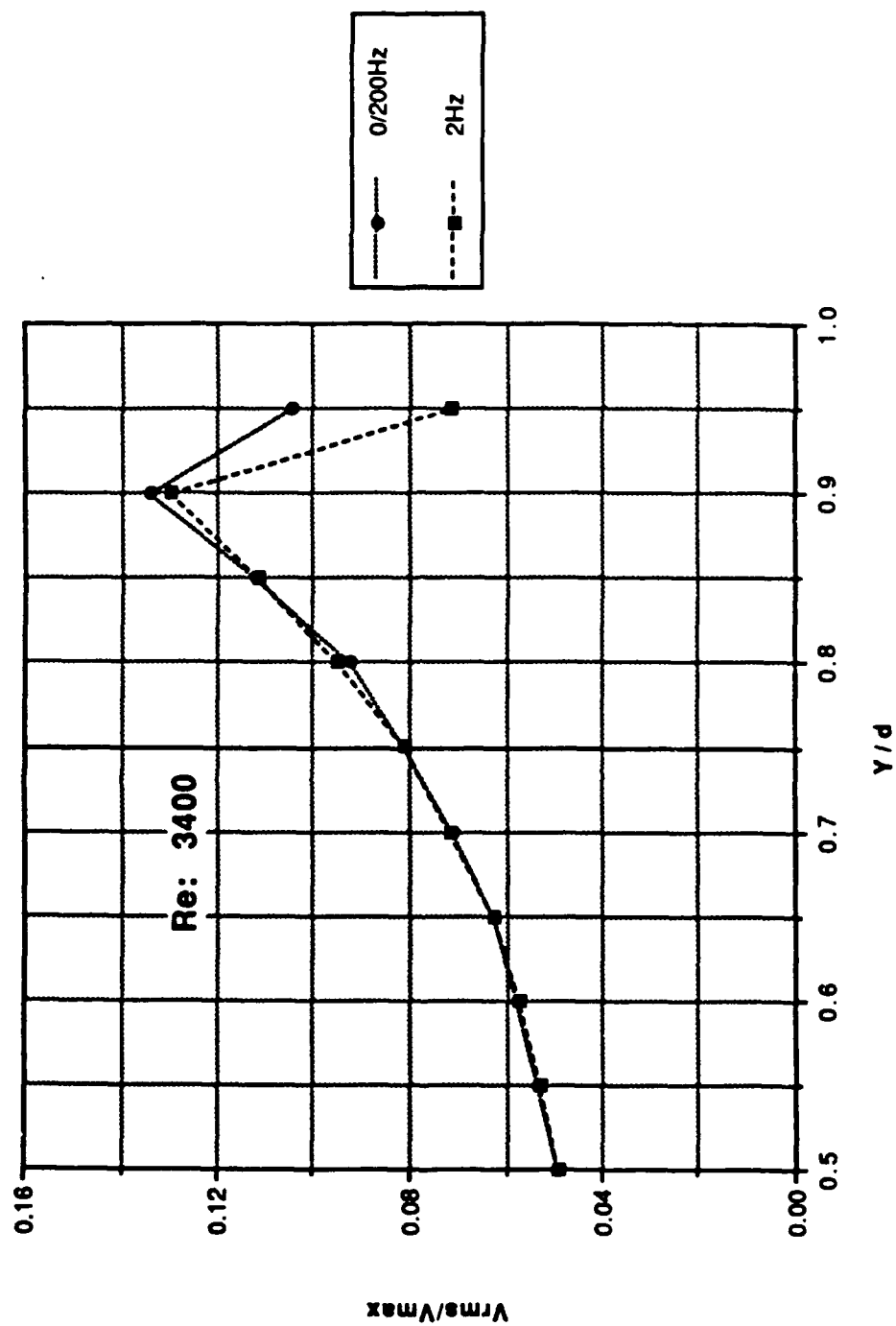


Figure 96. Profile Data: Longitudinal Turbulence Intensity Normalized by the Centerline Velocity vs y/d ; Re: 3400

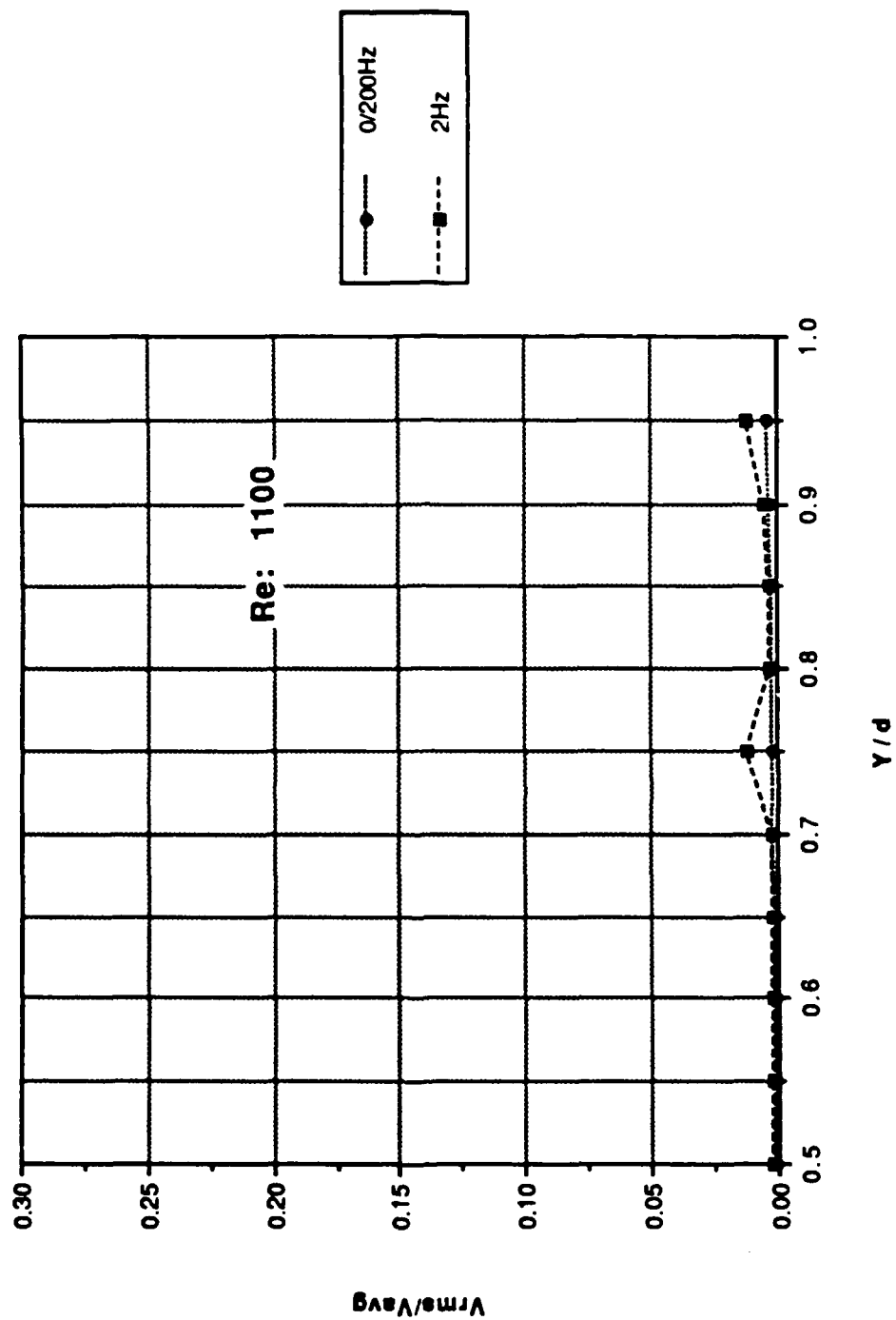


Figure 97. Profile Data: Longitudinal Turbulence Intensity Normalized by the Mean Velocity vs y/d ; Re: 1100

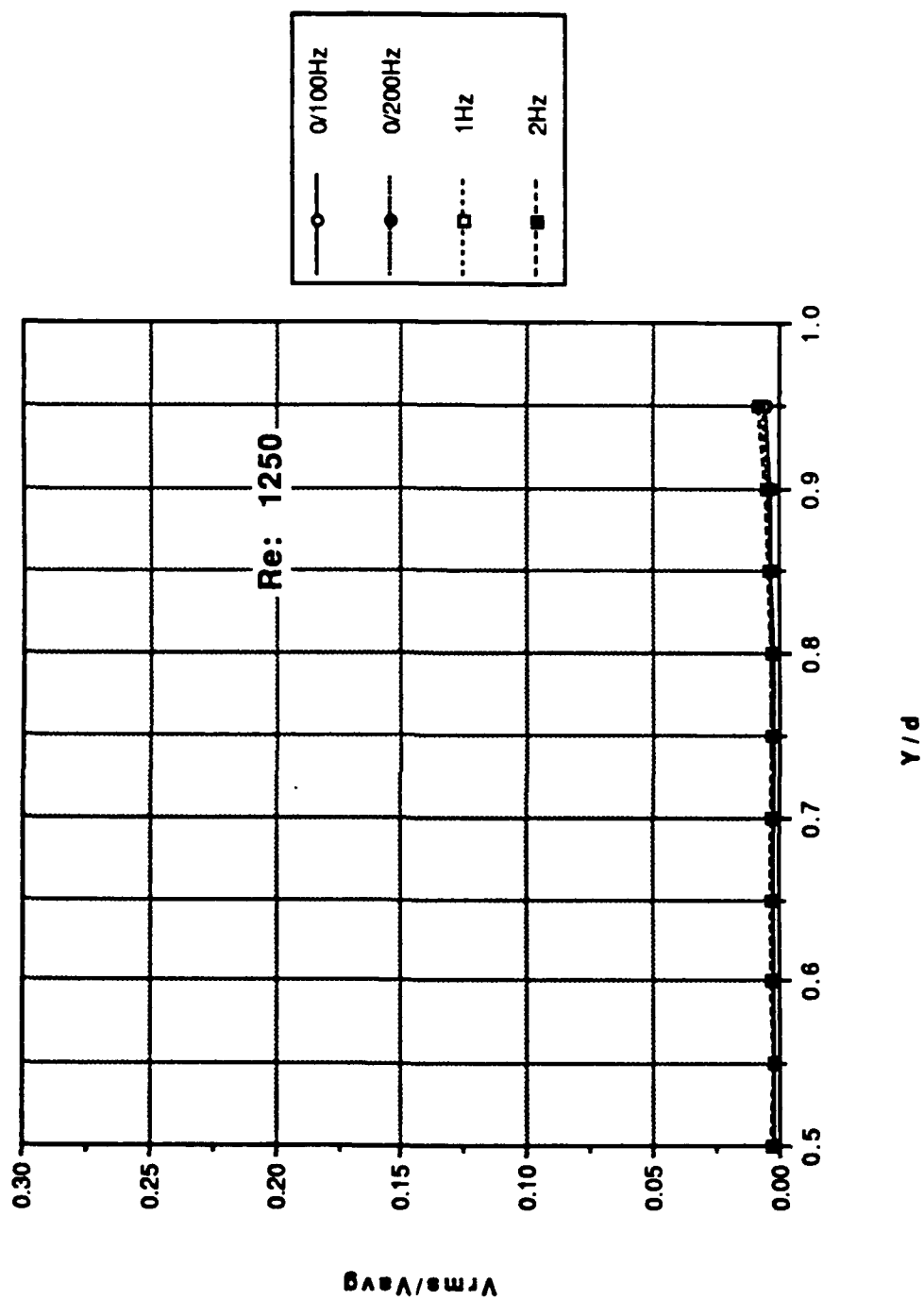


Figure 98. Profile Data: Longitudinal Turbulence Intensity Normalized by the Mean Velocity vs y/d ; Re: 1250

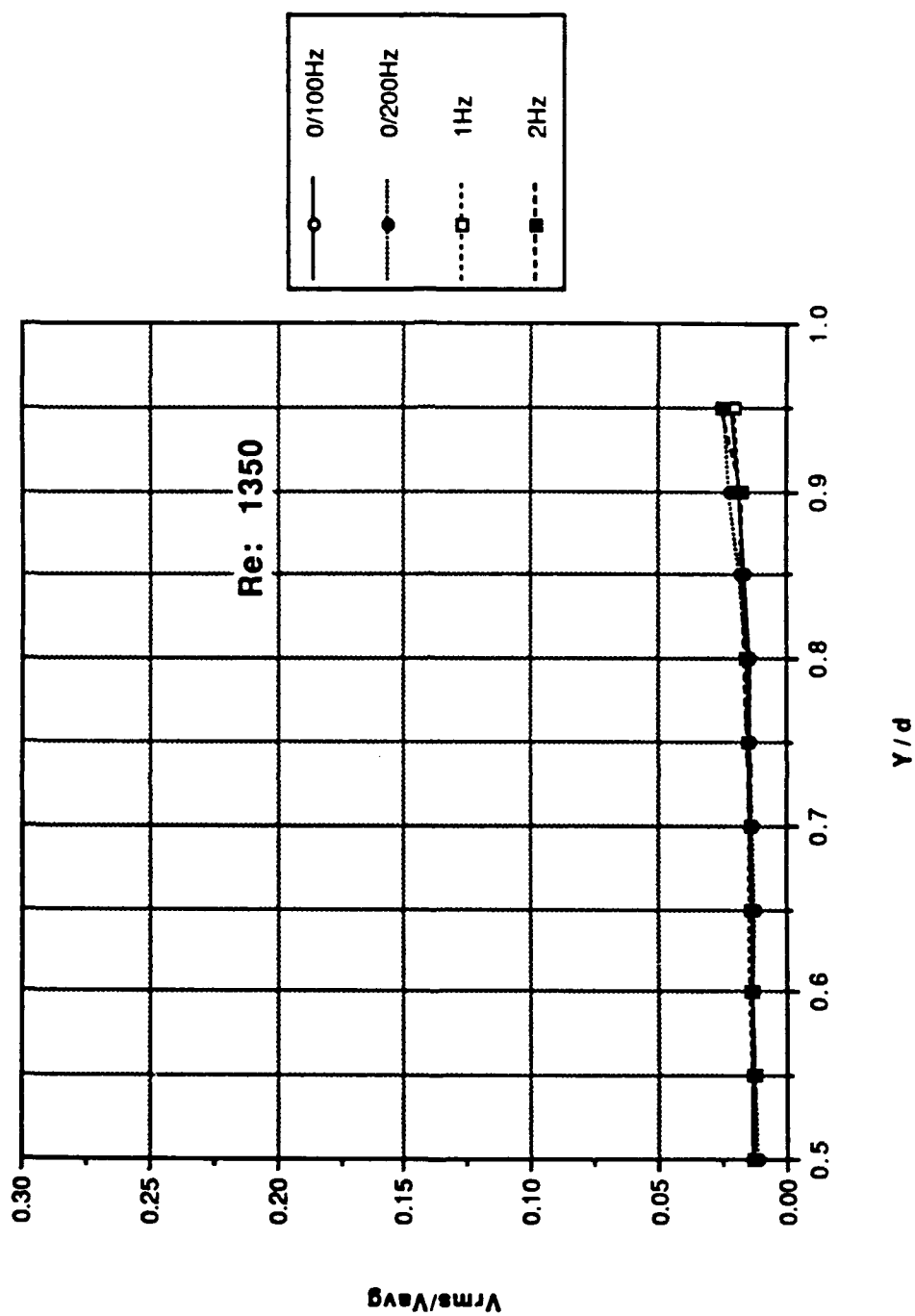


Figure 99. Profile Data: Longitudinal Turbulence Intensity Normalized by the Mean Velocity vs y/d ; $Re: 1350$

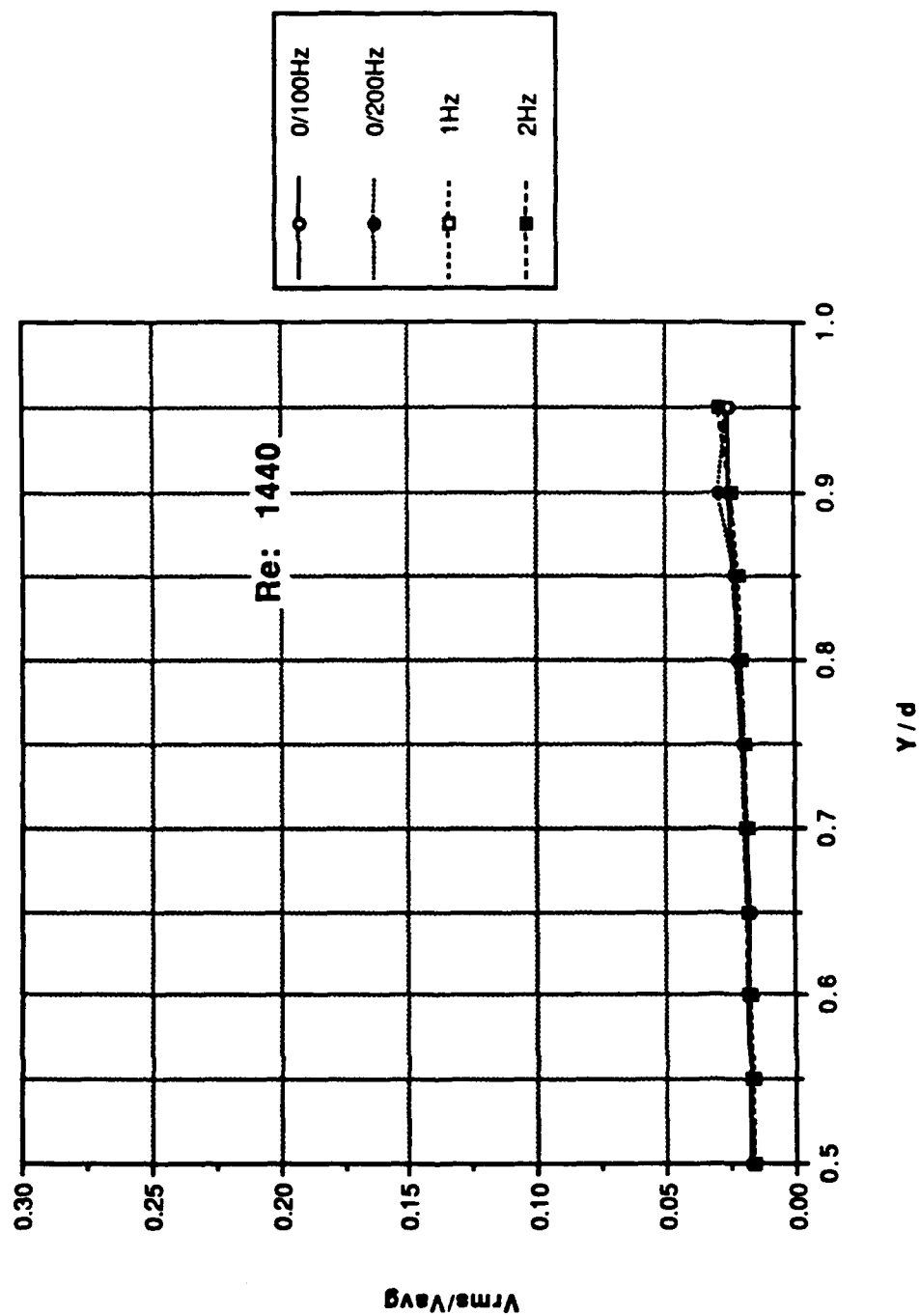


Figure 100. Profile Data: Longitudinal Turbulence Intensity Normalized by the Mean Velocity vs y/d ; $Re: 1440$

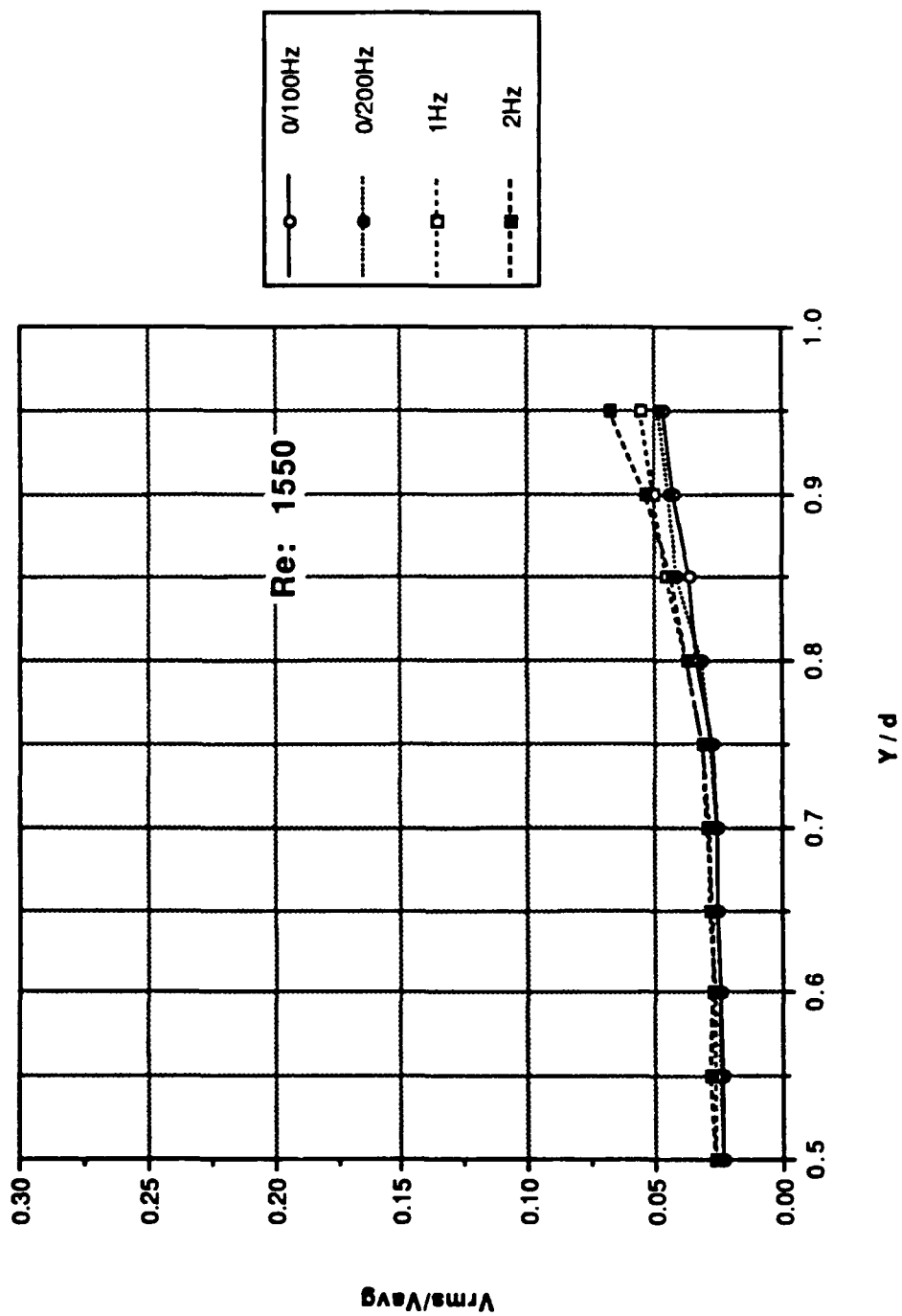


Figure 101. Profile Data: Longitudinal Turbulence Intensity Normalized by the Mean Velocity vs y/d ; Re: 1550

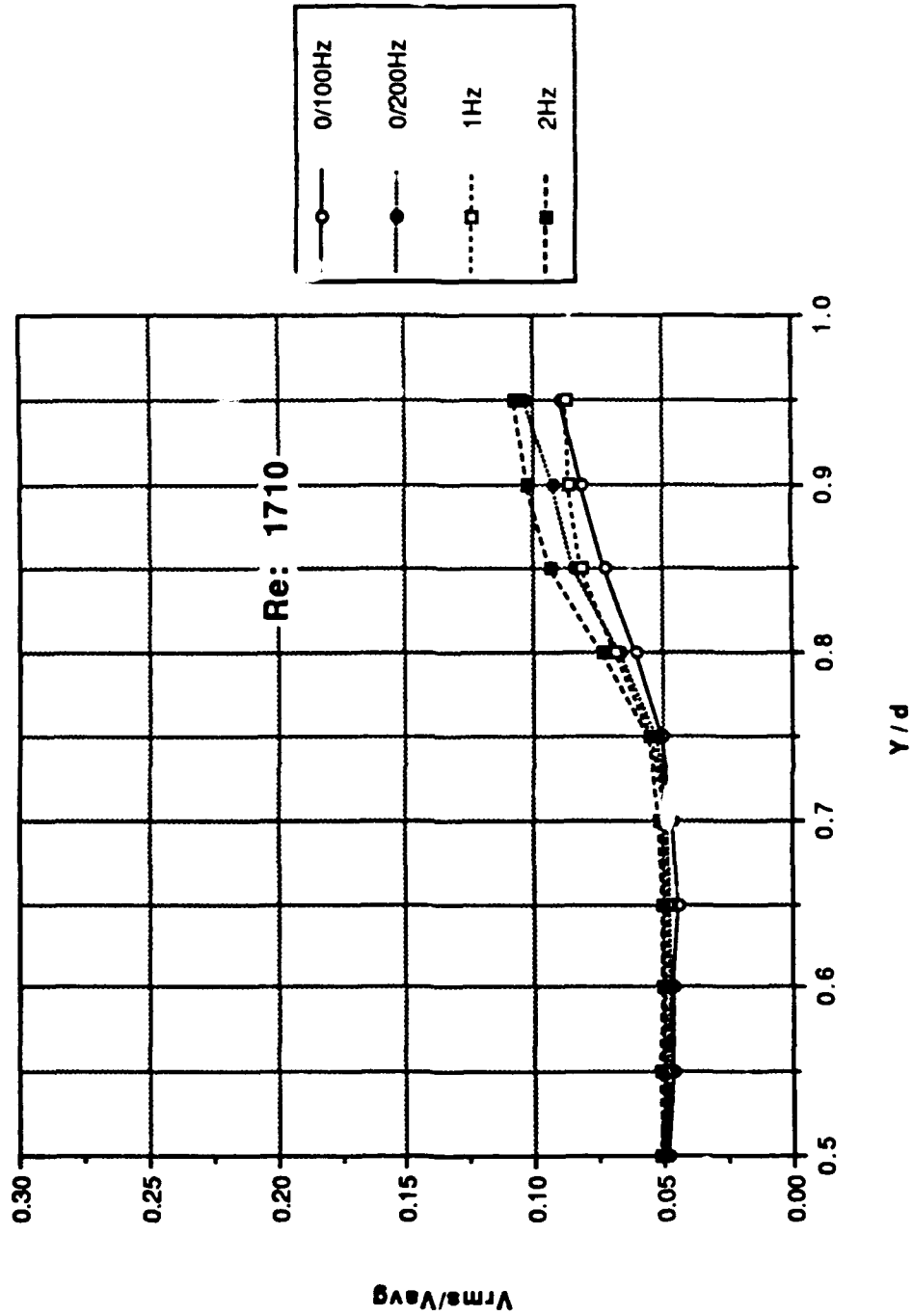


Figure 102. Profile Data: Longitudinal Turbulence Intensity Normalized by the Mean Velocity vs y/d ; Re: 1710

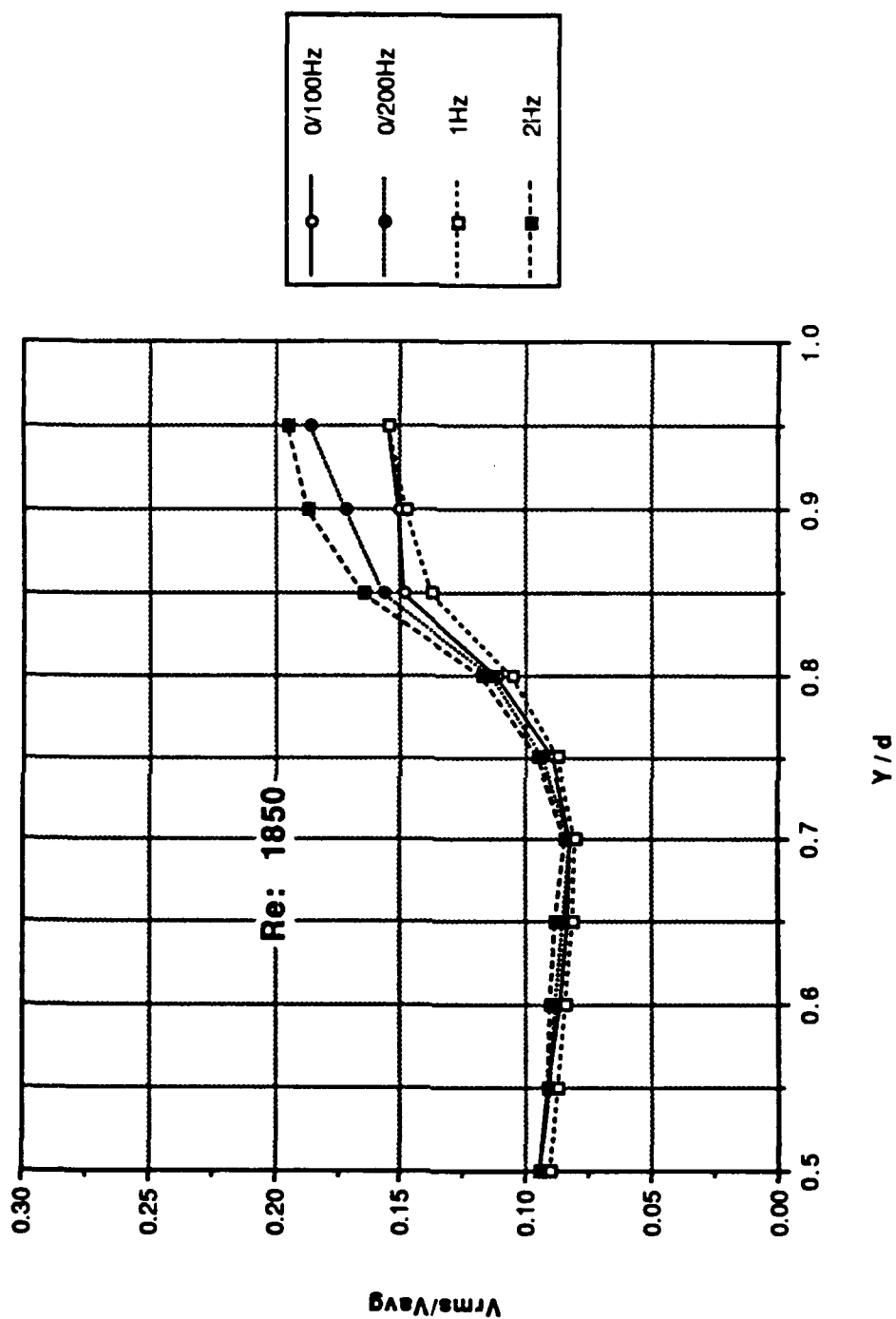


Figure 103. Profile Data: Longitudinal Turbulence Intensity Normalized by the Mean Velocity vs y/d ; Re: 1850

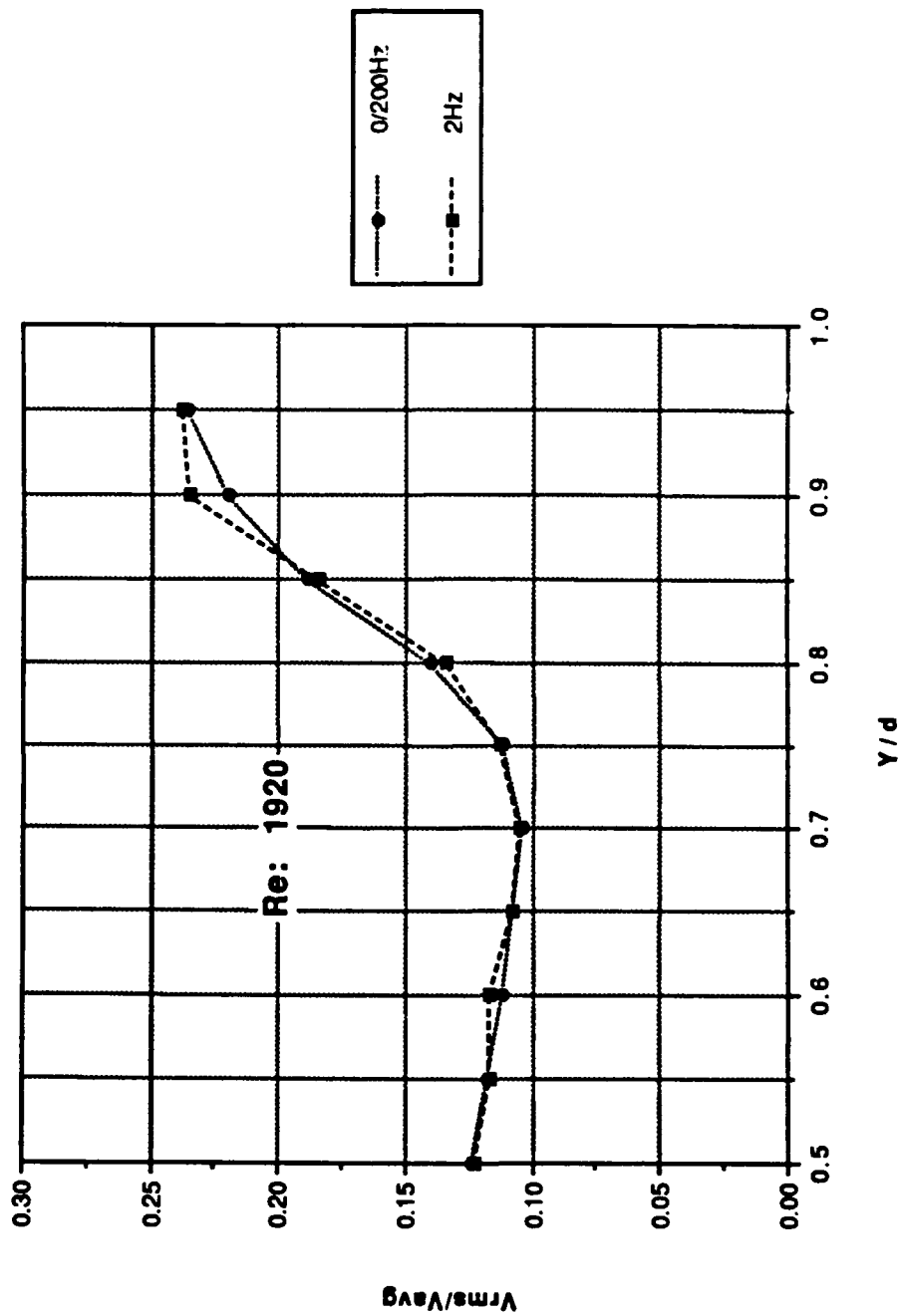


Figure 104. Profile Data: Longitudinal Turbulence Intensity Normalized by the Mean Velocity vs y/d ; Re: 1920

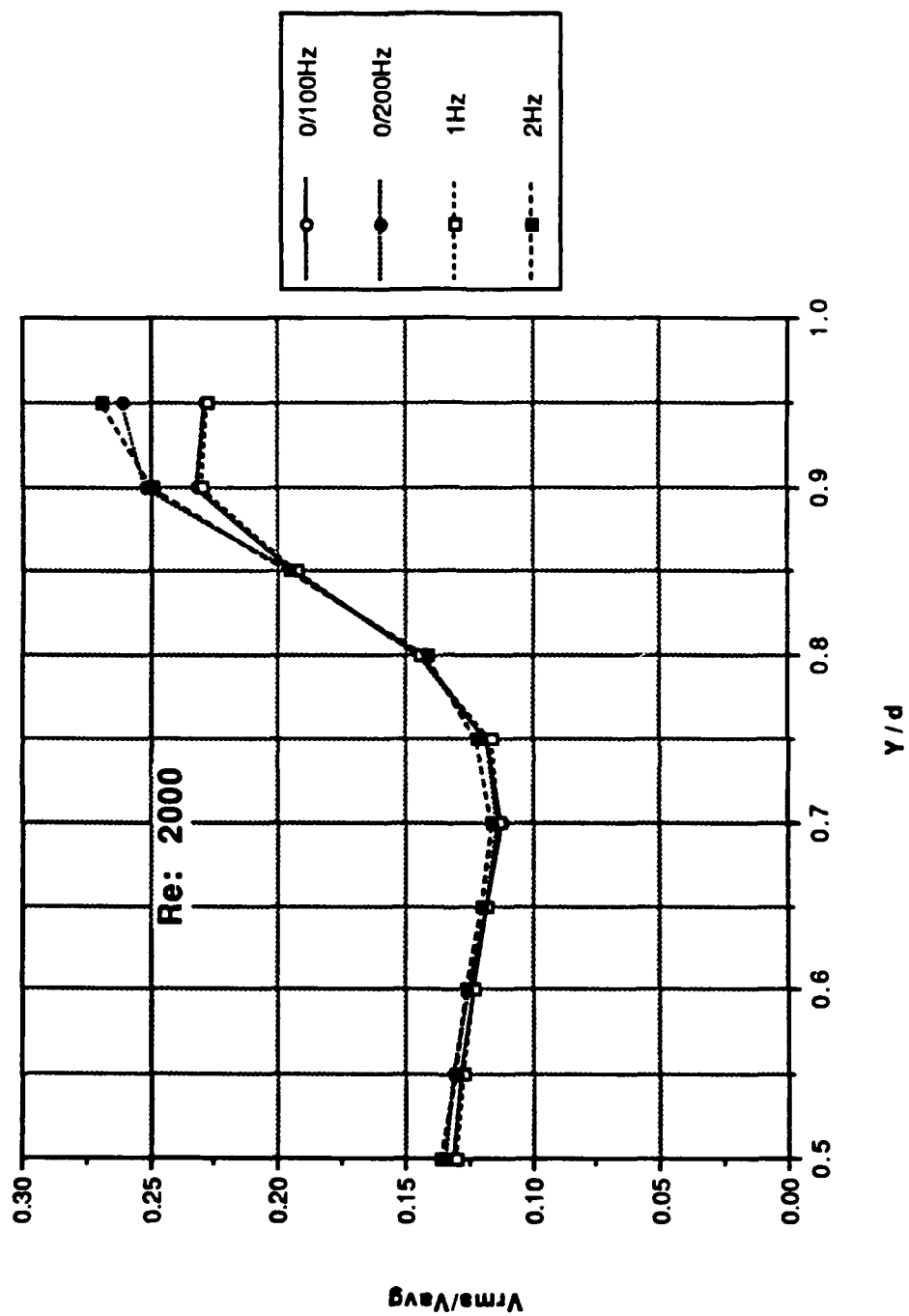


Figure 105. Profile Data: Longitudinal Turbulence Intensity Normalized by the Mean Velocity vs y/d ; Re: 2000

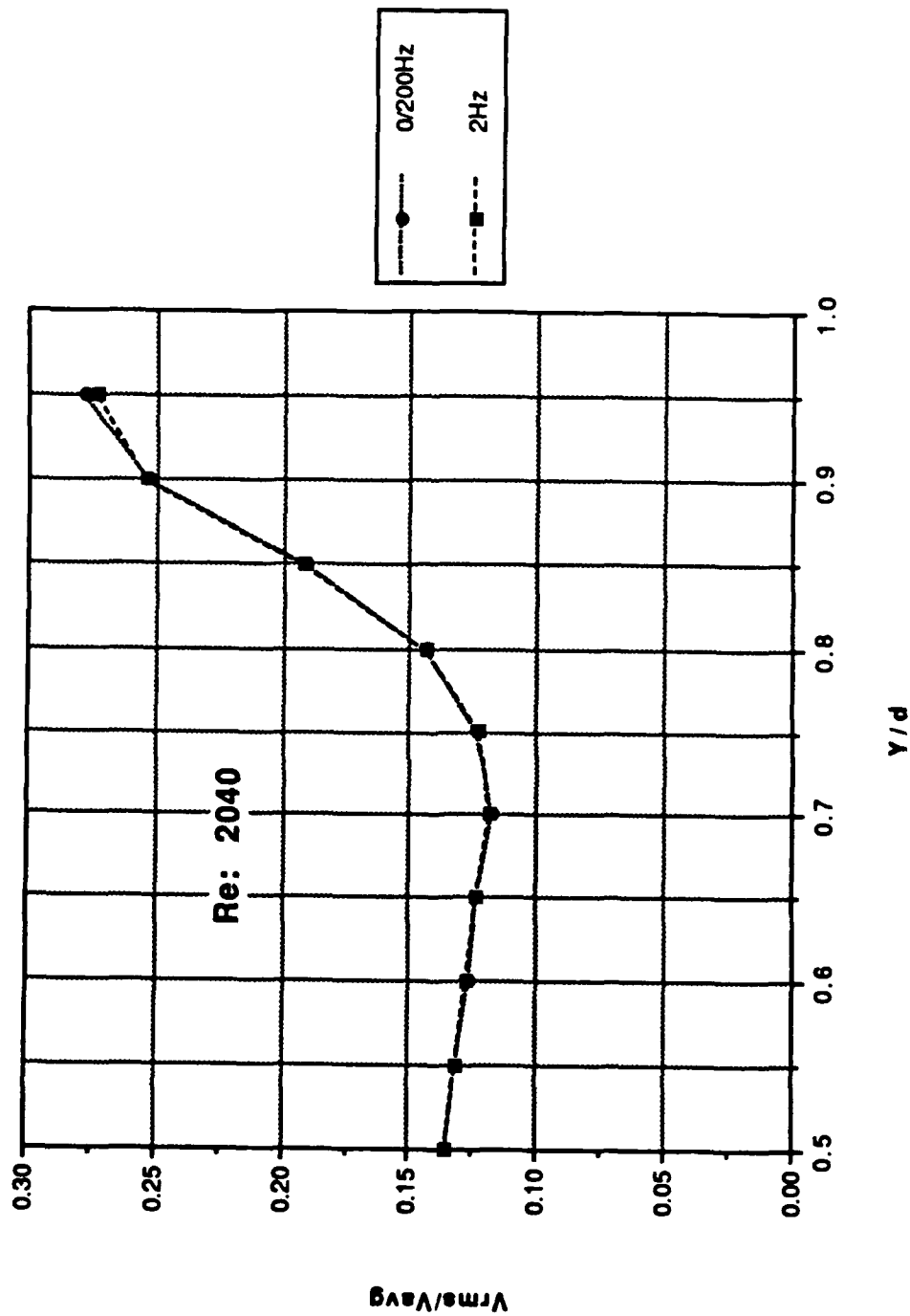


Figure 106. Profile Data: Longitudinal Turbulence Intensity Normalized by the Mean Velocity vs y/d ; Re: 2040

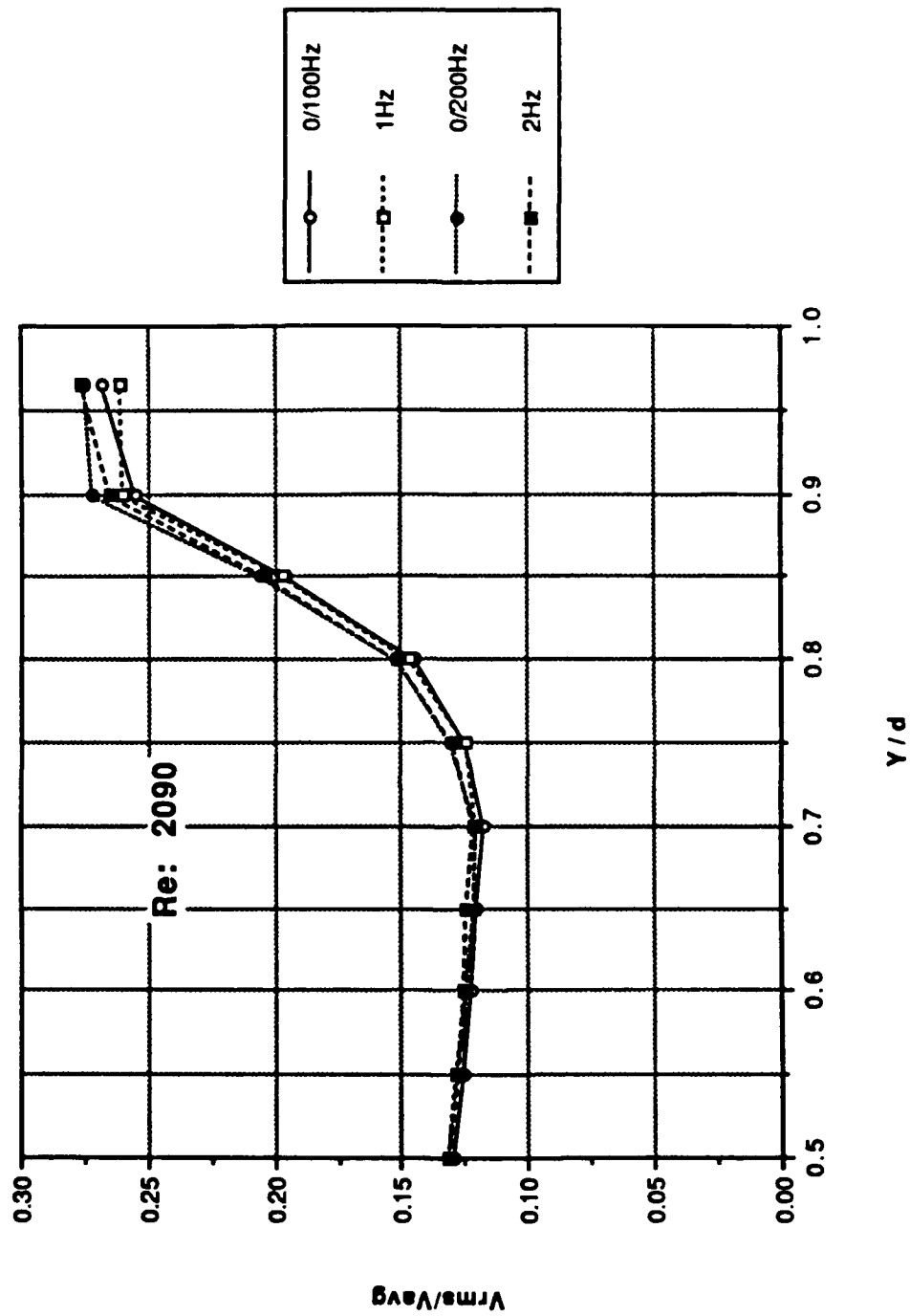


Figure 107. Profile Data: Longitudinal Turbulence Intensity Normalized by the Mean Velocity vs y/d ; Re: 2090

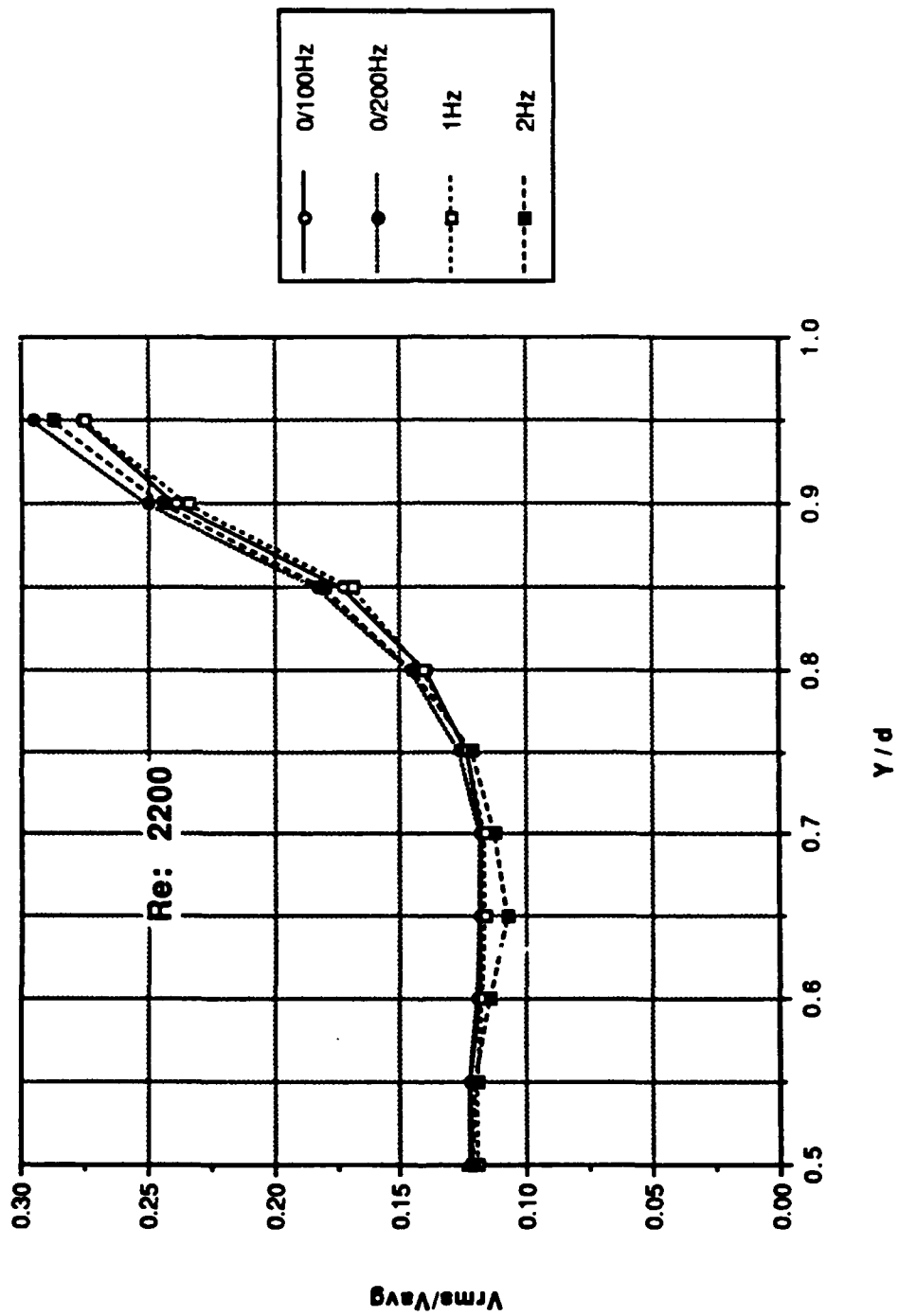


Figure 108. Profile Data: Longitudinal Turbulence Intensity Normalized by the Mean Velocity vs y/d ; Re: 2200

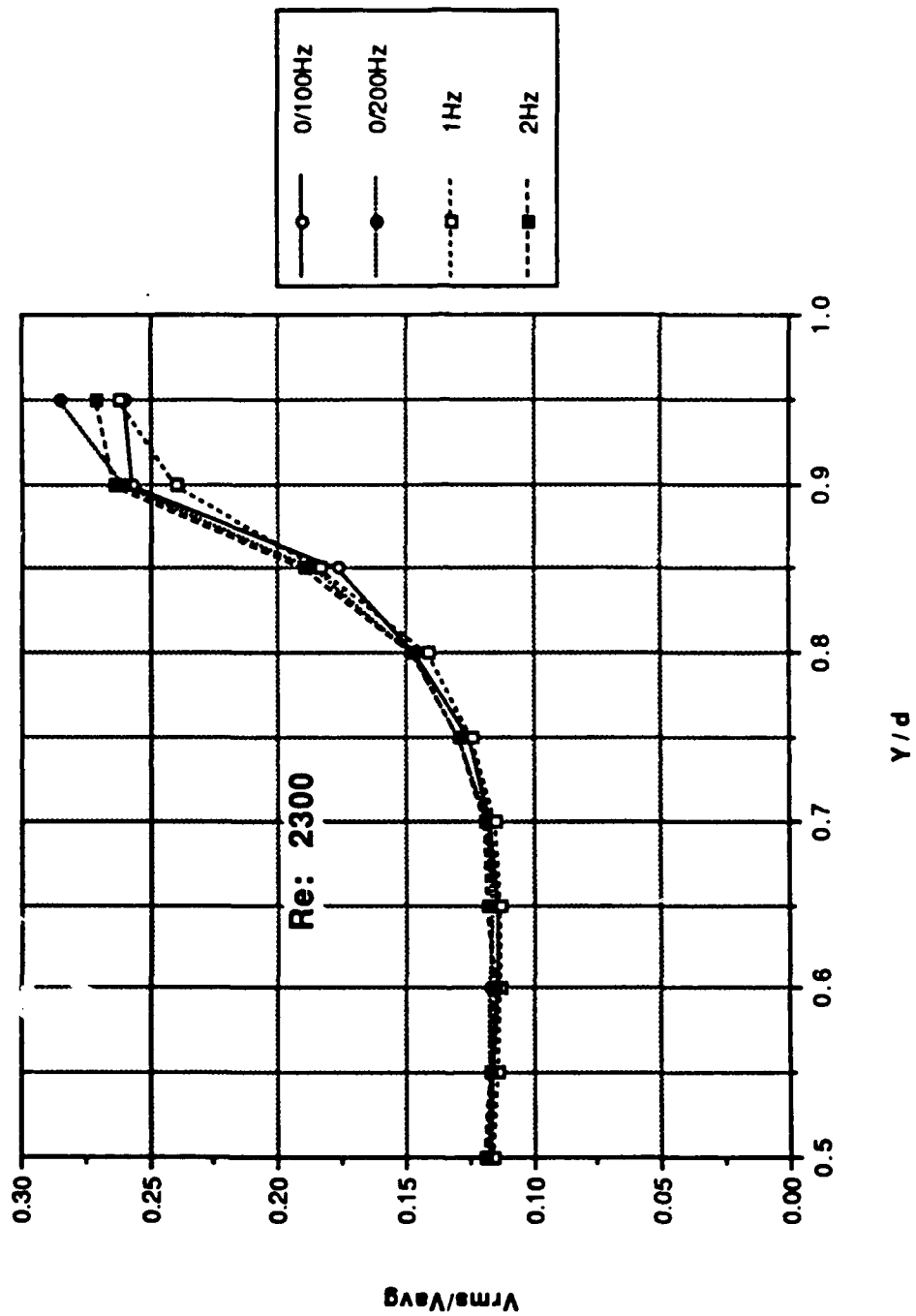


Figure 109. Profile Data: Longitudinal Turbulence Intensity Normalized by the Mean Velocity vs y/d ; Re: 2300

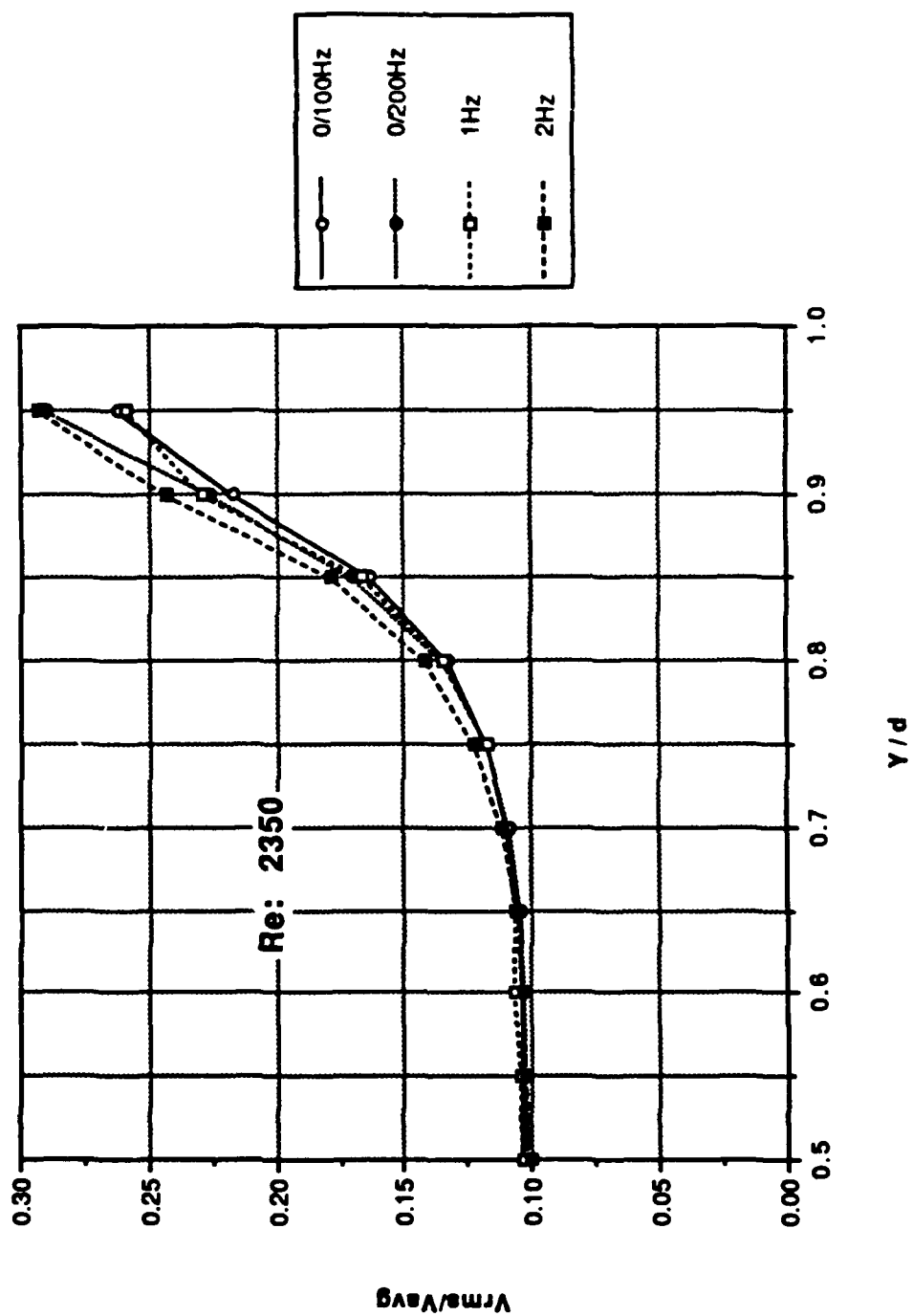


Figure 110. Profile Data: Longitudinal Turbulence Intensity Normalized by the Mean Velocity vs y/d ; Re: 2350

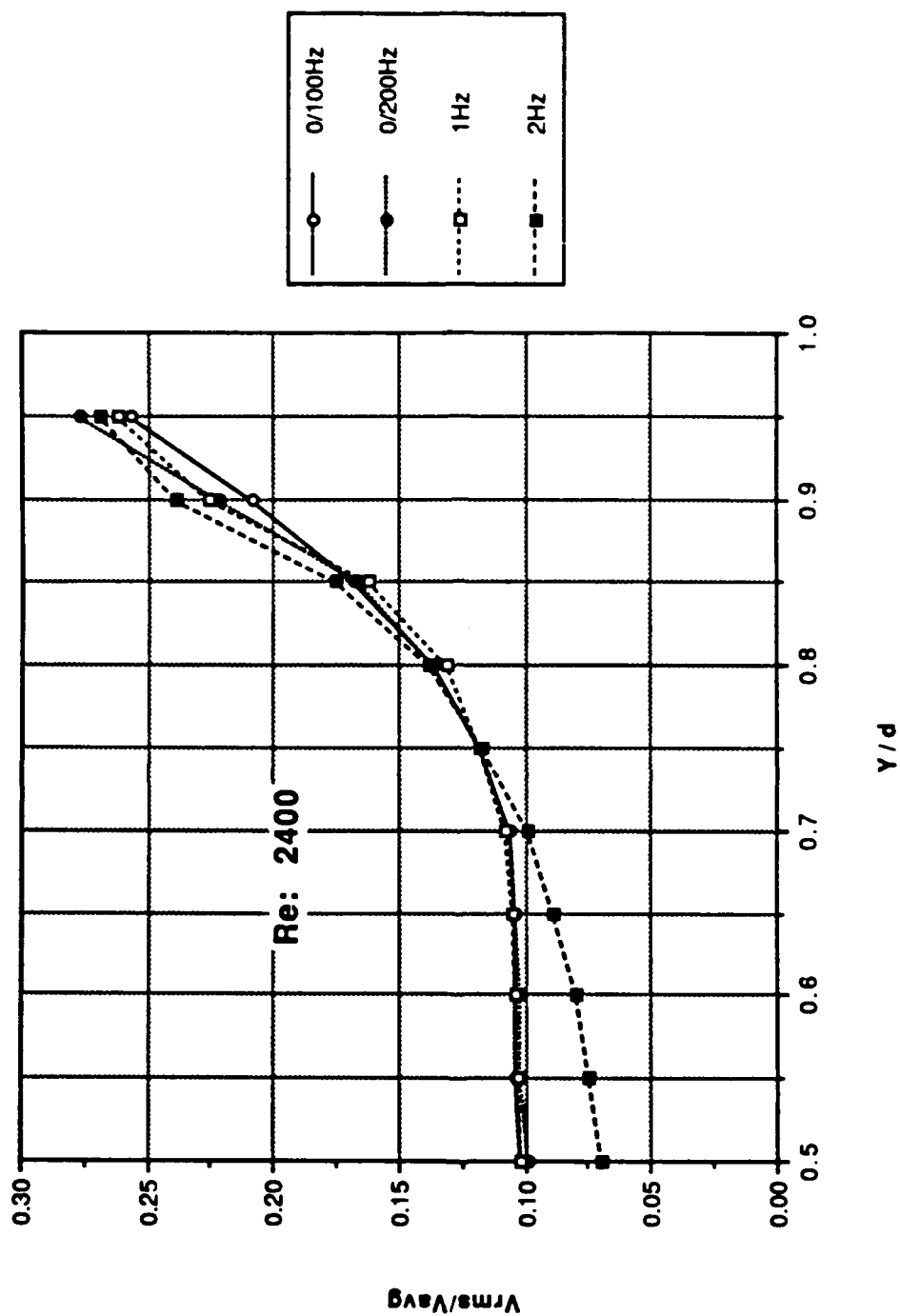


Figure 111. Profile Data: Longitudinal Turbulence Intensity Normalized by the Mean Velocity vs y/d ; Re: 2400

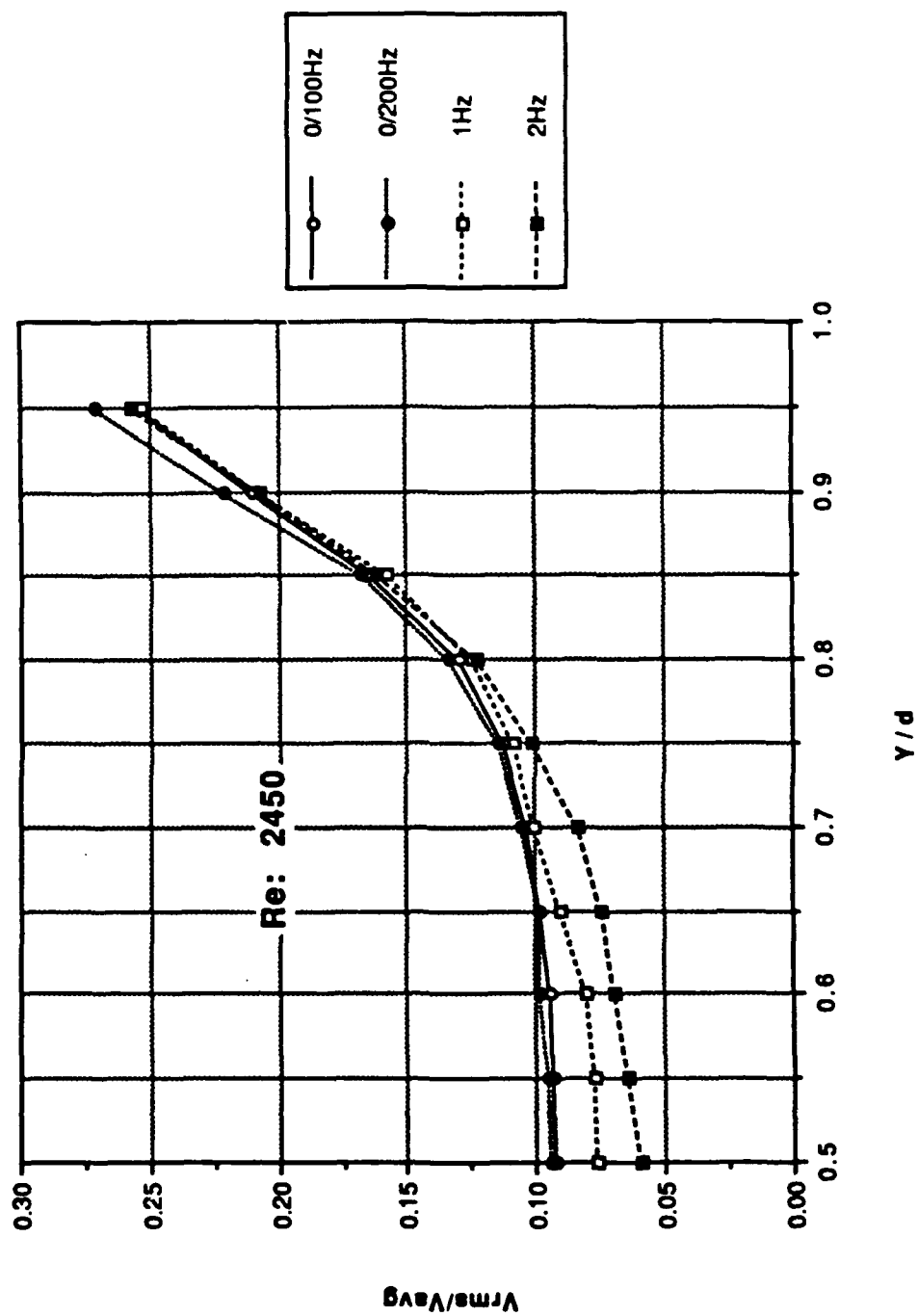


Figure 112. Profile Data: Longitudinal Turbulence Intensity Normalized by the Mean Velocity vs y/d ; Re: 2450

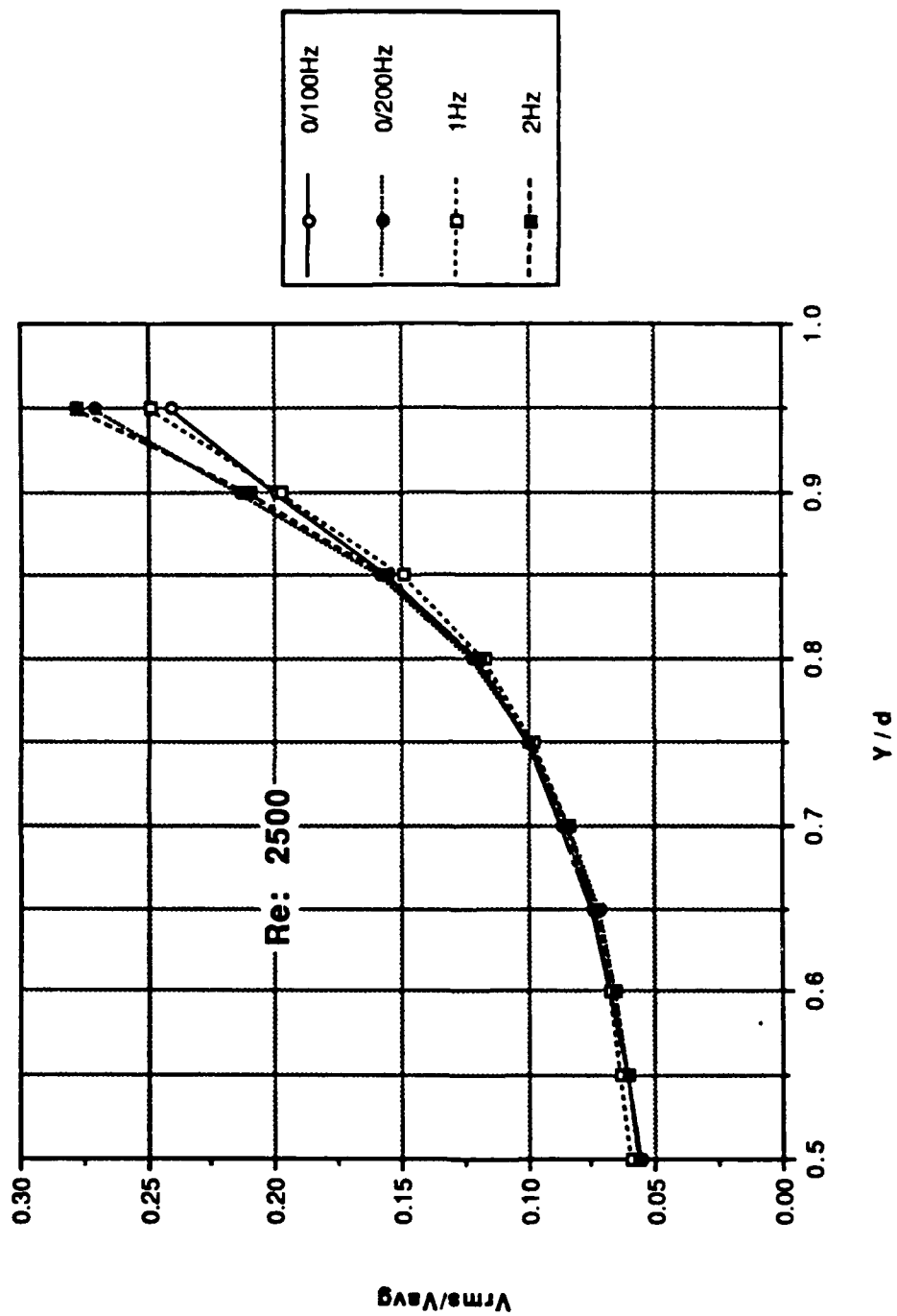


Figure 113. Profile Data: Longitudinal Turbulence Intensity Normalized by the Mean Velocity vs y/d ; Re: 2500

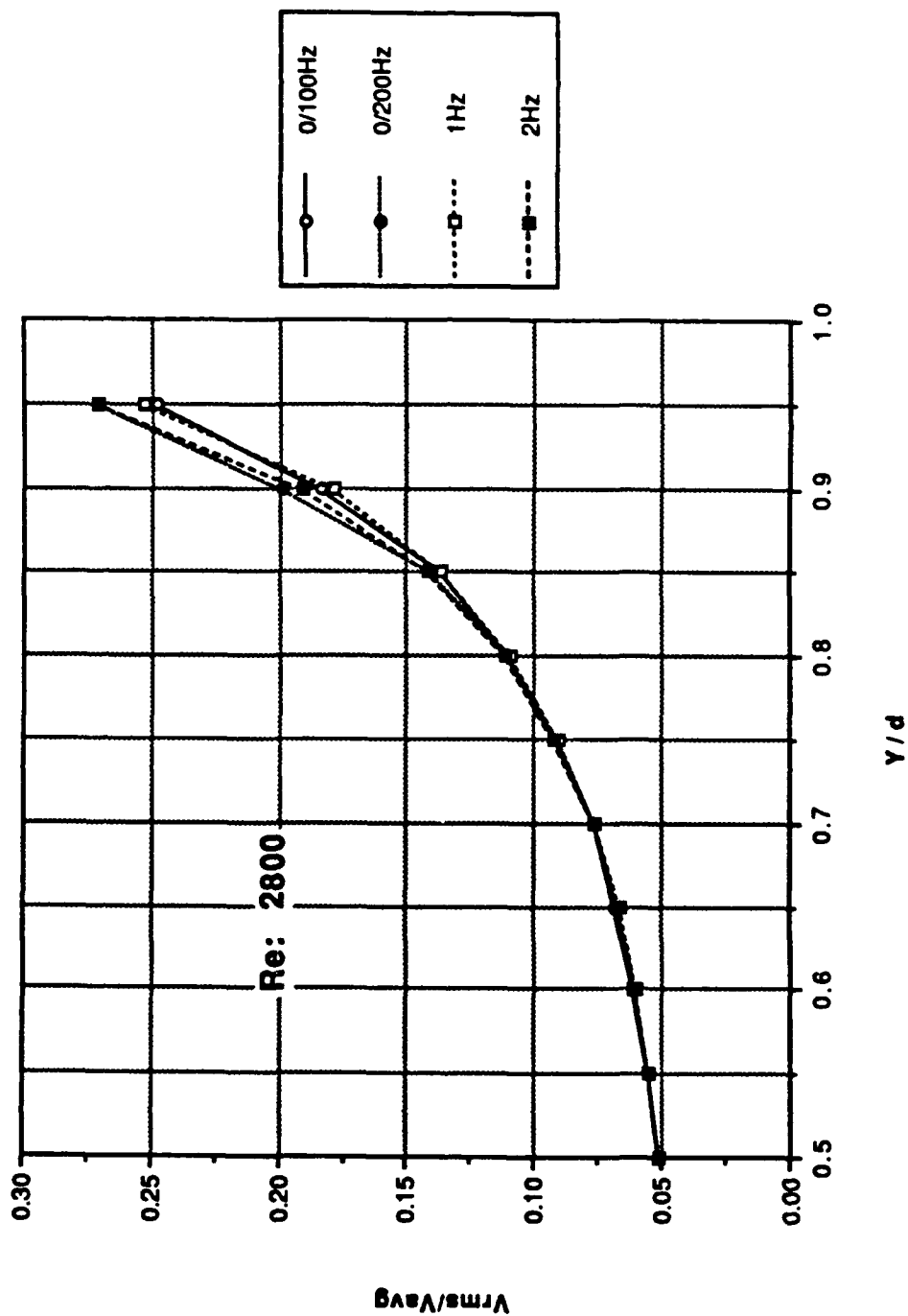


Figure 114. Profile Data: Longitudinal Turbulence Intensity Normalized by the Mean Velocity vs y/d ; Re: 2800

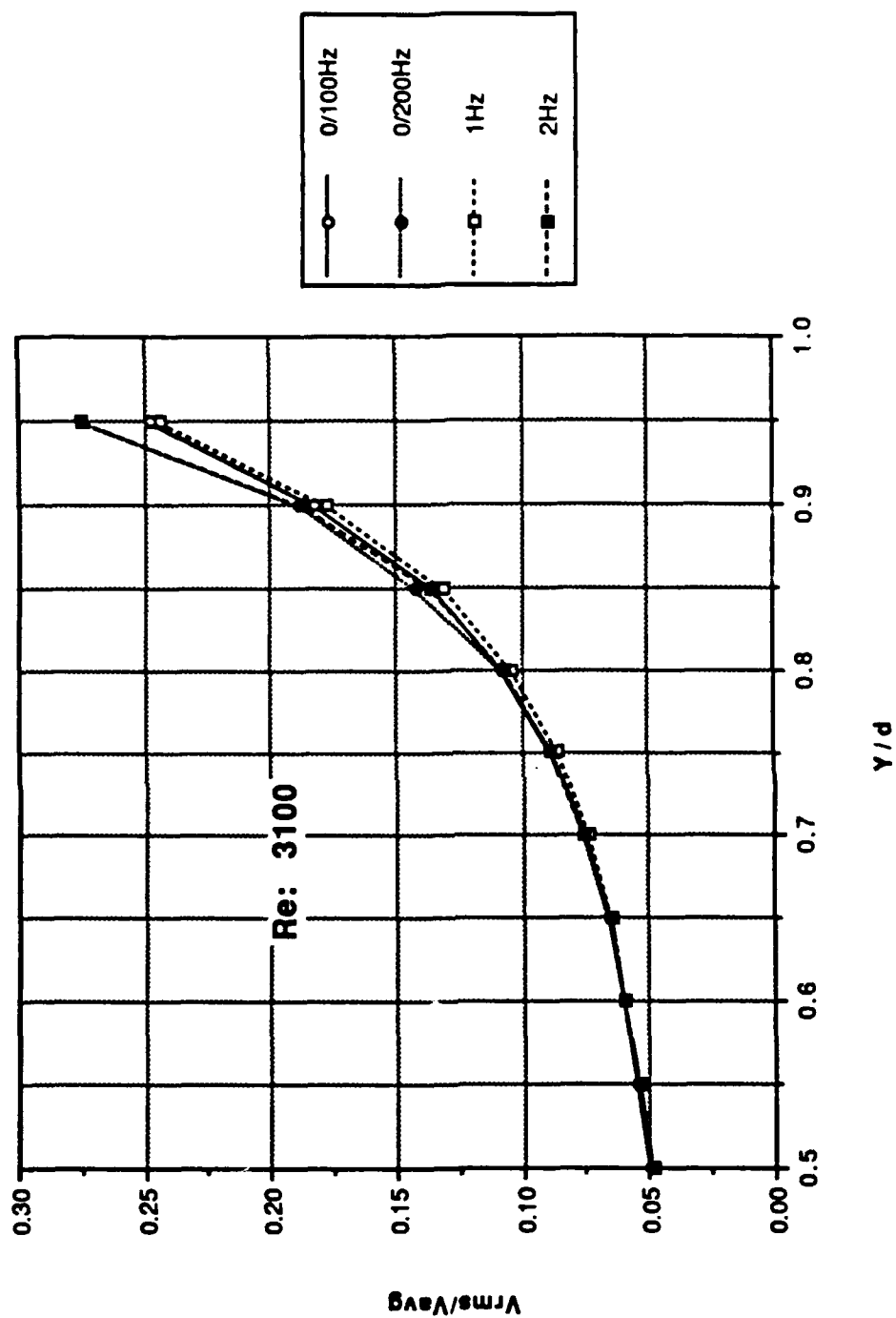


Figure 115. Profile Data: Longitudinal Turbulence Intensity Normalized by the Mean Velocity vs y/d ; Re: 3100

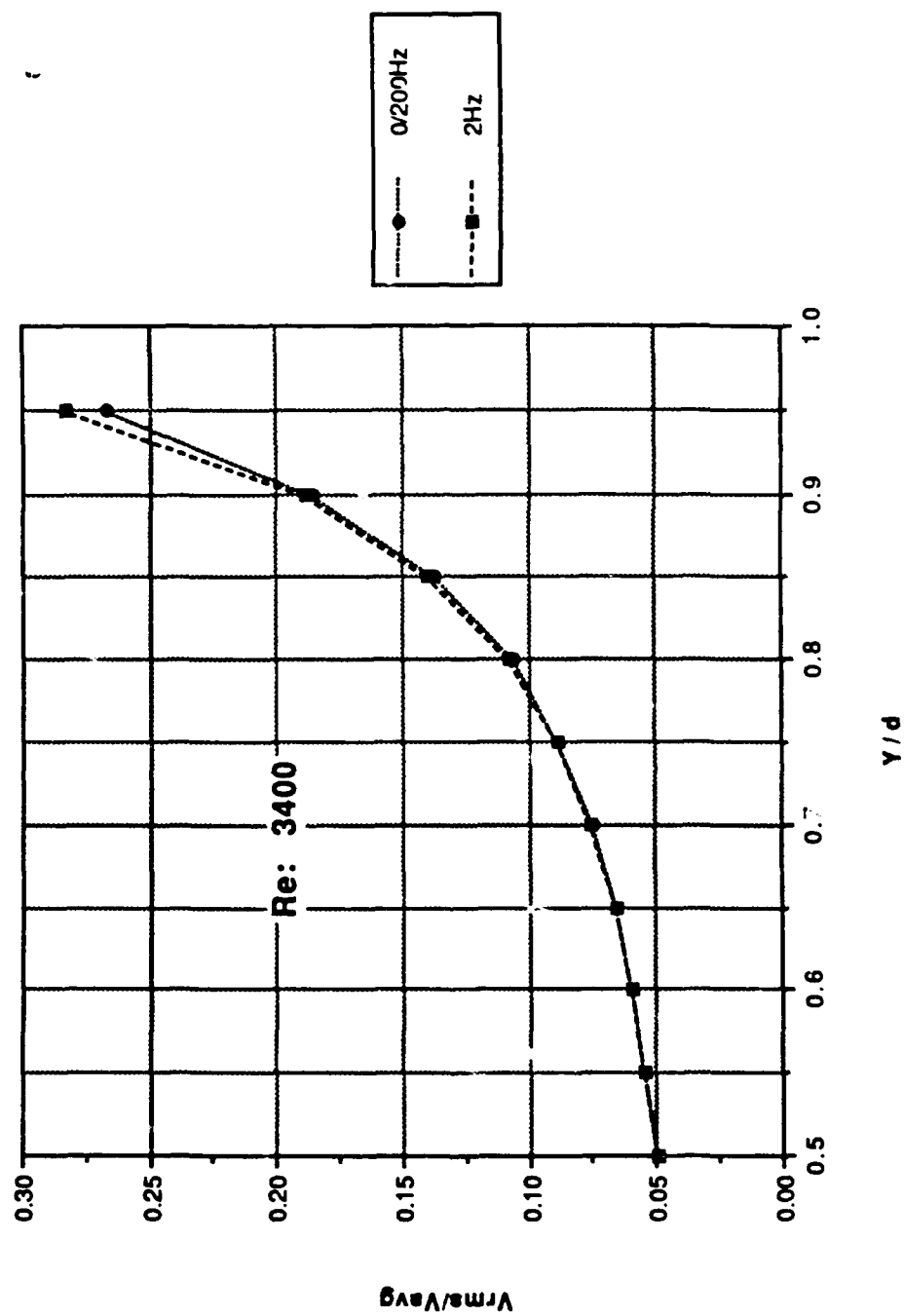


Figure 116. Profile Data: Longitudinal Turbulence Intensity Normalized by the Mean Velocity vs y/d ; Re: 3400

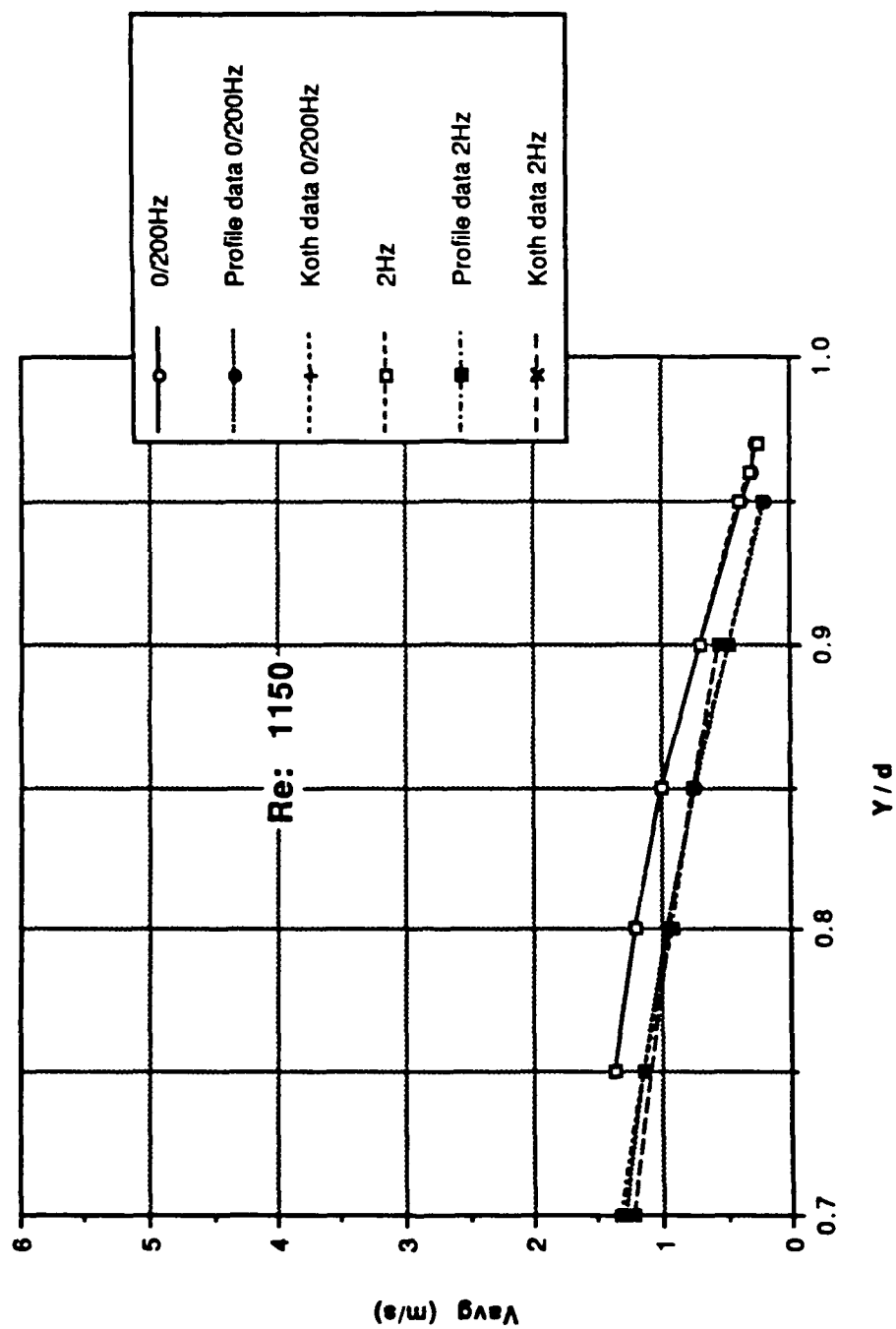


Figure 117. Near-Wall Data: Mean Velocity vs y/d; Re: 1150

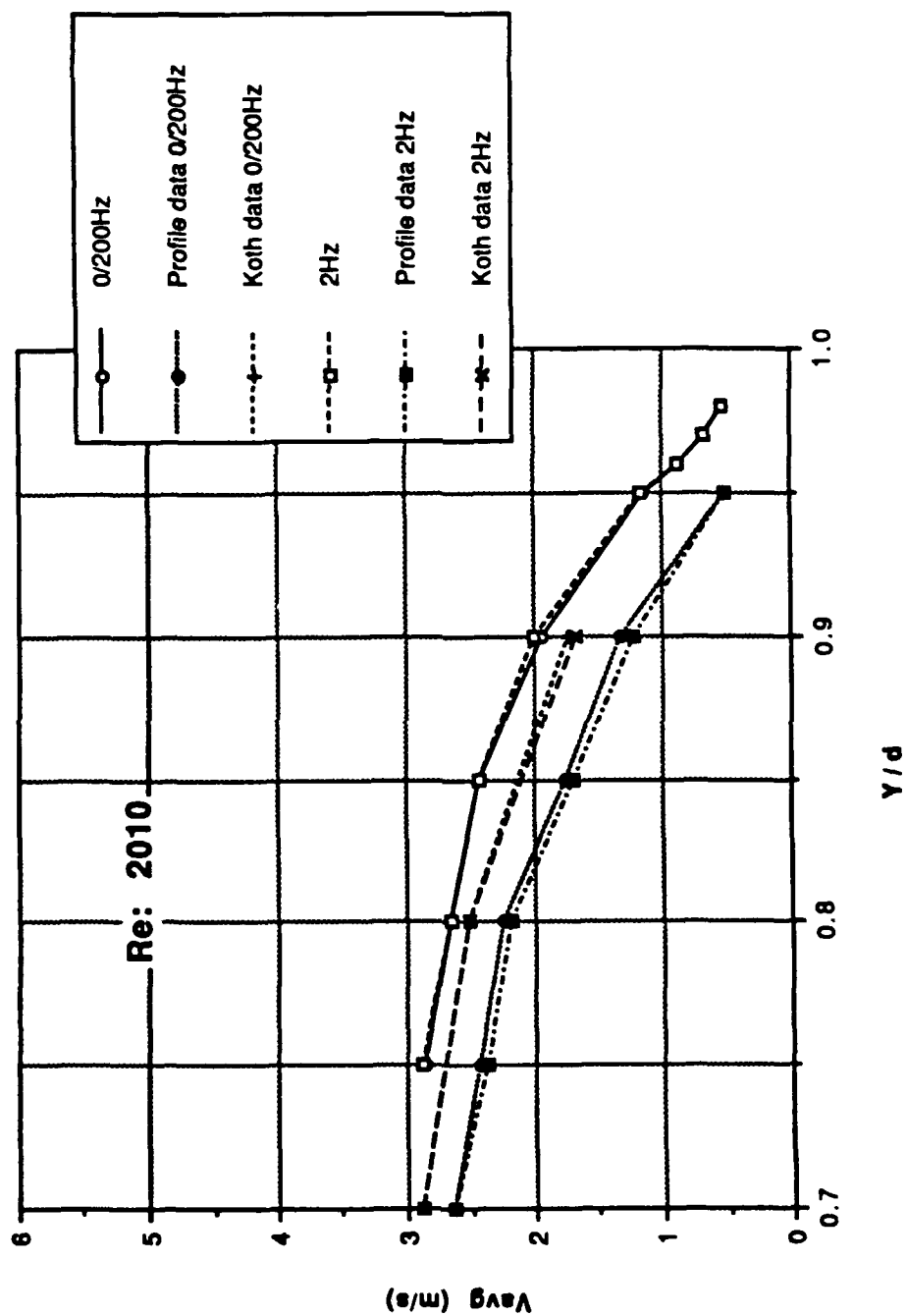


Figure 118. Near-Wall Data: Mean Velocity vs y/d ; Re: 2010

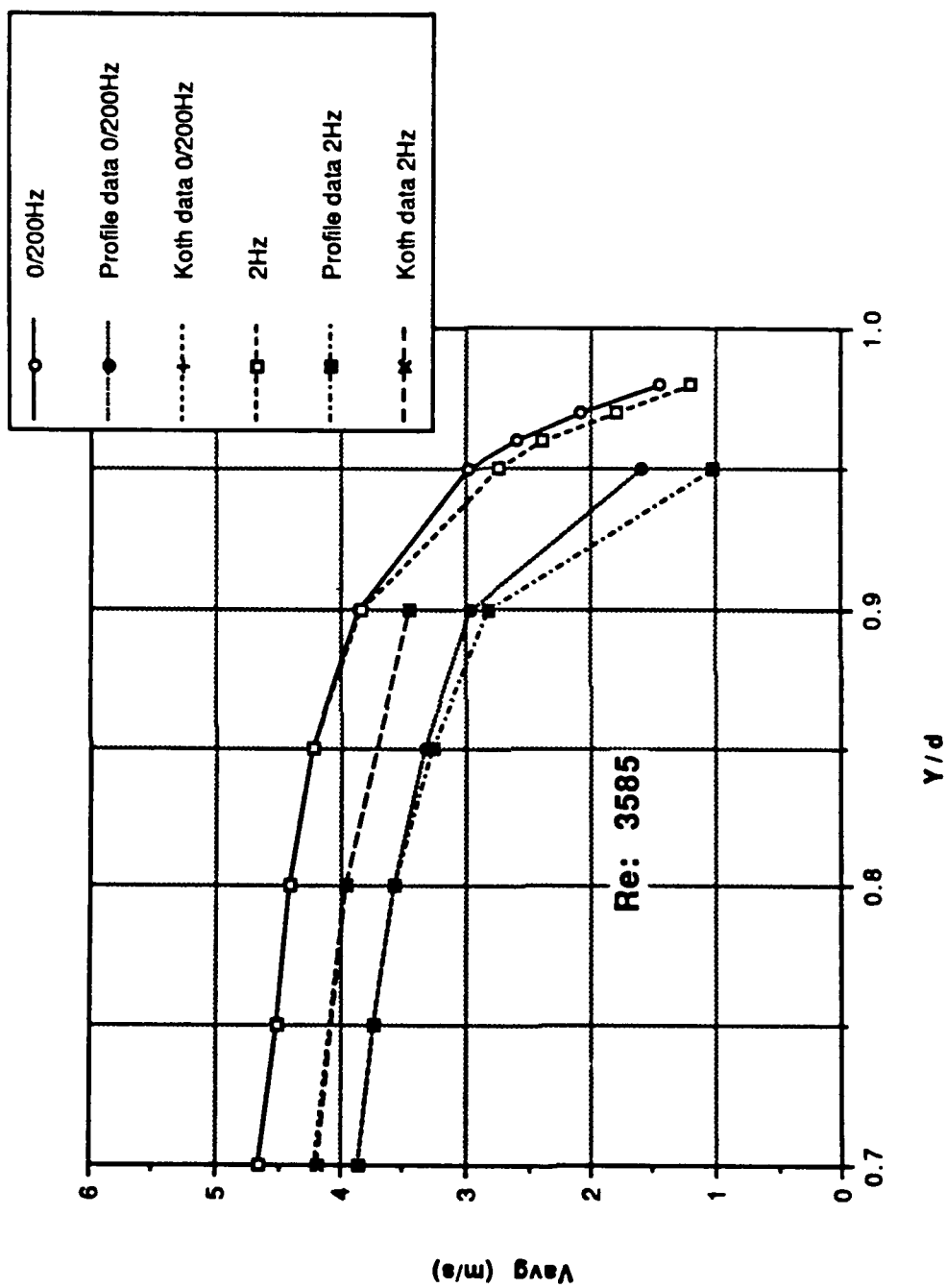


Figure 119. Near-Wall Data: Mean Velocity vs y/d ; Re: 3585

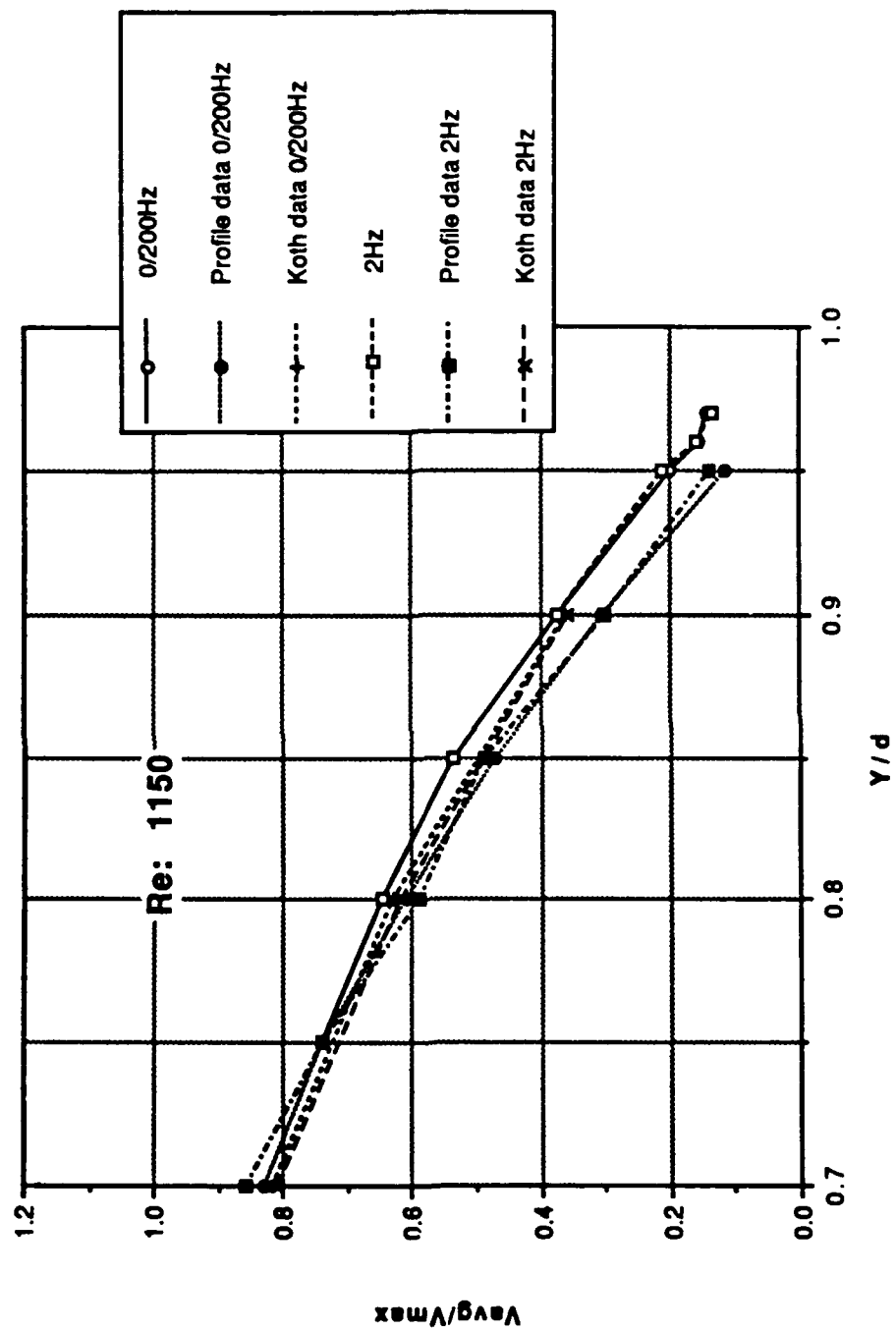


Figure 120. Near-Wall Data: Mean Velocity Normalized by the Centerline Velocity vs y/d ; $Re: 1150$

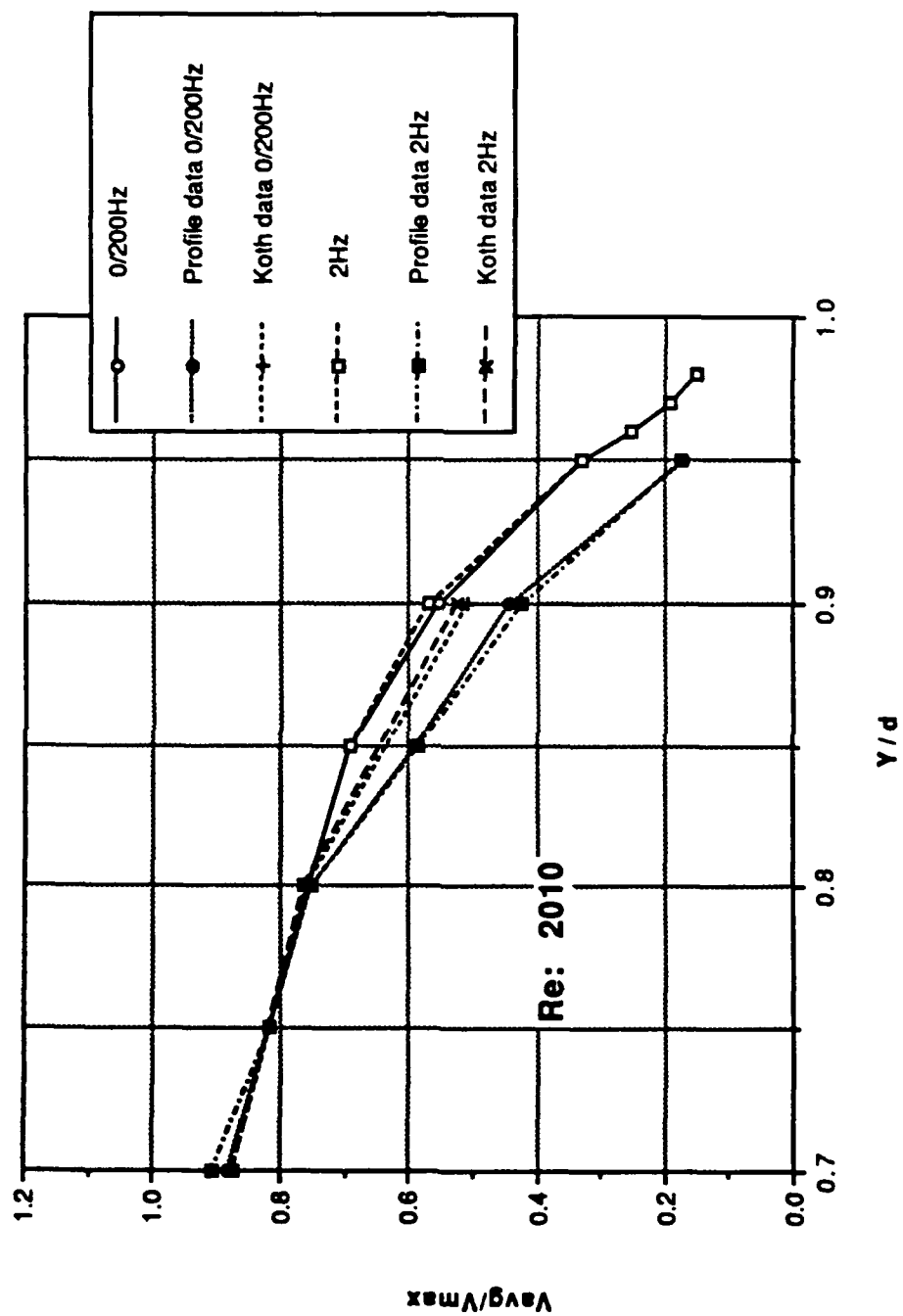


Figure 121. Near-Wall Data: Mean Velocity Normalized by the Centerline Velocity vs y/d ; $Re: 2010$

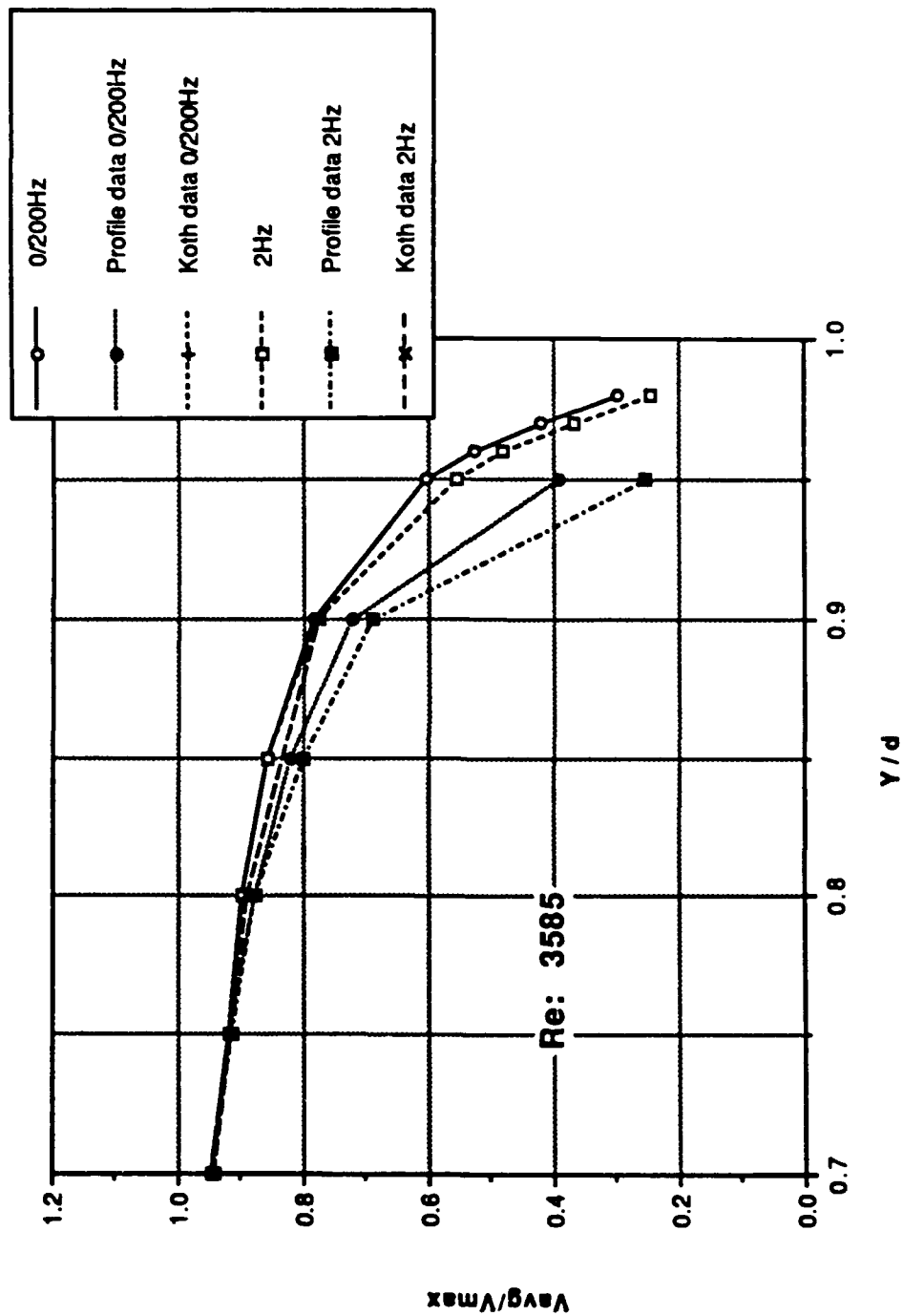


Figure 122. Near-Wall Data: Mean Velocity Normalized by the Centerline Velocity vs y/d ; $Re: 3585$

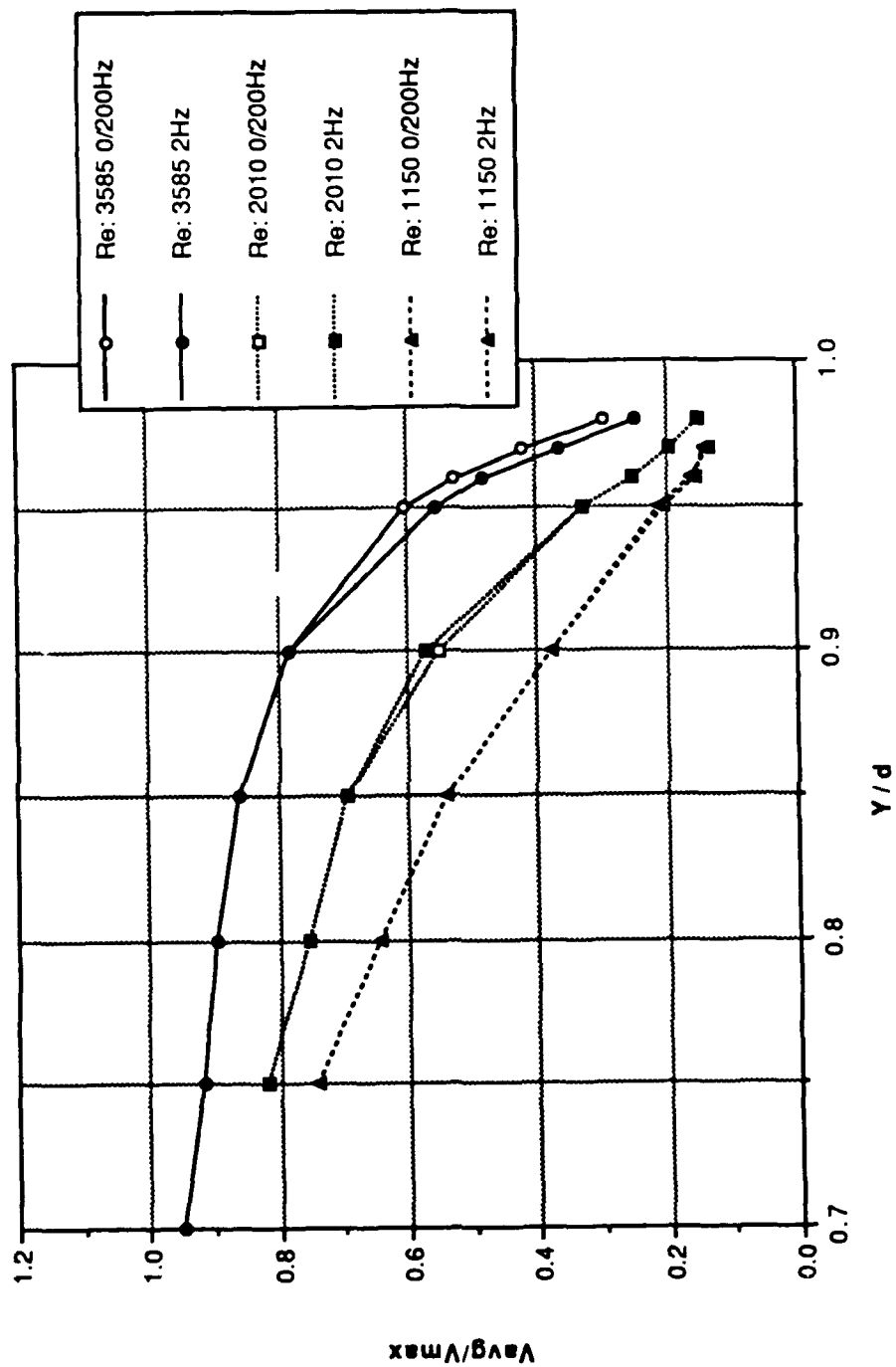


Figure 123. Near-Wall Data: Mean Velocity Normalized by the Centerline Velocity vs y/d ; Composite Near-Wall Profiles

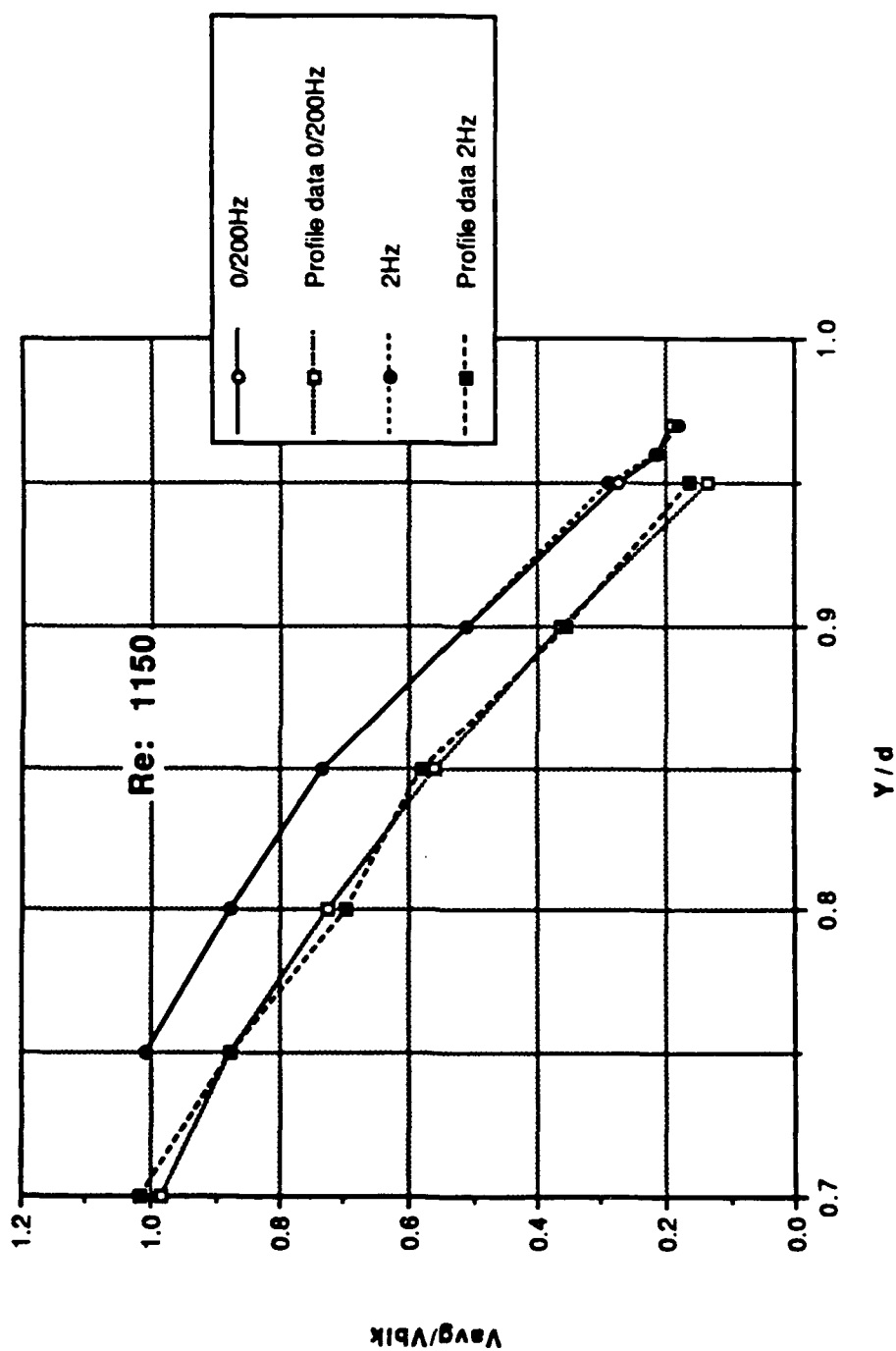


Figure 124. Near-Wall Data: Mean Velocity Normalized by the Bulk Velocity vs y/d ; Re: 1150

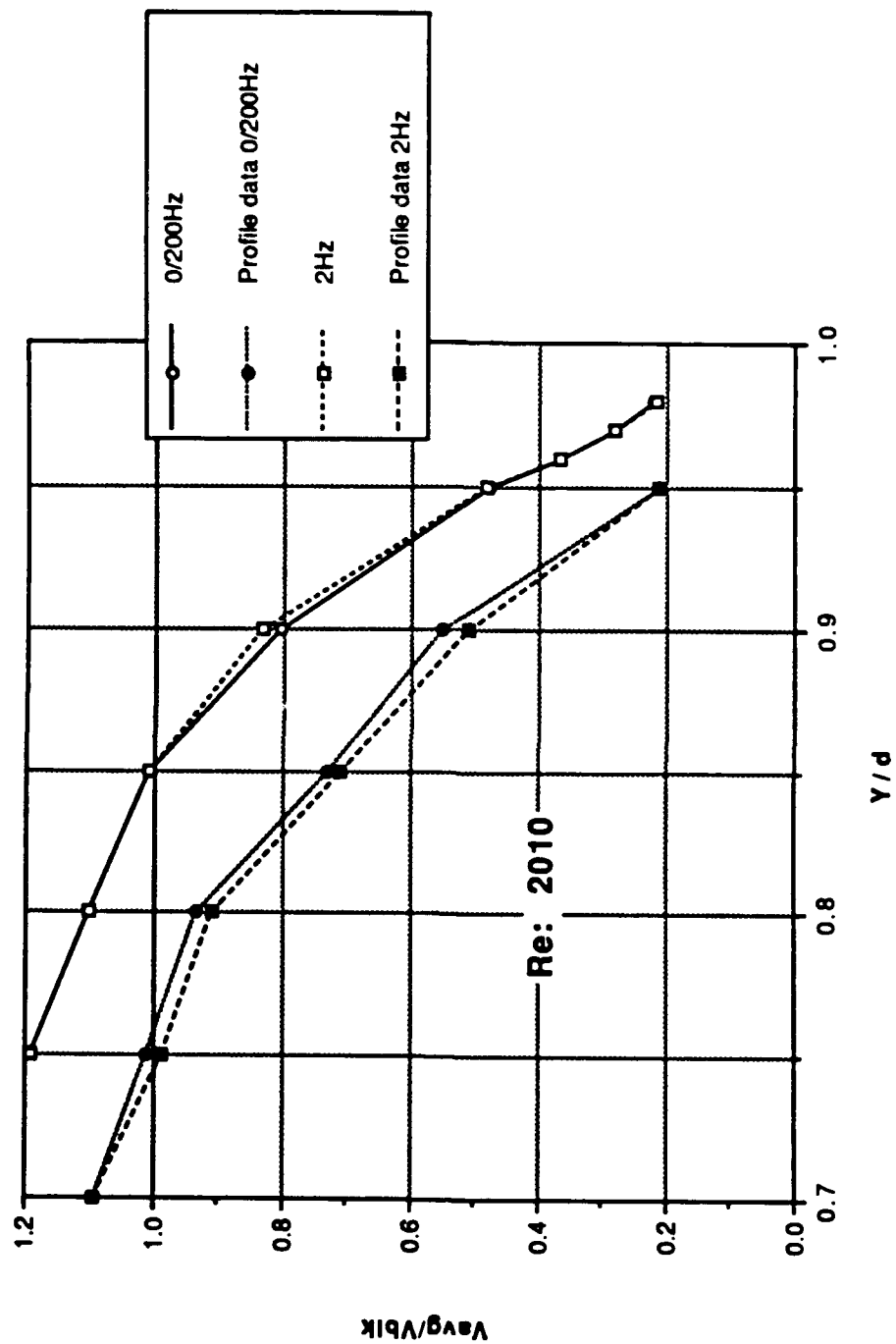


Figure 125. Near-Wall Data: Mean Velocity Normalized by the Bulk Velocity vs y/d ; Re: 2010

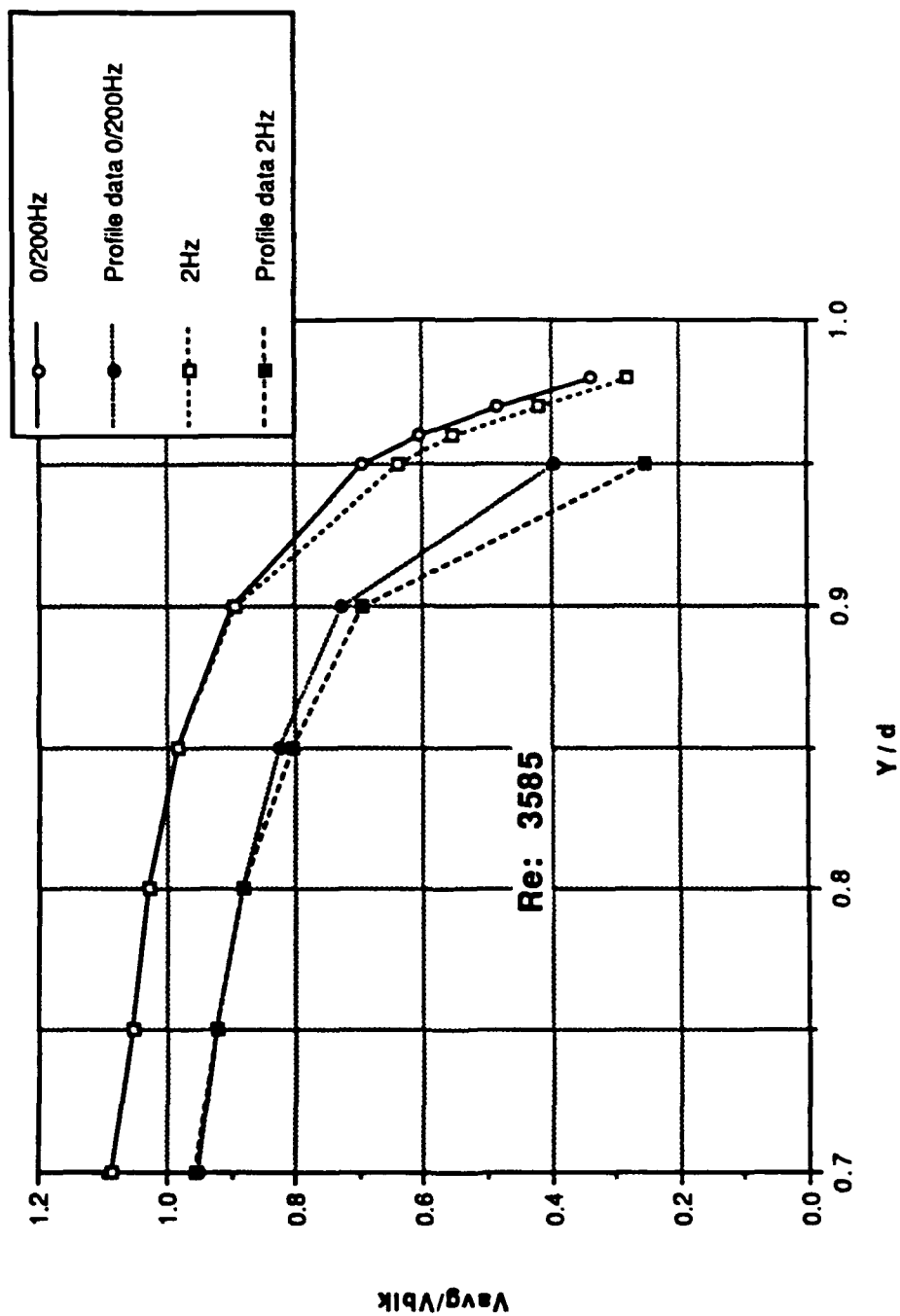


Figure 126. Near-Wall Data: Mean Velocity Normalized by the Bulk Velocity vs y/d ; $Re: 3585$

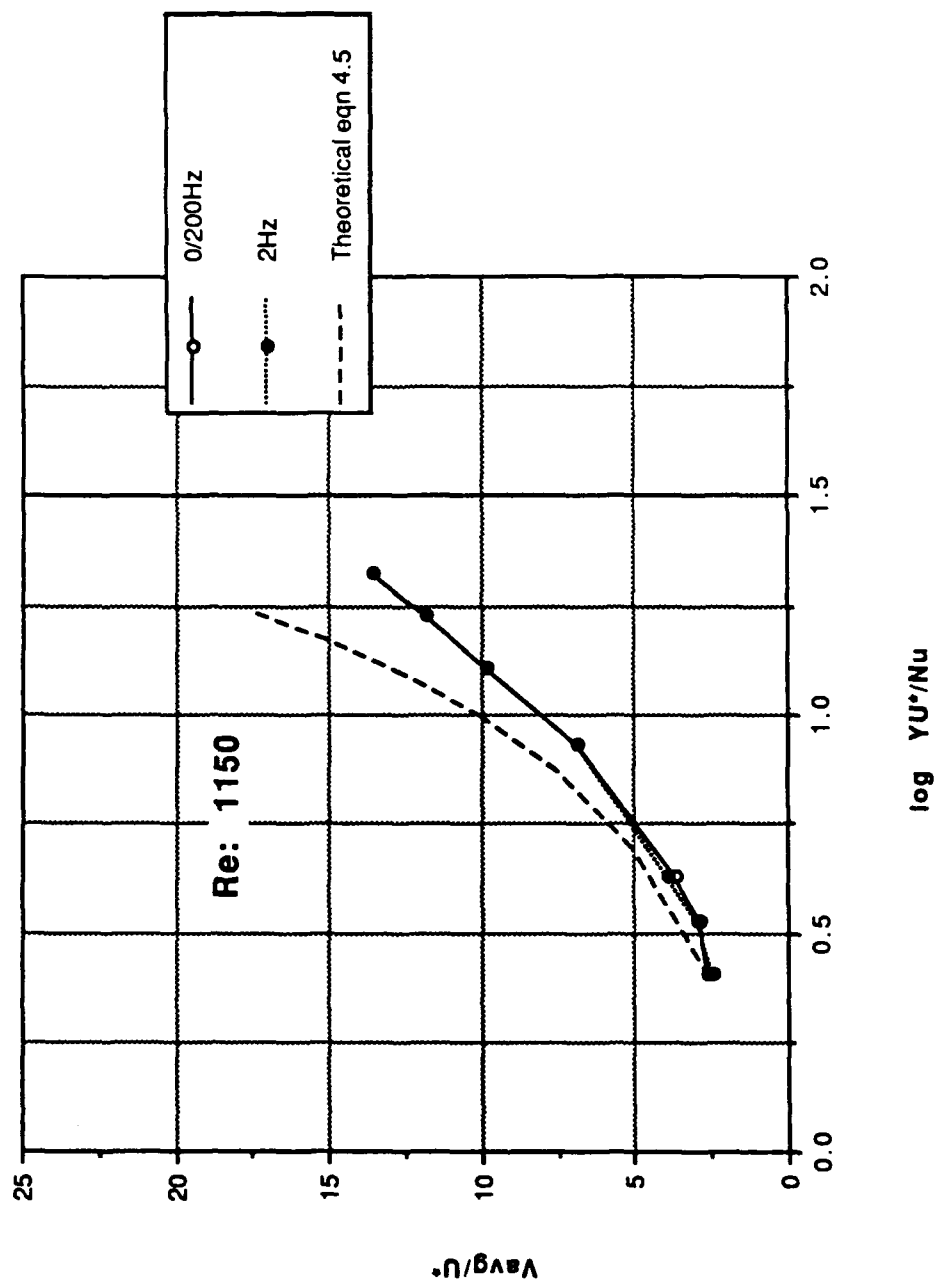


Figure 127. Near-Wall Data: Mean Velocity Normalized by the Shear Velocity vs $\log(yU^*/Nu)$; $Re: 1150$

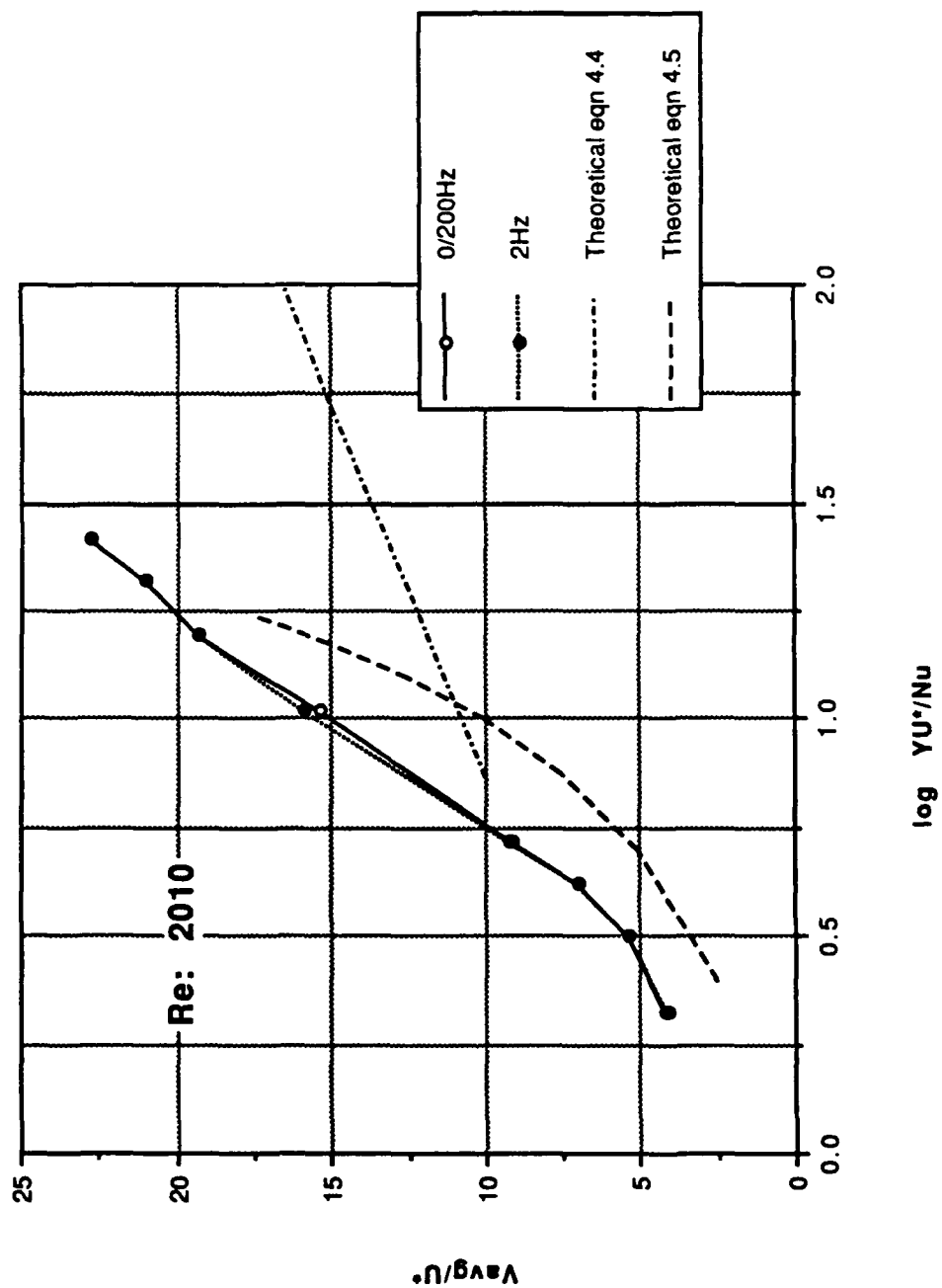


Figure 128. Near-Wall Data: Mean Velocity Normalized by the Shear Velocity vs $\log(yU^*/Nu)$; $Re: 2010$

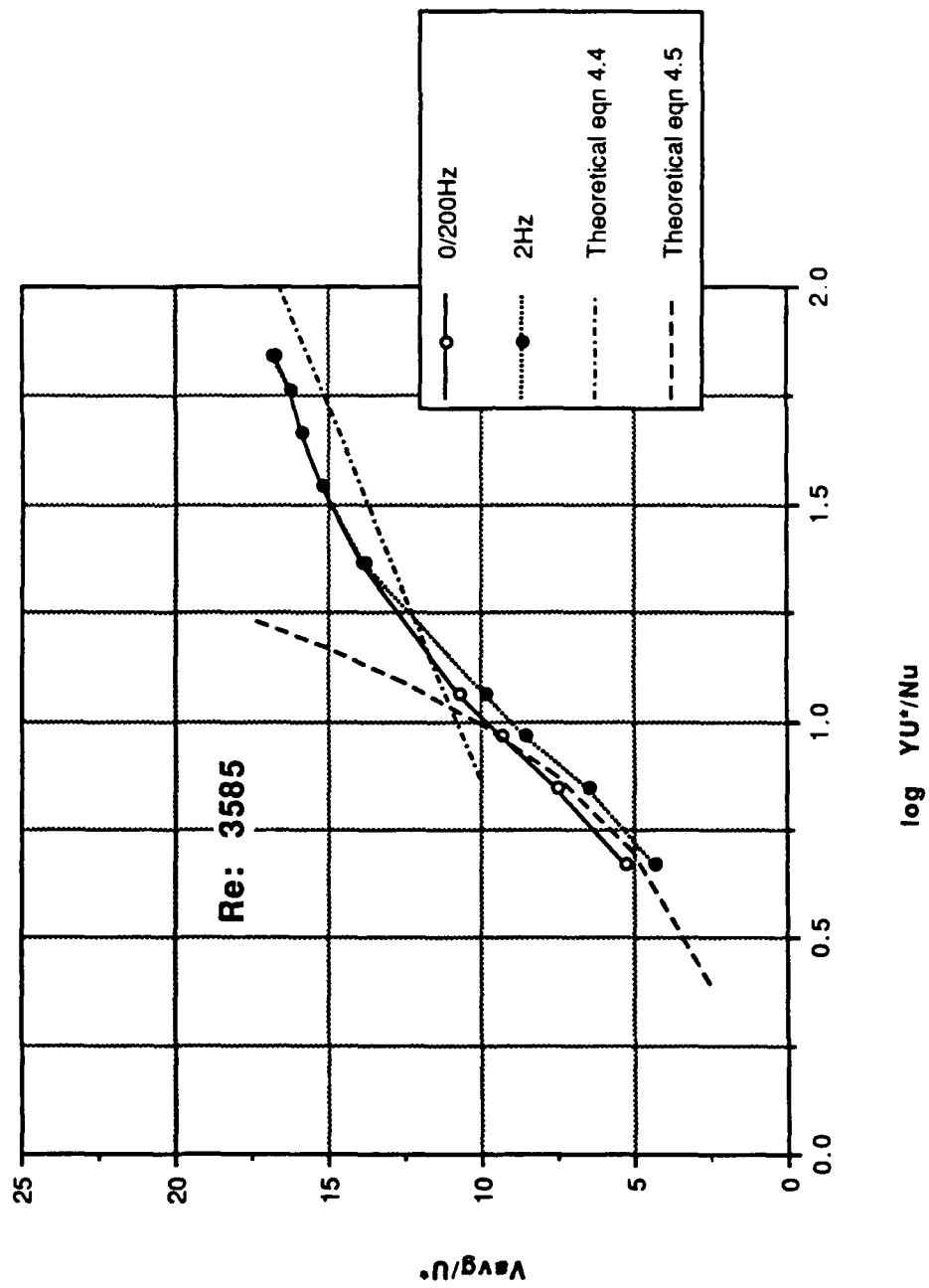


Figure 129. Near-Wall Data: Mean Velocity Normalized by the Shear Velocity vs $\log(yU^*/Nu)$; $Re: 3585$

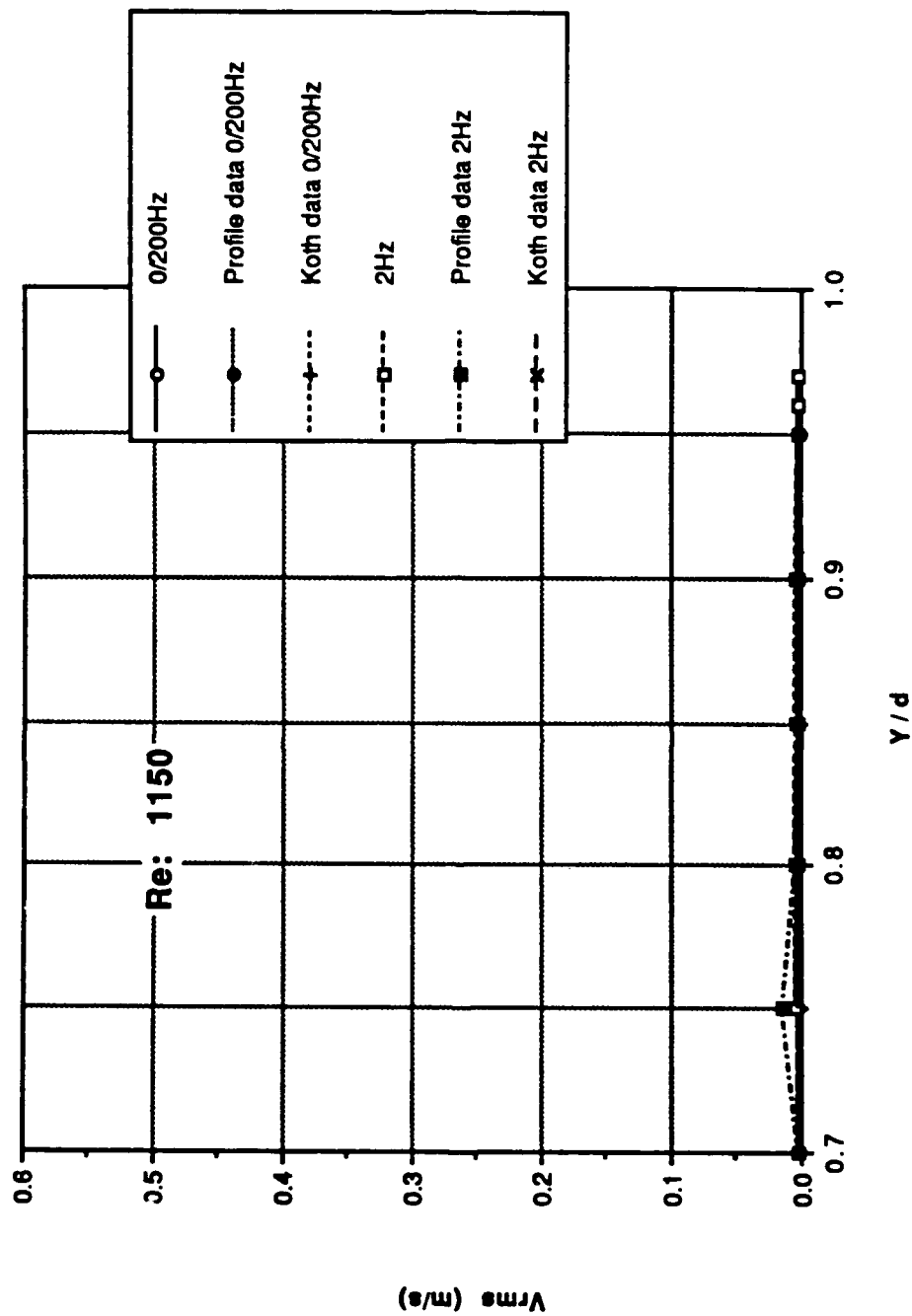


Figure 130. Near-Wall Data: Longitudinal Turbulence Intensity vs y/d ; Re: 1150

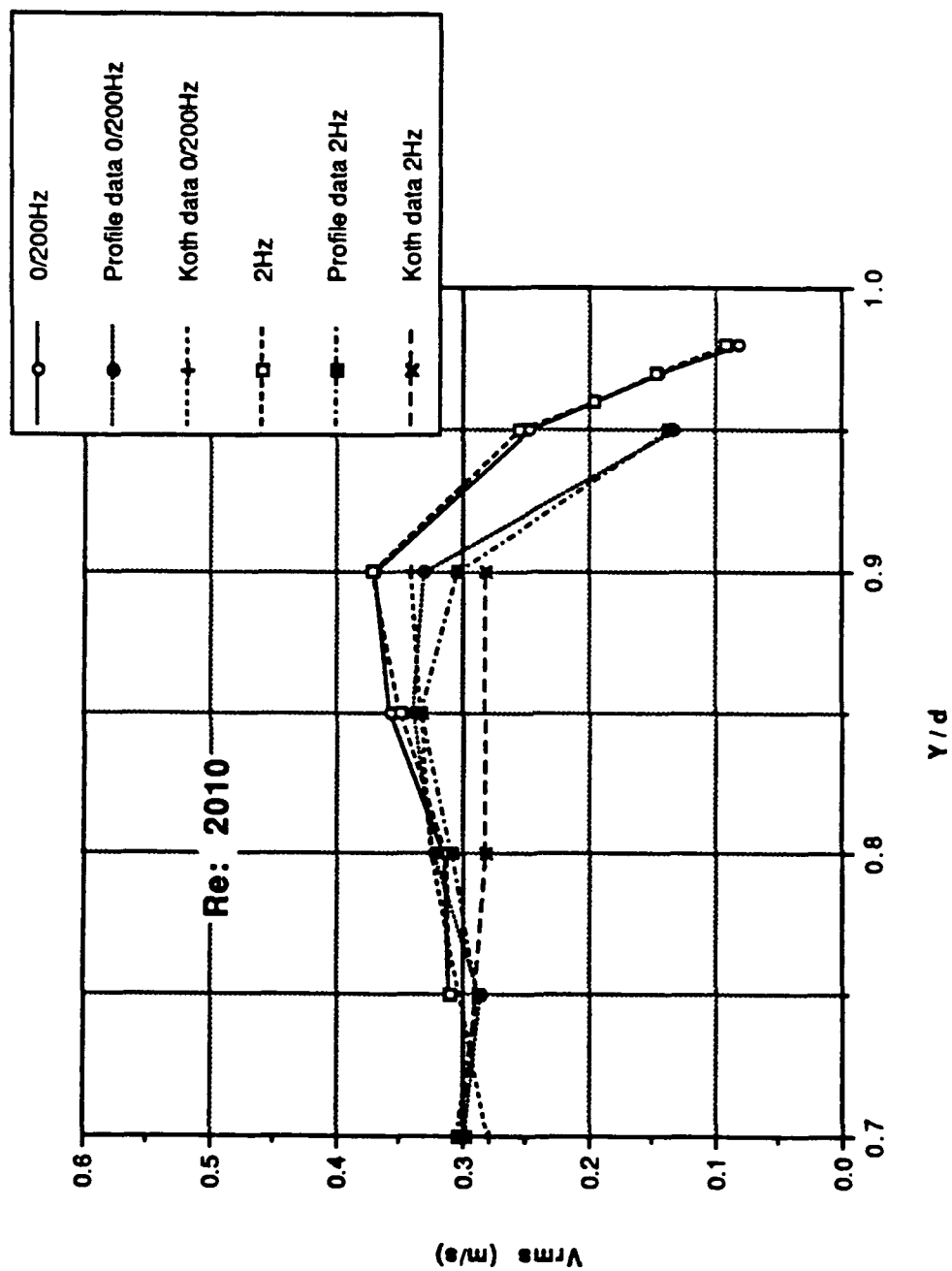


Figure 131. Near-Wall Data: Longitudinal Turbulence Intensity vs y/d ; Re: 2010

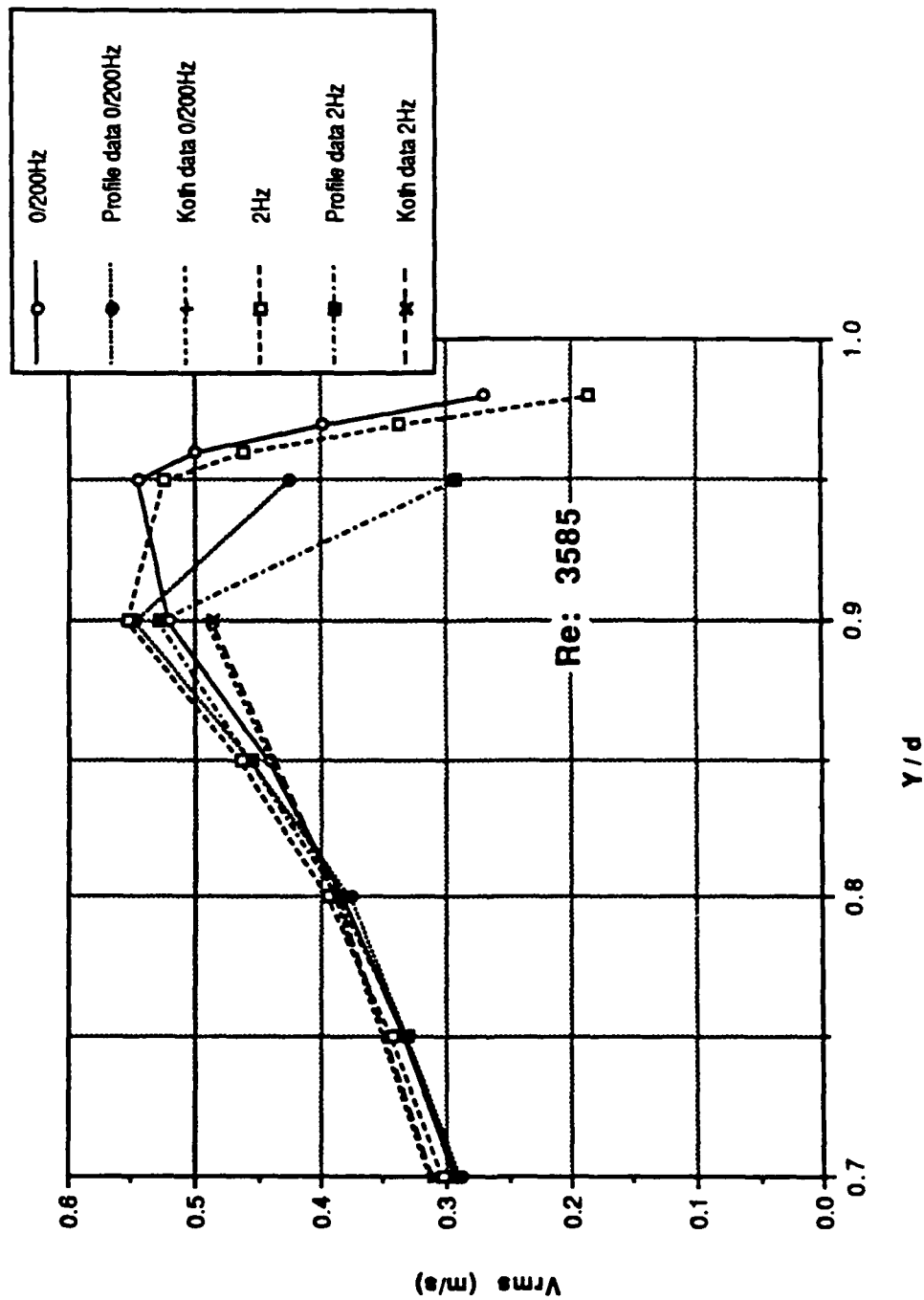


Figure 132. Near-Wall Data: Longitudinal Turbulence Intensity vs y/d ; $Re: 3585$

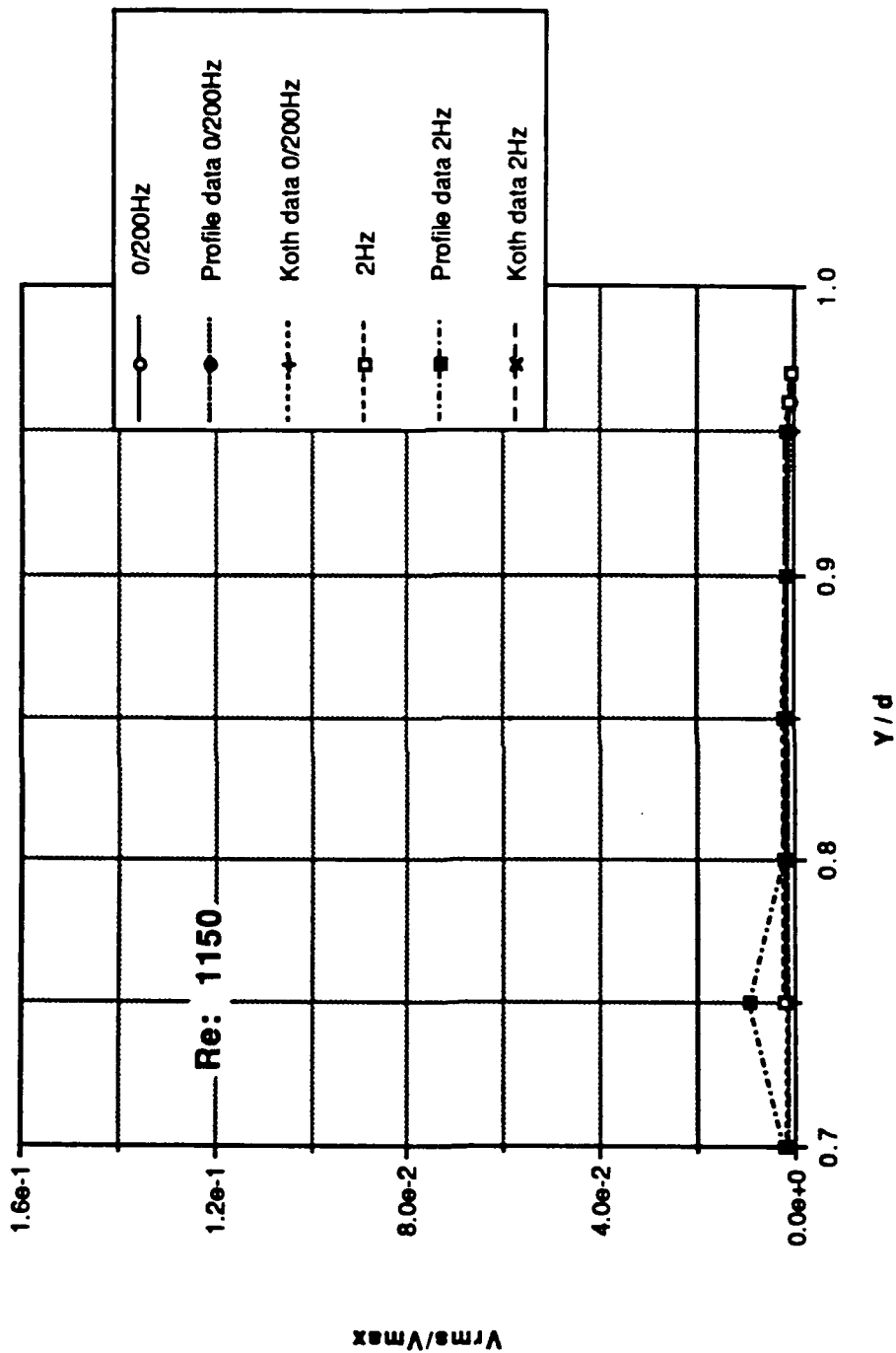


Figure 133. Near-Wall Data: Longitudinal Turbulence Intensity Normalized by the Centerline Velocity vs y/d ; Re: 1150

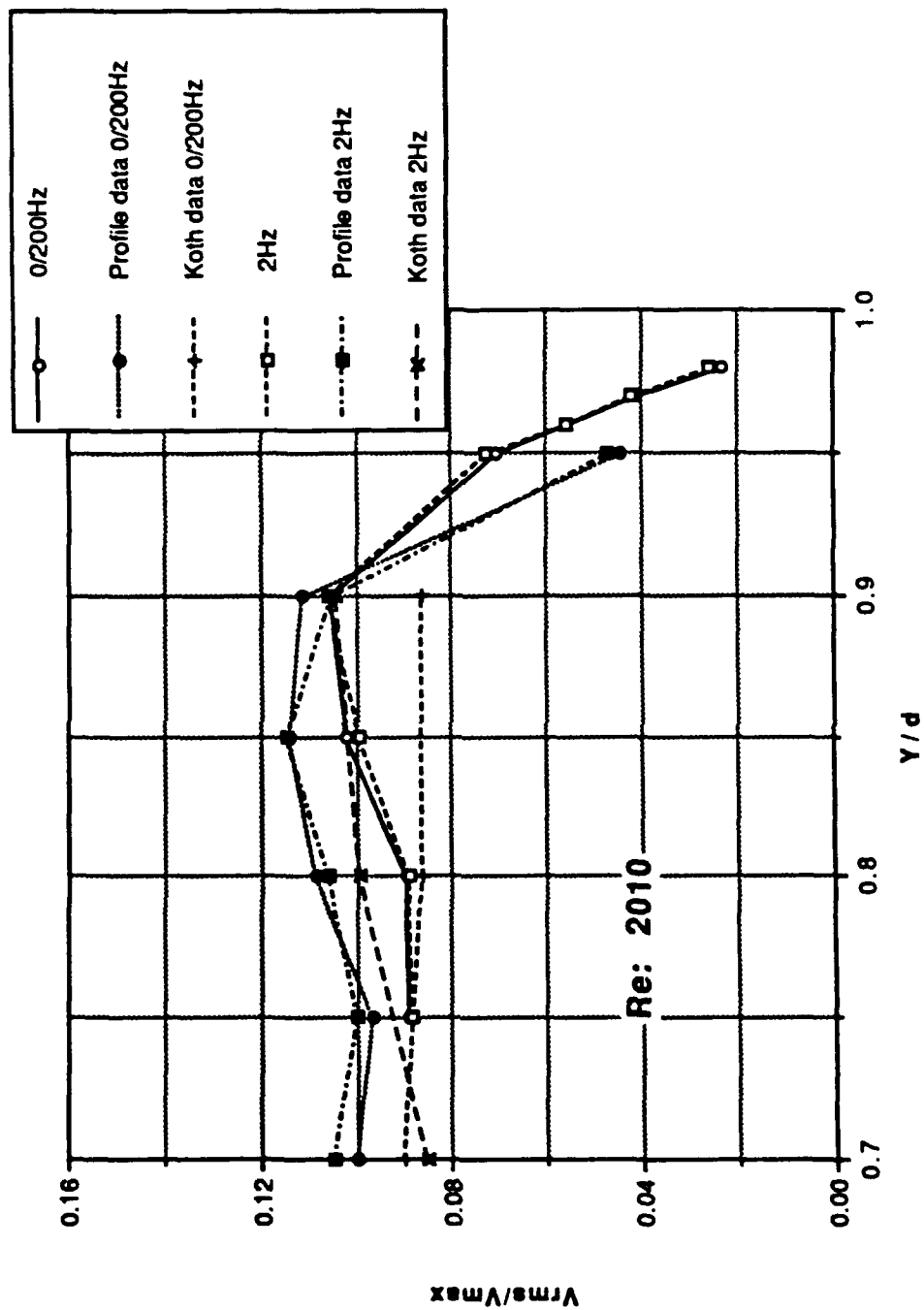


Figure 134. Near-Wall Data: Longitudinal Turbulence Intensity Normalized by the Centerline Velocity vs y/d ; Re: 2010

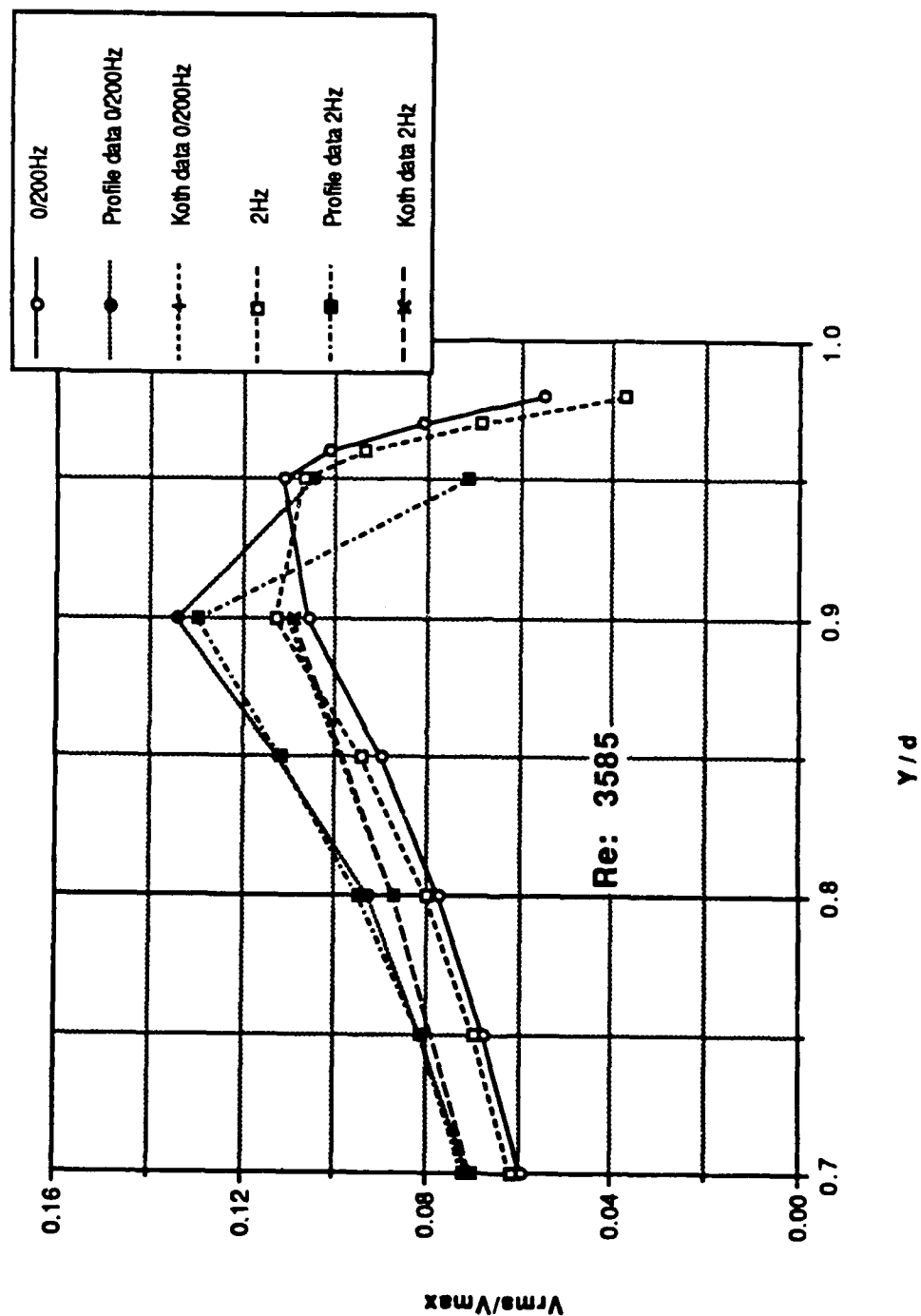


Figure 135. Near-Wall Data: Longitudinal Turbulence Intensity Normalized by the Centerline Velocity vs y/d ; Re: 3585

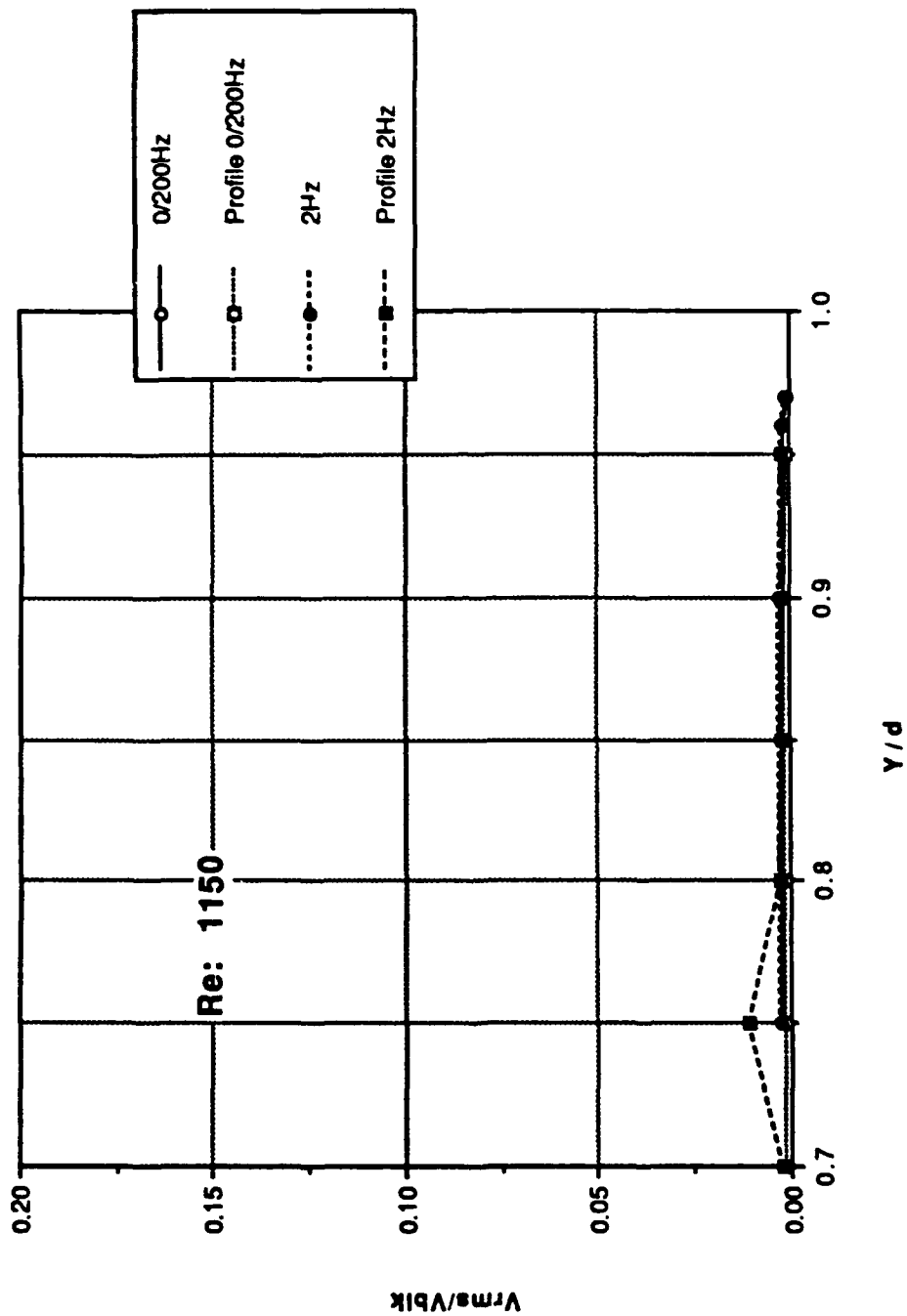


Figure 136. Near-Wall Data: Longitudinal Turbulence Intensity Normalized by the Bulk Velocity vs y/d ; Re: 1150

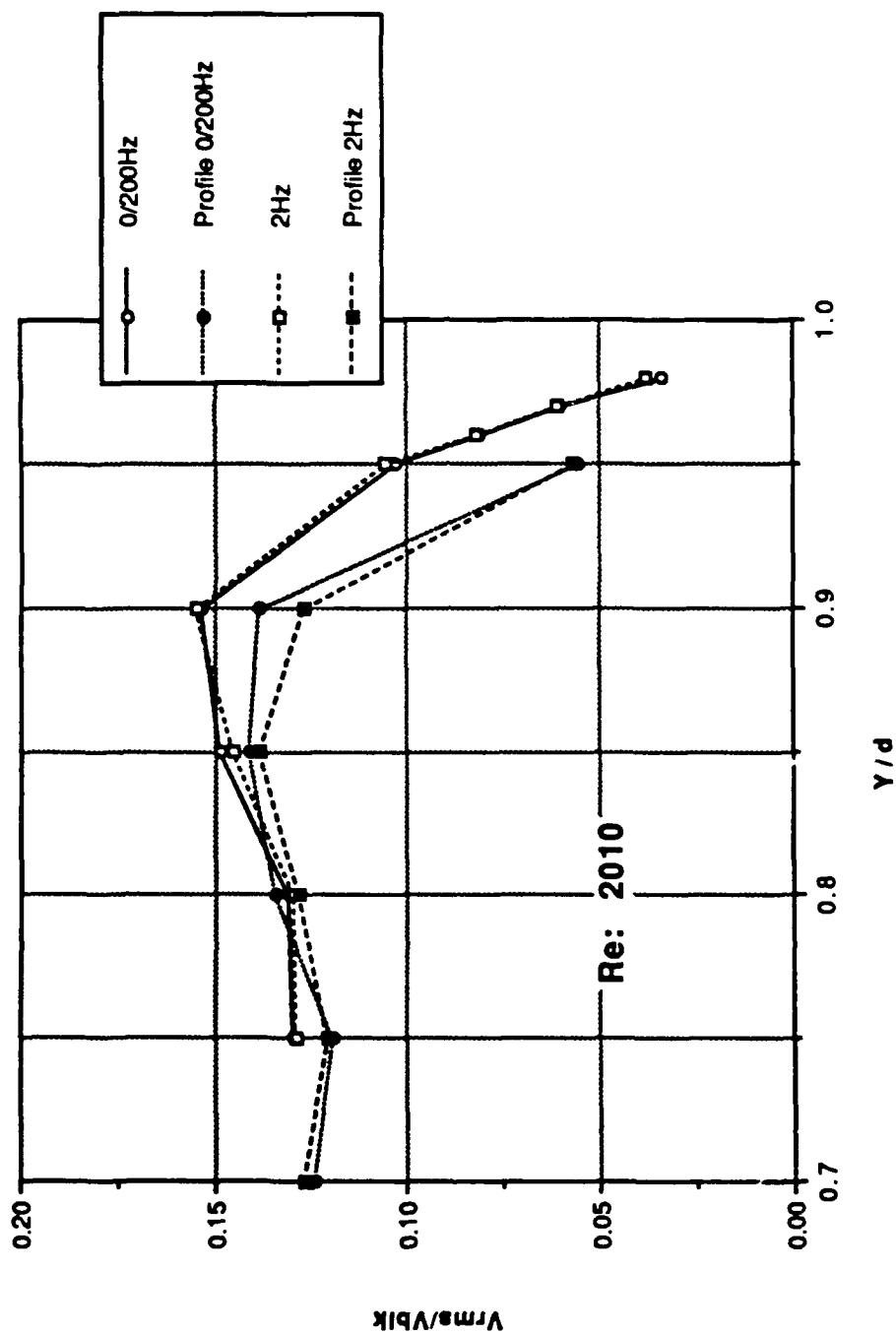


Figure 137. Near-Wall Data: Longitudinal Turbulence Intensity Normalized by the Bulk Velocity vs y/d ; Re: 2010

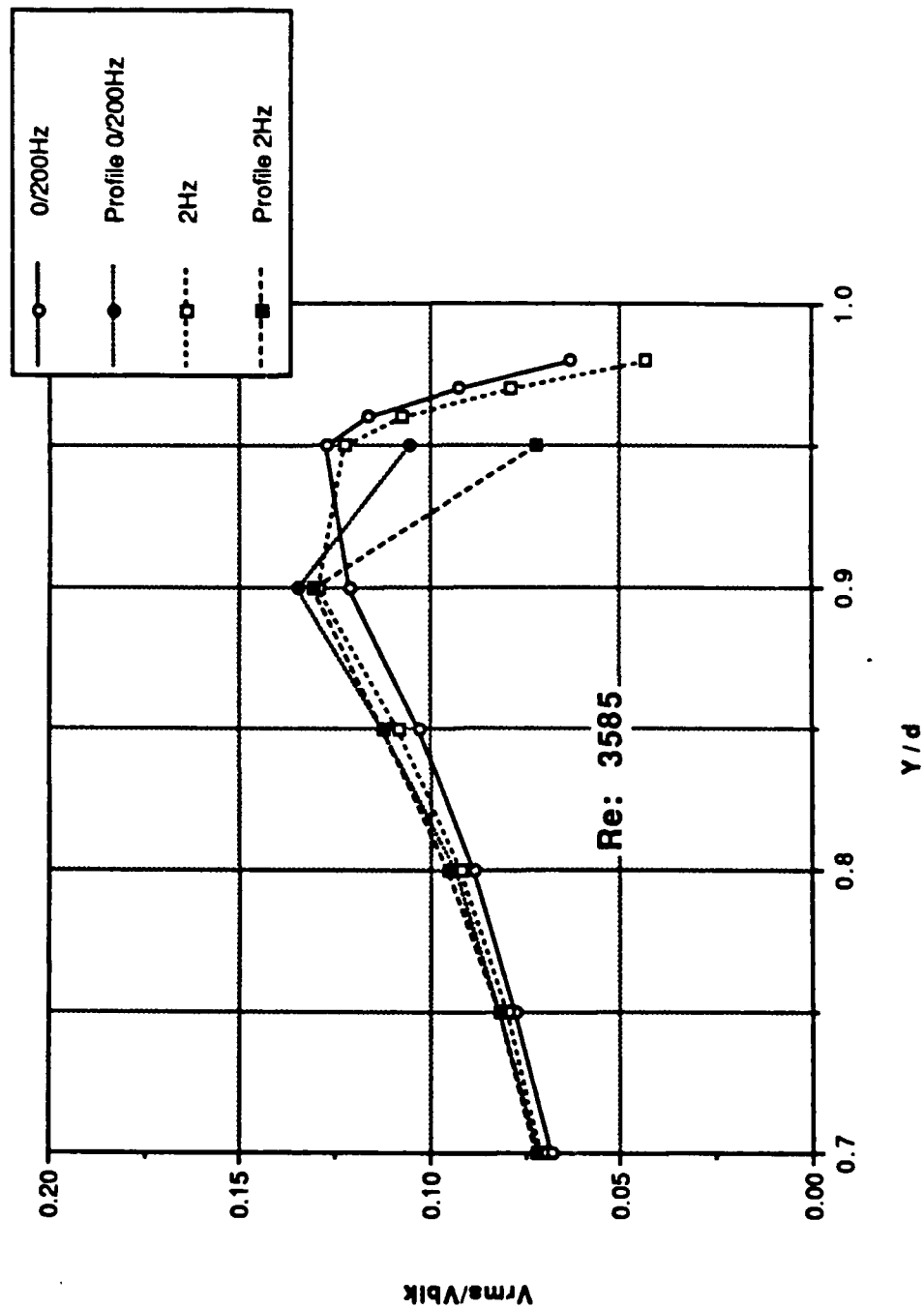


Figure 138. Near-Wall Data: Longitudinal Turbulence Intensity Normalized by the Bulk Velocity vs y/d ; Re: 3585

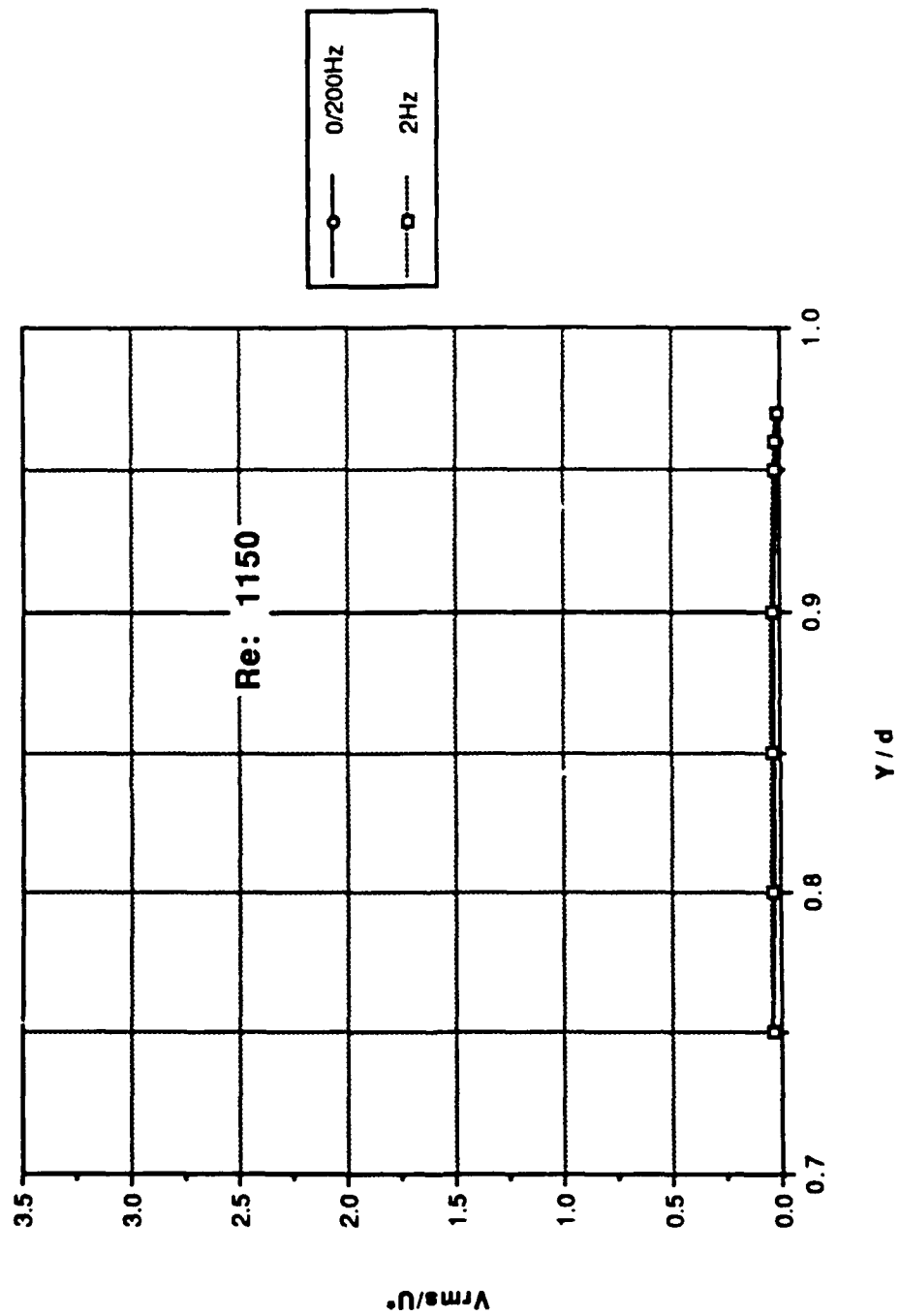


Figure 139. Near-Wall Data: Longitudinal Turbulence Intensity Normalized by the Shear Velocity vs y/d ; Re: 1150

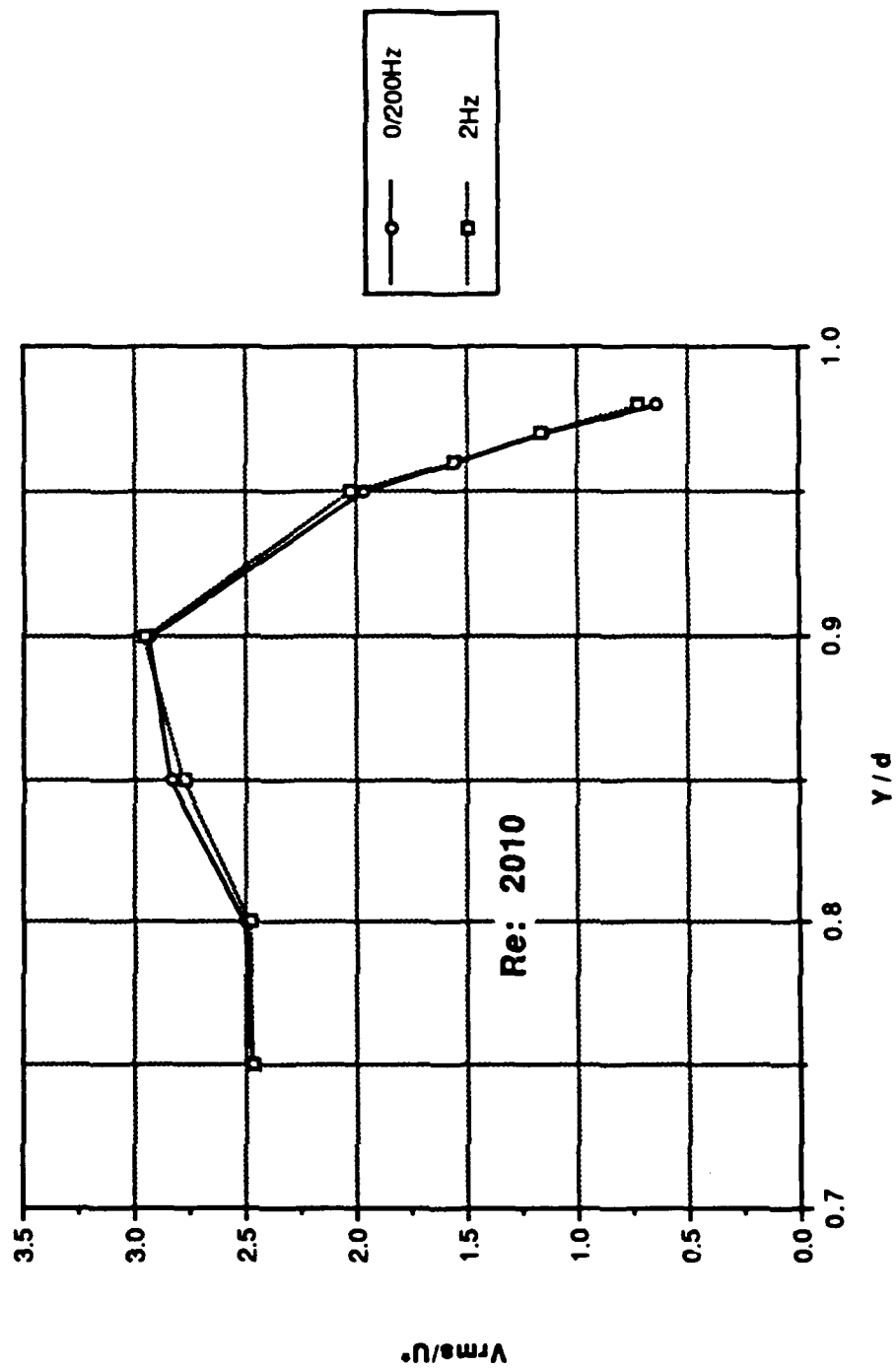


Figure 140. Near-Wall Data: Longitudinal Turbulence Intensity Normalized by the Shear Velocity vs y/d ; Re: 2010

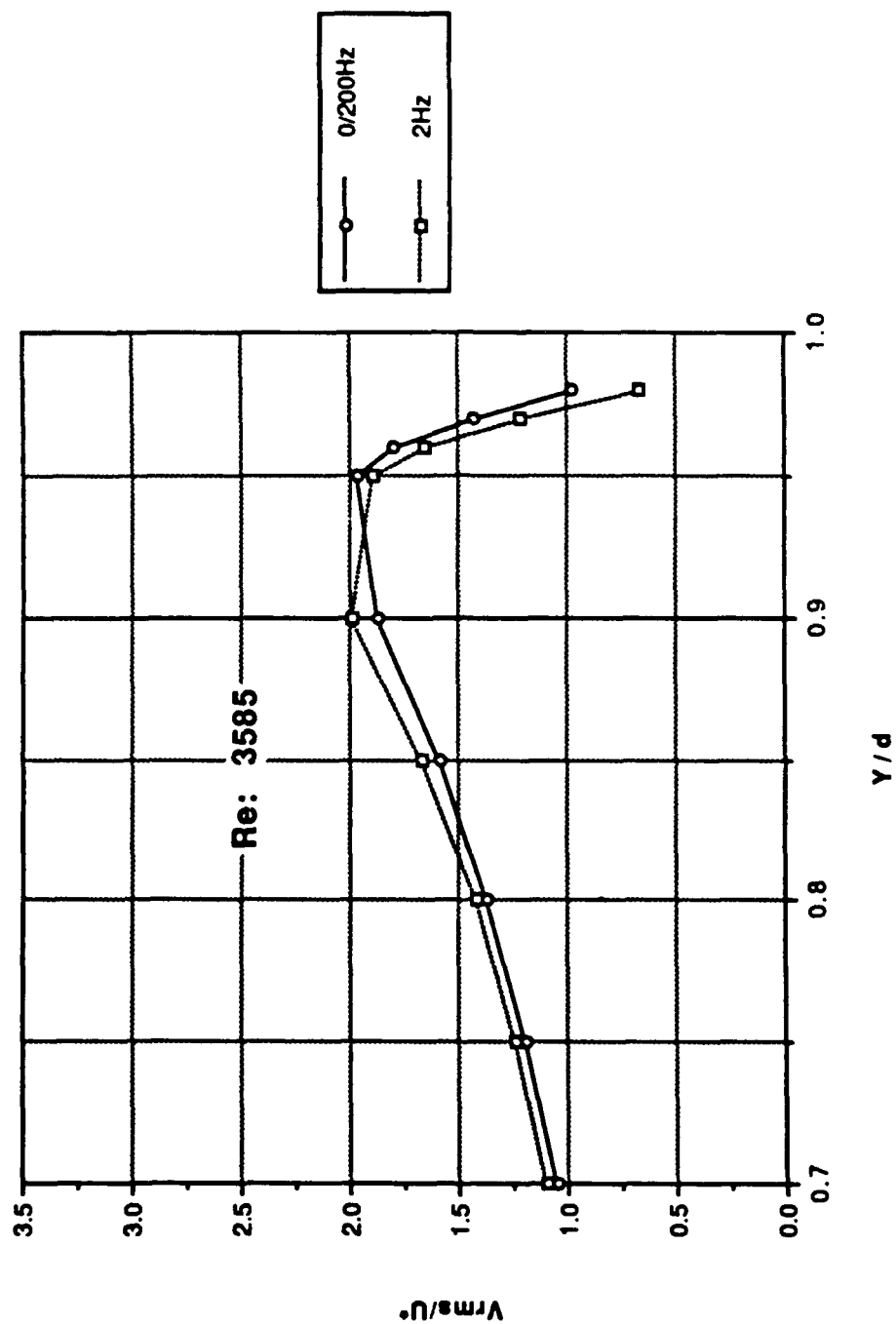


Figure 141. Near-Wall Data: Longitudinal Turbulence Intensity Normalized by the Shear Velocity vs y/d ; Re: 3585

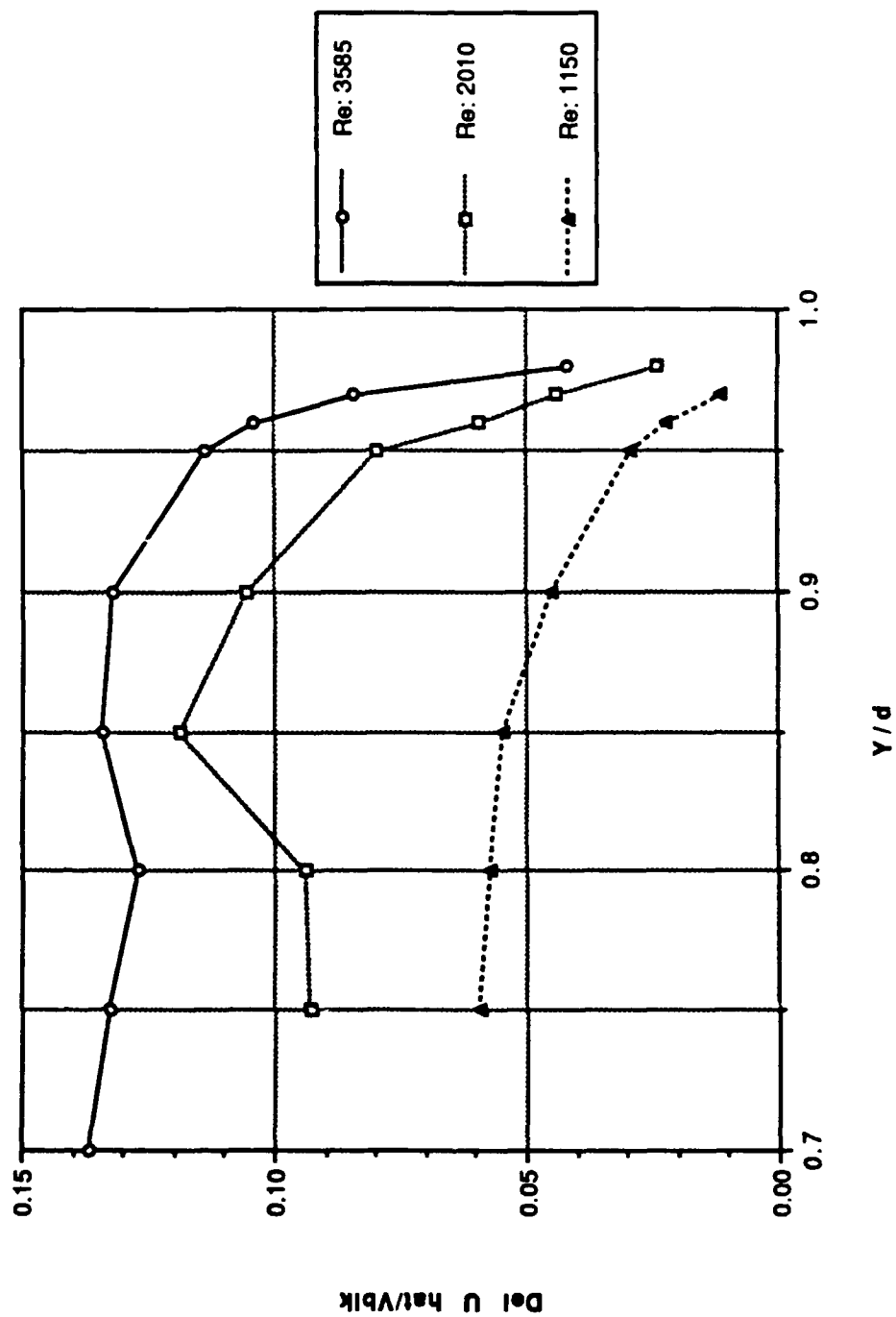


Figure 142. Phase Averaged Amplitude Normalized by the Bulk Velocity vs y/d ; Composite Near-Wall Profiles

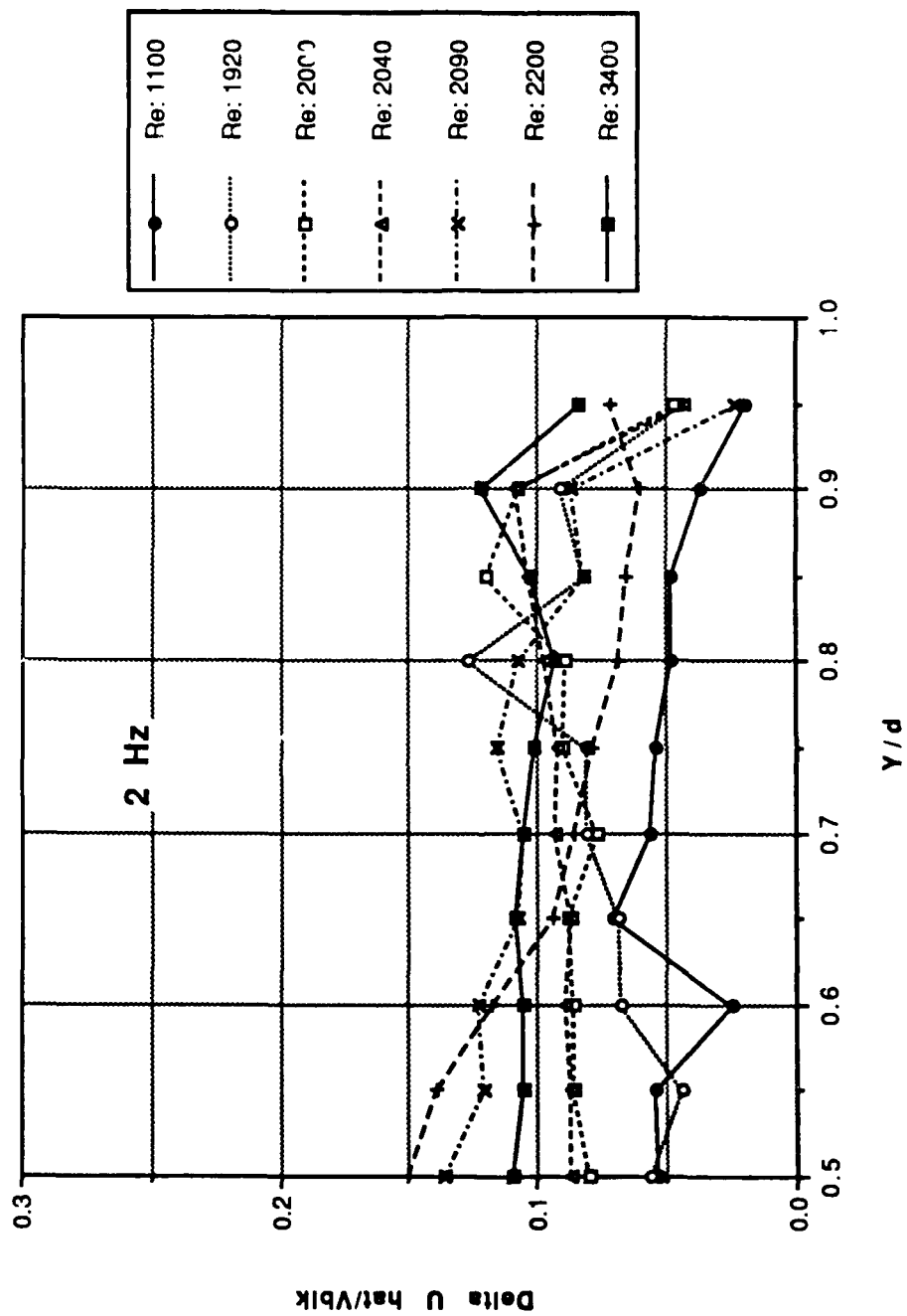


Figure 143. Phase Averaged Amplitude Normalized by the Bulk Velocity vs y/d ;
Composite of Pre-Transition Profiles

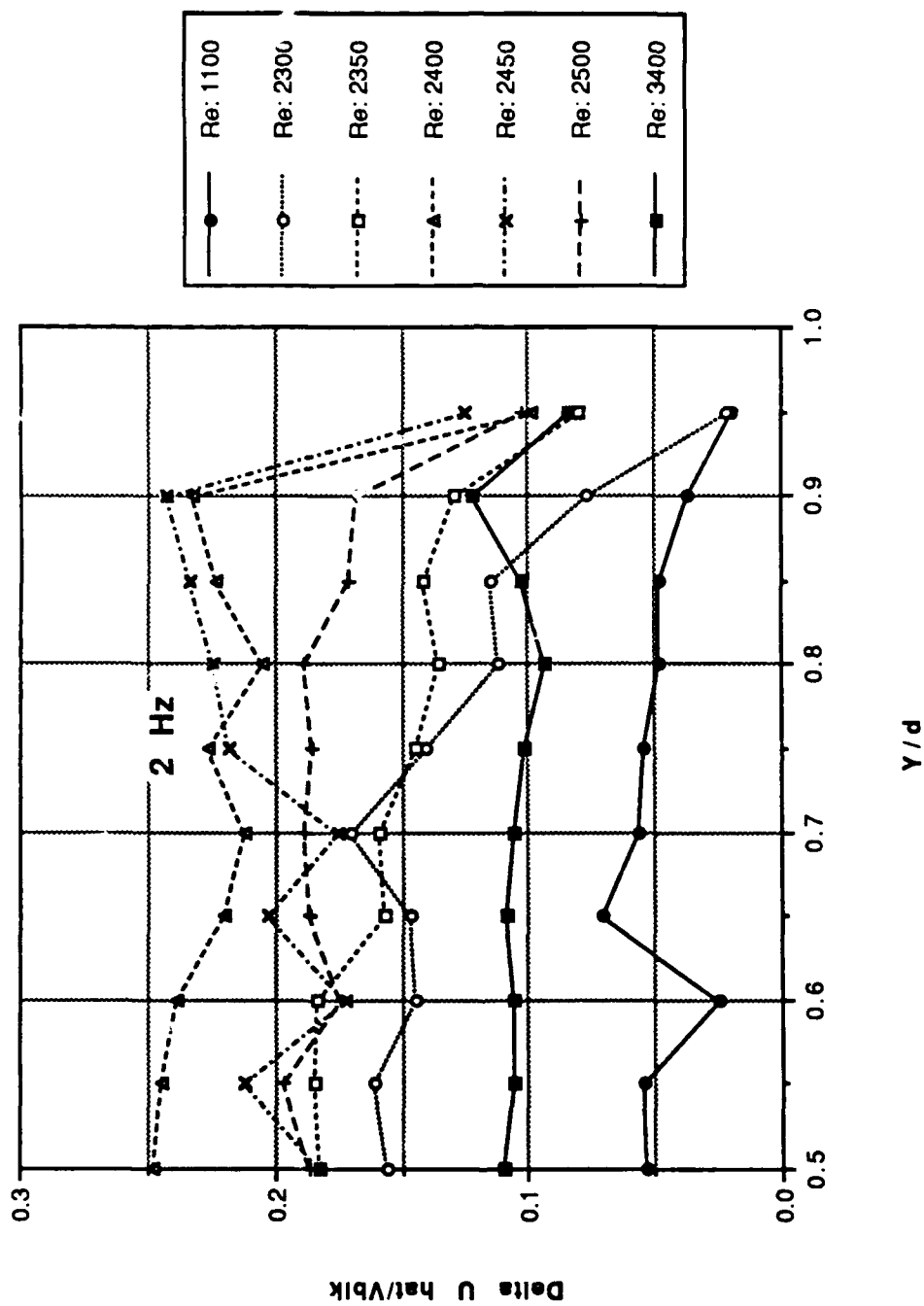


Figure 144. Phase Averaged Amplitude Normalized by the Bulk Velocity vs y/d ;
Composite of Transitional Profiles

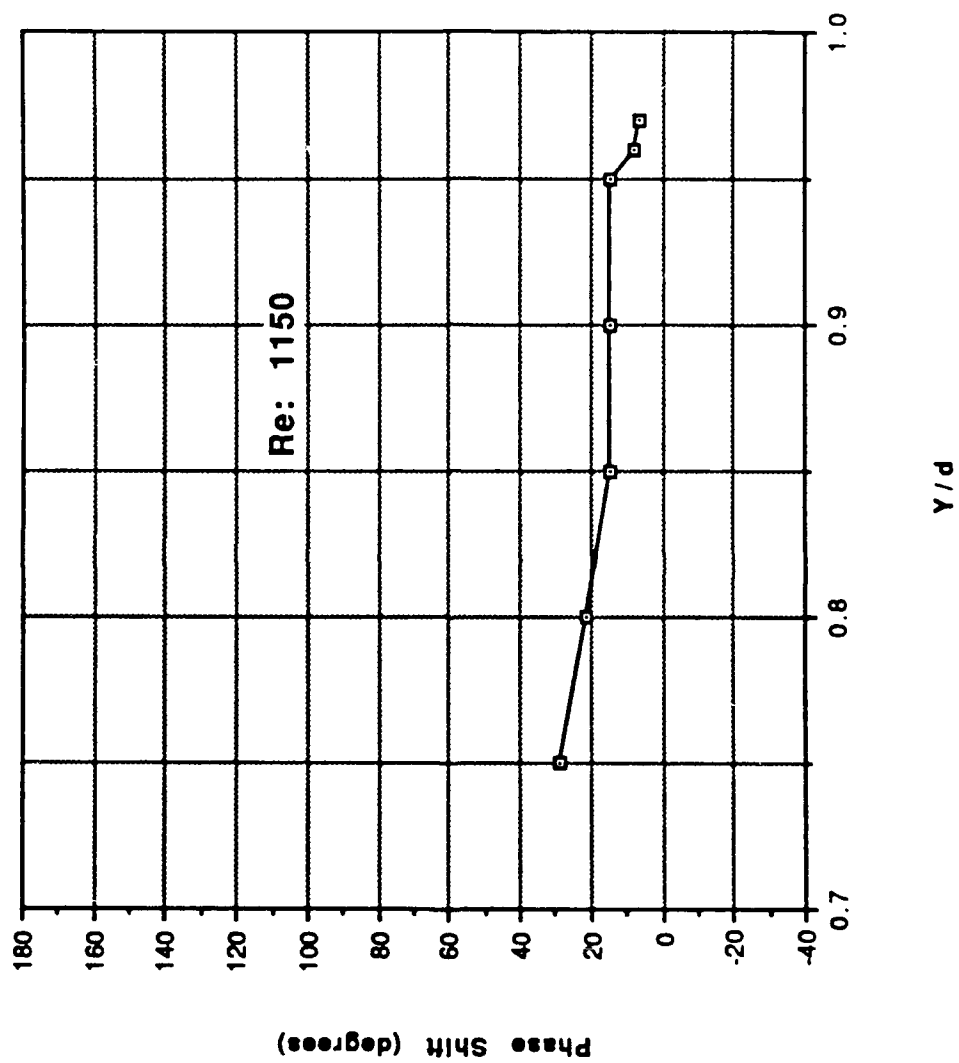


Figure 145. Near-Wall Data: Phase Shift vs y/d ; Re: 1150

LIST OF REFERENCES

1. Shemer, L., "Laminar-Turbulent Transition in a Slowly Pulsating Pipe Flow", *Phys. Fluids*, 28, pp. 3506-3509, 1985.
2. Tu, S. W. and Ramaprian, B. R., "Fully Developed Periodic Turbulent Pipe Flow. Part I. Main Experimental Results and Comparisons with Predictions," *J. Fluid Mech*, 137, pp. 31-58, 1983.
3. Ramaprian, B. R. and Tu, S. W., "An Experimental Study of Oscillatory Pipe Flow At Transitional Reynolds Numbers," *J. Fluid Mech*, 100, pp. 513-544, 1980.
4. Stettler, J. C. and Hussain, A. K. M. F., "On Transition of the Pulsatile Pipe Flow," *J. Fluid Mech*, 170, pp. 169-197, 1986.
5. Merkli, P. and Thomann, H., "Transition to Turbulence in Oscillating Pipe Flow," *J. Fluid Mech.*, 68, pp. 567-575, 1975.
6. Sergeev, S. I., "Fluid Oscillations in Pipes at Moderate Reynolds Numbers," *Fluid Dyn.*, Mekh 2H" 1, pp. 21-22, 1966.
7. Hino, M. and Sawamoto, M., "Linear Stability Analysis of an Oscillator Flow Between Parallel Plates," *Proc. 7th Symposium on Turbulence*, H. Sato and M. Ohji, Eds., pp. 1-7. Inst. of Space & Aeronautics, Univ. of Tokyo, 1975.
8. Hino, M., Sawamoto, M. and Takasu, S., "Experiments on Transition to Turbulence in an Oscillatory Pipe Flow," *J. Fluid Mech.*, 75, pp. 193-207, 1976.
9. Gerrard, J. H., "An Experimental Investigation of the Pulsating Turbulent Water Flow in a Tube," *J. Fluid Mech.*, 46, pp. 43-64, 1971.

10. Gilbrech, D. A. and Combs, G. D., "Critical Reynolds Numbers for Incompressible Pulsating Flow in Tubes," in *Developments in Theoretical and Applied Mechanics*, I. New York, Plenum Press, 1963.
11. Sarpkaya, T., "Experimental Determination of the Critical Reynolds Number for Pulsating Poiseuille Flow," *Trans. A. S. M. E. D. J. Basic Engrg.*, 88, pp. 589-598, 1966.
12. Simpson, R. L., Sallas, J. J. and Nasburg, R. E., "Tailoring the Wave Form of a Periodic Flow with a Programmable Damper," *J. Fluids Engrg.*, 100, pp. 287-290, 1978.
13. Grosch, C. E. and Salwen, H., "The Stability Of Steady and Time-Dependent Plane Poiseuille Flow," *J. Fluid Mech.*, 34, pp. 177-205, 1968.
14. Herbert, D. M., "The Energy Balance in Plane Poiseuille Flow," *J. Fluid Mech.*, 56, pp. 73-80, 1972.
15. Hall, P., "The Stability of Plane Poiseuille Flow Modulated at High Frequency," *Proc R. Soc. Lond. A.*, 344, pp. 453-464, 1975.
16. von Kerczek, C. H., "The Instability of Oscillatory Plane Poiseuille Flow," *J. Fluid Mech.*, 116, pp. 91-114, 1982.
17. Singer, B., Ferziger, J. H. and Reed, H., *Numerical Simulation of Laminar-Turbulent Transition in the Plane Channel*, Report TF-31, Thermosciences Division, Department of Mechanical Engineering, Stanford University, Stanford, May, 1987.
18. Singer, B., Ferziger, J. H. and Reed, H., "Numerical Simulation of Transition in Oscillatory Plane Channel Flow," *J. Fluid Mech.*, 208, pp. 45-66, 1989.
19. Tozzi, J. T., Ph. D. Thesis, Catholic University, 1982.
20. Davies, S., "Stability of Time Periodic Flows," *Ann. Rev. Fluid Mech.*, 8, pp. 57-74, 1976.

21. Ligrani, P. M., Subramanian, C. S., Coumes, T. M., Greco, F. J., Koth, H. and Longest, J. M., "Study of the Imposition of Bulk Flow Pulsations on a Plane Channel Flow at Moderate Strouhal Numbers", submitted to *Int'l J. of Experiments in Thermal & Fluid Sciences* 1990.
22. Han, L. S., "Hydrodynamic Entrance Lengths for Incompressible Laminar Flow in Rectangular Ducts," *J. of Appl. Mech.* 27, pp. 403-410, 1960.
23. Zang, T. A. and Krist, S. E., "Numerical Experiments on Stability and Transition in Plane Channel Flow," *Theoretical and Computational Fluid Dynamics*, 1, pp. 41-64, 1989.
24. Koth, H. E., *Effects of Imposed Bulk Flow Oscillations At 1, 2, 3 and 4 Hz on Transition in a Straight Channel With 40 to 1 Aspect Ratio*, Master's Thesis, Naval Postgraduate School, Monterey, California, June, 1990.

INITIAL DISTRIBUTION LIST

		No. Copies
1.	Defense Technical Information Center Cameron Station Alexandria, VA 22304-6145	2
2.	Library, Code 52 Naval Postgraduate School Monterey, CA 93943-5002	2
3.	Professor P. M. Ligrani, Code 69Li Department of Mechanical Engineering Naval Postgraduate School Monterey, CA 93943-5000	4
4.	Department Chairman, Code 69 Department of Mechanical Engineering Naval Postgraduate School Monterey, CA 93943-5000	1
5.	Naval Engineering Curricular Officer, Code 34 Department of Mechanical Engineering Naval Postgraduate School Monterey, CA 93943-5000	1
6.	Professor C. S. Subramanian, Code 69Su Department of Mechanical Engineering Naval Postgraduate School Monterey, CA 93943-5000	2
7.	LT Darrell S. Morrow Route 1, 608 Misquite Rd. Cuero, TX 77954	2